Studies on co-utilization of High ash coal under CO_2 atmosphere for Thermal treatment with Wastes in the context of Syngas and Electricity generation

A thesis

Submitted in Partial Fulfilment of the Requirements for the Degree of

DOCTOR OF PHILOSOPHY

By

Pradeep Sahu

Department of Chemical Engineering

Indian Institute of Technology Guwahati

Guwahati, Assam 781039

January 2023

Dedicated to

My Parents

Department of Chemical Engineering
Indian Institute of Technology Guwahati
Guwahati, Assam 781039

STATEMENT

I hereby declare that the matter embodied in this thesis entitled "**Studies on co-utilization of high ash coal under CO_2 atmosphere for thermal treatment with wastes in context of syngas and electricity generation**" is the result of investigations carried out by me in the Department of Chemical Engineering, Indian Institute of Technology Guwahati, Assam, India under the supervision of **Dr. Prabu Vairakannu.**

In keeping with the general practice of reporting scientific observations, due acknowledgement has been made wherever the work described is based on the findings of other investigations.

Guwahati — **Pradeep Sahu**

January, 2023 — (Roll No. 166107016)

Department of Chemical Engineering
Indian Institute of Technology Guwahati
Guwahati, Assam 781039

CERTIFICATE

It is certified that the work described in this thesis, entitled "**Studies on co-utilization of high ash coal under CO_2 atmosphere for thermal treatment with wastes in the context of syngas and electricity generation**", done by **Mr. Pradeep Sahu** for the award of degree of philosophy is an authentic record of the results obtained from the research work carried out under my supervision in the department of Chemical Engineering, Indian Institute of Technology Guwahati, India and this work has not been submitted elsewhere for the award of any other degree or diploma.

This thesis in my opinion, has reached the standard fulfilling the requirements for the award of the degree of Doctor of philosophy in accordance with the regulations of the institute.

Date: January, 2023

(Dr. Prabu Vairakannu)
Associate Professor
Department of Chemical Engineering
Indian Institute of Technology Guwahati
Guwahati, 781039

ACKNOWLEDGEMENTS

It gives me immense pleasure to extend my sincere gratitude to acknowledge each individual who led me to the completion of the dissertation. I am highly obliged to all the people who have encouraged me during all these years.

First and foremost, I would like to express my sincere thanks to my thesis supervisor, **Dr. Prabu Vairakannu**, for providing relentless support and valuable guidance in various stages of my research journey. His positive attitude and encouragement boosted my inner confidence and helped me to excel even after multiple failures. I am fortunate that he took me under his wings and considered me working under his esteemed guidance. I am greatly indebted for sharing his profound knowledge with me. I have thoroughly enjoyed working with him and I strongly believe that he brought out the best in me in every aspect.

I am grateful to my doctoral committee members **Prof. Tamal Banerjee** (Department of Chemical Engineering), **Prof. Vaibhav V. Goud** (Department of Chemical Engineering), **Dr. Narayanasamy Selvaraju** (Department of Biosciences and Bioengineering) for their valuable suggestions, intensive assessment, and their active cooperation during my research progress.

I would like to acknowledge all the centres for providing me instrumental facilities for the characterization purposes such as the Analytical Lab Facility (Department of Chemical Engineering), Central Instrument Facility (CIF), Guwahati Biotech Park (for ultimate analysis).

I am grateful to all the staff and faculty members of the Chemical Engineering Department for showering their profound knowledge as soon as I enrolled myself as the research scholar in this institute.

I would like to thank my friends, labmates and my well-wishers for providing me healthy research environment. Finally, I would like to thank my family for showering their endless love, care and encouragement throughout my life. They have always pushed me to set goals and helped me to achieve them.

Pradeep Sahu

ABSTRACT

Municipal solid waste (MSW) generated over the years has created many problems for the society. MSW pollutes the environment and affects human health. Most of the MSW generated is dumped in open landfills in India. MSW can be treated by thermo-chemical methods as they are faster and require less area as compared to landfills. Incineration is one of the common thermo-chemical methods for treating it. MSW power plants are partly carbon neutral as biomass are a major part of it. MSW based thermal power plants have very low net thermal efficiency due to the low calorific value of MSW. To improve the efficiency, MSW can be co-combusted with conventional fuels like coal. India possesses majorly high ash coals (HAC) and co-utilization of MSW with HAC is one of the options for efficient production of syngas and electricity. Hence, experimental and power plant simulation studies are required to evaluate the process and economic feasibility of co-utilization of HAC and wastes.

Plastics and e-wastes are non-biodegradable components of MSW. Plastics are high calorific components of MSW. This makes thermo-chemical treatment of plastics favourable by pyrolysis and gasification processes to generate electricity and chemicals. Gasification of COVID waste based plastics is necessary to convert it into valuable products. Further, printed circuit boards (PCB) are major components of e-wastes. PCB can be treated by pyrolysis and gasification and further, the valuable metal components in the board can also be recovered. Utilizing CO_2 for oxy-incineration and gasification of fuels can produce syngas/CO_2 enriched flue gas.

The feasibility of co-gasification of plastics and HAC, fixed bed gasification experiments under CO_2 atmosphere is analysed. In this study, four wastes materials are considered as the fuel feedstock for co-utilization with HAC. The wastes such as (i) high density polyethylene (HDPE), (ii) COVID based overall gown (OG) and (iii) various components of PCB are co-pyrolyzed and co-gasified with HAC. Reaction mechanism of HAC with HDPE, OG and PCB components is analysed. Kinetic parameters of the chemical reactions are estimated using various kinetic models. Further, co-incineration of MSW with HAC in sub/supercritical steam turbine based thermal power plants is simulated using Aspen Plus software.

Co-gasification of HAC and HDPE produces ester and carboxylic acid molecules in the presence of carbon and Al_2O_3 in HAC. The surface area and pore diameter of char obtained during co-pyrolysis is doubled at 1000°C due to the effective dispersion of ethylene into the inorganic enriched char matrix and further their reactivity with coal volatiles and the pyrolysis agent, CO_2. At 1000°C, HDPE globules are devolatilized and this results in the formation of porous residue with a surface area of 70 m^2/gm whereas HAC residue has 29.95 m^2/gm. Hence by the addition of HDPE, the maximum calorific value of syngas can be improved from 2.5 MJ/Nm^3 to 22 MJ/Nm^3 at 1000°C.

Co-gasification of HAC with OG increased the calorific value of syngas by 20.39% to 51.77% with increase in the OG proportion in the feed from 5 to 20%. It showed an adverse effect that the surface area of the residue decreases from 147.61 to 77.87 m^2/gm with OG in feed is increased from 0 to 20% due to the ash hindrance layer. OG gasification performed at 900°C and 1000°C produced the syngas with a calorific value of around 6.3 MJ/ Nm^3, which is higher than HAC based syngas. An oil with a yield of 17% was produced under N_2 conditions at 900ºC whereas a reduced oxygen content in the oil was observed (absence of C-O) under CO_2 conditions.

Pyrolysis of PCB at 500°C under N_2 conditions produces 7.5% of tar yield with a calorific value of 31.28 MJ/kg. The co-gasification of HAC with PCB (resin, plastic, and PCB mixture) under a 4:1 ratio generated the syngas with as high as 33-35% CO and 3.0-4.9% H_2 under CO_2 conditions with a net calorific value of 5.1-5.2 MJ/nm^3. The co-gasification residue showed the generation of surface area as high as 186 m^2/g and therefore, it can be suitable as a catalyst for cracking reactions. Further, $CaCO_3$, TiO_2, and SnO_2 in the residue can be used as potential additives in the concrete material for buildings.

Co-combustion of MSW with HAC and low ash coals (LAC) in steam turbine based thermal power plants is simulated in Aspen plus under air and oxy-fuel conditions. The results had shown that the addition of 25% MSW to LAC could give a similar plant thermal efficiency and LCOE to that of HAC under subcritical conditions without carbon capture. Adding MSW to Indian coals can decrease specific CO_2 emission by 711.9 to 772.8 kg/MWh without CCU. Co-combustion of coals decrease LCOE of the power plants by 19.8 and 22.2 $/MWh when HAC and LAC were used respectively.

Keywords: Co-gasification, High ash coal, Printed circuit boards, Plastic wastes, Thermal power plant

Table of contents

LIST OF TABLES

LIST OF FIGURES

This page is intentionally left blank

This page is intentionally left blank

CHAPTER 1

INTRODUCTION

In this chapter, a brief discussion on electronic and plastic waste management is presented along with their adverse effects. Different treatment methods of e-wastes and plastic wastes are discussed elaborately. Gasification of above wastes would reduce the formation of pollutants and produce syngas. Fossil fuels have remained a major source of electricity over the years and these are non-renewable sources of energy and hence a search for alternative sources of energy is necessary. Gasification of coal produces syngas, which can be used to produce electricity, secondary fuels, and chemicals. Co-gasification of plastic wastes and e-wastes with coal would not only reduce the volume of wastes and pollutants but also generate syngas.

1.1.Municipal Solid Waste

The amount of municipal solid waste (MSW) produced has increased significantly over the years from 1.3 billion tonnes in 2012 to 2.1 billion tonnes in 2016. It is expected to increase to 3.4 billion tonnes in 2030. This can lead to severe stress on waste management practices (Kaza et al., 2018). Mismanagement of MSW can lead to overflowing of dumpsites (Kulkarni, 2020). Composition of MSW varies from location to location and depends on the income of the people living in the region. In low to middle-income countries, MSW can contain 50% organics whereas it reduced to 32% in high-income countries (Kaza et al., 2018). If MSW is not dumped properly, it can release greenhouse gases such as CH_4 and CO_2 (Yang et al., 2013). Figure 1.1 gives the overall waste composition of MSW in different income group countries. Lower income, lower middle, upper middle and upper income countries produce 0.4, 0.53, 0.69 and 1.87 kg/capita/day of wastes, respectively.

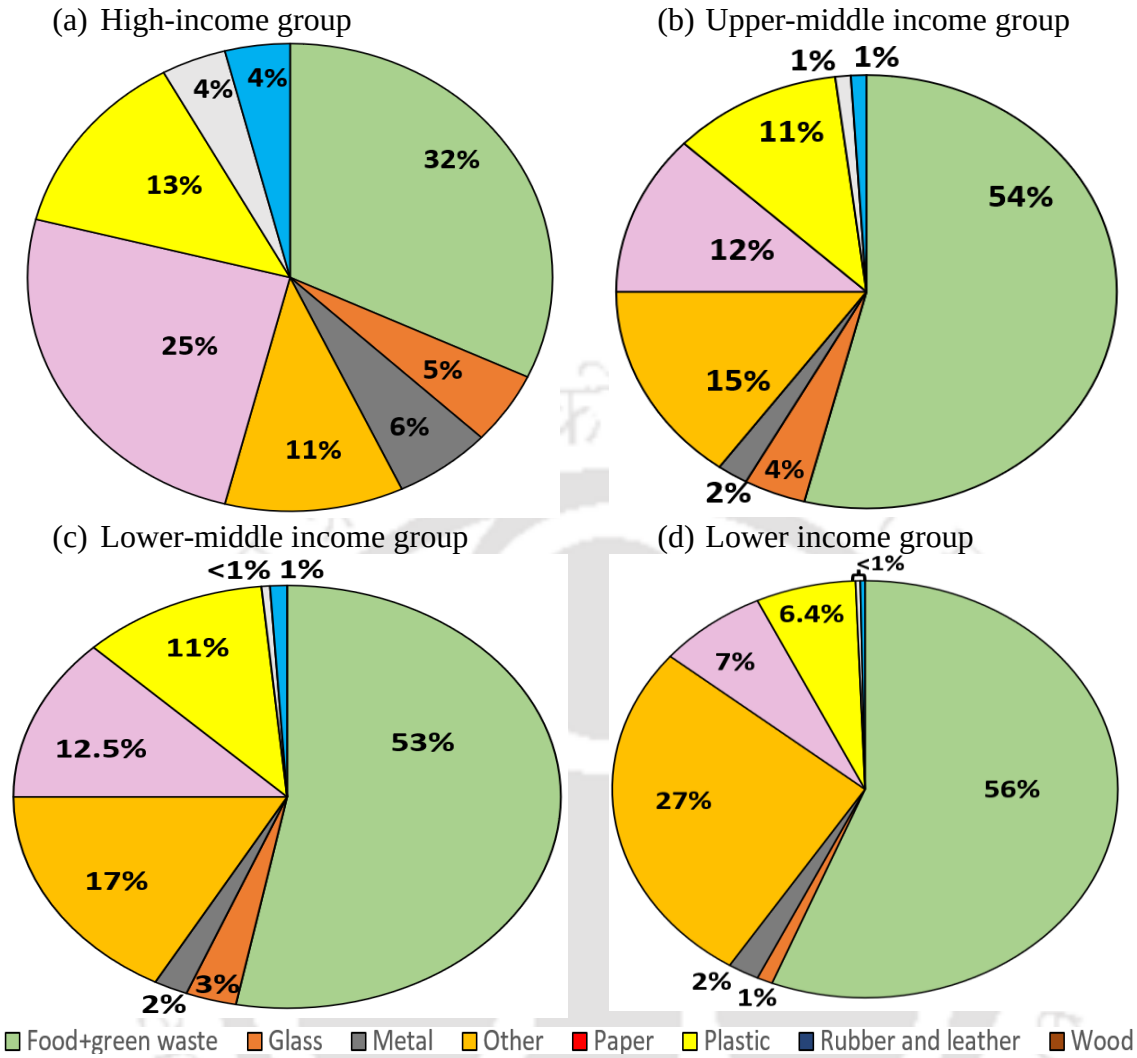

Fig. 1.1. MSW composition varying with income groups (Kaza et al., 2018)

After organic and paper wastes, the contribution of plastic wastes towards MSW is significant. Organic and paper wastes are biodegradable and take about 7-30 days to degrade. Plastic wastes constitute around 9-12% of total waste generated (Kaza et al., 2018). They can take 100-1000 years to degrade which is markedly higher than organic wastes, clothes, and paper wastes (Babaremu et al., 2022). Additives are used to improve the thermal and mechanical properties of plastics depending on their applications. However, additives like lead and tributyl tin are toxic (Thompson et al., 2009). These toxic chemicals can be released when plastics disintegrate to form microplastics (Cverenkárová et al., 2021). Plastics are hazardous to human as they remain in the gastrointestinal tract and take a long time for digestion. These toxic additives are known endocrine disruptors (Cverenkárová et al., 2021). Other components of MSW like glass,

rubber and metals are similar to plastics, which also take a long time for bio-degradation (Babaremu et al., 2022).

Table 1.1. Harmful effects of heavy metals and other plastics (Ankit et al., 2021),("Acute Expo. Guidel. Levels Sel. Airborne Chem.," 2011)

Heavy metals	Harmful effects
Antimony	It is a known carcinogen. Inhalation affect stomach and cause ulcers
Arsenic	It can cause skin disease, lung cancer, and impaired nerve signaling
Barium	Brain swelling, muscle weakness
Beryllium	Lung cancer, skin disease
Bromine	Toxic vapours emitted on incineration, causing pulmonary edema and respiratory tract irritation
Cadmium	Kidney damage
Chromium	DNA and eye damage
Lead	Brain, nervous system, and Kidney damage especially in children
Nickel	Allergic reaction and reduced lung function
Selenium	Selenosis
PBDE, PBB, TBBA	Foetus memory and learning affects

E-wastes can act as a source of plastic wastes, metallic wastes and glasses. According to the United States Environmental Protection Agency (USEPA), e-wastes contributes 8% of total global waste generated and 2-5% of total volume of waste generated (Hossain et al., 2015) (Ankit et al., 2021). Electronic wastes constitute 30% of organic wastes, 30% of ceramic wastes, and 40% of metallic wastes. Organic wastes are in the form of plastics.

Different materials in electronic waste have various toxicity levels. Electronic wastes contain heavy metals like mercury, chromium, beryllium, palladium, and gallium. These heavy metals can enter the food chain and seriously affect human and animal health. Mercury can form mercury phthalate, which is neurotoxic for humans and animals (Ankit et al., 2021). A brief description of the harmful effects caused by heavy metals and other plastics in electronic wastes is given in Table 1.1.

1.2. Treatment of plastic and e-wastes

Plastic wastes can be treated by biological or thermochemical treatment methods. Biological treatment methods use living organism like invertebrates, bacteria, fungi, algae, worms, and enzymes to degrade plastics. Biological treatment methods are time-consuming as compared to thermochemical treatment methods (Zhang et al., 2021). Landfilling of wastes can effect underground water sources (Okunola A et al., 2019). Other alternative method of utilising MSW is thermochemical methods, which include incineration, pyrolysis, and gasification. These treatment methods can be scaled up to treat higher quantities of unsorted waste (Dai et al., 2022). Improper incineration of plastic wastes can release toxic and greenhouse gases (Zhang et al., 2021). Pyrolysis is an endothermic process that requires external energy leading to higher energy penalty. Liquid and gaseous fuels are major products of pyrolysis producing wide range of chemicals. It is difficult to obtain narrow product distribution to simplify downstream processes (Dai et al., 2022).

Table 1.2. Chemical reactions occurring inside the gasifier (Saebea et al., 2020)

Reaction	Heat of reaction kJ/mol
$C + CO_2 \leftrightarrow 2CO$	172
$C + H_2O \leftrightarrow CO + H_2$	131
$C + 2H_2 \leftrightarrow CH_4$	-74.8
$CO + H_2O \leftrightarrow CO_2 + H_2$	-41.2
$CO + 3H_2 \leftrightarrow CO_2 + H_2$	-206
$2CO + 2H_2 \leftrightarrow CH_4 + CO_2$	-247
$CO_2 + 2H_2 \leftrightarrow CH_4 + 2H_2O$	-165
$CH_4 + H_2O \leftrightarrow CO + 3H_2$	206

Gasification of waste is carried out at high temperatures in the range of 700-1300°C, with the presence of gasifying media and a limited supply of oxygen. As compared to incineration, gasification produces a low amount of greenhouse gases. Gasifying media reacts with plastics and forms syngas. Air, Steam, and CO_2 can act as gasifying medium. Air gasification of plastics generally leads to dilution of syngas with inert gas like N_2. This can be eliminated with the supply of pure oxygen to gasifier with a significant energy penalty. The main reactions taking place inside the gasifier are given in Table 1.2 these are only indicative reactions and not complete list. Gasification of chemicals also reduced the formation of toxins (difurans and dioxins) as this process is carried out at high temperatures with a limited flow of oxygen. Syngas produced from gasification process

has wide applications. Syngas can be used to produce heat, electricity, secondary fuels (methanol and dimethyl ether), and other chemicals (Dai et al., 2022). Syngas produced from plastics can have very high calorific value.

In a gasifier, various thermo-chemical reactions such as drying, pyrolysis, oxidation and reduction take place.

Drying: Drying of particles takes place between 100 and 250°C. In this stage, the hot gases from oxidation stage comes in contact with the particles resulting in the release of moisture.

Pyrolysis: This process occurs in the absence of oxygen. It can occur at around 300°C to 600°C depending upon the nature of feedstock. In this stage, volatile matter from feed is released (CO_2, CH_4, H_2 and CO) and followed by, there is a formation of char and tar.

Oxidation: In this stage, partially, solid fuel is combusted and the generated heat is utilized in the pyrolysis and gasification reactions. The temperature of this stage can vary from 600 to 1400°C depending on the nature of the particle.

Reduction (or) gasification: The gases or products from previous stages reacts with gasifying media like steam/air or CO_2 to form various gases like H_2, CO or CH_4. The reactions taking place in this stage are endothermic and the energy from oxidation stage is utilized for reactions to occur. Temperature in this stage can be around 600-950°C depending upon the feed (Koido & Iwasaki, 2017).

E-wastes can be treated by thermal, chemical, and mechanical methods. Chemical recycling of e-wastes generally consists of using chemicals to dissolve specific metals. After dissolution, the metals are extracted from the solution. Metal dissolution is a very slow process. The solutions used in this process are toxic i.e., cyanides are used for gold recovery. Pyrometallurgical processes can be used for mass treatment of e-wastes irrespective of their type (Park et al., 2019). Incineration of e-wastes contributes to global emissions of Hg and Cd. Other toxins such as dioxins and difurans can also be released (Ankit et al., 2021). Pyrolysis of e-wastes has been performed to reduce the formation of such toxic chemicals in the absence of oxygen (Manikkampatti Palanisamy et al., 2022). These processes can reduce the volume of waste and the recovery of metals is easier as

e-wastes become brittle. The liquid products from pyrolysis contain phenols that can be used for the production of phenolic group based chemicals (Wang et al., 2017).

The syngas composition can be changed by feeding suitable gasifying medium depending upon the product requirement. Utilizing steam improves hydrogen concentration in syngas whereas CO_2 improves the CO level (Lee & Sohn, 2022). To improve the quality of syngas, it must be purified to remove other pollutants like SO_X, NO_X, and tar. Steam and CO_2 can be used with air or O_2 to gasify the solid fuels.

1.3. Energy Sources

Over the years, energy demand has increased globally from 420.23 TJ in 2010 to 599.29 TJ in 2018. According to the projections, energy demand is supposed to grow to 16311 by the year 2030. In the present scenario, 64% of energy is generated from fossil fuels (IEA (International Energy Agency), 2020). Energy generated from fossil fuels is a major source of greenhouse gases like CO_2, CH_4, SO_X, and NO_X. Fossil fuels like coal, natural gas, and petroleum leave a large carbon footprint on combustion. These non-renewable sources of energy are fast depleting. According to the current rate of the usage, these sources will last around 100 years (Shafiee & Topal, 2009). In India, around 55 % of the energy produced is from coal (Nagarkatti & Kolar, 2021).

Gasification based power plants generally have higher net efficiency than combustion-based plants. The majority of the Indian coals have high ash and this decreases the calorific value of the syngas produced (Chavan et al., 2012). Alternative fuels should be co-gasified with these coals to improve the calorific value of syngas. Plastic wastes have generally high calorific value and low ash content. This could improve the calorific value of syngas. Co-gasification of e-wastes with coal not only helps in decreasing pollutant emissions but also helps in the production of valuable syngas. Utilizing plastics/e-wastes with high ash coal can decrease the dependence on coal, and further the volume of residue can be reduced. Comparatively, e-waste have a very low calorific value as they contain metals and other non-combustible materials. Due to this, high temperature gasification of e-wastes is difficult. This makes utilizing them with coal necessary to achieve high temperature in during the gasification process.

1.4. Motivation for current work

In India, 55% of electricity is produced by coal (Nagarkatti & Kolar, 2021). As it is a non-renewable source of energy, utilizing it with other sources of energy is useful to increase the longevity of coal resources. The main intent of this thesis is to solve two prime issues: (a) blending coal with other alternative sources and (b) waste minimization strategies using thermal treatment methods.

- Gasification of plastic and e-wastes would not only reduce the volume of waste, and pollutants but also help in the generation of secondary fuels or electricity. Utilizing these wastes for the generation of power decreases the reliability on coal. Gasification makes further treatment of e-wastes easy as they become brittle and removal of metal from residue becomes comparatively easier.
- Gasification of fuels in CO_2 conditions presents an opportunity for the recycling and sequestration of high-purity CO_2. As the gasification of plastics and e-wastes is not a completely developed technology, the co-gasification of these wastes with coal is important to utilize e-wastes without much effect on the downstream processes.

1.5. Organization of the Thesis

The complete thesis is organized into seven chapters. The basic outline of each chapter is discussed below:

Chapter 1 discusses the management and treatment of plastics, and e-wastes. The importance of co-gasification of these waste with coal is discussed.

Chapter 2 presents the literature available regarding the co-gasification of coal with plastics and e-waste. The knowledge gap regarding the same is described.

Chapter 3 gives a brief description of the procedure followed for gasification experiments. The key parameters needed to estimate the conversion are discussed.

Chapter 4 highlights the effects of HDPE addition on the gasification of coal in CO_2 conditions. Thermogravimetric analysis of the same is carried out to calculate activation energy, Arrhenius constant, and reaction model.

Chapter 5 probes deeper into the co-gasification of coal and biomedical waste under CO_2 conditions at various temperatures.

Chapter 6 investigates the effect of co-gasifying printed circuit boards and their components in CO_2 conditions. Printed circuit boards are pyrolyzed and gasified at different temperatures and atmospheric conditions. The impact of gasification using individual components of PCB is investigated.

Chapter 7 examines the energy analysis on co-combustion of coal and MSW. Different parametric studies are performed to determine their effects on net power production. Further, the economic analysis is evaluated on the basis of Levelized cost of electricity (LCOE) for each case.

Chapter 8 discusses the conclusions and future scope related to the co-gasification of plastics and e-waste with Indian coals.

References

Acute Exposure Guideline Levels for Selected Airborne Chemicals. (2011). In *Acute Exposure Guideline Levels for Selected Airborne Chemicals* (Vol. 9). The National Academic Press. https://doi.org/10.17226/13247

Ankit, Saha, L., Kumar, V., Tiwari, J., Sweta, Rawat, S., Singh, J., & Bauddh, K. (2021). Electronic waste and their leachates impact on human health and environment: Global ecological threat and management. *Environmental Technology and Innovation*, *24*, 102049. https://doi.org/10.1016/j.eti.2021.102049

Babaremu, K. O., Okoya, S. A., Hughes, E., Tijani, B., Teidi, D., Akpan, A., Igwe, J., Karera, S., Oyinlola, M., & Akinlabi, E. T. (2022). Sustainable plastic waste management in a circular economy. *Heliyon*, *8*(7), e09984. https://doi.org/10.1016/j.heliyon.2022.e09984

Chavan, P., Datta, S., Saha, S., Sahu, G., & Sharma, T. (2012). Influence of high ash indian coals in fluidized bed gasification under different operating conditions. *Solid Fuel Chemistry*, *46*(2), 108–113. https://doi.org/10.3103/S0361521912020048

Cverenkárová, K., Valachovičová, M., Mackul'ak, T., Žemlička, L., & Bírošová, L. (2021). Microplastics in the food chain. *Life*, *11*(12), 1–18. https://doi.org/10.3390/life11121349

Dai, L., Zhou, N., Lv, Y., Cheng, Y., Wang, Y., Liu, Y., Cobb, K., Chen, P., Lei, H., & Ruan, R. (2022). Pyrolysis technology for plastic waste recycling: A state-of-the-art

review. *Progress in Energy and Combustion Science*, *93*(September 2021), 101021. https://doi.org/10.1016/j.pecs.2022.101021

Hossain, M. S., Al-Hamadani, S. M. Z. F., & Rahman, M. T. (2015). E-waste: A challenge for Sustainable Development. *Journal of Health and Pollution*, *5*, 3–11.

IEA (International Energy Agency). (2020). Key World Energy Statistics 2020. *Int. Energy Agency*, *33*(August), 4649. https://www.iea.org/reports/key-world-energy-statistics-2020

Kaza, S., Yao, L., Bhada-Tata, P., & Van Woerden, F. (2018). What a Waste 2.0 Introduction -"Snapshot of Solid Waste Management to 2050." Overview booklet. In *Urban Development Series*. https://openknowledge.worldbank.org/handle/10986/30317

Koido, K., & Iwasaki, T. (2017). Biomass Gasification: A Review of Its Technology, Gas Cleaning Applications, and Total System Life Cycle Cleaning Applications, and Total System Life Cycle Analysis. *Intech*, *25*(4), e275–e281. https://doi.org/10.3747/co.25.3884

Kulkarni, B. N. (2020). Environmental sustainability assessment of land disposal of municipal solid waste generated in Indian cities – A review. *Environmental Development*, *33*, 100490. https://doi.org/10.1016/j.envdev.2019.100490

Lee, R., & Sohn, J. M. (2022). A study on the effect of the CO2/steam mixtures and the addition of natural minerals on the reactivity of Adaro coal gasification. *International Journal of Hydrogen Energy*, *xxxx*. https://doi.org/10.1016/j.ijhydene.2022.04.280

Manikkampatti Palanisamy, M., Myneni, V. R., Gudeta, B., & Komarabathina, S. (2022). Toxic Metal Recovery from Waste Printed Circuit Boards: A Review of Advanced Approaches for Sustainable Treatment Methodology. *Advances in Materials Science and Engineering*, *2022*. https://doi.org/10.1155/2022/6550089

Nagarkatti, A., & Kolar, A. K. (2021). Advanced Coal Technologies for sustainable power sector in India. *Electricity Journal*, *34*(6), 106970. https://doi.org/10.1016/j.tej.2021.106970

Okunola A, A., Kehinde I, O., Oluwaseun, A., & Olufiropo E, A. (2019). Public and

Environmental Health Effects of Plastic Wastes Disposal: A Review. *Journal of Toxicology and Risk Assessment*, *5*(2). https://doi.org/10.23937/2572-4061.1510021

Park, H. S., Han, Y. S., & Park, J. H. (2019). Massive Recycling of Waste Mobile Phones: Pyrolysis, Physical Treatment, and pyrometallurgical processing of Insoluble Residue. *ACS Sustainable Chemistry and Engineering*, *7*. https://doi.org/10.1021/acssuschemeng.9bo2725

Saebea, D., Ruengrit, P., Arpornwichanop, A., & Patcharavorachot, Y. (2020). Gasification of plastic waste for synthesis gas production. *Energy Reports*, *6*, 202–207. https://doi.org/10.1016/j.egyr.2019.08.043

Shafiee, S., & Topal, E. (2009). When will fossil fuel reserves be diminished? *Energy Policy*, *37*(1), 181–189. https://doi.org/10.1016/j.enpol.2008.08.016

Thompson, R. C., Moore, C. J., Saal, F. S. vom, & Swan, S. H. (2009). Plastics, the environment and human health: current consensus and future trends. *Philosphical Transactions of The Royal Society B*. https://doi.org/doi:10.1098/rstb.2009.0053

Wang, H., Zhang, S., Li, B., Pan, D., Wu, Y., & Zuo, T. (2017). Recovery of waste printed circuit boards through pyrometallurgical processing: A review. *Resources, Conservation and Recycling*, *126*(August), 209–218. https://doi.org/10.1016/j.resconrec.2017.08.001

Yang, N., Zhang, H., Shao, L. M., Lü, F., & He, P. J. (2013). Greenhouse gas emissions during MSW landfilling in China: Influence of waste characteristics and LFG treatment measures. *Journal of Environmental Management*, *129*, 510–521. https://doi.org/10.1016/j.jenvman.2013.08.039

Zhang, F., Zhao, Y., Wang, D., Yan, M., Zhang, J., Zhang, P., Ding, T., Chen, L., & Chen, C. (2021). Current technologies for plastic waste treatment: A review. *Journal of Cleaner Production*, *282*, 124523. https://doi.org/10.1016/j.jclepro.2020.124523

This page is intentionally left blank

This page is intentionally left blank

CHAPTER 2

LITERATURE REVIEW

In this chapter, the general treatment methods of the potential feedstocks such as plastics, biomedical waste, and printed circuit boards (PCB) are discussed. The literature report on pyrolysis and gasification of PCB are analyzed. The effect of utilizing different types of gasifying agents on coal and plastics gasification is investigated. Thermal power plant studies utilizing coal and the plastic waste products are analyzed. Literature gap based on analysis of experimental and simulation work is presented. Objectives of the thesis are presented based on the literature gap.

2.1. Introduction

There is widespread recognition that global greenhouse gas emissions should be reduced in order to mitigate adverse impacts on the climate (Valérie Masson-Delmotte et al., 2018). Current global electric power production is dominated by coal and natural gas, emitting 65.2% of global CO_2 gas emissions from fuel combustion in 2018(IEA (International Energy Agency), 2020). Total CO_2 emissions from combustion of fossil fuels has increased from 15460 MT in 1973 to 32840 MT in 2017. If the same trend would continue without any control measures then meeting the limits of Paris agreement to restrict global warming to 1.5°C would be difficult (Valérie Masson-Delmotte et al., 2018). Reductions in greenhouse gas emissions from coal can be achieved by a variety of methods, including:

- Improving thermal efficiency and reducing demand
- Substituting coal with fuels which have lower carbon footprints
- Utilizing renewables such as solar and wind
- Applying CO_2 capture, utilisation, and storage (CCUS)

Over the past two decades, there has been significant progress in improving thermal efficiency and in the substitution of high carbon fuels with low carbon fuels in many developed countries (IEA (International Energy Agency), 2020). It is expected that the

percentage share of power production from fossil fuels, and especially coal, will decrease in the most of the organization for economic co-operation and development (OECD) countries unless CO_2 mitigating technologies are deployed at a large scale. In addition, the focus on renewable energy and improved waste management means that waste feedstocks such as municipal solid waste (MSW) are likely going to be increasingly used for energy production, electricity and chemicals in the future. However, waste feedstocks have various challenges, such as low energy density, high levels of heterogeneity and are widely dispersed (Muthuraman et al., 2010). Even with increased use of renewables the share of fossil fuel power production is still forecast to be significant for years to come. For example, in Australia electric power production from coal is forecast to remain between 52 and 57% in 2030 and between 19 and 26% in 2050, while natural gas use could vary between 4 to 29% by 2050 depending upon various policy scenarios(Finkel, 2017). Similarly, on a global level, total primary energy supply in 2040 is still expected to be dominated by coal, oil and natural gas (IEA (International Energy Agency), 2020).

2.2. Details on waste treatment

The accumulation of municipal solid waste (MSW) creates a major problem in urban areas. Mismanagement of MSW dumpsites could cause a health hazard to human beings and animals. Numerous studies have been reported the effect of MSW on land, air, and water. Rainfall near MSW landfills can pollute groundwater sources. The leachate from MSW moves with rainwater and gets percolated with groundwater and causes water-borne diseases(Ferronato & Torretta, 2019). Further, heavy metals in MSW can deteriorate the soil quality and fertility leading to affect the plant growth (S. M. Ali et al., 2014). One of the most common methods of treating MSW is incineration technology. Landfills are the third largest producer of methane. Methane is not only a combustible gas but also has more global warming potential than CO_2(Vallero, 2019). The combustible nature of landfill gases caused fire hazard in Deonar, Mumbai and Ghazipur, New Delhi (Kulkarni, 2020). Hence appropriate management of MSW is essential for maintaining a clean environment. The calorific value of MSW in Indian cities ranges from 6-10 MJ/kg subject to the composition of MSW(Saini et al., 2012). The content of MSW varies with the location depending on the social-economic conditions of the region (Rajaeifar et al., 2017). The collection of MSW is a major task for urban local bodies. The quantity of MSW generated in India was 1.2×10^5 t/day in 2011(Saini et al., 2012).

In Maharashtra (India), the local bodies collect almost the entire wastes that are generated on day to day basis. Many states in India could treat at least 50% of the generated waste and a few states such as Karnataka (India) can treat all the wastes collected. On an average 70% of the generated waste is collected in India and 12.45% of its content is treated. The amount of waste generated in India by 2050 would expect to be 300 million tonnes per year and the land needed for its dumping would be 1450 km^2. If India continues the landfilling for dumping the MSW, 23.5×10^7 m^3 space and 1175 hectares of land per year would be required by the year 2031(Joshi & Ahmed, 2016).

Collection of waste is important step prior to treatment. Wastes are collected in bins generally made up of concrete or steel. Next step, the wastes are segregated according to wet and dry nature. Collection efficiency of Indian states can vary from 30-90%. Segregation of wastes is performed by rag pickers and some materials is recycled depending upon their usage, which in turn reduce the volume of waste. After pre-treatment, the wastes are transported using specifically designed trucks.

Various treatment methods of MSW in India are thermal treatment, open dumping, landfilling, and biological methods. Landfilling is an accepted practice in urban centres. In 2011, India had 59 landfilling sites and further, 376 were further planned. Karnataka had 12 landfilling sites whereas West Bengal had 19. Two incineration plants were installed in various locations in Delhi (One in Okhla and other in Gazipur installed in 2012 and 2015 respectively). Bengaluru (capital of Karnataka) also contains an 8 MW incineration plant. Other Incineration plants are found in Maharashtra and Telangana. As Indian MSW mostly contains biological sources, biological treatment of MSW is favourable. Bengaluru has the largest vermi-composting centre capable of treating 100 million tonnes of waste daily. Smaller units have also emerged in Telangana, Maharashtra, and Uttar Pradesh (Joshi and Ahmed 2016).

Pyrolysis, gasification, incineration and bio-methanation are few of the thermochemical processes for energy generation from waste. Out of the above processes, incineration is the most common technique for energy generation in India (Azam et al., 2019). The US had 71 waste to energy plants, which could generate 2300 MW of energy in the year 2015 (Somaiya, 2016). Further, the US has increased its facilities to 77, which could generate 2547 MW, in the year 2019 (Michaels & Krishnan, 2018). European Union had a total of 461 waste to energy plants generating heat and electricity with a capacity of 0.41 EJ in

the year 2015(*Biomass Explained Waste-to-Energy (Municipal Solid Waste)*, 2018). According to the Indian government report for the year 2015-16, it was estimated that a 538 MW of electricity could be produced in India by incineration method at the initial stages of execution and this can be increased to 1075 MW in 2031 and, 2780 MW in 2050 from MSW. However, out of the total proposed capacity of energy generation, only 92.4 MW of electricity was generated due to the various reasons of the operational difficulties (Azam et al., 2019). India has constructed only a few wastes based energy plants for incineration and it is essential to build more infrastructure to handle the generated MSW for clean environment and effective utilization. Shalivahana power plant in Karimnagar, Andhra Pradesh, India uses a mixture of MSW, RDF, coal and biomass. It has a capacity of 12MW. Bottom ash is reused as fertiliser mixing it with cow dung and fly ash is used as for making bricks (Scarlat et al., 2019).

The inherent properties of MSW and its calorific value have great impact on its utilization. The biomass content in MSW, which generally consists of kitchen and agricultural wastes, can become a carbon-neutral fuel if all the carbon emissions are sequestered by the growth of crops (Nixon et al., 2017). However, coal-fired power plants are carbon emitters as coal is a carbon-positive fuel source. The co-combustion of MSW with coal in thermal power plants would reduce the impact of the carbon footprint in the environment. Hence the co-combustion of MSW with fossil fuels could be a possible solution for tackling the CO_2 emissions and further the management of MSW. As compared to coal and other fossil fuels, the combustion of MSW in thermal power plants had shown a net efficiency as low as 18.47% (Heller et al., 2004). This could be due to the factors of low calorific value of MSW and the additional power consumption for fuel drying. The addition of MSW as a co-feed to coal could increase the associated costs and may affect the net thermal efficiency of the power plants. Further the moisture content in MSW should be less than 15% for its utilization in thermal power plants(Ding et al., 2018a). In Italy, MSW with a moisture content as high as 25% was used in incineration process (Diaz et al., 2005). MSW with heating value less than 5 MJ/kg is not suitable for incineration (Ragazzi et al., 2007). According to the U.S standards, the calorific value of MSW used for incineration should not be below 6 MJ/kg (Rajaeifar et al., 2017). MSW with a heating value higher than 10 MJ/kg can be incinerated without the addition of any auxiliary fuel (Ragazzi et al., 2007). The calorific value of MSW in India has been continuously increasing over time. The heating value of MSW in Delhi (India) has

increased from 2.77 MJ/kg to 8.37 MJ/kg between the year 1981 and 2010. Due to the low calorific value of MSW, it needs to be utilized with other solid fuels such as coal and biomass for electricity production.

2.2.1. Details on Plastic Wastes

Plastics have become a very important source for the production of various materials. Properties of plastics can be improved by adding various chemicals. After usage, the plastics can be divided into two types depending on their end users such as post-industrial and post-consumer. Industrial waste plastics are consistent in composition depending upon their quality. In 2015, 381 million tonnes of plastic were produced. Out of the plastics generated, only 19.5% is recycled whereas 55% is discarded and the rest 25.5% is incinerated. Consumer plastics are dirty containing different types of foreign materials like glasses, organics and metals (Qureshi et al., 2020). Polyethylene (PE) and polypropylene (PP) constitute 49% of total demands of plastics. Plastics are generated from various sources like packaging materials, building materials, electrical/electronic equipments and these are the major sources of waste plastic generation (Hannah & Max, 2022). Details regarding sources of waste plastic source are given in Figure 2.1. PE and PP are mostly used as packaging materials (76%) (F. Zhang et al., 2021). Keeping in view of the high amount of plastics generated, treatment of plastics is necessary to maintain a clean environment.

Plastics can be treated by biological, chemical and thermochemical methods. Biological method uses worms, microorganisms to treat plastics. In this method, the plastics are converted into simpler compounds like CO_2, CH_4 and H_2O or its monomers. The thickness of the plastics slows down the process of degradation. The time taken by invertebrates and microorganisms to degrade plastics is high as compared to other methods. Chemical methods utilize different types of chemicals like isocyanates, methanol and glycols to depolymerize polymers (F. Zhang et al., 2021). Various thermochemical methods are described in this section.

Biomedical wastes are also a source of plastic wastes. In various countries, plastics composition in biomedical wastes can vary from 11-75% in hazardous category and 2-33% in non-hazardous category (Gill et al., 2022). Biomedical wastes are divided into different types with colour code depending upon their hazardous nature. As these plastics

have been in contact with viruses, bacteria and other infectious substances, management of these plastics is mandatory. Plastics from different sources like gloves, tubes, masks and gowns are generally red coded (Subramanian et al., 2021). Plastics which have not come in contact with infectious substances can be mixed with virgin plastics to enhance their recycling. Plastics can be sorted and separated to different type of plastics. They can be washed to remove organics, and then they can be grinded. The plastics generated after grinding has lower molecular weight than original plastic and hence thermomechanical degradation of plastics is imminent during recycling (Joseph et al., 2021). By thermochemical methods of plastic treatment, oils, gas and char can be recovered. Oils can be used as furnace oil. Gas released can be recycled to heat pyrolysis system. Syngas released can be used to generate electricity or chemicals.

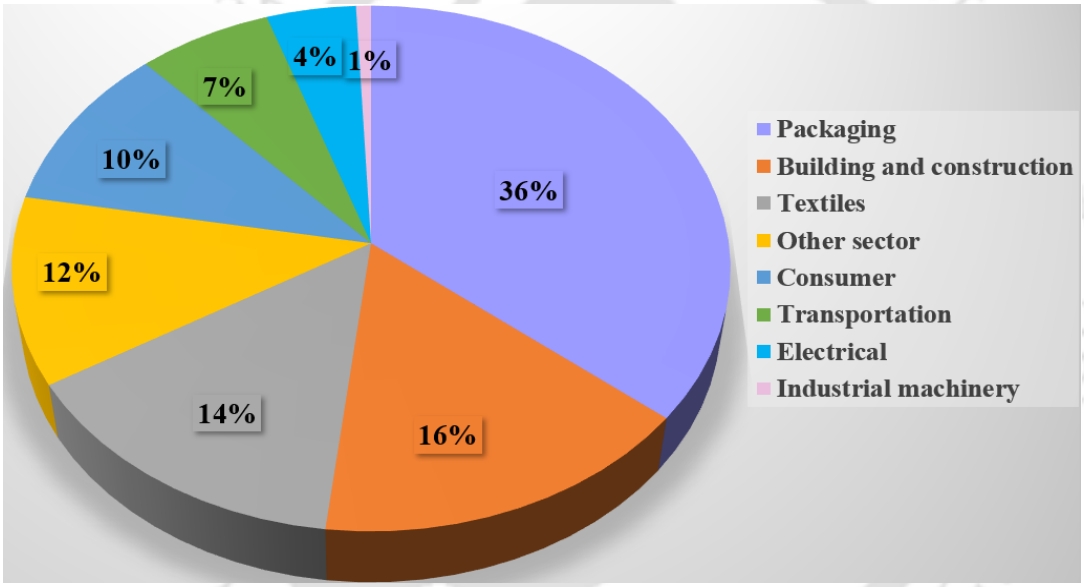

Figure 2.1. Sources of plastics pollution (Hannah and Max 2022)

Biomedical wastes are also a source of plastic wastes. In various countries, plastics composition in biomedical wastes can vary from 11-75% in hazardous category and 2-33% in non-hazardous category (Gill et al., 2022). Biomedical wastes are divided into different types with colour code depending upon their hazardous nature. As these plastics have been in contact with viruses, bacteria and other infectious substances, management of these plastics is mandatory. Plastics from different sources like gloves, tubes, masks and gowns are generally red coded (Subramanian et al., 2021). Plastics which have not come in contact with infectious substances can be mixed with virgin plastics to enhance their recycling. Plastics can be sorted and separated to different type of plastics. They can be washed to remove organics, and then they can be grinded. The plastics generated after

grinding has lower molecular weight than original plastic and hence thermomechanical degradation of plastics is imminent during recycling (Joseph et al., 2021). By thermochemical methods of plastic treatment, oils, gas and char can be recovered. Oils can be used as furnace oil. Gas released can be recycled to heat pyrolysis system. Syngas released can be used to generate electricity or chemicals.

2.2.1.1. Plastic incineration

Incineration and landfilling are the most common method to treat plastics. According to calculations carried out by Eriksson and Finnveden, if plastics are used to generate to electricity with high efficiency, then replacing it with power generated from fossil fuels can result in carbon negative process (Eriksson & Finnveden, 2009). Out of the plastics generated in OECD countries, 29% of the plastics is incinerated and these decreases to 10% in non-OECD countries. The world average for plastic incineration is 19%(Organisation for Economic Co-operation and Development (OECD), 2022). Incineration should be carried out under controlled conditions to prevent emissions of toxic pollutants. Minerals or ceria nanoparticles can be added to plastics during incineration to decrease pollutant emissions(Vejerano et al., 2014). According to the studies carried out by Khoo et al., the gasification process releases low amount of CO_2 as compared to incineration. Gasification releases around 380-900 kg CO_2/kg of plastic waste as compared to 1000-1600 kg CO_2/kg plastic during incineration. Also, pyrolysis similar to gasification releases low CO_2 per kg of plastics utilized as compared to incineration (Khoo, 2019).

2.2.1.2. Plastic Pyrolysis

Pyrolysis of plastics is an endothermic process that requires external energy. Plastic pyrolysis produces three types of products such as oil/tar, char, and gas. The gas produced does have calorific value gases like H_2, CO, CH_4, etc. Oil is the major product of plastic pyrolysis. To enhance the cracking of plastics, catalytic cracking or double-stage pyrolysis is explored by researchers. Product distribution can be managed by varying the heating rate of the process. A low heating rate (0.1-1°C/sec) can result in char being the major product. Whereas a high heating rate (1-1000°C/sec) can result in product distribution being shifted to a liquid and gaseous state (Kartik et al., 2022).

Operating temperature plays an important role in determining the chemical composition of the oil and gas produced. According to the studies carried out by Alvarez et al., as the operating temperature is increased from 625 to 675°C, the quantity of aromatic components increases in the product gas. The concentration of aromatic compounds is directly dependent on the residence time of vapours released (Gracida-Alvarez et al., 2018). With increase in the the residence time of pyrolysis from 1.4 to 5.6 seconds, the concentration of aromatics compounds increased from 10% to 25% at 675°C and further the concentration of alkanes and alkenes decreased from 80 to 65%. Oil characteristics depend upon the source of plastics. Polystyrene pyrolysis produces high amounts of aromatics in oil (91%), whereas polyolefin pyrolysis produces 50-55% aromatics (Dai et al., 2022).

Scaling up of pyrolysis reactors is a major hurdle in the commercialization of the process. Fluidized bed reactors can suffer from defluidization when plastics are pyrolyzed. Impurities in plastics like dyes, coatings, and pigments can affect the quality of oil produced. Mixed plastics may also contain PVC which might produce hydrochloric acid corroding the reactor and affecting oil quality. A high amount of olefins produced in pyrolysis oil restricts its use in the transportation sector. Olefins might produce gums in engines. The quality of naphtha produced from plastic pyrolysis is not of the same quality as produced from fossil fuels. Replacing naphtha and transportation fuels from plastic pyrolysis should not be done keeping given the disadvantages associated with it (Dai et al., 2022). Hence, pyrolysis of plastics alone may not be beneficial or the product gas should be treated to remove the corrosive components.

2.2.1.3. Plastic gasification

Gasification of plastics has been carried out in various reactors and gasifying media. Plastics has high amount of volatile matter and hence, the amount of tar formation during its gasification is a major hurdle. To overcome this, a two stage or catalytic gasification of plastics has been reported. Tables 2.1-2.3 give a summary of gasification trials reported using various plastics and with co-gasification of biomass/coal and plastics.

2.2.1.3.1. Steam gasification of plastics

Steam gasification of plastics comparatively produces higher amount of tar as compared to air gasification. To decrease the tar content, catalysts like olivine, dolomite and

activated carbon can be used (Lopez et al., 2018). Wilk and Hofbauer utilized olivine as a catalyst to decrease tar content. They carried steam gasification of polypropylene (PP) and polyethylene (PE) at 850°C with steam to plastic ratio of 2. They found that compared to PE, PP produces higher amount of CH_4 as it contains methyl side groups favouring methane formation. PP syngas contains higher methane gas by 10% than PE syngas. Steam to plastic ratio in steam gasification plays an important role in determining the syngas composition.

Wu and Williams carried out steam gasification of plastics in two stages. In first stage, pyrolysis was carried out at 500°C. In the second stage, the vapours from the first stage were cracked in the presence of steam and catalyst (Ni-Mg-Al). The gas yield by using catalyst can be as high as 90% under steam conditions (C. Wu & Williams, 2010). Hydrogen production was enhanced by 10 to 20 times when catalyst was added. Similar results were also obtained by He et al. when they used NiO-Al_2O_3 as catalyst. They found catalytic gasification increases the concentration of H_2 by around 8%, as compared to steam gasification, consequently decreasing CO, CH_4 and C2 hydrocarbon concentration (He et al., 2009). Friengfung et al. conducted steam gasification of plastics with and without catalysts (Dolomite impregnated with Ni). They found that by using this catalyst, the gas yield has been improved by around 20%. Gas yield of PS (polystyrene) is the least as compared to PP (polypropylene), HDPE (high density polyethylene) and LDPE (low density polyethylene). This could be due to side phenyl groups, which hinder devolatilization process (Friengfung et al., 2014).

2.2.1.3.2. Air gasification of plastics

Air gasification of plastics conducted by researchers has been given in Table 2.2. Syngas based on air gasification is highly dependent on equivalent ratio (ER). ER is defined as the ratio of the quantity of air provided for gasification to the air needed by fuel for complete combustion. According to Lera et al., cold gas efficiency and carbon conversion efficiency increased by around 20% when ER increases from 0.25 to 0.35 (Martínez-Lera et al., 2013). The higher oxygen content enhanced the reactivity with hydrocarbons and foms H_2 and CO (equation 2.1) and thus decreasing hydrocarbon concentration in syngas (Arena & Di Gregorio, 2014).

$$C_nH_m + {}^{n}/_{2}\, O_2 \rightarrow nCO + {}^{m}/_{2}\, H_2 \qquad (2.1)$$

The tar content should be less than 10 mg/Nm^3 for the syngas to be utilized in power generation process. This is reduced by changing the bed material from inert sand to olivine, which reduced the tar content. Decreasing tar content improves carbon conversion efficiency (Lopez et al., 2018). Choi et al. carried out air gasification of PET in two stages, maintaining similar operating temperature in fluidized bed reactor and tar reactor. When activated carbon is used for tar cracking, the concentration of H_2 and CO increases from 3 and 15% to 17 and 21% when no cracking agent was used (Choi et al., 2021). The performance of activated carbon is better than dolomite for reducing tar concentration (J. W. Kim et al., 2011).

2.2.1.3.3. Co-gasification of plastics with other fuels

When plastics like PE are co-gasified with other fuels like biomass or coal, the concentration of H_2 and CH_4 increases parallelly by decreasing CO and CO_2 concentration (F Pinto et al., 2002). In their other studies, they showed that by adding plastics, hydrocarbon concentration also increases. This can countered by improving equivalent ratio to increase reactions occurring between oxygen and hydrocarbons (Filomena Pinto et al., 2003). Co-gasification of PE with Puertollano based coal increased gas and tar yield as compared to coal alone (Filomena Pinto et al., 2009). Pinto et al. carried out co-gasification of rice husk and PE using various gasifying media such as air, steam, O_2, CO_2 and their mixtures. When compared to air gasification, steam gasification produces higher amount of hydrogen whereas, air gasification enhances the amount of CO and CO_2 in syngas. Higher residence time of syngas in gasifier enhanced the cracking reactions thus decreasing the amount of hydrocarbons. When air and steam is used as a gasifying agent, by improving ER from 0.2 to 0.3, CO and CO_2 concentration in the syngas increases by around 2-4% owing to the reactions occurring between hydrocarbons and oxygen. Increasing oxygen content in inlet gas mixture also decreases tar, CO and hydrocarbons content in syngas (Filomena Pinto et al., 2016). It also increases H_2/CO ratio which makes it useful for manufacturing liquid fuels.

2.2.1.3.4. Co-gasification under CO_2 conditions

Pinto et al. used O_2/CO_2 as gasifying agent and the concentration of CO in the syngas increases by 10% as compared to O_2 gasification due to Boudouard reaction (reaction

2.2) and reverse water gas shift reaction. Further, CO_2 gasification decreases CH_4 concentration due to dry reforming reaction (Filomena Pinto et al., 2016).

$$C + CO_2 \rightarrow 2CO \quad (2.2)$$

$$CO_2 + H_2 \leftrightarrow CO + H_2O \quad (2.3)$$

Wang et al. carried out co-gasification of pine wood and PET/HDPE plastics in 1:1 ratio. Mixing pine wood and HDPE increased H_2 concentration in syngas (36.7%) and further had a positive synergy with respect to the release of C2-C3 hydrocarbons (Z. Wang et al., 2021). Li et al. carried out CO_2 gasification of pine wood (PW) and HDPE. They had treated pinewood in acid, alkali, and water and gasification was carried out using various ratios of PW and HDPE (1:0, 3:1, 1:1, 1:3, 0:1). Acid treated PW decreased H_2 concentration in syngas whereas, alkali treated PW had a reverse effect due to the progress of alkali promoted char gasification and cyclization reactions. CO release can be split in two stages, first due to volatile release and then due to gasification of char. Acid treated PW with HDPE favoured the formation of CO during volatile matter release stage and alkali treated PW favoured CO formation during the char gasification stage (Li et al., 2021).

Table 2.1. Steam gasification of plastics

Reference	Reactor type	Reactor conditions	Plastic type	Gas composition (Volume %)				
				H_2	CO	CH_4	C2-C4	Calorific value (MJ/m^3)
C. Wu & Williams, 2010	Two stage reactors	T: 800°C	HDPE	4	24.5	16	54	-
			HDPE+catalyst (Ni+Mg+Al)	25.5	64	7	2.5	-
			PP	18	0	26	55	-
			PP+catalyst (Ni+Mg+Al)	62	28	2	0	-
			PS	51	21	10	16	-
			PS+catalyst (Ni+Mg+Al)	55.5	34.5	2	1	-
Wilk & Hofbauer, 2013	Dual fluidized bed	S/P: 2 T: 850°C	PE	38	7	30	-	25.8
		S/P: 2 T: 850°C	PP	34	4	40	-	27.2
Erkiaga et al., 2013	Spouted bed	S/P: 1 T: 900°C Bed: Olivine	PE	58	27	7	-	16.2
		S/P: 1 T: 900°C Bed: γ-Alumina	PE	59	26	8	-	16.2
Friengfung et al., 2014	Fixed bed	S/O_2:1.1 T: 850°C	PS	29	43	1.7	-	
			HDPE	35	43	11	-	
			PP	38	45	9	-	
Akkache et al., 2016	Fixed bed	850°C	Plastic waste	44	19	20	-	20.4

T: Temperature, S/P: Steam to plastic ratio, Bed: Bed material

Table 2.2. Air gasification of plastics

Reference	Reactor type	Operating Conditions	Plastic type	Gas composition (Volume %)			
				H_2	CO	CH_4	Calorific Value (MJ/m^3)
Arena et al., 2010	Bubbling fluidized bed	T: 845-897°C ER: 0.2-0.31 Bed: Sand	PE	9.1-9.5	2.8-2.2	10.4-7.1	7.9-6.3
		T: 807-850°C ER: 0.2-0.29 Bed: Olivine	PE	30.1-29.1	18.4-20.9	3.4-1.5	7.6-6.3
		T: 869-914°C ER: 0.22-0.31 Bed: Olivine	Waste plastic mixture	6.8-6.6	3.7-4.8	7.6-6.3	6.8-5.2
Arena & Di Gregorio, 2014	Bubbling fluidized bed	T: 887°C ER: 0.25 Bed: Olivine	Mixed plastic wastes	5.9	6.4	6.6	6.6
Martínez-Lera et al., 2013	Bubbling fluidized bed	T: 750°C ER: 0.3 Bed: Sand	PE	2.7	6.1	7	3.9
		T: 750°C ER: 0.3 Bed: Sand	Waste PE	3	8.7	8.7	4.9
		T: 750°C ER: 0.3 Bed: Sand	Waste polyolefins	3	8.5-10	8.5-10	4.9-5.7
Zaccariello & Mastellone, 2015	Bubbling fluidized bed	T: 877°C ER: 0.25 Bed: Sand	Recycled plastic	6	6.6	6.5	7.9

ER: Equivalent ratio, Bed: Bed material

Table 2.3. Co-gasification of plastics with other fuels (Fluidized bed)

Reference	Gasifying media	Operating Conditions	Feed mixture	Gas composition (Volume %)		
				H_2	CO	CH_4
Pinto et al., 2002	Steam	T: 740-880°C S/F: 0.8	Pine wood +PE (0.9/0.1)	25-44	34-31	15-10
Filomena Pinto et al., 2003	Steam/air	T: 850°C ER: 0.2 S/F: 0.85	Coal + PE (0.9/0.1)	40	17	17
Filomena Pinto et al., 2016*	Steam	T: 850°C S/F: 1	Rice husk + PE (0.8/0.2)	41	15	11
	CO_2	T: 850°C S/F: 1 ER: 0.2		37	20	10
	Air	T: 850°C ER: 0.2		19	24	12
	Oxygen	T: 850°C ER: 0.2		38	12	12
Ruoppolo et al., 2012	Air	T: 780°C ER: 0.23 Bed: Sand	Pine wood + PE (0.9/0.1)	17	16	12
	Air	T: 780°C ER: 0.23 Bed: γ-Al_2O_3	-	30	14	3
Brachi et al., 2014	Steam/air	T: 752°C ER: 0.1 S/F:0.76 Bed: γ-Al_2O_3	Olive husk + PET (0.75/0.25)	33	12	9

S/F: Steam to feed ratio

Reference	Gasifying media	Operating Conditions	Feed mixture	Gas composition (Volume %)		
				H_2	CO	CH_4
Brachi et al., 2014	Steam/air	T: 845°C ER: 0.1 S/F:0.62 Bed: Ni-γ-Al_2O_3	Olive husk +PET (0.75/0.25)	40	22	5.5
Wilk & Hofbauer, 2013	Steam	T: 850°C S/F:1.6 Bed: Olivine	Wood +PE (0.7/0.3)	41	23	14
	Steam	T: 850°C S/F:0.94 Bed: Olivine	Wood + Plastics (0.5/0.5)	35	24	6
Robinson et al., 2016	Air	T: 725-875°C ER:0.19-0.31 Bed: Olivine	Wood + PET (0.5/0.5)	4.3-5.4	13-9	3-2.7
Aznar et al., 2006	Air	T: 850°C ER:0.36 Bed: Sand-dolomite	Coal + polyolefins (0.6/0.4)	11	12	2
			Coal +polyolefins +biomass (0.6/0.2/0.2)	14	13	2
Zaccariello & Mastellone, 2015 (BFB)	Air	T: 872°C ER:0.25 Bed: Silica sand	Recycled plastic +wood (0.8/0.2)	10	7	8
	Air	T: 868°C ER:0.36 Bed: Silica sand	Coal+ Recycled plastic +wood (0.5/0.3/0.2)	14	13	2

2.2.2. Electronic waste treatment methods

Due to technological advances in recent years, e-waste generation has increased significantly and the lifetime of e-waste has decreased. Printed circuit boards (PCB) are a major constituent of electronic wastes. The weight percentage of PCB in total electronic wastes can vary from 5-10% (Vermesan et al., 2020). PCB contains a mixture of metals, epoxy resins and plastics. Different electronic items like resistors, diodes etc are mount on boards. PCB is a multi-layered structure of glass fibers, brominated epoxy resins and metal layer (P. Zhu et al., 2013). Plastics in PCB can be of various types like High impact polystyrene, Acrylonitrile butadiene styrene, Polycarbonate, Poly phenylene oxide etc. These plastics contain brominated compounds which act as flame retardants (Reena et al., 2011). PCB contains heavy metals, which can be recycled by various processes like hydrometallurgical, pyrometallurgical and mechanical processes. Hydrometallurgical processes use solvents, which leaches out metals from PCB. The solvents used can be toxic in nature (Ankit et al., 2021).

Different pyrometallurgical processes used to treat PCB are incineration, pyrolysis and gasification. Incineration of PCB can result in the formation of toxic compounds like difurans/dioxins. Non-metallic components in PCB plastics are combusted. PCB after incineration becomes brittle and the precious heavy metals can be recovered by mechanical processes (Jie et al., 2008). To destroy pollutants, PCB must be incinerated at high temperature (900-1000°C)(Ankit et al., 2021).

2.2.2.1. PCB pyrolysis

Pyrolysis of PCB is carried out at comparatively lower temperatures than incineration in inert atmosphere to recover oils and other important products. Pyrolysis of PCB is carried out at a temperature between 400°C to 900°C. Most of the researchers have obtained maximum yield of oil at around 500°C-600°C. The oil obtained in these conditions can have bromine related compounds. Details of the PCB pyrolysis performed are given in Table 2.4.

Table 2.4. Optimal yield of oil from PCB pyrolysis

Reference	Operating conditions	O_Y (%)	Sample weight (gm)	Oil calorific value (MJ/kg)
Chen et al., 2021	T:550°C Time: 1 h	19.7	10	26.97
	T:800°C Time: 1 h	13.5		29.71
Nie et al., 2020	T:400°C Time: 2 h	28.87	30	-
Lin & Chiang, 2014	T:500°C Time:0.5 hr.	38	5	37.5
	T:400°C Time:0.5 hr.	29		32.3
Long et al., 2010 (Vacuum pyrolysis)	T:550°C Time:2 hr. P:20 kPa	10	3000	-
Jie et al., 2008	T:500°C Time:0.5 hr	9.06	50	30.52
	T:600°C Time:0.5 hr	9.13		30.79
	T:700°C Time:0.5 hr	8.87		30.66
Guo et al., 2010	T:600°C U: 0.19m/s	~24	314	-
	T:600°C U: 0.48m/s	~18		-
Quan et al., 2010	T:700°C Time:0.5 hr	20.1	160	-
Wu & Qiu, 2014	T:600°C Time:0.5 hr. P:10 kPa	21.6	10	-

U: Superficial gas velocity, T: Temperature, P: Pressure, Oy: Oil yield

According to the studies carried out by Chen et al., the maximum oil yield was observed at 550°C. Oil yield was heavily dependent on time duration and operating temperature. As operating temperature is increased from 550°C, thermal cracking of PCB increases thus improving gas yield. The oil obtained contained phenolic compounds. The epoxy resin in PCB undergoes chain scission reactions. The radicals released in this process undergoes recombination reactions to generate phenolic compounds (W. Chen et al., 2021). Non-metallic components of PCB can be separated easily by mechanical process (shaking table). Oil yield can increase to 28.87% when non-metallic components are removed from PCB (Nie et al., 2020). Hydrocarbons present in PCB oil changes with operating temperature. As the operating temperature is increased from 300 to 400°C, the carbon number of pyrolysed oil improves from C5-C9 to C5-C21. The quantity of

bromine in oil declines from 18.85% to 11.5% when temperature is increased from 300 to 500°C. This was due to constant degradation and debromination of oil products with temperature (Lin & Chiang, 2014).

Jie et al. observed similar physical property of oil when pyrolysis was carried out from 500-700°C. Oil yield was reported between 9.06% and 8.87% and the calorific value was found between 30.52 and 30.66 MJ/kg. H/C ratio of oil should be higher and it denotes the domination of aromatic compounds in pyrolysis oil obtained. The H/C ratio of oil decreases from 1.29 to 1.13 when the operating temperature is increased from 300 to 700°C (Jie et al., 2008). A similar result with decrease in H/C ratio was reported under fluidized bed conditions. At 400°C, the H/C ratio was 1.33 and at 700°C, it decreased to 1.2 (Guo et al., 2010).

Quan et al. in their studies utilized the oil obtained by PCB pyrolysis for manufacturing carbon nano tubes. This shows that the oil obtained can also be used for non-conventional applications (Quan et al., 2010). Wu and Qiu carried out co-pyrolysis of Chinese sawdust with PCB's in different mass ratio. They found that by adding sawdust, the weight of residue obtained was higher. This could be due to blocking of PCB pores by sawdust, thus preventing the release of volatile matter from PCB (W. Wu & Qiu, 2014). Kim et al. carried out co-pyrolysis of PCB with HDPE and PP. They observed that HDPE and PP had a positive effect on weight loss rate. Epoxy resins in PCB could breakdown to hydrogen and bromine radicals. When HDPE and PP melted, they get deposited over the pores of PCB. Reaction between hydrogen/bromine radicals with plastics can increase the decomposition rate of HDPE/PP. Co-pyrolyzing HDPE/PP with PCB increases the amount of alkylated olefins and phenols in the oil produced (Y. M. Kim et al., 2017). When coal is mixed with PCB, the temperature range in which pyrolysis occurs increases as compared to PCB alone (Hao et al., 2014).

2.2.2.2. PCB Gasification

A very few literature reported PCB gasification processes. Zhang et al. carried out PCB gasification in the presence of eutectic LNK carbonates. They found that as compared to pyrolysis, the steam gasification of PCB resulted in the complete utilization of PCB. The amount of tar produced is less under gasification conditions by around 14%. Gas yield under gasification conditions is higher than pyrolysis conditions by around 34%. The amount of hydrogen produced by steam gasification is nearly 20 fold higher than PCB

pyrolysis (63.42×10^{-3}mol v/s 3.82×10^{-3}mol). This was due to two stage release of hydrogen from PCB. During devolatilization of PCB, H_2 is released and further gasification of subsequent char produces H_2 (S. Zhang et al., 2013). Further, they found that adding Ni powder to the feed mixture enhance the rate of hydrogen generation with decrease in the gasification reaction temperature from 927°C to 727°C (Salbidegoitia et al., 2015).

Table 2.5. Syngas composition on gasification of PCB plastics

Sample		WEEE plastic*	HIPS*	ABS*
Experiment		Gas composition (vol.%)		
No catalyst	H_2	42	57	42
	CO	7	5	7.5
	CH_4	21	20	26
	C2-C4	20	16	22.5
5%Ni/Al_2O_3	H_2	52	63	63
	CO	15	25.5	12
	CH_4	11	7.5	14
	C2-C4	10.5	2	8
10% Ni/Al_2O_3	H_2	57	65	65
	CO	21	26	15
	CH_4	7.5	5	10
	C2-C4	7	1	7

*WEEE: waste electrical and electronic equipment, HIPS: High Impact Polystyrene, ABS: Acrylonitrile Butadiene Styrene

Plastic components in electrical/electronic equipments were made up of flame retarding compounds like polybrominated diphenyl ethers (PBDE). High temperature gasification (~1150-1200°C) and then shock cooling of syngas to below 200°C can decrease the amount of pollutants dioxins and difurans (Yamawaki, 2003). Steam gasification of waste electrical and electronic equipment (WEEE) plastics with sand and Ni catalyst was carried out by Acomb et al. (Acomb et al., 2013). They concluded that when Ni is used as catalyst for steam gasification of WEEE plastic, the concentration of H_2 and CO increases due to reforming reactions between steam and hydrocarbons. When the weight fraction of Ni in catalyst mixture is increased from 0 to 10%, the concentration of H_2 and CO in syngas increases by 15% and 14%, respectively. They also concluded the possibility of HIPS (High Impact Polystyrene) and ABS (Acrylonitrile Butadiene

Styrene) being a constituent of WEEE plastics. Table 2.5 gives a summary of gasification experiments carried out by Acomb et al. on WEEE, HIPS and ABS plastic.

2.3. Utilizing CO_2 as pyrolyzing, gasifying and combustion media

When CO_2 is utilized as a media for pyrolysis, gasification and combustion, the syngas/ flue gas produced is rich in CO_2. H_2O is another major component of the flue gas generated after combustion. When pure O_2 is utilized for combustion, it is called oxy-fuel combustion. The flue gas generated can be purified by various steps like condensation and desulfurization to generate high purity CO_2. A part of CO_2 generated can be recycled and the rest can be sequestered. This can help in reducing greenhouse gas emissions. Similarly, syngas generated could be used to generate various chemicals (methanol, Dimethyl Ether) and electricity through IGCC (Integrated Gasification Combined cycle) process. Figure 2.2 shows the schematic of utilization of CO_2 in combustion power plants. Syngas can be generated with the help of O_2 and recycled flue gas (RFG). The syngas can be purified to remove sulphur based impurities. After purification it can be combusted. In the with the help of RFG this results in generation of flue gas with high CO_2 content. The flue generated can be purified further to remove NO_X and SO_X emissions. A section of flue gas can be recycled to gasifier and combustor section.

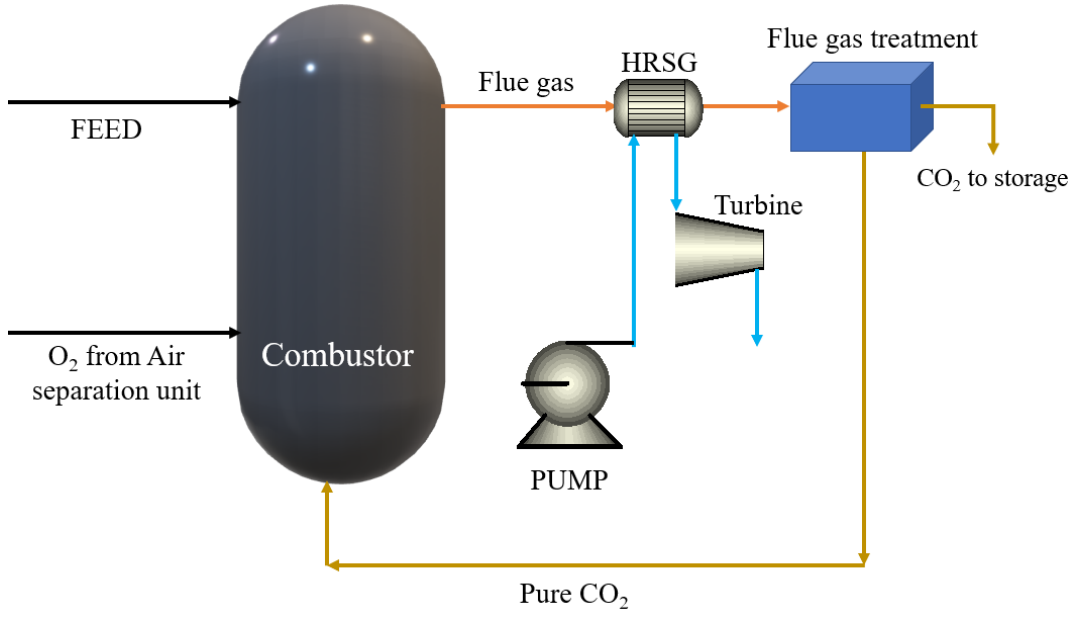

Figure 2.2. Schematic diagram of oxy-fuel combustion.

2.3.1. CO_2 as a Pyrolyzing media

2.3.1.1. Impact of CO_2 on lighter components

H_2 and CO constitute the major light gases released during pyrolysis. Generally, it is found that when pyrolysis is undertaken in an atmosphere of CO_2 instead of N_2, Ar or He, that the yields of light gases (eg.CO) are higher (Yuzbasi & Selçuk, 2011). The effect is greater at higher temperatures, where the CO_2 can react directly with the solid according to the Boudouard reaction. The presence of CO_2 inhibits the decomposition of carboxyl groups to CO_2, thereby reducing the CO_2 yield. The influence of CO_2 on CO yield is negligible at low temperatures, but at around 500°C, CO_2 promotes the decomposition of carbonyl and hydroxyl groups and ether bridges, leading to an increased yield of CO under fast pyrolysis conditions(Gao et al., 2013). The presence of inherent catalytic components in a feedstock could improve the reactivity of CO_2 with the fuels. Calcite is a constituent of ash in coal and thermal cracking of calcite is inhibited by the presence of CO_2 at high partial pressure.

By gradual replacement of N_2 with CO_2 under fast pyrolysis conditions, H_2 productivity was increased due to the destruction of H_2 containing char structures and further the cleavage of C-H bond. With further increase in the concentration of the feed CO_2, H_2 production decreases due to the progress of reverse water gas shift reaction (equation 2.3), which would increase the CO production (Guizani et al., 2014). Reverse water gas shift reaction would also occur in slow pyrolysis conditions decreasing H_2 content (Q. Wang et al., 2018).

During CO_2 pyrolysis of plastics such as poly ethylene terephthalate (PET) and poly vinyl chloride (PVC), CO_2 reacts with the tars, volatile organic compounds or pyrolytic oil to produce higher quantity of CO than expected at temperatures exceeding 600°C (T. Lee et al., 2017). Increase in the degradation of char and reaction with volatile organic compounds under CO_2 conditions could lead to the increase in yield of pyrolytic gases(J. Lee,).

Lee et al. also analysed the flue gases evolving from the synthetic MSW containing mixture of biomass, polyethylene and polystyrene(J. Lee, Choi, et al., 2017). It was reported that hydrogen concentration increases with an increase in the pyrolytic temperature. Methane concentration remains similar in both environments for a low concentration of biomass in the feed. The released methane gas gets cracked and produces hydrogen gas at 450°C. At above 450°C, CO concentration increases with temperature in

CO_2 atmosphere whereas in N_2 atmosphere it is negligible. This is due to the reaction between CO_2 and pyrolytic oil, which is produced from thermal degradation of biomass or plastics.

The influence of CO_2 on the evolution of light hydrocarbons during pyrolysis is complex and depends on a variety of parameters. Generally volatile yields are slightly higher in an atmosphere of CO_2 than in inert gas. However, often the measured differences (~2 – 3%) are typically on the order of the variation of volatile yields measured between samples(Zellagui et al., 2016). While overall yields increase in the presence of CO_2, at higher temperatures, equilibrium favours the formation of CO over hydrocarbons. When lignite was subjected to slow pyrolysis in the presence of CO_2, the yields of CH_4 and C_2H_6 decreased compared to experiments in the presence of N_2(Q. Wang et al., 2018). However, under fast heating conditions, the presence of CO_2 can enhance the formation of light hydrocarbons such as CH_4 (550°C to 850°C) by degradation of the macromolecular structure of the parent feedstock (Gao et al., 2013). At high temperatures, the experimental results are more consistent, showing that CO_2 hinders light hydrocarbon formation and enhances the yield of CO. Since the difference in yield increases with temperature, it may be due to enhanced tar cracking with CO_2, via the reaction (2.1).

2.3.1.2. Impact of CO_2 on higher hydrocarbons

Impact of addition of CO_2 on the formation of tar, char and secondary reaction was described by Guizani et al. (Guizani et al., 2014). The evolution of tar and heavy hydrocarbons (C_{6+}) during pyrolysis in the presence of CO_2 is affected by the heating rate and properties of the parent feedstock. The introduction of CO_2 causes tar cracking, polymerization and further char gasification. CO_2 can react with tar and improves the gas yield. Jamil et al. undertook pyrolysis of Victorian brown coal under fast heating conditions in He and CO_2 between 600°C and 1000°C and found that tar yields were not affected(Jamil et al., 2004). They argued that the tar evolves so quickly from the coal at low temperatures, that CO_2 does not have time to participate in intra-particle reactions to influence tar formation. However, under slow pyrolysis conditions, Wang et al. found that tar yields for a Chinese lignite in the presence of CO_2 were significantly higher in N_2 atmosphere (Q. Wang et al., 2018). In N_2 atmosphere, tar yields were ~4 – 5 wt%. CO_2/N_2

mixed atmosphere is used varying CO_2 from 20 – 60 vol%, tar yield varies from ~6 wt% at 400°C, to ~8 – 9 wt% at 600°C and reduced to ~7 – 8 wt% at 800°C.

The general increase in tar yield was attributed to higher conversion of hydroxyl groups and methylene groups to phenols and aliphatic molecules in tar(Q. Wang et al., 2018). The reduction of the tar yield at higher temperatures is probably due to enhanced tar cracking with CO_2, via the reaction (2). The total acidic component of bio-oil produced in CO_2 pyrolysis is comparatively lesser than N_2 conditions. This improved the quality of bio-oil and make it more preferable. Fast pyrolysis is inherent in all combustion and gasification techniques, but is also being seen as a potential standalone technology to convert waste materials into bio-crude and bio-chars. The thermally cracked species reacts with CO_2 resulting in lower number of variations of chemical species. Pyrolytic oil obtained under CO_2 conditions had higher amount of aromatic content and oxygenated compounds (aldehydes and ketones). Higher acetic acid content in pyrolytic oil under CO_2 conditions is resulted due to the reaction of CO_2 with primary volatiles and solid residue(H. Zhang et al., 2011)(Fang et al., 2018). The increase in the unsaturated hydrocarbon structures and decrease in the chain structures in bio-oils should also be taken as the evidence for increased cracking under CO_2 conditions. Further, bio-oil produced under CO_2 conditions was more stable because it consists of higher quantity of mono-functional phenol groups with less methoxy containing compounds, which are precursors to polymerization in bio-oil.

2.3.1.3. Impact of CO_2 on char structure

Char yields are often lower when CO_2 is used in place of an inert has such as N_2 or He in pyrolysis experiments. The reduction in yield can be negligible at low temperatures – typically below 700°C. Under slow pyrolysis conditions, Wang et al. found that the char yield of a high-ash Chinese lignite remained the same at temperatures up to 700°C in a range of different gas atmospheres, including with CO_2(Q. Wang et al., 2018).

The studies performed by Zhu et al. were conclusive in proving the effect of temperature on the surface area of char under CO_2 pyrolysis conditions(S. Zhu, Bai, Hao, et al., 2017). They found that the char surface areas (measured using BET CO_2 chemisorption) were increased in CO_2 relative to those measured in N_2, by ~10 – 40 % depending upon the coal. A significant difference in the generation of surface area in char between N_2 and

CO_2 atmosphere was reported at the temperature interval between 600°C and 800°C. Experiments using a Chinese lignite found that in comparison with N_2, CO_2 could inhibit the release of volatiles at low temperatures and in fact cause a small increase (< 10%) in char yields at temperatures of 500°C – 600°C due to its higher density and thermal properties(S. Zhu, Bai, Hao, et al., 2017). Rathnam et al. studied the pyrolysis behaviour of four Australian coals in N_2 and CO_2 atmosphere and found that the higher apparent yield of volatiles was estimated in CO_2 conditions and this could be attributed to the char-CO_2 gasification reaction above 700°C. The normalized rate of weight loss at 927°C is 0.0014 (s^{-1})(Kumar et al., 2009). Other researchers have found similar trends, with the greatest impact on char yield occurring above 700°C, when the char-CO_2 reaction occurs at an appreciable rate(Kumar et al., 2009). The CO_2 promotes the rupture of methylene groups in the coal samples but inhibits the decomposition of methyl groups at higher temperature. Zhu et al. pyrolyzed lignite and sub-bituminous coals at 800°C in a fixed bed reactor and found that compared with N_2 atmosphere chars obtained under CO_2 atmosphere had larger specific surface area and lower ratios of small to large aromatic rings(S. Zhu, Bai, Luo, et al., 2017). Similar results showing increase in the surface area by 10-40% were also obtained by Rathnam et al. (Kumar et al., 2009). Gao et al. performed pyrolysis of lignite under pure N_2 and 50% N_2-50% CO_2 conditions(Gao et al., 2013). The presence of CO_2 promoted the cracking of hydroxyl, methyl and methylene groups in lignite. Lignite char adsorbs CO_2 under pyrolysis conditions on the active sites of char developed. The aliphatic and aromatic O-containing functional groups present on the coal surface are removed during pyrolysis generating active sites for CO_2 adsorption. CO_2 reactions promote the removal of hydroxyl, methyl functional groups and further enhance the cracking of aromatic structure of char. During the reaction of CO_2 with these functional groups, higher H radicals are generated than N_2 pyrolysis conditions and this leads to generating the crosslinking between the fragments generated and causes macromolecular structure of char. CO_2 could help in developing the pore structure of char by opening closed pores and development of the internal pore structure.

Under CO_2 conditions, the surface area of char is higher as compared to N_2 conditions with an increase of about 50 and 60% at 700°C and 800°C, respectively. Micropore volume developed under CO_2 conditions is higher, indicating the development of the porous structure and increase in surface area of char under CO_2 conditions. It is reported

that the micropore volume developed under N_2 conditions is 0.084 cm^3/gm whereas in CO_2 conditions, it is 0.135 cm^3/gm(Gao et al., 2013).

Generally high rank coals possess large number of micro-pores and thus higher surface area is created whereas low rank coal contains mainly macro-pores(Kumar et al., 2009). Butterman and Castaldi compared H_2O/N_2 pyrolysis condition with CO_2 pyrolysis condition(Butterman & Castaldi, 2012). CO_2 enhanced the macro-pores in lignin pyrolyzed in a TGA and subjected to a slow heating rate of 1°C/min.(Butterman & Castaldi, 2012). The maximum size of the pores increased from 80 μm in H_2O/N_2 to 325 μm in CO_2. The diffusion of H_2O in the pores is slower than the rate of gasification of H_2O with char. Hence H_2O molecule remains at the entrance of mesopores increasing its entry diameter by steam gasification. Whereas CO_2 could achieve strong internal diffusion in meso and macropores and can access the surface area of char and thereby increasing the pore diameter further by gasification. Under CO_2 conditions, the macropores formed can coalesce and could increase their diameter even further. SEM micrographs showed that the reactive CO_2 was able to access the lignin char structure and convert the char more uniformly than H_2O/N_2 under the same conditions more completely. Pyrolysis in CO_2 produced a greater number of mesopores and macropores and a wider distribution of pore diameters. Char, which are micro-porous in nature, can reach a maximum surface area on pyrolysis and with increase in the char conversion, surface area would start to decrease due to pore coalescence. However, this effect was not found in non-porous char (e.g. food waste and plastics) at higher char conversion(Hla et al., 2016). Sawdust char produced under CO_2 conditions has more rounded cavities as compared to N_2, which had resulted in higher surface area of char(Farrow et al., 2015).

Heating rate had a strong influence on the formation of pore structure in the char. At higher heating rates, the volatile matter does not get sufficient time to release from the internal matrix of fuels. The inorganics in the matrix would try to migrate out of micro-pores and agglomerate under CO_2 gasification conditions and as a result, bubbles may form and would get ruptured at higher temperature/heating rate. Under these conditions, a glassy structure is formed, which is inaccessible to CO_2 molecules(Butterman & Castaldi, 2012). At temperatures lower than 600°C, CO_2 would act as inert gas and not aid in tar release. Higher heating rate during pyrolysis could result in higher concentration of radicals on char surface, enhancing the rate of CO_2 reactions(Jamil et al., 2004).

Table 2.6. Thermal behaviour of coal under various conditions

Reference	Sample	Initial weight loss temperature (˚C)	Char combustion (CO_2 atmosphere only) /VM Release Temperature range(˚C)	Temperature of maximum weight loss during TGA(˚C)	Number of weight loss peaks	Gas atmosphere under which TGA performed
Naidu et al., 2016	Godavari khani coal	300	800-1150	1075	2	CO_2
	Bellampalli coal	300	700-1110	980	2	CO_2
	Bilaspur coal	300	800-1150	1007	2	CO_2
	Neyveli lignite coal	200	700-1030	937	2	CO_2
Yuzbasi & Selçuk, 2011	Lignite coal	216.7	800-950	481	2	CO_2
Zellagui et al., 2016	South african coal	400	$900\text{-}1200_c$	1100	2	CO_2
Lu et al., 2013	Anthracite coal	420	420-520	465	1	N_2
Yuzbasi & Selçuk, 2011	Lignite coal	230.8	$230.8\text{-}550_c$	482.9	1	N_2
Zellagui et al., 2016	South african coal	400	$400\text{-}600_c$	475	1	N_2
Muthuraman et al., 2010	Indian coal	300	380-520	420	1	Air
	Indonesian coal	250	250-520	360	2	Air
Biswas et al., 2006	Indian coal (21.1 % ash)	349	349-492	400,427	2	Air
	Indian coal (43.4 % ash)	355	355-478	394.3	1	Air
Zhuo et al., 2017	Coal	500	$500_a\text{-}750_a$	524.8	1	Air
Yuzbasi & Selçuk, 2011	Lignite coal	224	224-546.7	426.2	2	79% N_2/21% O_2

Reference	Sample	Initial weight loss temperature (˚C)	Char combustion (CO_2 atmosphere only) /VM Release Temperature range(˚C)	Temperature of maximum weight loss during TGA(˚C)	Number of weight loss peaks	Gas atmosphere under which TGA performed
	Shenmu lignite char	380.1	380.1-573.2	500_c	1	80% N_2/20% O_2
G. D. Shen et al., 2016	Shenmu bituminous coal char	483.2	483.2-657.6	600_c	1	80% N_2/20% O_2
Tahmasebi et al., 2013	Victorian brown coal	215	256.8-450	366.3	1	79% N_2/21% O_2
	Chinese lignite char	381.4	381.4-509.5	450	1	80% CO_2/20% O_2
G. D. Shen et al., 2016	Chinese bituminous coal char	462.9	462.9-588.8	510	1	80% CO_2/20% O_2
Tahmasebi et al., 2013	Victorian brown coal (lignite)	215	259.3-450	368.7	1	79% CO_2/21% O_2
Yuzbasi & Selçuk, 2011	Lignite coal	225.8	225.8-550	347.1	2	79% CO_2/21% O_2

c: calculated by author

Table 2.7. Thermal behaviour of MSW under various conditions

Reference	Sample	VM release temperature range(˚C)	VM release Peaks(˚C)	Char combustion Temperature (˚C) (peaks, range)	Temperature of maximum weight loss during TGA(˚C)	Number of weight loss peaks	Gas atmosphere under which TGA performed
Singh et al., 2012	RDF (Refuse derived fuel)	240-380 410-500	345 474	-	345	2	N_2
	MSW plastic	410-500	478	-	478	1	N_2
	Waste tyre rubber	310-410 420-500	377 437	-	377	2	N_2
Fang et al., 2016	MSW	250-410	297.5	410-880,459.2	297.5	2	N_2
	Paper sludge	280-540 540-750(tar coke pyrolysis)	414.7 724.6	750-850,822.9	724.6	3	N_2
J. Chen et al., 2015	Petrochemical waste water sludge	192-387 388-477	327_c 430_c	-	327	2	N_2
J. Lee, Choi, et al., 2017	Modelled MSW	300-500 (biomass,PE and PS)	300,400,500	-	-	2	N_2
	Modelled MSW	300-500 (biomass,PE and PS)	300,400,500	800-900, 850_c	400	3	CO_2

Reference	Sample	VM release temperature range(˚C)	VM release Peaks(˚C)	Char combustion Temperature (˚C) (peaks, range)	Temperature of maximum weight loss during TGA(˚C)	Number of weight loss peaks	Gas atmosphere under which TGA performed
J. Chen et al., 2015)	Petrochemical waste water sludge	201-380 381-471	327_c 430_c	777-910, 877_c	327	3	CO_2
Lai et al., 2011	MSW	200-350 (biomass) 350-450(plastic)	310.8 400	450-550,480	310.8	3	80% N_2/20% O_2
B. Shen & Qinlei, 2006	MSW	$250\text{-}350_a$ $350\text{-}450_a$	300 425	450-550,475	300	3	Air
Lai et al., 2011	MSW	200-350 (biomass) 350-450(plastic)	310.4 405	450-550,480	310.4	3	80% CO_2/20% O_2

c: calculated by author

2.3.1.4. Thermogravimetric analysis of fuels

During CO_2 pyrolysis of feedstock, moisture release begins at 100°C and the volatile matter release depends upon the nature and composition of feedstock. Each feed stock has its specific range and initial release temperature. The gasification under CO_2 atmosphere could result in higher utilization of fuel. MSW having higher volatile matter than coal resulted in higher weight loss rates, as compared to coal, at the temperature interval between 200°C and 500°C. Tars are high molecular weight hydrocarbons (eg. C_6H_9), which form liquids at standard temperature and pressure. TGA behaviour of solid fuels such as coal and MSW under pyrolysis and combustion conditions are compared and summarized in Tables 2.6 and 2.7. The initial volatile matter loss temperature of biomass and MSW is almost identical in the range of 177°C to 277°C due to the presence of high quantity of biomass in MSW. It results in both MSW and biomass samples having similar maximum volatile release temperature.

The major components of MSW are biomass and plastics The initial volatile matter release temperature of plastics is higher than that of coals, but the temperature range of volatile matter release is lower because of higher weight loss rate associated with plastics(Zellagui et al., 2016). The weight loss of MSW happens at various stages owing to its constituents. At low to moderate temperatures, most studies reveal that the pyrolysis of coal in CO_2 has very little effect on volatile matter release(Zellagui et al., 2016)(Jamil et al., 2004). Even during rapid pyrolysis of coal at 600°C, volatile matter weight loss was less as compared to N_2 conditions(Chang et al., 2017). A similar observation was reported by Meng et al. for coal gangue(F. Meng et al., 2013). It was found that the maximum volatile release temperature was higher for coal gangue under CO_2 conditions. In South African coal and Xuzhou bituminous coal, by replacing N_2 with CO_2, the mass loss rate had increased during the release of volatile matter(L. Duan et al., 2009). This is due to the reaction of CO_2 with free radicals generated from the volatile matter and simultaneous occurrence of thermal cracking reactions(L. Duan et al., 2009).

2.3.2. Impact of CO_2 on gasification and combustion

Table 2.8. Effect of gasifying agents on yield of product gases

Reference	Operating conditions and raw materials used	CO/ H_2 maximum obtained	Conditions for maximum CO/ H_2 obtained.
Billaud et al., 2016	Reactor(R): Drop tube reactor Biomass(B): Beech sawdust (0.315 mm to 0.45 mm) Gasifying medium: Steam, Air, CO_2 Bed temperature range(T): 800-1400°C	CO_2 gasifying media: 3 (CO- 15 mol/kg dry mass H_2O gasifying media: 3 Air gasifying media: 5	CO_2: 800°C H_2O: 800°C Air: 800°C, ER:0.4
Fremaux et al., 2015	Fluidized bed, B:Wood residue below 5mm Bed material: Silica 0.5mm T: 900°C Gasifying medium: steam Minimum fluidization velocity: 0.1 to 0.14 m/s	0.9	At 0.5 steam to biomass ratio.
Pacioni et al., 2016	Fixed bed tubular reactor Apple pomace, spent coffee grounds, saw dust Gasifying medium: steam T: 650-900°C	0.86 for apple pomace	At 0.5 conversion and 850°C
Valin et al., 2016	Fluidized bed, Operating temperature: 850°C B: Wood sawdust(1-2mm) Gasifying medium: CO_2, steam and their mixture	2	Complete replacement of steam with CO_2 as a gasifying medium
Hanaoka et al., 2013	Downdraft fixed bed gasifier Operating Pressure: 1.5 bar Operating temperature: 900˚C Japanese cedar and gulfweed (< 2mm) Gasifying medium: CO_2, O_2, He and their various proportions in the gasifying media mixture	3.05	79 % CO_2 21% O_2 ER 0.3 He/CO_2/O_2=55/30/15

The main oxidizing agents used in gasification systems are air, steam/air and steam/oxygen mixtures and water/oxygen. Table 8 shows the effect of gasifying agents

on syngas production, while Table 9 provides a summary of the main advantages and disadvantages of various gasifying agents. Table 2.10 and 2.11 compare the behaviour of different power generating systems and their efficiencies when steam and CO_2 are used as a gasifying agent, respectively.

Table 2.9. Advantages and disadvantages of gasifying agents, (Richardson et al., 2015).

Parameters	Advantages	Disadvantages
Air	1. Provides partial combustion for heat supply of gasification 2. Yields moderate char and tar concentrations	1. Provides low heating value syngas (3 – 6 MJ/Nm^3) 2. High concentration of N_2 in syngas (~50 vol%) 3.Yields ER of 0.2 to 0.4
Steam	1. Yields high heating value syngas (10 – 15 MJ/Nm^3) 2. Yields H_2 rich syngas 3.Easier integration with steam utilities	1.Requires indirect or external heat supply for gasification 2.Yields high tar content in syngas 3.May require catalytic reforming of tar
Carbon dioxide	1. Yields high heating value syngas 2. Yields high H_2 and CO and low CO_2 contents in syngas	1.Requires indirect or external heat supply for gasification 2.May require catalytic reforming of tar 3. CO_2 separation and recycle equipment required

CO_2 can be used as a gasifying agent together with O_2 and as a moderator (Prabu & Geeta, 2015)(Perkins & Vairakannu, 2017). Research on using CO_2 as a gasifying agent is at an early stage and to our knowledge there are no commercial gasification systems in continuous operation with pure CO_2/O_2 mixtures. Valin et al. used steam, CO_2 and their mixtures as the gasifying medium and found that the cold gas efficiency, total gas yield and CO_2 net emissions did not change with respect to CO_2 content in a mixture of CO_2 and H_2O(Valin et al., 2016). They concluded that with increase in CO_2 concentration, the water gas shift reaction occurs in the reverse direction, which increases CO and decreases

H_2 yield. Hanaoka et al. studied CO_2/O_2 gasification of gulfweed and Japanese cedar(Hanaoka et al., 2013). They found that CO_2 concentration in the gasifying media increases the concentration of CO in the product gas. Maximum CO/H_2 ratio obtained was 3.05 for gulfweed at 79 vol% CO_2 and 21 vol% O_2 as gasifying media. Analysis of the generated tar in GC-MS showed that the concentration of CO increased due to the degradation 3 to 5 ring aromatic structures. Ca and Mg in gulfweed acted as catalysts during gasification process. Highest concentration of syngas (CO and H_2) was observed at 69.7% by volume at a ratio of 45 vol% CO_2 and 55 vol% O_2 of gasifying medium. Maintaining equivalence ratio and optimum ratio of oxidant to gasifying medium is crucial for achieving best results during CO_2 gasification. Billaud et al. carried out experiments with steam, CO_2 and air as gasifying mediums (Billaud et al., 2016). It can be seen that air as a feed gas produces higher yield of CO than for the case of CO_2 and steam gasification agents. This may due to the incomplete combustion of fuel in air atmosphere. However, CO_2 and steam atmosphere had shown a similar yield of CO/H_2 as 3. Overall, CO_2 gasification agent produces a higher yield of CO/H_2 in the range of 2 to 3 (Table 8).

Jayaraman et al. studied the kinetic parameters for char-steam-CO_2 gasification for high ash coals (Jayaraman et al., 2017). They estimated that 156-173 kJ/mol of activation energy for steam gasification and 162-196 kJ/mol for steam blended CO_2 gasification. Aranda et al. estimated the reaction order of 0.6 for CO_2 gasification whereas it was 1.1 for steam gasification(Aranda et al., 2016). The rate of steam gasification is approximately twice as high as CO_2 gasification. Using CO_2 in place of N_2 in the gasifying agent would decrease the gasifier temperature due to its higher specific heat capacity(Liang et al., 2017).

Table 2.10. Steam based gasifying media power plant calculations without CCS.

Reference	Fuel	Gasifying media	Syngas composition (volume %)						Calorific value (HHV) (MJ/Nm^3)	Gasifier used	Gasifier operating conditions		Plant type
			CO_2	H_2	N_2	CH_4	CO	H_2O			Temperature (°C)	Pressure (Atm.)	
Craig & Mann, 2014	Biomass	Steam(S/B:0.53-1.1)	13.5	21.3	1	15.8	43.2	-	14.3_c	EBG	826	1.67	Biomass IGCC
	Biomass	Steam (steam/wood: 0.32 air/wood: 1.07)	13.5	8.9	24.2	6.5	6.7	39.9	4.6_c	1 stage FBG	830	31.3-ADGT 20-UGT	Biomass IGCC
Liszka et al., 2013	Coal	Steam (Steam /fuel:0.005 w/w)	6.6	21.7	8.2	-	48	14.3	8.7_c	EFG	1639	41.84	IGCC/CHP
A. M. Cormos et al., 2015	Coal + MBM (4:1)	Steam+O_2 (Steam/ O_2 =0.14 w/w)	3.4	28.7	5.5	-	54.9	6.4	10.6_c	EFG	1450	39.47	IGCC
C. C. Cormos, 2012	Coal	Steam + O_2 (Steam/O_2 :0.14 w/w)	4.2	26.2	4.8	-	57.2	6.6	10.5_c	EFG	>1400	39.47	IGCC
Sues et al., 2010	Biomass	Steam	3-10	52-53	1	1-3	33-46	3-9	16-19	CFB	700-800	1	IGCC
O. H. Ali et al., 2013	Biomass	Steam	5.4	55.8	15.6	5.6	0.6	16.8	9.4	FBG	500	3.95	PSOFC/GT

Reference	Fuel	Gasifying media	Syngas composition (volume %)						Calorific value (HHV) (MJ/Nm^3)	Gasifier used	Gasifier operating conditions		Plant type
			CO_2	H_2	N_2	CH_4	CO	H_2O			Temperature (°C)	Pressure (Atm.)	
Kuo & Wu, 2016	Raw wood	Steam (S/C:0.4)	0.7	38.5	0	0	60	0	29.3	FB	900	1	Three stage steam turbine
	TW	Steam (S/C:0.8)	0.6	38	0	0	61.4	0	29.46	FB	900	1	
	Coal	Steam (S/C:1.35)	0.5	42	0	0	57	0	28.4	FB	900	1	

*: *other gas composition not given; EBG: Entrained bed gasifier; FBG: fluidized bed gasifier; Sub: Subcritical conditions; Sup: Supercritical; U: Ultra-supercritical; MBM: Meat bone meal; CFB: Circulatory fluidized bed; BFB: Bubbling fluidized bed; EFG: Entrained flow gasifier; HP: High pressure; MP: Medium pressure; LP: Low pressure; FB:Fixedbed;TW: torrefied wood; ccs: CO_2 captured; CHP: combined heat and power; ADGT: Aeroderivative gas turbine; UGT: utility gas turbine; S/B: Steam to biomass ratio*

Table 2.11. CO_2 based gasifying media power plant calculations with CCS

Reference	Fuel	Gasifying media	Syngas composition (volume %)						Calorific value (HHV) (MJ/Nm^3)	Gasifier used	Gasifier operating conditions		Plant type	Plant efficiency %
			CO_2	H_2	N_2	CH_4	CO	H_2O			Temperature (°C)	Pressure (Atm.)		
Hasegawa, 2012	Coal	CO_2/O_2 (ER-2.58)	4.9	23.8	1.5	0.3	66.2	3.2	11.5	EFG	1257	-	IGCC	41.9_{te}
Prabu & Geeta, 2015;Marcourt et al., 1983	Coal	CO_2/O_2 (0.99)	25.5	9.1	0.5	1.7	63.1	0	9.86_c	UCG	1200-1500	27	IGCC/UCG	41 $_{ccs}$
	Coal	CO_2/O_2 (2.98)	56	5.6	0.5	1.3	36.5	0	5.87_c	UCG	1200-1500	3.6	UCG	27 $_{ccs}$
	Coal	CO_2/O_2 (0.99)	25.2	9	0.5	2.5	6.3	0	9.8_c	UCG	1200-1500	9.42	PEMFC/IGCC	37.95 $_{ccs}$
	Coal	CO_2/O_2 (0.99)	25.2	9	0.5	2.5	6.3	0	9.8_c	UCG	1200-1500	9.42	PEMFC/IGCC/ CLR	43.59 $_{ccs}$
Prabu, 2015; Marcourt et al., 1983	Coal	CO_2/O_2 (2.98)	56	5.6	0.5	1.3	36.5	0	5.87_C	UCG	1200-1500	3.6	CLC/ST (3 stage)	29.42 $_{ccs}$ Sub 32.55 $_{ccs}$ Sup 35.4 $_{ccs}$ U
	Coal	CO_2/O_2 (0.99)	25.2	9	0.5	2.5	6.3	0	9.8_c	UCG	1200-1500	9.42	CLC/GT/ST /air turbine	42.53 $_{ccs}$
Marcourt et al., 1983	Coal	CO_2/O_2 (2.03)	39	5.2	0.3	1.8	53.3	-	8_c	Packed bed	>1200	9.17		
	Coal	CO_2/O_2 (1.95)	41	6.4	0.2	2.2	49.5	-	7.8_c	Packed bed	>1200	26.64		

Liang et al., 2017	Coal	CO_2/O_2 (0.79/0.21)	72.5	6.7	0	3	18.2	-	4.35_c	CFB	~1000	1	-	-

te: thermal efficiency; ccs: CO_2 captured; Sub: subcritical conditions; Sup: Supercritical conditions; U: Ultra supercritical conditions; RW: raw wood; TW: torrefied wood; CFB: Circulatory fluidized bed; BFB: Bubbling fluidized bed; EFG: Entrained flow gasifier; CLC: chemical looping combustion; CLR: Chemical looping reforming; ER: Equivalent ratio; S/C: Steam to carbon ratio

2.3.3. Utilizing CO_2 as a moderator

CO_2/O_2 mixture can be used in combustion instead of air. Using this mixture requires the use of air separation unit (ASU) and carbon capture and storage unit (CCS). Due to this capital cost increases significantly. This consequently affects cost of electricity (LCOE).

2.3.3.1. Oxy-fuel combustion of coal

The CO_2 concentration in the flue gas of conventional pulverised fuel plants is rather low, typically between 10 and 15%(Ahn et al., 2014). Oxy-fuel combustion aims to increase the concentration of CO_2 in the effluent stream, by using CO_2 as the moderating medium in the oxidant, thereby making the capture of CO_2 from the process more economical. In oxy-fuel combustion, the oxygen is diluted with RFG instead of nitrogen. In oxy-fuel combustion technology, the final flue gas contains mostly CO_2, H_2O (steam) and trace amounts of fuel N_2, sulphur impurities etc. A pure stream of CO_2 flue gas can be obtained on condensation of steam in a condenser. In this technology, the utilization of oxygen leads to a high temperature combustion front and therefore, it is essential to control the adiabatic flame temperature (AFT) due to material constraints of the boiler and operating temperatures of the power systems. The AFT can be controlled by the addition or recycling of the end products of combustion such as CO_2 and H_2O.

Riaza et al. investigated the ignition temperature and burnout of a semi-anthracite and a high volatile bituminous coal under oxy-fuel combustion conditions(Riaza et al., 2011). They found that in an atmosphere of 21 vol% O_2 and 79 vol% CO_2, the ignition temperature of coal was higher and the burnout was lower than in air due to the higher specific molar heat of CO_2 compared with N_2 and the lower molecular diffusivity of O_2 in CO_2 than in N_2. When the O_2 concentration under oxy-fuel conditions was increased to between 30 – 35 vol%, the ignition temperature was lower than in air and the burnout value was higher.

The key issues which must be considered are: heat transfer, fuel ignition and combustion stability, char combustion rates, pollutant formation, gas cleaning systems and selection of the type of recycle flue gas. Due to the different heat transfer properties of CO_2 in comparison to N_2, the transitions between the controlling reaction regimes are altered.

Table 2.12. Advantages and disadvantages of oxy-fuel combustion (Buhre et al., 2005)

Advantages	Disadvantages
• Industry familiar with oxy-fuel combustion and it potentially represents a lower commercial and technical risk than pre-combustion CO_2 capture, eg. gasification technology.	• Significantly reduced efficiency compared with existing PF technology.
• Can deliver near zero emissions.	• Not yet demonstrated at commercial scale, so technical and commercial risks remain.
• Has potential to be retrofitted to existing plants as either oxy-fuel with CO_2 liquefaction or as direct flue gas liquefaction.	• May require SO_x removal.
• Can be implemented in new plants by modifying furnace and boiler technologies commonly used in power industry.	• Large oxygen separation plant required compared to other near-zero technologies.
• Low NOx emissions relative to conventional PF technology.	• Oxy-fuel is based on near-zero emissions and electricity generation and cannot be adapted to production of hydrogen.
	• Relies on carbon sequestration, for which suitable sites may not be available or possible to permit in locations desirable for operation of oxy-fuel combustion power plants.

One of the main advantages of oxy-fuel combustion is that the technology is quite similar to existing combustion power plant technology and may be retrofitted to existing furnaces/boilers. It can deliver near-zero CO_2 emissions and significant reductions in NO_x and SO_x emissions depending upon specific design choices. The main disadvantages with oxy-fuel technology are the reduced efficiency of plant, due to additional power consumption for oxygen separation, flue gas recycle and CO_2 compression. Table 2.12 provides a summary of the main advantages and disadvantages of oxy-fuel combustion. A major hurdle to development and deployment of commercial oxy-fuel power plants is that the CO_2 must be sequestered and there are significant challenges in developing and permitting sequestration sites. To date, most CO_2 sequestration sites have been used for

enhanced oil recovery, where the geology and reservoirs are well known and there is an economic driver to inject CO_2.

2.3.3.2. Oxyfuel Combustion of Wastes

The application of oxy-fuel combustion to the processing of waste feedstocks is immature, with research and development efforts just starting to emerge. The major challenge of processing waste feedstocks at industrial scale is their variability and heterogeneous nature.

Ding et al. developed a steady-state process model of the oxy-fuel combustion of municipal solid waste in Aspen Plus(Ding et al., 2018b). The model was validated against the conventional air-blown incineration plant and the model was used to explore a range of oxy-fuel combustion scenarios. Fu et al. evaluated the techno-economics of oxy-enriched combustion of MSW and found that using 25% O_2-enriched air yielded similar combustion characteristics as co-incineration with 20% mass ratio of coal(Fu et al., 2015). Tang et al. investigated the enrichment of heavy metals in MSW ashes during oxy-fuel combustion(Tang et al., 2015). The replacement of N_2 with CO_2 in the carrier gas was found to delay oxidation of the feed, which could be compensated for by increasing the O_2 concentration in the oxidant. High concentrations of CO_2 also promoted the formation of secondary products such as H_2, CO and CH_4(López-González et al., 2017). Similarly, Chen et al. found that replacing N_2 by CO_2 also delayed the drying and devolatization stages during oxy-fuel combustion of petrochemical wastewater(J. Chen et al., 2015).

Jang et al. conducted combustion experiments with waste sludge at air and oxy-fuel conditions in a circulating fluidized bed reactor(Jang et al., 2016). They found temperature for combustion of the waste sludge was 800°C and that the flue-gas temperatures of oxy-fuel combustion with O_2 in the range of 21-25 vol% were higher than other scenarios investigated. Heavy and trace metals in bottom ashes were markedly increased for the case of 40 vol% O_2 during oxy-fuel combustion, while heavy and trace metals in the fly ashes were not significantly affected(Jang et al., 2016). Sung et al. investigated the co-combustion of sewage sludge and wood pellets, under oxy-fuel conditions using a circulating fluidised bed(Sung et al., 2018). Stable burning was achieved across a range of conditions, with the sludge proportion being varied from 30% to 100% of the feed. The flue gas temperatures under oxy-fuel conditions were highly

dependent on volatile matter content of fuel. Higher content of wood pellets in fuel mixture (sewage sludge and wood pellet mixture) significantly increased flue gas temperature.

Coal which has been main the source of generating power in India. Most of the coal resources in Indian context are of low quality containing high ash. Power from coal can be generated by combustion and gasification processes. Utilizing wastes with coal can not only decrease carbon footprint but also help in managing landfills. Combustion of MSW is one of the most common methods to treat it. Gasification of wastes is an important process to help in recycling and produce energy or various chemicals. Utilizing CO_2 for combustion of wastes can produce flue gas with high concentration CO_2. The flue gas can be purified to remove pollutants to achieve high purity CO_2 which can be used for various applications (Enhanced oil recovery) or sequestration. This can decrease net CO_2 emissions. Using CO_2 as a combustion or gasifying media helps in decreasing pollutants like (NO_X and SO_X).

2.4. Research Gaps

Based on the literature review, the following research gaps are found.

- The literature lacks studies on co-gasification of HAC and plastics under CO_2 conditions. The impact of CO_2 on the co-gasification of plastics and coal is yet to be reported. The reaction mechanism and physical changes in the coal structure occurring during the gasification process are not reported.
- Techno-economic studies on utilizing HAC with MSW in thermal power plant industries has not been performed. Further, the impact of carbon capture on MSW based power plants has not yet been explored.

2.5 Research objectives and scope

The main aim of this thesis is to study the impact of waste utilization along with HAC for syngas production and electricity generation under CO_2 atmosphere. Based on the literature gap, the following objectives are framed,

1. To conduct laboratory scale fixed bed reactor studies by CO_2 and N_2 pyrolysis and gasification of plastic wastes such as high density polyethylene (HDPE) and Covid plastic wastes with HAC to analyze the interaction between these wastes.

2. Study of the co-gasification of HAC with electronic wastes such as PCB under CO_2 conditions. Impact of addition of PCB fuels (PCB plastic, PCB resin PCB mixture) on coal gasification process.
3. Kinetic studies on the HAC with the waste plastics under CO_2 conditions
4. Characterization of gasification residue, tar and syngas generated during N_2 pyrolysis and CO_2 gasification.
5. Execution of co-combustion of MSW and Indian coals (HAC and low ash coal (LAC)) under air and oxy-fuel conditions to analyze the performance of thermal power plants by energy, economic and environmental analysis using Aspen plus software.

The scope of the present work is to conduct fixed bed reactor experiments using three different solid feedstocks such as (i) HAC, (ii) HDPE, (iii) PCB and their individual components such plastics, resins etc. and (iv) Covid based waste based plastics (overall gown) under N_2 and CO_2 atmospheres. Thermogravimetric analysis are conducted using these plastics to estimate the kinetic parameters. Using Aspen plus software, the impact of co-combustion of MSW with two types of Indian coal (high ash coal and low ash coal) under air and oxy-fuel conditions on the thermal efficiency of the power plants in terms of net efficiency, specific CO_2 emissions and levelized cost of electricity (LCOE) is evaluated.

The results of these studies are explained in the subsequent chapters.

References

Acomb, J. C., Nahil, M. A., & Williams, P. T. (2013). Thermal processing of plastics from waste electrical and electronic equipment for hydrogen production. *Journal of Analytical and Applied Pyrolysis*, *103*, 320–327. https://doi.org/10.1016/j.jaap.2012.09.014

Ahn, S., Choi, G., & Kim, D. (2014). The effect of wood biomass blending with pulverized coal on combustion characteristics under oxy-fuel condition. *Biomass and Bioenergy*, *71*, 144–154. https://doi.org/10.1016/j.biombioe.2014.10.014

Akkache, S., Hernández, A. B., Teixeira, G., Gelix, F., Roche, N., & Ferrasse, J. H. (2016). Co-gasification of wastewater sludge and different feedstock: Feasibility

study. *Biomass and Bioenergy*, *89*, 201–209. https://doi.org/10.1016/j.biombioe.2016.03.003

Ali, O. H., Hossein, G., & Hooman, F. (2013). Energy Efficiency Improvement Analysis Considering Environmental Aspects in Regard to Biomass Gasification PSOFC/GT Power Generation System. *Procedia Environmental Sciences*, *17*, 831–841. https://doi.org/10.1016/j.proenv.2013.02.101

Ali, S. M., Pervaiz, A., Afzal, B., Hamid, N., & Yasmin, A. (2014). Open dumping of municipal solid waste and its hazardous impacts on soil and vegetation diversity at waste dumping sites of Islamabad city. *Journal of King Saud University - Science*, *26*(1), 59–65. https://doi.org/10.1016/j.jksus.2013.08.003

Ankit, Saha, L., Kumar, V., Tiwari, J., Sweta, Rawat, S., Singh, J., & Bauddh, K. (2021). Electronic waste and their leachates impact on human health and environment: Global ecological threat and management. *Environmental Technology and Innovation*, *24*, 102049. https://doi.org/10.1016/j.eti.2021.102049

Aranda, G., Grootjes, A. J., Meijden, C. M. Van Der, Drift, A. Van Der, Gupta, D. F., Sonde, R. R., Poojari, S., & Mitra, C. B. (2016). Conversion of high-ash coal under steam and CO 2 gasi fi cation conditions. *Fuel Processing Technology*, *141*, 16–30. https://doi.org/10.1016/j.fuproc.2015.06.006

Arena, U., & Di Gregorio, F. (2014). Energy generation by air gasification of two industrial plastic wastes ina pilot scale fluidized bed reactor. *Energy*, *68*, 735–743. https://doi.org/10.1016/j.energy.2014.01.084

Arena, U., Zaccariello, L., & Mastellone, M. L. (2010). Fluidized bed gasification of waste-derived fuels. *Waste Management*, *30*(7), 1212–1219. https://doi.org/10.1016/j.wasman.2010.01.038

Azam, M., Jahromy, S. S., Raza, W., Jordan, C., Harasek, M., & Winter, F. (2019). Comparison of the combustion characteristics and kinetic study of coal, municipal solid waste, and refuse-derived fuel: Model-fitting methods. *Energy Science and Engineering*, *7*(6), 2646–2657. https://doi.org/10.1002/ese3.450

Aznar, M. P., Caballero, M. A., Sancho, J. A., & Francés, E. (2006). Plastic waste elimination by co-gasification with coal and biomass in fluidized bed with air in

pilot plant. *Fuel Processing Technology*, *87*(5), 409–420. https://doi.org/10.1016/j.fuproc.2005.09.006

Billaud, J., Valin, S., Peyrot, M., & Salvador, S. (2016). Influence of H_2O, CO_2 and O_2 addition on biomass gasification in entrained flow reactor conditions: Experiments and modelling. *Fuel*, *166*, 166–178. https://doi.org/10.1016/j.fuel.2015.10.046

Biomass explained Waste-to-energy (Municipal Solid Waste). (2018). EIA. https://www.eia.gov/energyexplained/biomass/waste-to-energy.php

Biswas, S., Choudhury, N., Sarkar, P., Mukherjee, A., Sahu, S. G., Boral, P., & Choudhury, A. (2006). Studies on the combustion behaviour of blends of Indian coals by TGA and Drop Tube Furnace. *Fuel Processing Technology*, *87*(3), 191–199. https://doi.org/10.1016/j.fuproc.2005.05.002

Brachi, P., Chirone, R., Miccio, F., Miccio, M., Picarelli, A., & Ruoppolo, G. (2014). Fluidized bed co-gasification of biomass and polymeric wastes for a flexible end-use of the syngas: Focus on bio-methanol. *Fuel*, *128*, 88–98. https://doi.org/10.1016/j.fuel.2014.02.070

Buhre, B. J. P., Elliott, L. K., Sheng, C. D., Gupta, R. P., & Wall, T. F. (2005). Oxy-fuel combustion technology for coal-fired power generation. *Progress in Energy and Combustion Science*, *31*(4), 283–307. https://doi.org/10.1016/j.pecs.2005.07.001

Butterman, H. C., & Castaldi, M. J. (2012). Experimental investigation of lignin decomposition and char structure during CO_2 and H_2O/N_2 gasification. *Waste and Biomass Valorization*, *3*(1), 49–60. https://doi.org/10.1007/s12649-011-9086-2

Chang, Q., Gao, R., Li, H., Dai, Z., Yu, G., Liu, X., & Wang, F. (2017). Effects of CO_2 on coal rapid pyrolysis behavior and chemical structure evolution. *Journal of Analytical and Applied Pyrolysis*, *128*(September), 370–378. https://doi.org/10.1016/j.jaap.2017.09.012

Chen, J., Mu, L., Cai, J., Yao, P., Song, X., Yin, H., & Li, A. (2015). Pyrolysis and oxy-fuel combustion characteristics and kinetics of petrochemical wastewater sludge using thermogravimetric analysis. *Bioresource Technology*, *198*, 115–123. https://doi.org/10.1016/j.biortech.2015.09.011

Chen, W., Chen, Y., Shu, Y., He, Y., & Wei, J. (2021). Characterization of solid, liquid

and gaseous products from waste printed circuit board pyrolysis. *Journal of Cleaner Production*, *313*(January), 127881. https://doi.org/10.1016/j.jclepro.2021.127881

Choi, M. J., Jeong, Y. S., & Kim, J. S. (2021). Air gasification of polyethylene terephthalate using a two-stage gasifier with active carbon for the production of H2 and CO. *Energy*, *223*. https://doi.org/10.1016/j.energy.2021.120122

Cormos, A. M., Dinca, C., & Cormos, C. C. (2015). Multi-fuel multi-product operation of IGCC power plants with carbon capture and storage (CCS). *Applied Thermal Engineering*, *74*(2015), 20–27. https://doi.org/10.1016/j.applthermaleng.2013.12.080

Cormos, C. C. (2012). Integrated assessment of IGCC power generation technology with carbon capture and storage (CCS). *Energy*, *42*(1), 434–445. https://doi.org/10.1016/j.energy.2012.03.025

Craig, K. R., & Mann, M. K. (2014). *Cost and Performance Analysis of Biomass-Based Integrated Gasification Combined-Cycle (BIGCC) Power Systems* (Vol. 24, Issue 6).

Dai, L., Zhou, N., Lv, Y., Cheng, Y., Wang, Y., Liu, Y., Cobb, K., Chen, P., Lei, H., & Ruan, R. (2022). Pyrolysis technology for plastic waste recycling: A state-of-the-art review. *Progress in Energy and Combustion Science*, *93*(September 2021), 101021. https://doi.org/10.1016/j.pecs.2022.101021

Diaz, L. F., Savage, G. M., & Eggerth, L. L. (2005). Production of Refuse-Derived Fuel (RDF). *Solid Waste Management*, 295–302. http://www.unep.org/ietc/InformationResources/Publications/SolidWasteManagementPublication/tabid/79356/Default.aspx

Ding, G., He, B., Cao, Y., Wang, C., Su, L., Duan, Z., Song, J., Tong, W., & Li, X. (2018a). Process simulation and optimization of municipal solid waste fired power plant with oxygen/carbon dioxide combustion for near zero carbon dioxide emission. *Energy Conversion and Management*, *157*(December 2017), 157–168. https://doi.org/10.1016/j.enconman.2017.11.087

Ding, G., He, B., Cao, Y., Wang, C., Su, L., Duan, Z., Song, J., Tong, W., & Li, X. (2018b). Process simulation and optimization of municipal solid waste fired power

plant with oxygen/carbon dioxide combustion for near zero carbon dioxide emission. *Energy Conversion and Management*, *157*(May 2017), 157–168. https://doi.org/10.1016/j.enconman.2017.11.087

Duan, L., Zhao, C., Zhou, W., Qu, C., & Chen, X. (2009). Investigation on coal pyrolysis in CO2 atmosphere. *Energy and Fuels*, *23*(7), 3826–3830. https://doi.org/10.1021/ef9002473

Duan, Y., Duan, L., Wang, J., & Anthony, E. J. (2019). Observation of simultaneously low CO, NOx and SO_2 emission during oxy-coal combustion in a pressurized fluidized bed. *Fuel*, *242*(January), 374–381. https://doi.org/10.1016/j.fuel.2019.01.048

Eriksson, O., & Finnveden, G. (2009). Plastic waste as a fuel-CO_2-neutral or not? *Energy and Environmental Science*, *2*, 907–914. https://doi.org/DOI:10.1039/b908135f

Erkiaga, A., Lopez, G., Amutio, M., Bilbao, J., & Olazar, M. (2013). Syngas from steam gasification of polyethylene in a conical spouted bed reactor. *Fuel*, *109*, 461–469. https://doi.org/10.1016/j.fuel.2013.03.022

Fang, S., Gu, W., Dai, M., Xu, J., Yu, Z., Lin, Y., Chen, J., & Ma, X. (2018). A study on microwave-assisted fast co-pyrolysis of chlorella and tire in the N_2 and CO_2 atmospheres. *Bioresource Technology*, *250*(November 2017), 821–827. https://doi.org/10.1016/j.biortech.2017.11.080

Fang, S., Yu, Z., Lin, Y., Lin, Y., Fan, Y., Liao, Y., & Ma, X. (2016). Effects of additives on the co-pyrolysis of municipal solid waste and paper sludge by using thermogravimetric analysis. *Bioresource Technology*, *209*, 265–272. https://doi.org/10.1016/j.biortech.2016.03.027

Farrow, T. S., Sun, C., & Snape, C. E. (2015). Impact of CO_2 on biomass pyrolysis, nitrogen partitioning, and char combustion in a drop tube furnace. *Journal of Analytical and Applied Pyrolysis*, *113*, 323–331. https://doi.org/10.1016/j.jaap.2015.02.013

Ferronato, N., & Torretta, V. (2019). Waste mismanagement in developing countries: A review of global issues. *International Journal of Environmental Research and Public Health*, *16*(6). https://doi.org/10.3390/ijerph16061060

Finkel, A. (2017). Independent Reveiw Into Future Security of National Energy Market. *Journal of Chemical Information and Modeling*, *8*(1), 43. http://www.environment.gov.au/system/files/resources/1d6b0464-6162-4223-ac08-3395a6b1c7fa/files/electricity-market-review-final-report.pdf

Fremaux, S., Beheshti, S. M., Ghassemi, H., & Shahsavan-Markadeh, R. (2015). An experimental study on hydrogen-rich gas production via steam gasification of biomass in a research-scale fluidized bed. *Energy Conversion and Management*, *91*, 427–432. https://doi.org/10.1016/j.enconman.2014.12.048

Friengfung, P., Jamkrajang, E., Sunphorka, S., Kuchonthara, P., & Mekasut, L. (2014). *NiO / Dolomite Catalyzed Steam / O_2 Gasification of Di ff erent Plastics and Their Mixtures*.

Fu, Z., Zhang, S., Li, X., Shao, J., Wang, K., & Chen, H. (2015). MSW oxy-enriched incineration technology applied in China: Combustion temperature, flue gas loss and economic considerations. *Waste Management*, *38*(1), 149–156. https://doi.org/10.1016/j.wasman.2014.12.026

Gao, S. P., Zhao, J. T., Wang, Z. Q., Wang, J. F., Fang, Y. T., & Huang, J. J. (2013). Effect of CO_2 on pyrolysis behaviors of lignite. *Ranliao Huaxue Xuebao/Journal of Fuel Chemistry and Technology*, *41*(3), 257–264. https://doi.org/10.1016/s1872-5813(13)60017-1

Gill, Y. Q., Khurshid, M., Abid, U., & Ijaz, M. W. (2022). Review of hospital plastic waste management strategies for Pakistan. *Environmental Science and Pollution Research*, *29*(7), 9408–9421. https://doi.org/10.1007/s11356-021-17731-9

Gracida-Alvarez, U. R., Mitchell, M. K., Sacramento-Rivero, J. C., & Shonnard, D. R. (2018). Effect of Temperature and Vapor Residence Time on the Micropyrolysis Products of Waste High Density Polyethylene. *Industrial and Engineering Chemistry Research*, *57*(6), 1912–1923. https://doi.org/10.1021/acs.iecr.7b04362

Guizani, C., Escudero Sanz, F. J., & Salvador, S. (2014). Effects of CO_2 on biomass fast pyrolysis: Reaction rate, gas yields and char reactive properties. *Fuel*, *116*, 310–320. https://doi.org/10.1016/j.fuel.2013.07.101

Guo, Q., Yue, X., Wang, M., & Liu, Y. (2010). Pyrolysis of scrap printed circuit board

plastic particles in a fluidized bed. *Powder Technology*, *198*(3), 422–428. https://doi.org/10.1016/j.powtec.2009.12.011

Hanaoka, T., Hiasa, S., & Edashige, Y. (2013). Syngas production by gasification of aquatic biomass with CO2/O2 and simultaneous removal of H_2S and COS using char obtained in the gasification. *Biomass and Bioenergy*, *59*, 448–457. https://doi.org/10.1016/j.biombioe.2013.08.017

Hanaoka, T., Sakanishi, K., & Okumura, Y. (2012). The effect of $N_2/CO_2/O_2$ content and pressure on characteristics and CO_2 gasification behavior of biomass-derived char. *Fuel Processing Technology*, *104*, 287–294. https://doi.org/10.1016/j.fuproc.2012.05.024

Hannah, R., & Max, R. (2022). *Plastic Pollution*. https://ourworldindata.org/plastic-pollution

Hao, J., Wang, H., Chen, S., Cai, B., Ge, L., & Xia, W. (2014). Pyrolysis characteristics of the mixture of printed circuit board scraps and coal powder. *Waste Management*, *34*(10), 1763–1769. https://doi.org/10.1016/j.wasman.2013.10.043

Hasegawa, T. (2012). Development of Semiclosed Cycle Gas Turbine for Oxy-Fuel IGCC Power Generation with CO_2 Capture. *Intech*, 13. http://dx.doi.org/10.1039/C7RA00172J%0Ahttps://www.intechopen.com/books/advanced-biometric-technologies/liveness-detection-in-biometrics%0Ahttp://dx.doi.org/10.1016/j.colsurfa.2011.12.014

He, M., Xiao, B., Hu, Z., Liu, S., Guo, X., & Luo, S. (2009). Syngas production from catalytic gasification of waste polyethylene: Influence of temperature on gas yield and composition. *International Journal of Hydrogen Energy*, *34*(3), 1342–1348. https://doi.org/10.1016/j.ijhydene.2008.12.023

Heller, M. C., Keoleian, G. A., Mann, M. K., & Volk, T. A. (2004). Life cycle energy and environmental benefits of generating electricity from willow biomass. *Renewable Energy*, *29*(7), 1023–1042. https://doi.org/10.1016/j.renene.2003.11.018

Hla, S. S., Lopes, R., & Roberts, D. (2016). The CO2 gasification reactivity of chars produced from Australian municipal solid waste. *Fuel*, *185*, 847–854. https://doi.org/10.1016/j.fuel.2016.08.039

IEA (International Energy Agency). (2020). Key World Energy Statistics 2020. *Int. Energy Agency*, *33*(August), 4649. https://www.iea.org/reports/key-world-energy-statistics-2020

Jamil, K., Hayashi, J. I., & Li, C. Z. (2004). Pyrolysis of a Victorian brown coal and gasification of nascent char in CO2 atmosphere in a wire-mesh reactor. *Fuel*, *83*(7–8), 833–843. https://doi.org/10.1016/j.fuel.2003.09.017

Jang, H. N., Kim, J. H., Back, S. K., Sung, J. H., Yoo, H. M., Choi, H. S., & Seo, Y. C. (2016). Combustion characteristics of waste sludge at air and oxy-fuel combustion conditions in a circulating fluidized bed reactor. *Fuel*, *170*, 92–99. https://doi.org/10.1016/j.fuel.2015.12.033

Jayaraman, K., Gökalp, I., & Jeyakumar, S. (2017). Estimation of synergetic effects of CO2 in high ash coal-char steam gasification. *Applied Thermal Engineering*, *110*, 991–998. https://doi.org/10.1016/j.applthermaleng.2016.09.011

Jiang, L., Yang, X. R., Gao, X., Xu, Q., Das, O., Sun, J. H., & Kuzman, M. K. (2020). Pyrolytic kinetics of polystyrene particle in nitrogen atmosphere: Particle size effects and application of distributed activation energy method. *Polymers*, *12*(2). https://doi.org/10.3390/polym12020421

Jie, G., Ying-Shun, L., & Mai-Xi, L. (2008). Product characterization of waste printed circuit board by pyrolysis. *Journal of Analytical and Applied Pyrolysis*, *83*(2), 185–189. https://doi.org/10.1016/j.jaap.2008.08.007

Joseph, B., James, J., Kalarikkal, N., & Thomas, S. (2021). Recycling of medical plastics. *Advanced Industrial and Engineering Polymer Research*, *4*(3), 199–208. https://doi.org/10.1016/j.aiepr.2021.06.003

Joshi, R., & Ahmed, S. (2016). Status and challenges of municipal solid waste management in India: A review. *Cogent Environmental Science*, *2*(1), 1–18. https://doi.org/10.1080/23311843.2016.1139434

Kartik, S., Balsora, H. K., Sharma, M., Saptoro, A., Jain, R. K., Joshi, J. B., & Sharma, A. (2022). Valorization of plastic wastes for production of fuels and value-added chemicals through pyrolysis – A review. *Thermal Science and Engineering Progress*, *32*(April), 101316. https://doi.org/10.1016/j.tsep.2022.101316

Khoo, H. H. (2019). LCA of plastic waste recovery into recycled materials, energy and fuels in Singapore. *Resources, Conservation and Recycling*, *145*(November 2017), 67–77. https://doi.org/10.1016/j.resconrec.2019.02.010

Kim, J. W., Mun, T. Y., Kim, J. O., & Kim, J. S. (2011). Air gasification of mixed plastic wastes using a two-stage gasifier for the production of producer gas with low tar and a high caloric value. *Fuel*, *90*(6), 2266–2272. https://doi.org/10.1016/j.fuel.2011.02.021

Kim, Y. M., Han, T. U., Kim, S., Jae, J., Jeon, J. K., Jung, S. C., & Park, Y. K. (2017). Catalytic co-pyrolysis of epoxy-printed circuit board and plastics over HZSM-5 and HY. *Journal of Cleaner Production*, *168*, 366–374. https://doi.org/10.1016/j.jclepro.2017.08.224

Kulkarni, B. N. (2020). Environmental sustainability assessment of land disposal of municipal solid waste generated in Indian cities – A review. *Environmental Development*, *33*, 100490. https://doi.org/10.1016/j.envdev.2019.100490

Kumar, R., Elliott, L. K., Wall, T. F., Liu, Y., & Moghtaderi, B. (2009). Differences in reactivity of pulverised coal in air (O_2/N_2) and oxy-fuel (O_2/CO_2) conditions. *Fuel Processing Technology*, *90*(6), 797–802. https://doi.org/10.1016/j.fuproc.2009.02.009

Kuo, P., & Wu, W. (2016). Thermodynamic analysis of a combined heat and power system with CO_2 utilization based on co-gasi fi cation of biomass and coal. *Chemical Engineering Science*, *142*, 201–214. https://doi.org/10.1016/j.ces.2015.11.030

Lai, Z. Y., Ma, X. Q., Tang, Y. T., & Lin, H. (2011). A study on municipal solid waste (MSW) combustion in N_2/O_2 and CO_2/O_2 atmosphere from the perspective of TGA. *Energy*, *36*(2), 819–824. https://doi.org/10.1016/j.energy.2010.12.033

Lee, J., Choi, D., Tsang, Y. F., Oh, J. I., & Kwon, E. E. (2017). Employing CO_2 as reaction medium for in-situ suppression of the formation of benzene derivatives and polycyclic aromatic hydrocarbons during pyrolysis of simulated municipal solid waste. *Environmental Pollution*, *224*, 476–483. https://doi.org/10.1016/j.envpol.2017.02.028

Lee, J., Lee, T., Tsang, Y. F., Oh, J. I., & Kwon, E. E. (2017). Enhanced energy recovery

from polyethylene terephthalate via pyrolysis in CO_2 atmosphere while suppressing acidic chemical species. *Energy Conversion and Management*, *148*, 456–460. https://doi.org/10.1016/j.enconman.2017.06.026

Lee, T., Lee, J., Ok, Y. S., Oh, J. I., Lee, S. R., Rinklebe, J., & Kwon, E. E. (2017). Utilizing CO2 to suppress the generation of harmful chemicals from thermal degradation of polyvinyl chloride. *Journal of Cleaner Production*, *162*, 1465–1471. https://doi.org/10.1016/j.jclepro.2017.06.181

Li, J., Burra, K. R. G., Wang, Z., Liu, X., & Gupta, A. K. (2021). Co-gasification of high-density polyethylene and pretreated pine wood. *Applied Energy*, *285*(September 2020), 116472. https://doi.org/10.1016/j.apenergy.2021.116472

Liang, C., Zhang, H., Zhu, Z., Na, Y., & Lu, Q. (2017). CO_2-O_2 gasification of a bituminous coal in circulating fluidized bed. *Fuel*, *200*, 81–88. https://doi.org/10.1016/j.fuel.2017.03.032

Lin, K. H., & Chiang, H. L. (2014). Liquid oil and residual characteristics of printed circuit board recycle by pyrolysis. *Journal of Hazardous Materials*, *271*, 258–265. https://doi.org/10.1016/j.jhazmat.2014.02.031

Liszka, M., Malik, T., Budnik, M., & Zie, A. (2013). *Comparison of IGCC (integrated gasi fi cation combined cycle) and CFB (circulating fl uidized bed) cogeneration plants equipped with CO_2 removal*. *58*. https://doi.org/10.1016/j.energy.2013.05.005

Long, L., Sun, S., Zhong, S., Dai, W., Liu, J., & Song, W. (2010). Using vacuum pyrolysis and mechanical processing for recycling waste printed circuit boards. *Journal of Hazardous Materials*, *177*(1–3), 626–632. https://doi.org/10.1016/j.jhazmat.2009.12.078

López-González, D., Parascanu, M. M., Fernandez-Lopez, M., Puig-Gamero, M., Soreanu, G., Avalos-Ramírez, A., Valverde, J. L., & Sanchez-Silva, L. (2017). Effect of different concentrations of O_2 under inert and CO_2 atmospheres on the swine manure combustion process. *Fuel*, *195*, 23–32. https://doi.org/10.1016/j.fuel.2017.01.041

Lopez, G., Artetxe, M., Amutio, M., Alvarez, J., Bilbao, J., & Olazar, M. (2018). Recent

advances in the gasi fi cation of waste plastics . A critical overview. *Renewable and Sustainable Energy Reviews*, *82*(May 2017), 576–596. https://doi.org/10.1016/j.rser.2017.09.032

Lu, K. M., Lee, W. J., Chen, W. H., & Lin, T. C. (2013). Thermogravimetric analysis and kinetics of co-pyrolysis of raw/torrefied wood and coal blends. *Applied Energy*, *105*, 57–65. https://doi.org/10.1016/j.apenergy.2012.12.050

Marcourt, M., Paquay, V., Pie, A., Federal, G., & Fontaine, M.-. (1983). *Coal gasification at pressure by mixtures carbon dioxide and oxygen*. *62*, 823–828.

Martínez-Lera, S., Torrico, J., Pallarés, J., & Gil, A. (2013). Design and first experimental results of a bubbling fluidized bed for air gasification of plastic waste. *Journal of Material Cycles and Waste Management*, *15*(3), 370–380. https://doi.org/10.1007/s10163-013-0129-6

Meng, A., Chen, S., Long, Y., Zhou, H., Zhang, Y., & Li, Q. (2015). Pyrolysis and gasification of typical components in wastes with macro-TGA. *Waste Management*, *46*, 247–256. https://doi.org/10.1016/j.wasman.2015.08.025

Meng, F., Yu, J., Tahmasebi, A., & Han, Y. (2013). Pyrolysis and combustion behavior of coal gangue in O_2/CO_2 and O_2/N_2 mixtures using thermogravimetric analysis and a drop tube furnace. *Energy and Fuels*, *27*(6), 2923–2932. https://doi.org/10.1021/ef400411w

Michaels, T., & Krishnan, K. (2018). *Energy recovery council 2018 directory of waste-to energy facilities*.

Muthuraman, M., Namioka, T., & Yoshikawa, K. (2010). A comparative study on co-combustion performance of municipal solid waste and Indonesian coal with high ash Indian coal: A thermogravimetric analysis. *Fuel Processing Technology*, *91*(5), 550–558. https://doi.org/10.1016/j.fuproc.2009.12.018

Naidu, V. S., Aghalayam, P., & Jayanti, S. (2016). Evaluation of CO_2 gasification kinetics for low-rank Indian coals and biomass fuels. *Journal of Thermal Analysis and Calorimetry*, *123*(1), 467–478. https://doi.org/10.1007/s10973-015-4930-4

Nie, C., Wang, Y., Zhang, H., Zhang, Y., Zhang, Y., Yan, Z., Li, B., Lyu, X., Tao, Y., Qiu, J., Li, L., Zhang, G., & Zhu, X. (2020). Cleaner utilization of non-metallic

components in separation tailings of waste printed circuit board : Pyrolysis oil , calorific value and building aggregate. *Journal of Cleaner Production*, *258*, 120976. https://doi.org/10.1016/j.jclepro.2020.120976

Nixon, J. D., Dey, P. K., & Ghosh, S. K. (2017). Energy recovery from waste in India: An evidence-based analysis. *Sustainable Energy Technologies and Assessments*, *21*, 23–32. https://doi.org/10.1016/j.seta.2017.04.003

Organisation for Economic Co-operation and Development (OECD). (2022). *Plastic pollution is growing relentlessly as waste management and recycling fall short, says OECD*. OECD Better Policies for Better Lives. https://www.oecd.org/environment/plastic-pollution-is-growing-relentlessly-as-waste-management-and-recycling-fall-short.htm

Pacioni, T. R., Soares, D., Domenico, M. Di, Rosa, M. F., Moreira, R. de F. P. M., & José, H. J. (2016). Bio-syngas production from agro-industrial biomass residues by steam gasification. *Waste Management*, *58*, 221–229. https://doi.org/10.1016/j.wasman.2016.08.021

Park, Y. K., Han, T. U., Jeong, J., & Kim, Y. M. (2019). Debrominated high quality oil production by the two-step catalytic pyrolysis of phenolic printed circuit boards (PPCB) using natural clays and HY. *Journal of Hazardous Materials*, *367*(December 2018), 50–58. https://doi.org/10.1016/j.jhazmat.2018.12.040

Perkins, G., & Vairakannu, P. (2017). Considerations for oxidant and gasifying medium selection in underground coal gasification. *Fuel Processing Technology*, *165*, 145–154. https://doi.org/10.1016/j.fuproc.2017.05.010

Pinto, F, Franco, C., André, R. N., Miranda, M., Gulyurtlu, I., & Cabrita, I. (2002). Co-gasification study of biomass mixed with plastic wastes. *Fuel*, *81*(3), 291–297. https://doi.org/10.1016/S0016-2361(01)00164-8

Pinto, Filomena, André, R., Miranda, M., Neves, D., Varela, F., & Santos, J. (2016). Effect of gasification agent on co-gasification of rice production wastes mixtures. *Fuel*, *180*, 407–416. https://doi.org/10.1016/j.fuel.2016.04.048

Pinto, Filomena, André, R. N., Franco, C., Lopes, H., Gulyurtlu, I., & Cabrita, I. (2009). Co-gasification of coal and wastes in a pilot-scale installation 1: Effect of catalysts

in syngas treatment to achieve tar abatement. *Fuel*, *88*(12), 2392–2402. https://doi.org/10.1016/j.fuel.2008.12.012

Pinto, Filomena, Franco, C., André, R. N., Tavares, C., Dias, M., Gulyurtlu, I., & Cabrita, I. (2003). Effect of experimental conditions on co-gasification of coal, biomass and plastics wastes with air/steam mixtures in a fluidized bed system. *Fuel*, *82*(15–17), 1967–1976. https://doi.org/10.1016/S0016-2361(03)00160-1

Prabu, V. (2015). Integration of in-situ CO_2-oxy coal gasification with advanced power generating systems performing in a chemical looping approach of clean combustion. *Applied Energy*, *140*(x), 1–13. https://doi.org/10.1016/j.apenergy.2014.11.056

Prabu, V., & Geeta, K. (2015). CO 2 enhanced in-situ oxy-coal gasification based carbon-neutral conventional power generating systems. *Energy*, *84*, 672–683. https://doi.org/10.1016/j.energy.2015.03.029

Quan, C., Li, A., & Gao, N. (2010). Synthesis of carbon nanotubes and porous carbons from printed circuit board waste pyrolysis oil. *Journal of Hazardous Materials*, *179*(1–3), 911–917. https://doi.org/10.1016/j.jhazmat.2010.03.092

Qureshi, M. S., Oasmaa, A., Pihkola, H., Deviatkin, I., Tenhunen, A., Mannila, J., Minkkinen, H., Pohjakallio, M., & Laine-Ylijoki, J. (2020). Pyrolysis of plastic waste: Opportunities and challenges. *Journal of Analytical and Applied Pyrolysis*, *152*(March). https://doi.org/10.1016/j.jaap.2020.104804

Ragazzi, M., Rada, E. C., Panaitescu, V., & Aposto, T. (2007). Municipal solid waste pre-treatment: A comparison between two dewatering options. *WIT Transactions on Ecology and the Environment*, *102*, 943–949. https://doi.org/10.2495/SDP070902

Rajaeifar, M. A., Ghanavati, H., Dashti, B. B., Heijungs, R., Aghbashlo, M., & Tabatabaei, M. (2017). Electricity generation and GHG emission reduction potentials through different municipal solid waste management technologies: A comparative review. *Renewable and Sustainable Energy Reviews*, *79*(January), 414–439. https://doi.org/10.1016/j.rser.2017.04.109

Reena, G., Sangita, & Verinder, K. (2011). Ft-ir studies of e-plastic obtained from obsolete computers. *Journal of Chemical and Pharmaceutical Research*, *3*(5), 660–667.

Riaza, J., Álvarez, L., Gil, M. V., Pevida, C., Pis, J. J., & Rubiera, F. (2011). Effect of oxy-fuel combustion with steam addition on coal ignition and burnout in an entrained flow reactor. *Energy*, *36*(8), 5314–5319. https://doi.org/10.1016/j.energy.2011.06.039

Richardson, Y., Drobek, M., Julbe, A., Blin, J., & Pinta, F. (2015). Biomass Gasification to Produce Syngas. In *Recent Advances in Thermo-Chemical Conversion of Biomass* (pp. 213–250). Elsevier. https://doi.org/https://doi.org/10.1016/B978-0-444-63289-0.00008-9

Robinson, T., Bronson, B., Gogolek, P., & Mehrani, P. (2016). Comparison of the air-blown bubbling fluidized bed gasification of wood and wood-PET pellets. *Fuel*, *178*, 263–271. https://doi.org/10.1016/j.fuel.2016.03.038

Ruoppolo, G., Ammendola, P., Chirone, R., & Miccio, F. (2012). H 2-rich syngas production by fluidized bed gasification of biomass and plastic fuel. *Waste Management*, *32*(4), 724–732. https://doi.org/10.1016/j.wasman.2011.12.004

Saini, S., Rao, P., & Patil, Y. (2012). City Based Analysis of MSW to Energy Generation in India, Calculation of State-Wise Potential and Tariff Comparison with EU. *Procedia - Social and Behavioral Sciences*, *37*, 407–416. https://doi.org/10.1016/j.sbspro.2012.03.306

Salbidegoitia, J. A., Fuentes-Ordóñez, E. G., González-Marcos, M. P., González-Velasco, J. R., Bhaskar, T., & Kamo, T. (2015). Steam gasification of printed circuit board from e-waste: Effect of coexisting nickel to hydrogen production. *Fuel Processing Technology*, *133*, 69–74. https://doi.org/10.1016/j.fuproc.2015.01.006

Scarlat, N., Fahl, F., & Dallemand, J. F. (2019). Status and Opportunities for Energy Recovery from Municipal Solid Waste in Europe. *Waste and Biomass Valorization*, *10*(9), 2425–2444. https://doi.org/10.1007/s12649-018-0297-7

Shaddix, C. R., & Molina, A. (2011). Fundamental investigation of NOx formation during oxy-fuel combustion of pulverized coal. *Proceedings of the Combustion Institute*, *33*(2), 1723–1730. https://doi.org/10.1016/j.proci.2010.07.072

Shen, B., & Qinlei. (2006). Study on MSW catalytic combustion by TGA. *Energy Conversion and Management*, *47*(11–12), 1429–1437.

https://doi.org/10.1016/j.enconman.2005.08.016

Shen, G. D., Wang, Z. Q., Wu, J. L., He, T., Li, J. Q., Yang, J., & Wu, J. H. (2016). Combustion characteristics of low-rank coal chars in O_2/CO_2, O_2/N_2 and O_2/Ar by TGA. *Ranliao Huaxue Xuebao/Journal of Fuel Chemistry and Technology*, *44*(9), 1066–1073. https://doi.org/10.1016/s1872-5813(16)30048-2

Singh, S., Wu, C., & Williams, P. T. (2012). Pyrolysis of waste materials using TGA-MS and TGA-FTIR as complementary characterisation techniques. *Journal of Analytical and Applied Pyrolysis*, *94*, 99–107. https://doi.org/10.1016/j.jaap.2011.11.011

Somaiya, K. (2016). *Power Generation From Municipal Solid Waste*. http://164.100.47.193/lsscommittee/Energy/16_Energy_20.pdf

Spörl, R., Maier, J., & Scheffknecht, G. (2013). Sulphur oxide emissions from dust-fired oxy-fuel combustion of coal. *Energy Procedia*, *37*(0), 1435–1447. https://doi.org/10.1016/j.egypro.2013.06.019

Subramanian, A. K., Thayalan, D., Edwards, A. I., Almalki, A., & Venugopal, A. (2021). Biomedical waste management in dental practice and its significant environmental impact: A perspective. *Environmental Technology and Innovation*, *24*, 101807. https://doi.org/10.1016/j.eti.2021.101807

Sues, A., Juraščík, M., & Ptasinski, K. (2010). Exergetic evaluation of 5 biowastes-to-biofuels routes via gasification. *Energy*, *35*(2), 996–1007. https://doi.org/10.1016/j.energy.2009.06.027

Sung, J. H., Back, S. K., Jeong, B. M., Kim, J. H., Choi, H. S., Jang, H. N., & Seo, Y. C. (2018). Oxy-fuel co-combustion of sewage sludge and wood pellets with flue gas recirculation in a circulating fluidized bed. *Fuel Processing Technology*, *172*(December 2017), 79–85. https://doi.org/10.1016/j.fuproc.2017.12.005

Tahmasebi, A., Kassim, M. A., Yu, J., & Bhattacharya, S. (2013). Thermogravimetric study of the combustion of Tetraselmis suecica microalgae and its blend with a Victorian brown coal in O_2/N_2 and O_2/CO_2 atmospheres. *Bioresource Technology*, *150*, 15–27. https://doi.org/10.1016/j.biortech.2013.09.113

Tang, Y. T., Ma, X. Q., Yu, Q. H., Zhang, C., Lai, Z., & Zhang, X. (2015). Heavy metal

enrichment characteristics in ash of municipal solid waste combustion in CO2/O2 atmosphere. *Waste Management*, *43*, 247–254. https://doi.org/10.1016/j.wasman.2015.06.024

Valérie Masson-Delmotte, Pörtner, H.-O., Skea, J., Zhai, P., Roberts, D., & Priyadarshi R. Shukla. (2018). IPCC report Global warming of 1.5°C. In *Global Warming of 1.5°C. An IPCC Special Report on the impacts of global warming of 1.5°C above pre-industrial levels and related global greenhouse gas emission pathways, in the context of strengthening the global response to the threat of climate change*, (Vol. 2, Issue October). www.environmentalgraphiti.org

Valin, S., Bedel, L., Guillaudeau, J., Thiery, S., & Ravel, S. (2016). CO_2 as a substitute of steam or inert transport gas in a fluidised bed for biomass gasification. *Fuel*, *177*, 288–295. https://doi.org/10.1016/j.fuel.2016.03.020

Vallero, D. (2019). *Air Pollution Calculations: Quantifying Pollutant Formation, Transport,Transformation, Fate and Risks*. Elsevier.

Vejerano, E. P., Leon, E. C., Holder, A. L., & Marr, L. C. (2014). Characterization of particle emissions and fate of nanomaterials during incineration. *Environmental Science: Nano*, *1*(2), 133–143. https://doi.org/10.1039/c3en00080j

Vermesan, H., Tiuc, A.-E., & Purcar, M. (2020). Advanced Recovery Techniques for Waste Materials from IT and Telecommunication Equipment Printed Circuit Boards. *Sustainability*, *12(1)*, 74. https://doi.org/doi:10.3390/su12010074

Wang, Q., Li, K., Guo, Z., Fang, M., Luo, Z., & Cen, K. (2018). Effects of CO_2 atmosphere on slow pyrolysis of high-ash lignite. *Carbon Resources Conversion*, *1*(1), 94–103. https://doi.org/10.1016/j.crcon.2018.04.002

Wang, Z., Li, J., Burra, K. G., Liu, X., Li, X., Zhang, M., Lei, T., & Gupta, A. K. (2021). Synergetic Effect on CO_2-Assisted Co-Gasification of Biomass and Plastics. *Journal of Energy Resources Technology, Transactions of the ASME*, *143*(3), 1–9. https://doi.org/10.1115/1.4048062

Wilk, V., & Hofbauer, H. (2013). Conversion of mixed plastic wastes in a dual fluidized bed steam gasifier. *Fuel*, *107*, 787–799. https://doi.org/10.1016/j.fuel.2013.01.068

Wilk, Veronika, & Hofbauer, H. (2013). Co-gasification of plastics and biomass in a dual

fluidized-bed steam gasifier: Possible interactions of fuels. *Energy and Fuels*, *27*(6), 3261–3273. https://doi.org/10.1021/ef400349k

Wu, C., & Williams, P. T. (2010). Pyrolysis-gasification of plastics, mixed plastics and real-world plastic waste with and without Ni-Mg-Al catalyst. *Fuel*, *89*(10), 3022–3032. https://doi.org/10.1016/j.fuel.2010.05.032

Wu, W., & Qiu, K. (2014). Vacuum co-pyrolysis of Chinese fir sawdust and waste printed circuit boards. Part I: Influence of mass ratio of reactants. *Journal of Analytical and Applied Pyrolysis*, *105*, 252–261. https://doi.org/10.1016/j.jaap.2013.11.011

Yamawaki, T. (2003). The gasification recycling technology of plastics WEEE containing brominated flame retardants. *Fire and Materials*, *27*(6), 315–319. https://doi.org/10.1002/fam.833

Yuzbasi, N. S., & Selçuk, N. (2011). Air and oxy-fuel combustion characteristics of biomass/lignite blends in TGA-FTIR. *Fuel Processing Technology*, *92*(5), 1101–1108. https://doi.org/10.1016/j.fuproc.2011.01.005

Zaccariello, L., & Mastellone, M. L. (2015). Fluidized-bed gasification of plastic waste, wood, and their blends with coal. *Energies*, *8*(8), 8052–8068. https://doi.org/10.3390/en8088052

Zellagui, S., Schönnenbeck, C., Zouaoui-Mahzoul, N., Leyssens, G., Authier, O., Thunin, E., Porcheron, L., & Brilhac, J. F. (2016). Pyrolysis of coal and woody biomass under N2 and CO2 atmospheres using a drop tube furnace - Experimental study and kinetic modeling. *Fuel Processing Technology*, *148*, 99–109. https://doi.org/10.1016/j.fuproc.2016.02.007

Zhang, F., Zhao, Y., Wang, D., Yan, M., Zhang, J., Zhang, P., Ding, T., Chen, L., & Chen, C. (2021). Current technologies for plastic waste treatment: A review. *Journal of Cleaner Production*, *282*, 124523. https://doi.org/10.1016/j.jclepro.2020.124523

Zhang, H., Xiao, R., Wang, D., He, G., Shao, S., Zhang, J., & Zhong, Z. (2011). Biomass fast pyrolysis in a fluidized bed reactor under N_2, CO_2, CO, CH_4 and H_2 atmospheres. *Bioresource Technology*, *102*(5), 4258–4264. https://doi.org/10.1016/j.biortech.2010.12.075

Zhang, S., Yoshikawa, K., Nakagome, H., & Kamo, T. (2013). Kinetics of the steam

gasification of a phenolic circuit board in the presence of carbonates. *Applied Energy*, *101*, 815–821. https://doi.org/10.1016/j.apenergy.2012.08.030

Zhang, T., Mao, X., Qu, J., Liu, Y., Ali, A., & Ao, W. (2021). Microwave-assisted catalytic pyrolysis of waste printed circuit boards , and migration and distribution of bromine. *Journal of Hazardous Materials*, *402*(August 2020), 123749. https://doi.org/10.1016/j.jhazmat.2020.123749

Zhao, K., Jensen, A. D., & Glarborg, P. (2014). NO formation during oxy-fuel combustion of coal and biomass chars. *Energy and Fuels*, *28*(7), 4684–4693. https://doi.org/10.1021/ef402460h

Zhu, P., Chen, Y., Wang, L., Qian, G., Zhang, W. J., Zhou, M., & Zhou, J. (2013). Dissolution of brominated epoxy resins by dimethyl sulfoxide to separate waste printed circuit boards. *Environmental Science and Technology*, *47*(6), 2654–2660. https://doi.org/10.1021/es303264c

Zhu, S., Bai, Y., Hao, C., Li, F., & Bao, W. (2017). Investigation into the structural features and gasification reactivity of coal chars formed in CO_2 and N_2 atmospheres. *Journal of CO_2 Utilization*, *19*, 9–15. https://doi.org/10.1016/j.jcou.2017.02.017

Zhu, S., Bai, Y., Luo, K., Hao, C., Bao, W., & Li, F. (2017). Impacts of CO_2 on char structure and the gasification reactivity. *Journal of Analytical and Applied Pyrolysis*, *128*(November), 13–17. https://doi.org/10.1016/j.jaap.2017.11.005

Zhuo, Z., Liu, J., Sun, S., Sun, J., Kuo, J., Chang, K., Fu, J., & Wang, Y. (2017). Thermogravimetric characteristics of textile dyeing sludge, coal and their blend in N_2/O_2 and CO_2/O_2 atmospheres. *Applied Thermal Engineering*, *111*, 87–94. https://doi.org/10.1016/j.applthermaleng.2016.09.089

This page is left blank intentionally

CHAPTER 3

MATERIALS AND METHODOLOGY

In this chapter, the methods and procedures followed for characterization of the fuels used and subsequent products formed after gasification are described. Experimental procedure, feed preparation and operating conditions used for pyrolysis and gasification experiments are explained.

3.1. Fuel feedstock properties

In the present study, there were four fuel feedstocks used for gasification and pyrolysis experiments. The basic feed characterisation of the feedstocks such as high ash coal (HAC), high density polyethylene (HDPE), printed circuit board (PCB) and overall gown (OG) by proximate and ultimate analysis are given in Table 3.1. The calorific value of the fuels was estimated by a bomb calorimeter. HDPE was collected from Guwahati dumpsites by identifying with resin code. HDPE was also filed to produce a powdery mixture. PCB was collected from computer repair centres in a local market of Guwahati. PCB was a mixture of various metals, resins and plastics. In the present study, the components of PCB were segregated and their composition on weight basis is given in Table 3.2. PCB was broken into small pieces (20-30 mm) and it was separated into its components. PCB resin, plastics and metal components were powdered to -250 to +212 µm for the gasification experiments using a filer. The separated plastics and resins components of PCB were individually used as a feedstock with HAC for co-gasification operations. Further, a mixture of PCB components was prepared using the segregated metals, resins and plastics as per the composition given in Table 3.2. This mixture was used as a feedstock known as “PCB mixture”. Hence, three types of solid feed of PCB such as PCB mixture, PCB plastics and PCB resins were considered as fuel feed stock for gasification process. Another feedstock, overall gown, which is a biomedical plastic waste product, was made from plastic fibres. The OG used in the present study was brought from a pharmacy in Guwahati. OG was cut into smaller pieces by a scissor (20-30 mm). The photographs of fuel used is shown in Figure 3.1.

(a) HDPE (b) HAC (c) OG

(d) PCB Resin (e) PCB Plastic

Figure 3.1. Photographs of fuel used

Table 3.1. Proximate and ultimate analysis of fuels

	PCB Resin	PCB plastic	HAC	OG	HDPE
C	24.16	49.46	57.41	73.32	87.06
H	5.15	3.1	5.02	11.28	12.94
N	1.32	3.91	0.98	0.17	0
S	0	0	0	0	0
O	1.37	25.53	6.06	11.2	0
VM	29.7	49.8	19.47	89	100
FC	2.3	32.2	50	7.02	0
MC*	0	0	2	0	2
Ash	68	18	30.53	3.98	0
Calorific value (MJ/kg)	7.03	9.43	22.3	37.41	44.8

VM: volatile matter, FC: Fixed carbon, MC: moisture content; C.V: Calorific value (MJ/kg),
**As received basis, the rest are in dry basis*

Table 3.2. Composition of PCB mixture

Component	Weight, %
Copper	2.25
Aluminium	12.68
Tin aluminium alloy	5.49
PCB resin	60.95
PCB plastic	18.63

3.2. Experimental setup

All experiments were conducted using a laboratory scale fixed bed reactor. The experiments are conducted in batch mode. The schematic setup of the fixed bed reactor is given in Figure 3.2. The experiments were conducted at various operating temperatures. The temperature inside the reactor was measured by a K-type thermocouple. The fuel/fuel mixture was fed inside the reactor with the help of a hopper fixed at the top. Temperature inside the reactor was maintained by a PID controller. N_2/CO_2 gas cylinders were used to maintain inert/reactive atmosphere in the reactor and a gas flow rate of 0.3 litre per minute (LPM) was maintained using a mass flow controller (MFC) (Model: F-201-CV; Make M/s Boekhorst, Netherlands).

The syngas released during gasification/pyrolysis processes from the outlet of the reactor was passed through a condenser. A water chiller was used to cool the outlet water of the condenser and then, the cooled water is recirculated. After the removal of condensed gases, the syngas was sent through a bubble flow meter to measure the gas flow rate. The condensed gases such as tar/higher hydrocarbons in the condenser was recovered by washing it with a dichloromethane (DCM) solution. The liquid heavier hydrocarbons/tar components were dissolved in the DCM solution (Čepelioŋullar & Pütün, 2014). The DCM solution was recovered from the dissolved tar using a rotavapor (Model: R 300; Make M/s Buchi, Switzerland). The syngas obtained was collected in vacutainer tubes at different time intervals. The gas in the vacutainer tubes was analysed using a gas chromatograph. In Table 3.3, the list of experiments performed in this study is given. Experiments were conducted thrice in various conditions to detect repeatability of experiments.

Table 3.3. List of gasification experiments performed

Case	Fuels	Fuel ratio	Total fuel weight (gm)	Gas atmosphere	Temperature (°C)
1.	HAC	1	15	CO_2	900
			15		1000
			14		25-400
			14		25-600
			14		25-800
			14		25-1000
2.	HAC and OG	19:1	15	CO_2	1000
		9:1	15		1000
		17:3	15		1000
		4:1	15		1000
3.	HAC and PCB resin	4:1	15	CO_2	1000
	HAC and PCB plastic	4:1	15		1000
	HAC and PCB mixture	4:1	15		1000
4.	HAC and HDPE	1:1	14	CO_2	25-400
		1:1	14		25-600
		1:1	14		25-800
		1:1	14		25-1000
5.	PCB mixture	1	50	N_2 and CO_2	500
			50	N_2 and CO_2	700
			50	N_2 and CO_2	900
6.	PCB mixture	1	15	CO_2	1000
7.	OG	1	5	N_2 and CO_2	500
			5	N_2 and CO_2	700
			5	N_2 and CO_2	900

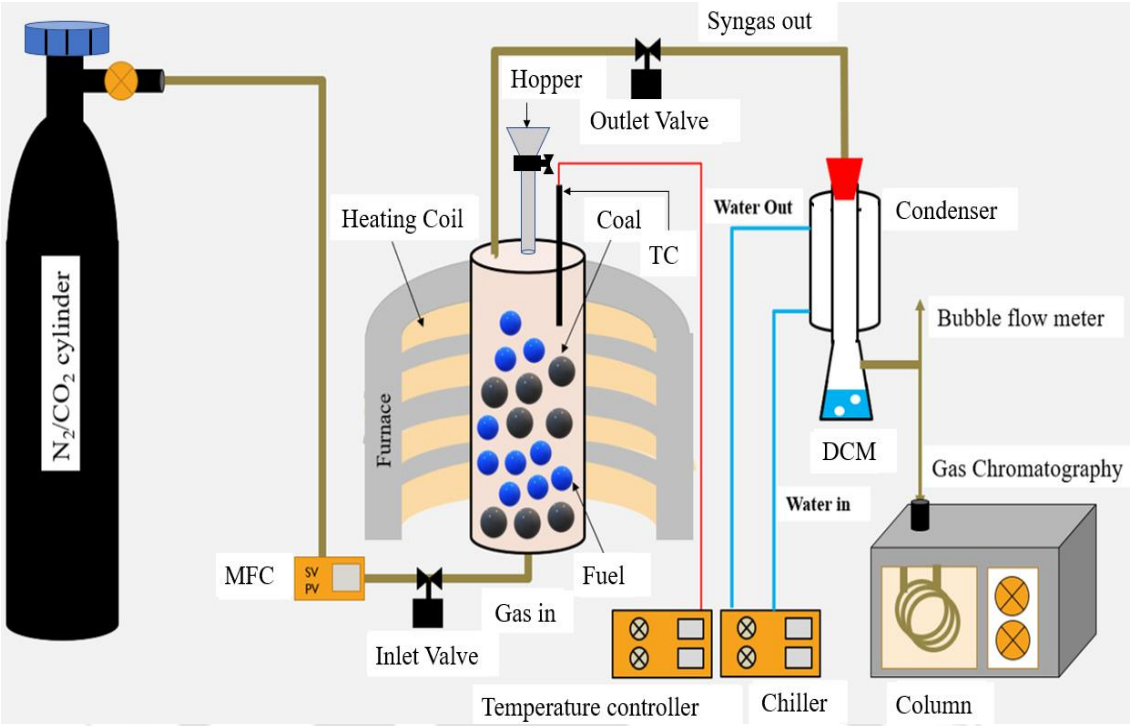

Figure 3.2. Schematic setup of fixed bed reactor *(*TC: K-type thermocouple)*

3.3. Characterization Methods

3.3.1. Proximate analysis

Proximate analysis of the fuel was used to estimate moisture content, ash, volatile matter and fixed carbon. This analysis has been performed according to Indian Standards IS:1350 (Bureau of Indian Standards, 1984). Muffle furnace and hot air oven were used for the analyses.

3.3.2. Ultimate analysis

By ultimate analysis of the fuels, the percentage of carbon, nitrogen, sulphur and hydrogen content in the fuel was estimated. Ultimate analysis was performed as per ASTM D 3176-09 standard using the facility available at Biotech Park, IIT Guwahati.

3.3.3. Calorific value of the feedstock

Calorific value of fuels is evaluated according to Indian Standards (IS: 1359- 1959) in a bomb calorimeter (Model: CC01/M3, Make: M/s Toshniwal Technologies Pvt. Ltd, India).

3.3.4. FTIR analysis

FTIR analysis of feed, residue and tar/oil samples obtained from various experiments was performed to examine the functional groups in the fuel. This analysis was carried out in the wavelength range of 400 to 4000 cm^{-1}. The dried KBr powder at 120°C was mixed with the fuel/residue powder in the ratio of 1:100 (KBr: fuel sample). A 100 mg of the prepared mixture is pelletized using a hydraulic press machine. FTIR analyses of these pellets were performed in the Centre of Environment, IIT Guwahati (Model: Spectrum two, Make: PerkinElmer, Singapore).

3.3.5. X- ray diffraction analysis (XRD)

XRD analysis of fuels is carried out to identify crystalline substances in the solid fuels scanned between 2θ ranges of 10-80° with a step size of 0.03°. This analysis was carried out for the ash components in the fuels to identify the metal oxides in clay components. Certain ash components like Na_2O, K_2O, CaO and MgO can act as catalyst in the gasification process. Alkali index of ash components is defined as the ratio of basic components (Na_2O, K_2O etc) to acidic components (SiO_2 and Al_2O_3) of ash (Hattingh et al., 2011).

$$Alkali\ index = Ash\% \times \left(\frac{Na_2O + MgO + CaO + K_2O + Fe_2O_3}{SiO_2 + Al_2O_3}\right) \quad (3.1)$$

High alkali index of the ash would enhance the gasification rate of the fuel. XRD (Model: Smartlab, Make: Rigaku Technologies, Japan) equipment in Central Instruments Facility (CIF), IIT Guwahati is used.

3.3.6. Field emission scanning electron microscope (FESEM) analysis

FESEM analysis of the solid fuel/residue samples was performed to examine their surface morphology. FESEM equipment (Model: Sigma 300, Make: M/s Zeiss, United Kingdom) in Central Instruments Facility, IIT Guwahati is used for the analysis.

3.3.7. Gas chromatography (GC)

A gas chromatograph was used to find the volume percentage each gas in the syngas mixture. Vacutainer tubes were used to collect and store the gases at various time intervals. The calibration of the gas chromatograph was done by using standard gases

brought from the vendor, Chemix specialty gases and equipment. Two types of detectors such as Thermal Conductivity Detector (TCD) and Flame Ionization Detector (FID) were used. In TCD, a carboxen column was used to analyse the permanent gases like H_2, N_2, CO, CH_4, CO_2, C_2H_2, C_2H_4 and C_2H_6. FID detector was used to analyse C_3 hydrocarbons in syngas. TG Bond-Q column was used in the FID detector with Argon as the carrier gas. The gas chromatograph (Model: CP-3800; Make M/s Varian, Netherland) in Chemical Engineering Department, IIT Guwahati was used for gas analysis.

3.3.8. Surface area and pore analysis

Surface area and pore diameter of the fresh fuels and residue obtained are estimated by BET analysis. Fuel and residue samples were dried at 125˚C to remove moisture content and further degassing was carried out at 125˚C for 4 hours. Liquid nitrogen (-196˚C) was used for adsorption and desorption on the surfaces and pores of the fuels/residues. BET analyser (Model: TriStar II, Make: Micromeretics, USA) in Dept. of Chemical Engineering, IIT Guwahati was used for the surface area and pore analysis.

3.3.9. Thermogravimetric analysis (TGA)

TGA studies were carried out to analyse pyrolysis and gasification behaviour of the fuel feedstocks under N_2 and CO_2 atmosphere. TGA (Model: TG 209 F1 Libra; Make M/s Netzsch, Germany) was carried out under non-isothermal conditions from 25 to 1000˚C. A 5 to 15 mg of the sample was used with N_2/CO_2 gas at a flow rate of 40 ml/min. TGA studies were conducted to analyse the reactivity of fuels and kinetic parameters (activation energy, Arrhenius constant and reaction order) by Coats-Redfern method.

3.3.9.1. Kinetic analysis

Coats-Redfern method is a kinetic model fitting method. The conversion of a fuel at any instant of the experiment can be defined as the amount of solid fuel converted to gaseous matter at that instant to the total mass of solid fuel reacted (Equation 3.2).

$$\alpha = \frac{m_o - m}{m_o - m_f} \tag{3.2}$$

In the above equation, α represents conversion, m_o, m and m_f represent the initial mass of fuel, mass of the fuel at any instant and mass of final sample left in the crucible, respectively.

$$\frac{d\alpha}{dt} = kf(\alpha) \tag{3.3}$$

Eq. 3.3 gives the expression for the decomposition of the fuel. 'k' is rate constant and f(α) is reaction model.

$$k = A \exp(-E/RT) \tag{3.4}$$

Rate constant is calculated using Equation 3.4, where 'A' is Arrhenius constant (s^{-1}), 'E' is activation energy (kJ/kmol) and T is temperature (K). 'R' is universal gas constant (8.314 $kJkmol^{-1}. K^{-1}$).

$$\frac{d\alpha}{dt} = A \exp\left(-\frac{E}{RT}\right).f(\alpha) \tag{3.5}$$

The above equation can also be represented by the following Equation 3.5 where β is heating rate.

$$\frac{d\alpha}{dT} = \frac{A}{\beta}\exp\left(-\frac{E}{RT}\right).f(\alpha) \tag{3.6}$$

The integral form of above equation can also be represented as,

$$\ln\left({}^{G(\alpha)}/_{T^2}\right) = \ln\left({}^{AR}/_{\beta E}\right) - E/RT \tag{3.7}$$

A graph was plotted between $\ln(G(\alpha)/T^2)$ and 1/T and the slope of the resultant line was used to calculate activation energy and the intercept of the plot was used to calculate Arrhenius constant (Noszczyk et al., 2021). In Table 3.4, the integral form of the reaction models is given.

Table 3.4. Reaction models

Reaction models	Integral form of reaction model (G(α))
First order model	$-\ln(1-\alpha)$
n^{th} order model	$[1-(1-\alpha)^{(1-n)}]^{-(1-n)}$
One dimensional diffusion model	α^2
2D diffusion model	$(1-\alpha)-\ln(1-\alpha)+\alpha$
3D diffusion model (Jander equation)	$(1-(1-\alpha)^{1/3})^2$
3D diffusion model (Ginstling - Brounshtein equation)	$\left(1-{}^{2\alpha}/_{3}\right)-(1-\alpha)^{2/3}$

3.3.9.2. Synergistic interactions between fuels

The comparison of the weight loss of the individual and co-feed conditions of the fuel samples provides the interaction between them. W_{act} is the actual weight loss of the blended fuels directly measured from TGA. W_{theo} is the estimated weight loss of the fuels for blended conditions using their individual weight loss found under unblended conditions. The following Equation is used to estimate W_{theo},

$$W_{theo} = X_1 W_1 + X_2 W_2 \quad (3.8)$$

X_1 and X_2 are the mass fractions of the fuels (0.5) and W_1 and W_2 are the individual weight loss of the fuels under unblended conditions. The synergism under blended conditions is determined by the following Equation 3.9.

$$\Delta W = W_{actual} - W_{theo} \quad (3.9)$$

If ΔW is positive, then the co-utilization of fuels has positive synergism whereas if it is negative, it indicates adverse effect.

3.4. Product Analysis

Tar and residue obtained from the experiments were analysed by various methods.

3.4.1. Product yield

Tar and residue obtained during/after gasification/pyrolysis process are weighed at the post operation stage. Residue and tar yield are calculated by the following Equation 3.10.

$$Yield_{R/T}\ (\%) = \frac{Weight\ of\ residue\ (or)\ tar}{Weight\ of\ feed}\ x\ 100 \quad (3.10)$$

$$Gas\ yield\ (\%) = 100 - tar\ yield - char\ yield \quad (3.11)$$

The remaining constituents are the gas and its yield is obtained using the Equation 3.11.

3.4.2. Syngas analysis

The flow rate of the syngas released was measured by a bubble flow meter. A graph is plotted between the gas flow rate and time elapsed during the experiments. The curve of the graph is integrated for the course of experiment and this gives the total amount of syngas generated (liters). This is represented in the equation 3.12.

$$V(liters) = \int_0^t v\,dt \tag{3.12}$$

'V' is the total volume of syngas generated, 'v' is the flow rate of syngas at any instant of time and 't' is total time period of the experiment. The volume of syngas generated per kg of the fuel used is calculated using the Equation 3.13.

$$Volume\ of\ syngas\ generated\ per\ kg\ of\ fuel\ \left(\frac{m^3}{kg}\right) = \frac{V}{M_{fuel}} \tag{3.13}$$

3.4.3. Carbon yield

Carbon yield is the ratio of carbon left in the residue to carbon initially present in the feed. The total carbon in the feed and residue is estimated by ultimate analysis and is used to calculate the carbon yield. Equation 3.14 is used estimate carbon yield.

$$Carbon\ yield\ (\%) = \frac{R \times R_C}{F \times F_C} \times 100 \tag{3.14}$$

'R' is the final weight of the residue obtained and 'R_C' is the percentage of carbon in the residue. 'F' is the initial weight of the feed and 'F_C' is the percentage of carbon in the feed.

References

Bureau of Indian Standards. (1984). *IS : 1350 (Part I) - 1984. Methods of test for coal and Coke. Part I Proximate Analysis (Reaffirmed 2001). 1*. https://law.resource.org/pub/in/bis/S11/is.1350.1.1984.pdf

Čepelioǂullar, Ö., & Pütün, A. E. (2014). Products characterization study of a slow pyrolysis of biomass-plastic mixtures in a fixed-bed reactor. *Journal of Analytical and Applied Pyrolysis*, *110*(1), 363–374. https://doi.org/10.1016/j.jaap.2014.10.002

Dhote, L., Ganduri, J., & Kumar, S. (2022). Evaluation of pyrolysis and gasification of distillery sludge and bio-compost mixed with coal. *Fuel*, *319*(February), 123750.

https://doi.org/10.1016/j.fuel.2022.123750

Hattingh, B. B., Everson, R. C., Neomagus, H. W. J. P., & Bunt, J. R. (2011). Assessing the catalytic effect of coal ash constituents on the CO_2 gasification rate of high ash , South African coal. *Fuel Processing Technology*, *92*(10), 2048–2054. https://doi.org/10.1016/j.fuproc.2011.06.003

Li, J., Burra, K. R. G., Wang, Z., Liu, X., & Gupta, A. K. (2021). Co-gasification of high-density polyethylene and pretreated pine wood. *Applied Energy*, *285*(September 2020), 116472. https://doi.org/10.1016/j.apenergy.2021.116472

Noszczyk, T., Dyjakon, A., & Koziel, J. A. (2021). Kinetic parameters of nut shells pyrolysis. *Energies*, *14*(3), 1–22. https://doi.org/10.3390/en14030682

Reyes, L., Abdelouahed, L., Campusano, B., Buvat, J. C., & Taouk, B. (2021). Exergetic study of beech wood gasification in fluidized bed reactor using CO_2 or steam as gasification agents. *Fuel Processing Technology*, *213*(November 2020), 106664. https://doi.org/10.1016/j.fuproc.2020.106664

This page is left blank intentionally

CHAPTER 4

CO-GASIFICATION OF INDIAN HIGH ASH COAL AND HIGH DENSITY POLYETHYLENE

In this chapter, the co-gasification of Indian high ash coal (HAC) and high-density polyethylene (HDPE) under CO_2 conditions has been carried out. Experiments have been carried out at various temperatures to analyze the impact of HDPE addition in the coal structure and composition of syngas. Experiments have been carried out with and without HDPE and further, kinetic analysis of co-pyrolysis and co-gasification of HAC with HDPE is carried by thermogravimetric analysis.

4.1. Experimental description

In this chapter, the co-gasification of HAC and HDPE using a thermogravimetric (TGA) apparatus and a fixed bed reactor is performed to evaluate their synergistic effects. Further, the kinetic parameters were estimated for the co-gasification reactions between HAC and HDPE. The effect of temperature on the char structure during the co-gasification of HDPE and HAC was evaluated at different temperature intervals from 400 to 1000˚C in a fixed bed reactor. The syngas composition obtained at different operating temperatures is analysed. Further the surface area and functional groups of the char were analysed by using a BET surface area analyser and FTIR instrument. Heating value of HDPE is almost double that of HAC (44.8 MJ/kg of HDPE and 22.3 MJ/kg of HAC). The list of experiments performed under CO_2 atmosphere is given in Table 4.1.

4.2. Co-pyrolysis and co-gasification of HAC with HDPE

In following sections kinetic analysis of HAC pyrolysis and co-pyrolysis with HDPE is reported. Gasification and co-gasification of the same is carried out in TGA instrument to estimate weight loss and kinetic triplets. Gasification and co-gasification experiments are carried out in fixed bed conditions.

Table 4.1. Summary of gasification and co-gasification experiments

Experiment	Sample	Temperature range (°C)
1	HAC	25-400
2	HAC	25-600
3	HAC	25-800
4	HAC	25-1000
5	HAC-HDPE (1:1)	25-400
6	HAC-HDPE (1:1)	25-600
7	HAC-HDPE (1:1)	25-800
8	HAC-HDPE (1:1)	25-1000

4.2.1. Thermogravimetric analysis

TGA and DTG graphs of the fuels are shown in Figure 4.1. A typical result, it can be observed that HDPE is completely volatilized at 500°C under the CO_2 atmosphere (Figure 4.1(a) and 4.1(c)). The maximum weight loss rate of HDPE under CO_2 conditions is higher than N_2 by 27% (Figure 4.1(c) and 4.1(d)). In HAC, there is only a 13.79% and 7.21% weight reduction by 500°C under CO_2 and N_2 atmosphere, respectively (Figure 4.1(a) and 4.1(b)). Interaction between CO_2 and HAC volatile matter could cause higher weight loss (6.58%) under gasification conditions. The lighter volatile gases are gradually liberated till 570˚C and then heavier volatiles are released at a slower rate than the lighter volatiles in HAC. There is no effective progress of gasification reaction that occurred above 900˚C in HAC. A higher weight loss with a total difference of 13.47% is estimated in the CO_2 atmosphere, compared to N_2 conditions in HAC above 900˚C. This difference in the weight loss during inert and reactive atmosphere is increased to 20% under the co-gasification conditions (Figure 4.1(a) and 4.1(b)). The temperature and range of weight loss of HAC and HDPE from the TGA are given in Table 4.2. T_i is the initial temperature denoting the beginning of volatile matter release and T_f is the complete devolatilization temperature. Volatile matter loss for HAC begins at 400˚C and in HDPE, it begins at 410˚C. As HDPE is a single species, the temperature range of HDPE degradation is low; whereas due to the presence of various species in HAC, it has a broader temperature range for the release of volatile matter. This range is similar to that observed by Meng et al. (Meng et al., 2015). This leads to a higher weight loss rate in HDPE as it is completely degraded in a particular temperature range.

Table 4.2. TGA and DTG of fuels and fuel blends

Fuel	T_i(ºC)	T_f(ºC)	DTG_{max}(ºC)	Range	$Rate_{max}$(%/min.)	Residue (wt. %)	ΔW	ΔC
CO_2 conditions								
HAC	400	572	508	172	1.74	64.12		
HDPE	410	493	466	83	31.76	0		
HAC-HDPE	413	500	473	87	13.81	22.27	9.79	0.16
N_2 conditions								
HAC	400	592	515	192	1.34	77.59		
HDPE	383	494	471	111	25.02	0		
HAC-HDPE	370	516	473	146	13.8	42.84	-4.04	-0.1

The maximum weight loss rate ($Rate_{max}$) of HDPE is 25.02 %/min, whereas it is 1.34 %/min for HAC under the inert atmosphere. $Rate_{max}$ increases in reactive (CO_2) atmosphere by 6.74 and 0.4 %/min in HDPE and HAC, respectively, compared to the inert atmosphere. DTG_{max} is the temperature at which the maximum weight loss rate occurred. The DTG_{max} of HDPE is less than HAC by around 40-44°C, compared to HAC in both atmospheres. DTG_{max} under co-pyrolysis and co-gasification conditions are very near to that of HAC. Temperature range in which volatile matter loss occurs is affected by HDPE addition. Temperature range in which volatile matter loss occurs decreases by 85°C and 46°C under co-gasification and co-pyrolysis conditions.

The effect of blending of HAC and HDPE on the weight loss and conversion is predicted by Equations 4.1 and 4.2,

$$W_{predicted} = X_1 W_{L1} + X_2 W_{L2} \quad (4.1)$$

$$\Delta W = W_{actual} - W_{predicted} \quad (4.2)$$

In Equation 4.1, X_1 and X_2 are the mass fractions of HAC and HDPE in the fuel blend, respectively. W_{L1} and W_{L2} denote the total weight loss of HAC and HDPE, respectively. ΔW represents the difference between the actual weight loss and predicted weight loss under the co-gasification conditions. Predicted weight loss is calculated by equation 4.2 based on the behaviour of individual fuel gasification and pyrolysis. Similarly, the conversion and their differences based on actual and predicted conditions (ΔC) are

estimated. The actual weight loss and the conversion under the co-gasification condition (CO_2 atmosphere) from TGA analysis are found as 77.73% and 91%, respectively, whereas, predicted weight loss and conversion using are 67.94% and 75%, respectively. Hence, one can notice the increase in weight loss by 9.79% and the conversion by 16% under the co-gasification conditions.

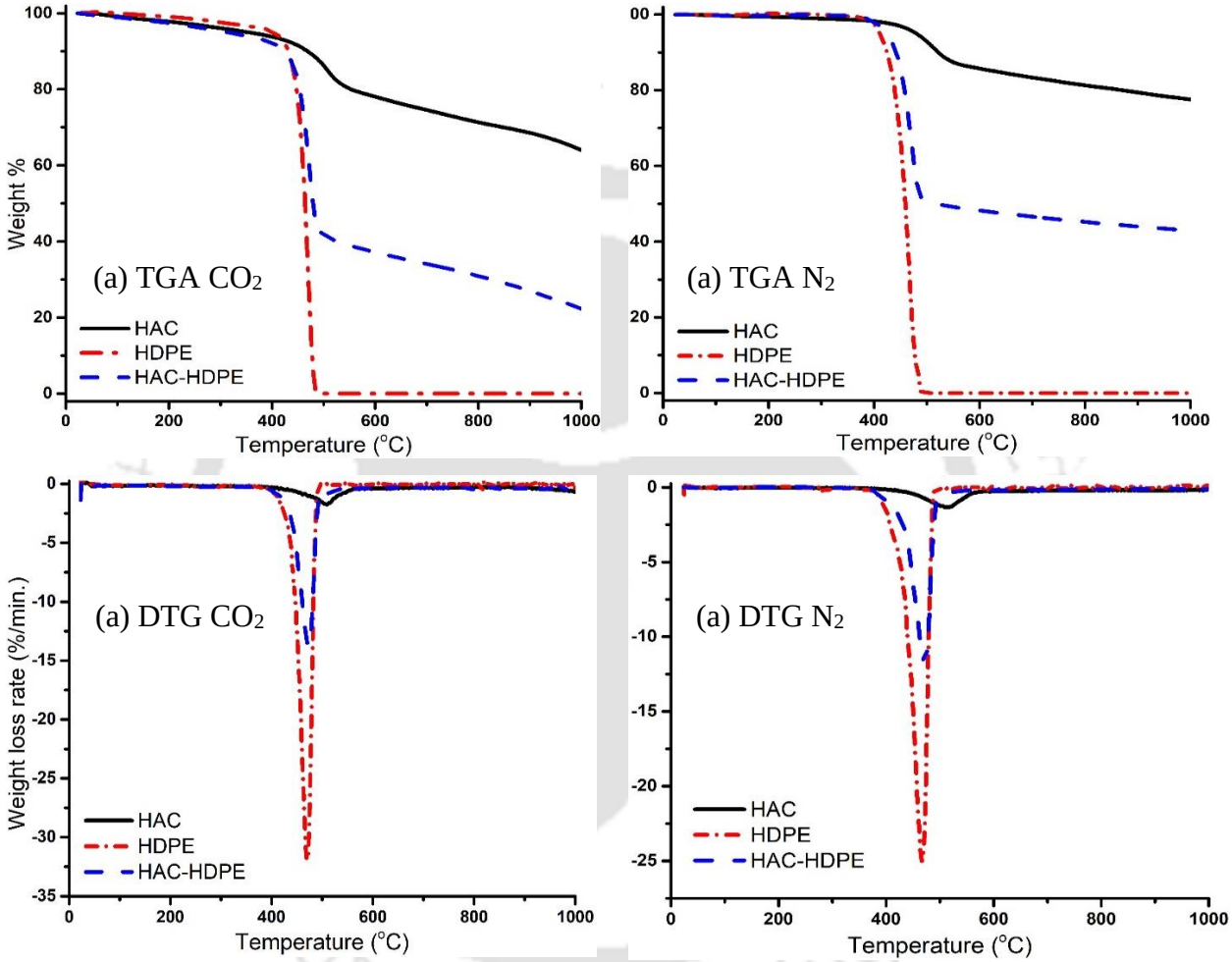

Figure 4.1. TGA and DTG curve of fuel and fuel blends

Predicted weight loss based on the individual behaviour of fuels during the release of volatile matter stage and char gasification stage is 54.92 and 2.22%, respectively. Corresponding actual weight losses at both stages are 54.09 and 4.63%, respectively. Although the difference in the weight loss is low in the volatile matter stage, there is an increase in the weight loss under the char gasification stage by 2.41%. Hence, the addition of HDPE alters the char structure and enhances char reactivity towards CO_2. The influence of HDPE addition in the char structure is further analyzed using SEM and BET equipment. Under N_2 conditions, the weight loss and conversion decreased under co-

pyrolysis conditions, which could be due to the blockage of pores in the coal char by the heavier hydrocarbons of the HDPE.

4.2.2. Kinetic analysis

The activation energy and Arrhenius constant of the gasification reactions under blended and unblended conditions of fuels are shown in Table 4.3 and 4.4. The activation energy was calculated in the temperature range between T_i and T_f for the volatile matter loss stage and gasification stage. It is found that the first-order homogeneous model can be the best fit for the volatile matter loss stage. Similar results were reported by Janajreh et al. (Janajreh et al., 2020). The activation energy for the volatile matter (VM) loss stage is the highest for HDPE (225.9 kJ/mol in N_2, 229.15 kJ/mol in CO_2) under both N_2 and CO_2 atmosphere. The estimated activation energy is found in line with the results of Meng et al. (Meng et al., 2015) (233 kJ/mol). In HAC, it was found that the activation energy under the CO_2 atmosphere is found low (29 kJ/mol), compared to the N_2 atmosphere (62 kJ/mol). Under blending conditions, the activation energy for volatile matter stage is lowered significantly (158 kJ/mol) as compared to pyrolysis conditions (180.4 kJ/mol).

The diffusional models were found to be the accurate fit in the char gasification stage (Fernandez et al., 2019). It was found that the 3-D diffusion model Jander equation (D3) was the most suitable and best fit for the char gasification stage. During char gasification reaction, diffusion of CO_2 through pores into reaction sites is predominant; whereas during the volatile matter stage (VM), HAC and HDPE undergo thermal degradation at moderate temperatures, homogeneous reaction order model is found to be the best fit at moderate temperatures. Hence, the model-fitting analysis reveals that the degradation follows different mechanisms at both weight reduction stages. The addition of HDPE increased activation energy in the gasification stage, using a 3-D model by 17.48 kJ/mol. This could be because of the breakage of bonds at higher temperatures.

Table 4.3. Activation energy of fuel and fuel blends by different models for volatile matter stage

Experiment	First-order			Second-order			Third-order		
	E (kJ/mol)	A (min^{-1})	R^2	E (kJ/mol)	A (min^{-1})	R^2	E (kJ/mol)	A (min^{-1})	R^2
HAC N_2	62.07	6.8×10^{3}	0.98	61.58	8.3×10^{3}	0.97	93.95	267.68	0.97
HAC CO_2	29.1	1.54×10^{6}	0.97	31.88	1.01×10^{6}	0.96	34.8	6.47×10^{5}	0.96
HDPE N_2	229.15	8.7×10^{12}	0.99	308.11	1.22×10^{19}	0.9	374.39	1.57×10^{24}	0.82
HDPE CO_2	225.88	3.9×10^{12}	0.98	291	4.7×10^{17}	0.81	391.4	2.3×10^{25}	0.71
HAC-HDPE N_2	180.4	1.5×10^{9}	0.99	217.38	1.2×10^{12}	0.97	178.5	2.5×10^{15}	0.94
HAC-HDPE CO_2	158.09	2.75×10^{7}	0.98	212.68	3.89×10^{11}	0.97	278.16	3.32×10^{16}	0.97

Table 4.4. Activation energy of fuel and fuel blends by different models for gasification stage

Experiment	D1 model			D2 model			D3 model			D4 model		
	E (kJ/mol)	A (min^{-1})	R^2	E (kJ/mol)	A (min^{-1})	R^2	E (kJ/mol)	A (min^{-1})	R^2	E (kJ/mol)	A (min^{-1})	R^2
HAC CO_2	13	5.8×10^{7}	0.96	15.42	9.6×10^{7}	0.96	18.09	3.4×10^{8}	0.973	16.31	4×10^{8}	0.97
HAC-HDPE CO_2	5.47	1.79×10^{7}	0.91	5.83	6.85×10^{6}	0.94	35.07	4.21×10^{6}	0.97	14.44	2.45×10^{7}	0.94

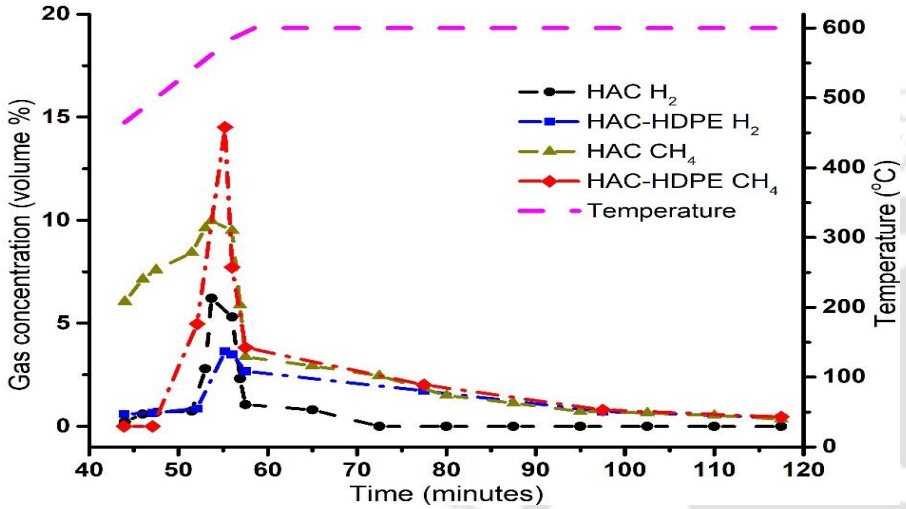

(a) 600ºC H_2 and CH_4

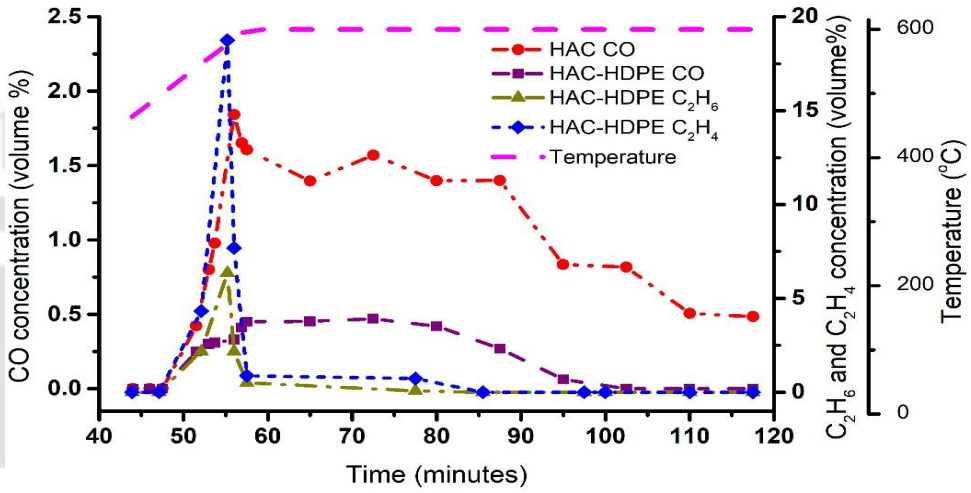

(b) 600ºC CO and C_2 compounds

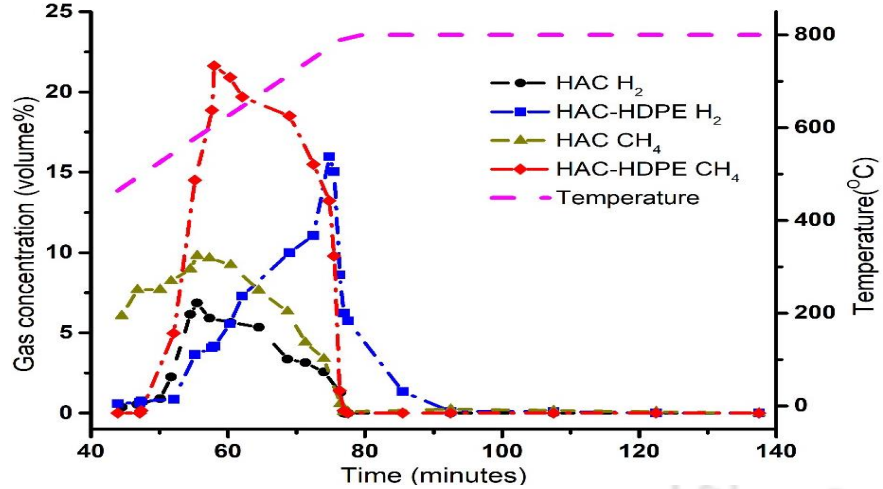

(c) 800ºC H_2 and CH_4

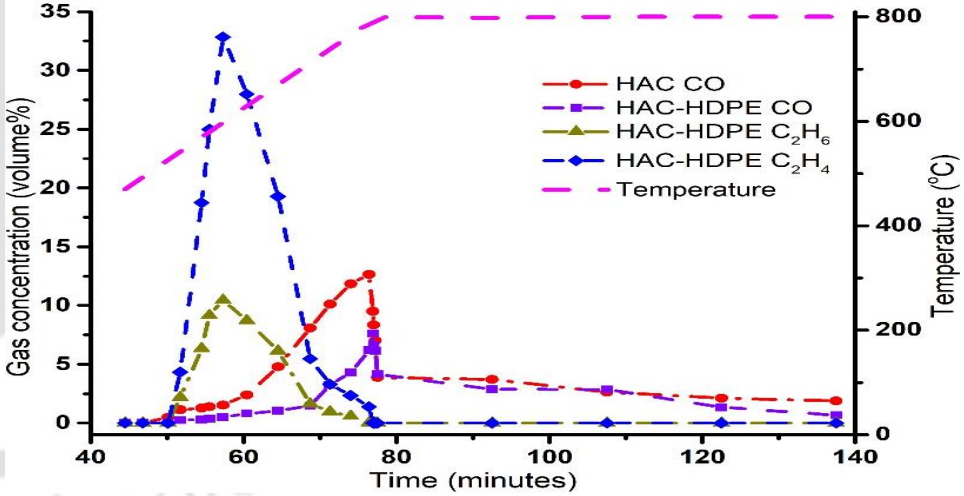

(d) 800ºC CO and C_2 compounds

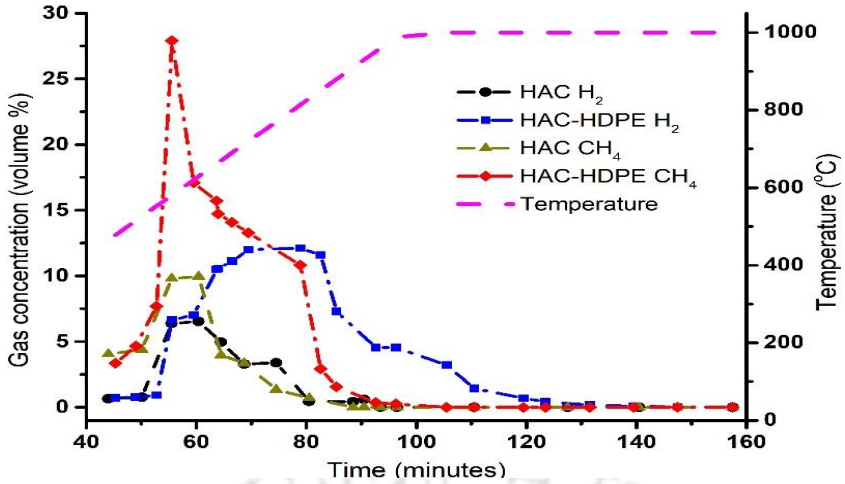

(e) 1000ºC H_2 and CH_4

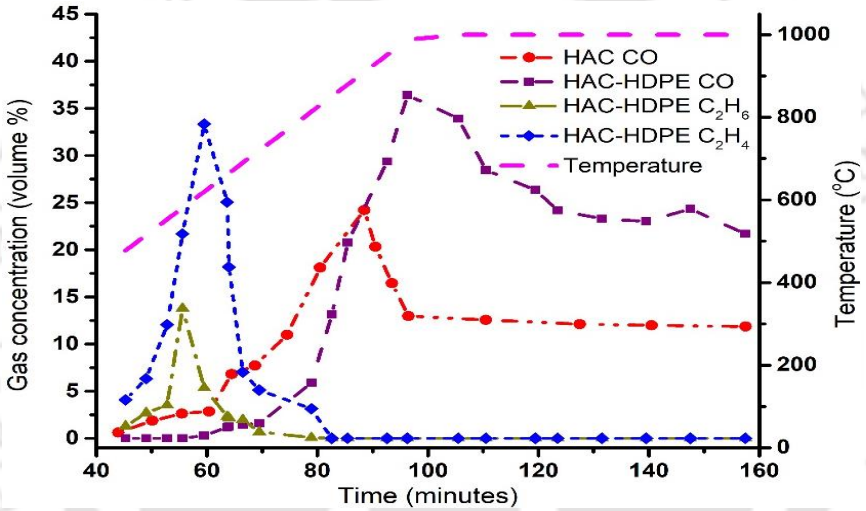

(f) 1000ºC CO and C_2 compounds

Figure 4.2. Variation of gas composition with operating temperature, HAC, and HAC-HDPE blend gasification at (a)&(b) 600ºC, (c)&(d) 800ºC and (e)&(f) 1000ºC

4.2.3. Fixed bed reactor studies

Fixed bed-based CO_2 gasification experiments are performed at 400, 600, 800, and 1000˚C with and without blending HAC and HDPE to observe the impact of HDPE addition on coal at various operating temperatures.

4.2.3.1. Effect of HDPE addition on syngas composition

The variation of syngas composition with operating temperatures for HAC and its blend with HDPE is given in Figure 4.2. At 400˚C, the thermal cracking of the HAC and HAC-HDPE blend has begun. The high concentration of gases such as H_2 and CH_4 could appear

at 550°C for both HAC and its blend with HDPE. There is a slight reduction in the concentration of H_2 by 2% under the co-gasification stage; the concentration of CH_4 becomes higher by 5% in HAC-HDPE blend. However, these gases are liberated for a short duration of 10-50 minutes. Other gases such as C_2H_6, C_2H_4, and CO were liberated at around 600°C at a low concentration level of 0.5-2.5% (Figures 4.2(a) & 4.2(b)). It can be observed that the percentage of CO in the outlet gas had decreased with the addition of HDPE. This reveals the role of HDPE, in hindering pyrolysis by forming a layer over HAC at 600°C. The CO concentration varied from 0.4 to 1.84% during HAC gasification, whereas the CO variation was found from 0.25 to 0.45% during the co-gasification of HAC-HDPE. A similar observation was obtained for H_2 gas with the highest percentage of 6.22% for HAC and this is reduced to 3.64% during the co-gasification condition.

When the operating temperature is increased from 600°C to 800°C, the concentration of CH_4 (15%) and H_2 (22%) is found higher than at 600°C under the blended conditions (Figures 4.2(c) & 4.2(d)). Further, the CO content also increased due to the thermal cracking of plastics at higher temperatures. Under blended conditions, at 630°C, a higher concentration of C_2H_4 (32.8%) and C_2H_6 (10%) is obtained with the highest methane content of 21.62%. Thus, the progress of thermal cracking and CO_2 cracking of HDPE raised the production of syngas. The HDPE particles, which had melted over the coal surface, cracked in the temperature range of 700 to 800°C. Consequently, the surface of coal particles is exposed to CO_2, resulting in higher production of CO due to the progress of char gasification reaction (Figure 4.2(f)).

When the reactor temperature is further increased from 800°C to 1000°C, the concentration of CO increased further to maximum concentration of 35% in the blended conditions. The highest concentration of CO obtained during HAC gasification was 22% (Figures 4.2(e) & 4.2(f)). At above 900°C, the char gasification reaction occurred and the residual plastics in the fuel blend reacted with CO_2 and formed ethane and ethylene. Further, the progress of dry reforming reaction between plastics and CO_2 led to a higher concentration of CO and H_2, compared to pure HAC gasification. Figure 4.3 shows the calorific value and the flow rate of the syngas at various operating temperatures. At 600°C, the syngas calorific value was found to be 3 MJ/Nm^3 for HAC and the addition of HDPE had raised the calorific value to 14 MJ/Nm^3 (Figure 4.3(a)) with the increase in the flow rate of syngas by 0.1 liters per minute (lpm).

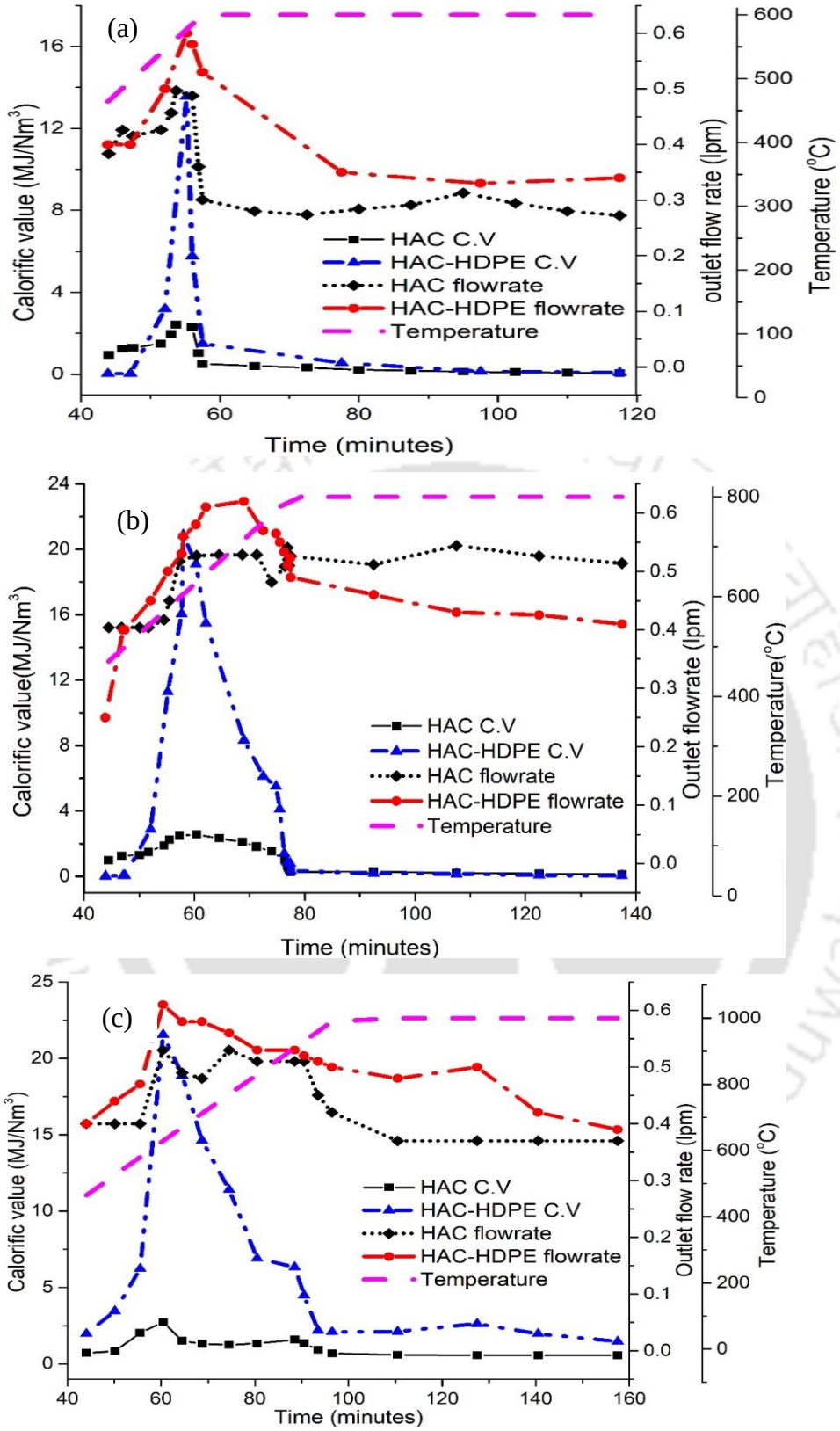

Figure 4.3. The calorific value (C.V.) and outlet flow rate of syngas obtained at (a) 600 ºC, (b) 800ºC and (c) 1000ºC

At the blended conditions, the heating value of syngas is obtained as high as 20 MJ/Nm^3 and 22 MJ/Nm^3 with a flow rate in the range of 0.4 to 0.6 lpm at 800°C and 1000°C, respectively (Figures 4.3(b) & 4.3(c)). The addition of HDPE with HAC nearly doubled the calorific value of syngas at higher temperatures (above 900°C) (Figure 4.3(c)).

The variation of CO_2 composition in the syngas is shown in Figure 4.4. At 600ºC, CO_2 concentration is found higher in the range of 85-99% and 55-99% during the gasification of HAC and HAC-HDPE blending conditions. This is only due to the release of volatiles matter from HAC and HDPE at 600ºC. However, at higher operating temperatures from 800ºC to 1000ºC, there is a decrease in the percentage of CO_2 in the syngas estimated in the range of 28-30% and 77-80% during HAC and HAC-HDPE blend, respectively. HAC. In Figure 4.4(c), it can be noticed that two inverse peaks of CO_2 gas are found at the 60th minute and 80-100th minute. This is because of increase in the cracking of volatile matters in the fuels and further due to the gasification of fixed carbon at higher temperatures. HDPE addition causes a delay in CO_2 gasification, which can be seen as the second peak is observed at the 80th minute in HAC gasification and 100th minute in HAC-HDPE blend gasification. This is due to the melting and plugging of HDPE particles over HAC, which restricts the access of CO_2 to HAC.

From Table 4.5, it can be observed that calorific value of syngas improves by 1 to 7 MJ/Nm^3 under co-gasification conditions. This was mostly due to high concentration of hydrocarbons formed. The calorific value of the syngas increases by 0.81MJ/Nm^3 for HAC and 6.72 MJ/Nm^3 under co-feed condition with increase in the operating temperature from 600 to 1000°C. One can also observe that concentration of CO increases significantly at 1000°C as compared to 800°C. This was mostly due to gasification reactions occurring between CO_2 and fuel. The volume of syngas generated at 600°C is higher under blending conditions due to HDPE cracking. With increase in the operating temperature from 600 to 800°C under blending conditions, the gasification reactions are hindered due to HDPE melting over HAC. This leads to decrease in the volume of syngas produced as compared to HAC. At 800°C, under blending conditions, the volume of syngas produced is 2.27 m^3/kg, whereas, for HAC alone it is 2.82 m^3/kg. As the operating temperature is further increased to 1000°C, due to porous structure formation and subsequent gasification reactions under blending conditions, the volume of syngas formed under blending conditions is higher (3.57 m^3/kg) than the non-blending conditions (3.42 m^3/kg).

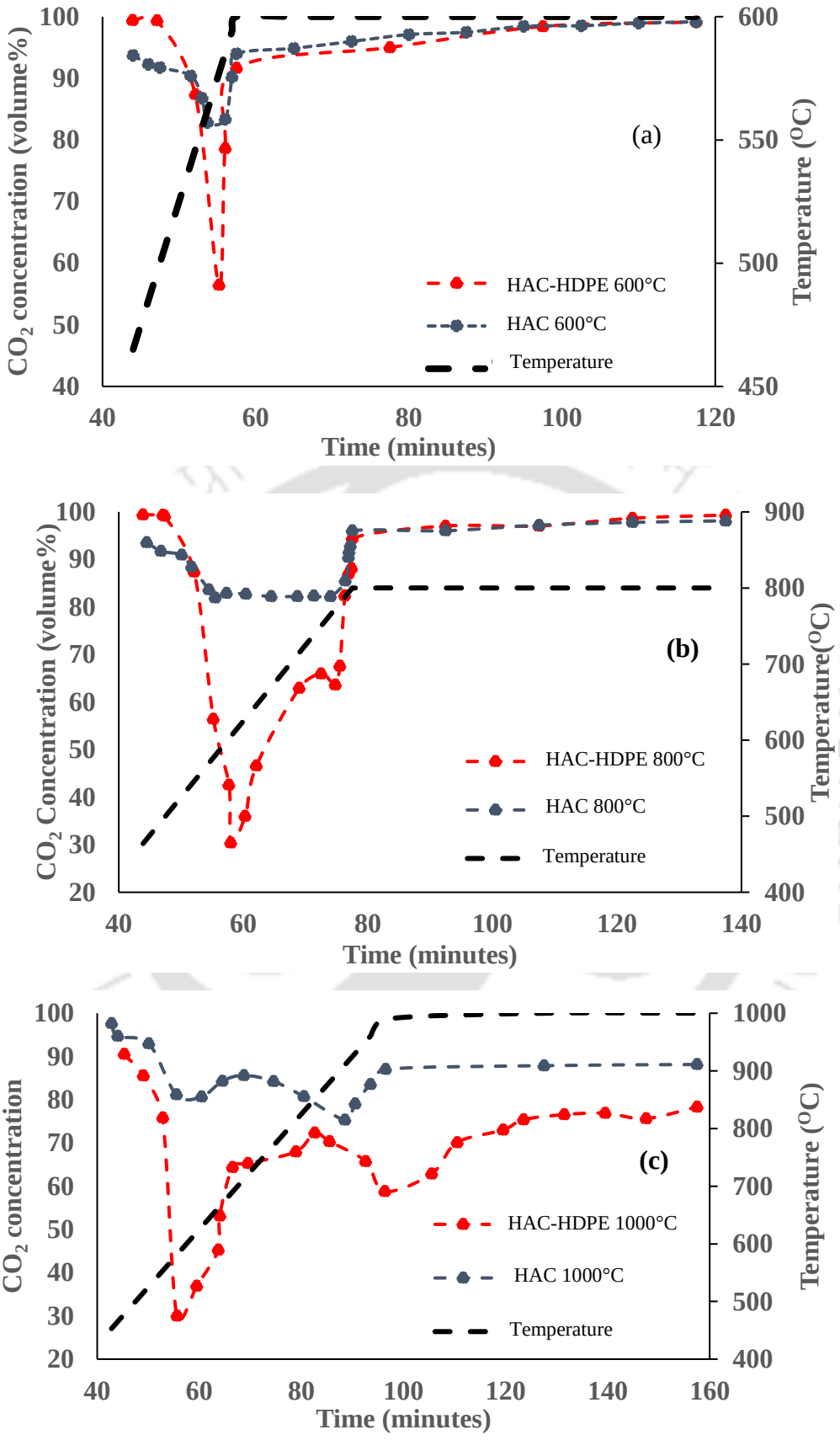

Figure 4.4. Variation of CO_2 concentration in the syngas at (a) 600ºC, (b) 800ºC, and (c) 1000ºC

Table 4.5. Overall syngas composition

Experiment	H_2	CO	CH_4	C2 hydrocarbons	Calorific value (MJ/Nm^3)	Syngas volume produced (m^3/kg)
HAC 600˚C	0.69±0.02	1±0.04	3.16±0.29	-	1.48	1.56
HAC 800˚C	1.2±0.03	3.48±0.24	2.36±0.35	-	1.54	2.82
HAC 1000˚C	1.33±0.07	11.35±0.7	1.74±0.14	-	2.29	3.42
HAC-HDPE 600˚C	1.87±0.1	0.35±0.03	2.83±0.25	0.46±0.05	2.52	1.79
HAC-HDPE 800˚C	2.77±0.11	2.09±0.25	5.39±0.55	5.61±0.74	6.41	2.27
HAC-HDPE 1000˚C	5.09±0.55	17.91±0.95	5.54±0.75	6.39±0.88	9.24	3.57

4.2.3.2. Residue characterization

Table 4.6. Mass balance estimated for HAC and HAC-HDPE

Experiment	Residue %	Tar %	Gas %
HAC 400˚C	93.71±3.14	0.00	6.29±0.95
HAC 600˚C	88.25±2.99	1.43±0.09	10.32±1
HAC 800˚C	86.3±3	2.14±0.15	11.56±0.88
HAC 1000˚C	75.14±2.85	3.21±0.7	21.65±2.53
HAC-HDPE 400˚C	97±3.03	0.00	3±0.3
HAC-HDPE 600˚C	49.07±2.03	9.2±1.53	41.73±1.03
HAC-HDPE 800˚C	45.43±2.83	10±1.83	44.57±1.06
HAC-HDPE 1000˚C	42±2.93	12.29±1	45.71±1.2

The mass balance of solid, liquid, and gas during pyrolysis at different experimental conditions is shown in Table 4.6. The surface area and pore size of the obtained solid residue are shown in Table 4.7 At 400°C, the percentage of solid residue is higher in HAC-HDPE blend; whereas it was reduced by 4% during HAC pyrolysis. This shows that the plastic melted at low temperatures and adhered on the surface of the coal particles. This is evident from the pore size measurement by the BET surface area analyzer (Table 4.7). With further increase in the temperature to 600°C, the solid residue had significantly decreased by 48%. Further, at 800°C and 1000°C, the solid residue is reduced by 3-5%.

In parallel, one could observe the increase in tar and gas evolution at higher temperatures due to the progress of pyrolysis and char gasification reactions. The surface area of HAC char increases from 2.41 m^2/gm to 29.95 m^2/gm and similarly, the pore size increases from 9.74 nm to 11.82 nm. Under blended conditions for HAC-HDPE, the surface area of the char residue increases from 2.67 m^2/gm to 70 m^2/gm and the pore size has increased from 8.68 nm to 22.7 nm.

Table 4.7. Surface area and pore size of the obtained char at different temperatures

Residue	Surface area (m^2/gm)	BJH adsorption pore size (nm)
HAC 400˚C	2.41	9.74
HAC 600˚C	3.64	10.07
HAC 800˚C	5.5	10.53
HAC 1000˚C	29.95	11.82
HAC-HDPE 400˚C	2.67	8.68
HAC-HDPE 600˚C	6.47	6.28
HAC-HDPE 800˚C	7.22	6.92
HAC-HDPE 1000˚C	70.04	22.7

4.2.3.3. FTIR analysis

FTIR analysis of the char has been carried out from 400 to 4000 cm^{-1} and the results are shown in Figure 4.5. The presence of ash has been observed at 1035 cm^{-1} in all the FTIR peaks of char obtained at various operating conditions. The raw HAC consists of aliphatic compounds-CH_2 bending and aromatic ring observed at 1436 cm^{-1} and 1600 cm^{-1}, respectively. Further, as a typical result, it is found that the area of various species in the FTIR peaks is continuously decreased with an increase in the operating temperature indicating the progress of pyrolysis and gasification reactions (Table 4.8).

FTIR of HDPE polymer revealed the presence of different functional groups such as –(CH_2=CH_2)- and -(CH_2)- in 2848, 2916 cm^{-1} and 718, 1472 cm^{-1}, respectively, (Singh et al., 2020). These groups are also found in the residual char obtained during the gasification of HAC-HDPE blend. These functional groups are completely released at 800˚C. CH_3 wagging deformation is found at 1366 cm^{-1}. HDPE could act as a hydrogen donor to stabilize the radicals released by coal macromolecules (Melendi-espina et al., 2015). Ester and carboxylic acid peaks are found in the char obtained by blending HAC

and HDPE at 1736 cm^{-1} and 1205 cm^{-1}, respectively. These peaks are not found in the char produced by HAC alone. These functional group formations could be due to reactions 4.3 and 4.4 between C_2 hydrocarbons and CH_4 released from HAC and HDPE with CO_2. As the HDPE cracks, methane and ethane gases are formed and these gases could react with CO_2 and form esters and acids. The peak at wavenumber 1366 cm^{-1} in the FTIR analysis showed the formation of esters and acids groups.

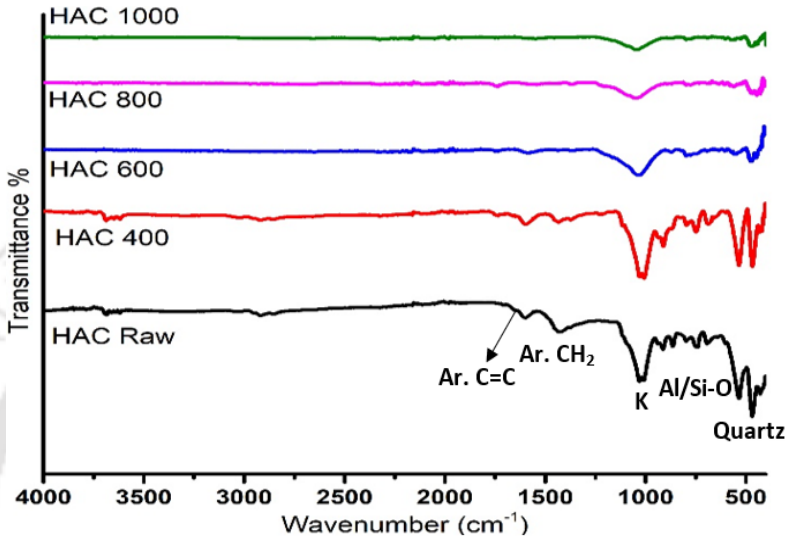

(a) HAC char

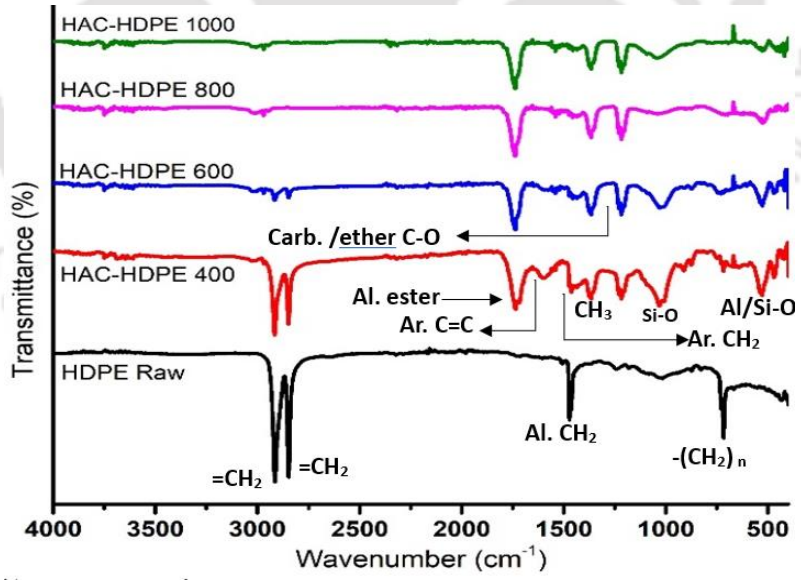

(b). HAC-HDPE char

Figure 4.5. FTIR of (a) HAC char, (b) HAC-HDPE residue (Al.-aliphatic, Ar.-Aromatic, Carb. – Carboxylic, K-Kaolinite). (O'Reilly & Mosher, 1983),(Gulmine et al., 2002),(Guo & Bustin, 1998), (Verma et al., 2015)

Table 4.8. Area of various FTIR peaks as calculated by Origin

Wavenumber (cm^{-1})	Functional group	HAC raw	HAC 400˚C	HAC 600˚C	HAC 800˚C	
1436	Aromatic C=C	174.61	153.22	39.72	33.94	
1600	Aliphatic CH_2	429.34	137.64	0	0	
HAC-HDPE char	Functional group	HDPE Raw	HAC-HDPE 400˚C	HAC-HDPE 600˚C	HAC-HDPE 800˚C	HAC-HDPE 1000˚C
1366	Aliphatic CH_3	0	170.5	148.26	133.36	126.14
1472	Aliphatic CH_2	166.38	0	0	0	0
1739	Aliphatic ester	0	410.37	330.81	329.03	311.36
2849	Symmetric CH_2	242.34	124.59	19.93	0	0
2914	Asymmetric CH_2	500.83	265.4	34.55	0	0

Reactions 4.3 and 4.4 could occur at 400˚C in the presence of catalyst alumina or carbon (Tommasi, 2017). The ash analysis of HAC using XRF showed the presence of 22.93% alumina. Alumina in HAC ash and carbon in coal could promote reactions 16 and 17, by acting as catalysts. With the increase in the operating temperatures, the concentration of acid and ester functional groups has decreased; however, even at 1000˚C, one can see the presence of a small proportion of acid and ester functional groups. The ultimate analyses of the resultant chars are shown in Table 4.9. The ultimate analysis of the residual char reveals higher oxygen content in HAC-HDPE blended chars due to the formation of ester and acid in the char. The oxygen content had decreased to 3.8% with the increase in the operating temperatures to 1000°C. This could be due to ester and carboxylic acid formation, which contain oxygen molecules obtained by reacting with CO_2 gasification agent. Carbon yield reflects the percent of carbon retained in the residue. From Table 4.9, one can observe that the residue of the HAC-HDPE mixture exhibited the lowest char yield of 34% at 1000°C. Whereas, HAC residue contains 85% of unutilized char at 1000°C due to the non-reactivity of coal. Hence, the experimental results clearly showed the addition of HDPE is highly beneficial for the thermal decomposition of high ash coal into syngas.

$$CH_4 + CO_2 \xrightarrow{C/Al_2O_3} CH_3COOH \quad (4.3)$$

$$CH_4 + CO_2 + C_2H_2 \xrightarrow{C/Al_2O_3} CH_3COOH = CH_2 \quad (4.4)$$

Table 4.9. Ultimate analysis of residue

Fuel	C	H	N	O	Ash	Carbon yield
HAC-HDPE 400	54.69	4.17	0.77	24.53	15.84	88.4
HAC-HDPE 600	55.41	2.97	0.38	10.13	31.11	86.48
HAC-HDPE 800	55.89	1.62	0.22	8.67	33.6	85.93
HAC-HDPE 1000	58.6	1.09	0.11	3.85	36.35	84.91
HAC-400	55.09	3.97	4.09	5.85	31	73.44
HAC-600	56.25	3.85	4	3.25	32.65	37.64
HAC-800	62.2	1.61	1.25	1.94	33	35.15
HAC-1000	64.87	0.3	0.26	0.08	34.49	34.07

4.2.3.4. SEM analysis and reaction mechanism

Figure 4.6 shows the mechanistic depiction of the positive synergistic interaction between HAC and HDPE as described in previous sections. The reaction between coal volatiles and ethylene forms acid and ester molecules at low temperatures and higher temperatures, the ester and HDPE molecules crack and are released from the residue. These cracks lead to the formation of a highly porous structure of char, which is favourable for Boudouard reaction. One interesting observation from the co-pyrolysis of HAC and HDPE is the tremendous increase in the surface area of char and their pore size at 1000°C. The char obtained from high ash coal at this temperature could be highly reactive and can be utilized effectively in gasification conditions. The reason behind the creation of a higher surface area in the char could be known from SEM images. The SEM images of raw HAC and HDPE are given in Figure 4.7. The SEM images of pyrolyzed HAC (Figure 4.8(a)) and HAC-HDPE blend (Figure 4.8(b)) at 400˚C had shown that the pores in the HAC char could not be observed at 2 KX magnification in Figure 4.8(b), whereas in the HAC-HDPE blend, the pores are filled with plastic particles (Figure 4.8(b)). This shows the coating of plastics over the pores of the coal and could reduce the gas evolution at low temperatures. At 600°C, the SEM micrographs show the presence of uniform globular structures in the HAC-HDPE based char, whereas, which was not observed for SEM images of pure HAC. This shows the bonding of HDPE with HAC (Figure 4.8(d)).

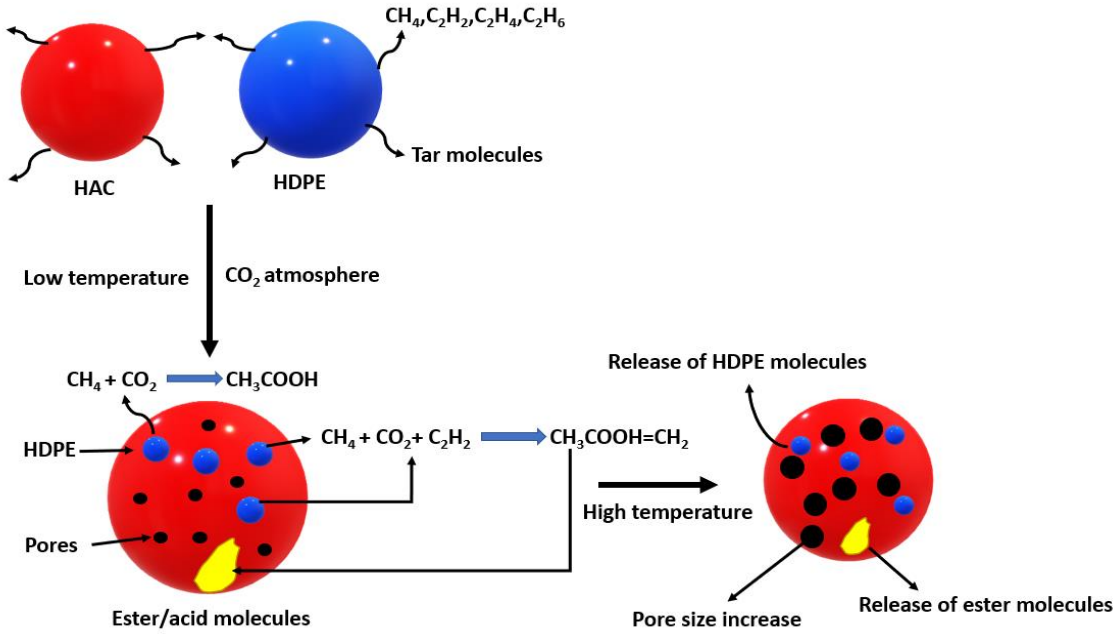

Figure 4.6. Mechanistic depiction of the interaction of HDPE and HAC during pyrolysis and gasification stages.

The distinct globular structures in the HAC-HDPE char had partially disappeared at 800˚C, and tiny structures are observed at higher magnification of 30 KX (Figure 4.8e) and 4.8(f)), compared to the image of solid residue obtained at 600˚C, which were observed clearly at 10 KX. At 1000˚C, a highly distinct morphology of char can be seen in the SEM image of HAC and HAC-HDPE blend residue (Figure 4.8(g) and Figure 4.8(h)). One can notice that the HAC char at 1000°C is non-porous and a compact structure alternatively, HAC-HDPE blend residue has a highly porous structure with a surface area of 70 m^2/gm, which is almost double that of HAC char at 1000°C. The pore diameter of the char also doubled with a pore size of 22.7 nm. The reason is explained based on the interaction between HDPE and HAC char. Due to the addition of HDPE, the compaction of coal pores is suppressed during the heat treatment and thus, the pore diameter is enlarged (Nomura et al., 2003). Coal consists of an aromatic nucleus, which is surrounded by peripheral groups, consisting of oxygen-based functional groups such as -COOH and –OH. Coking coals consist of highly ordered peripheral groups, which do not allow the crosslinking of molecules after the removal of volatile matter, and hence there is no compaction in the coal matrix (Basu, T.K., Mitra, P.K., Chowdhury, S.G., Roy, S.G., Chowdhury, 1996).

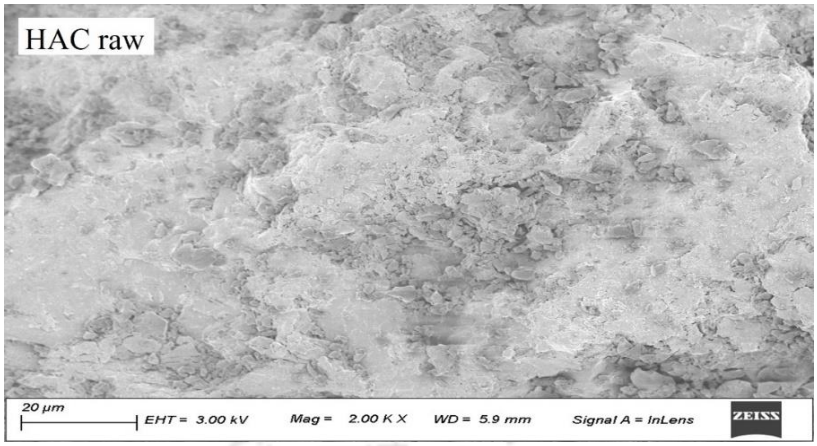

(a)

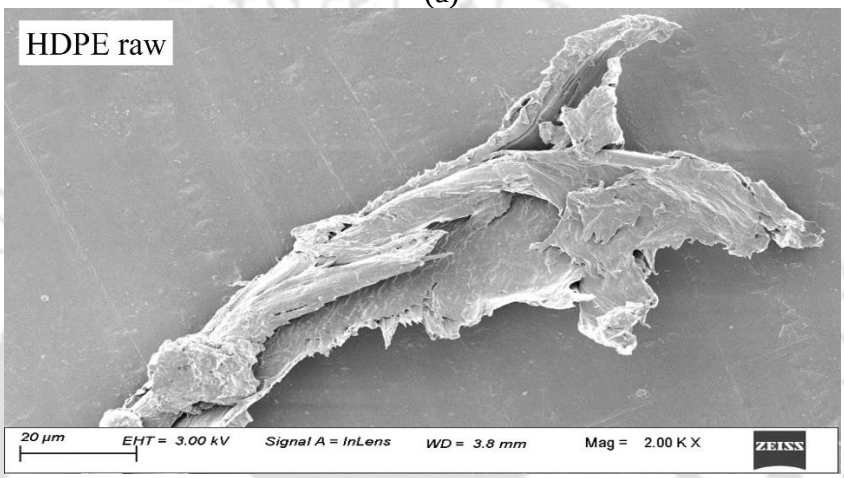

(b)

Figure 4.7. SEM images of raw fuel samples

However, in non-coking coals, the presence of disordered peripheral groups promotes crosslinking between the molecules, and hence, a packed structure is formed in the case of HAC char at 1000°C. This would make non-porous coal with a low specific surface area, which is not favourable for gasification. Whereas, for blended fuel gasification, the HDPE molecules fill these voids at low temperatures and decrease coke contraction. During the co-pyrolysis stage at 400°C-600°C, the HDPE molecules get added into the coal melt and did not allow the volatile matter to be released completely. Consequently, the HDPE molecules interact with the retained volatile matter of the coal and form carboxylic and ester bonds (explained in section 4.2.3.3). Further, with an increase in the operating temperature from 600°C to 1000°C, the HDPE molecules undergo thermal cracking and slowly the carboxylic and ester bonds break in the coal matrix. Due to the release of cracked products at high temperatures, a void space is created and this allows the CO_2 molecule to diffuse freely into the char matrix for gasification.

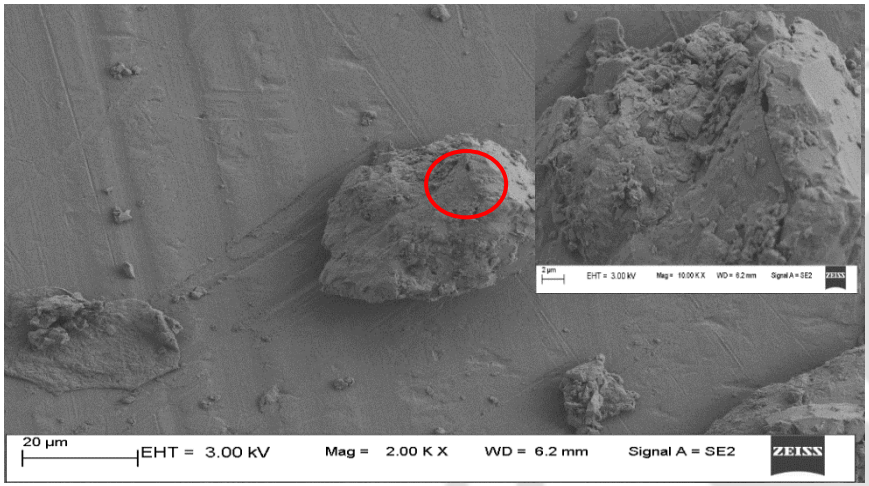

(a) HAC-400°C (2KX and 10KX)

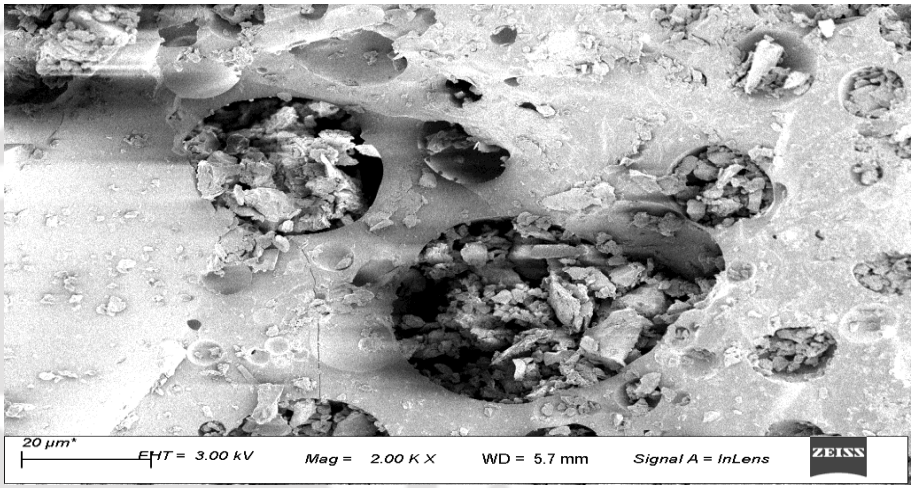

(b) HAC-HDPE 400ºC

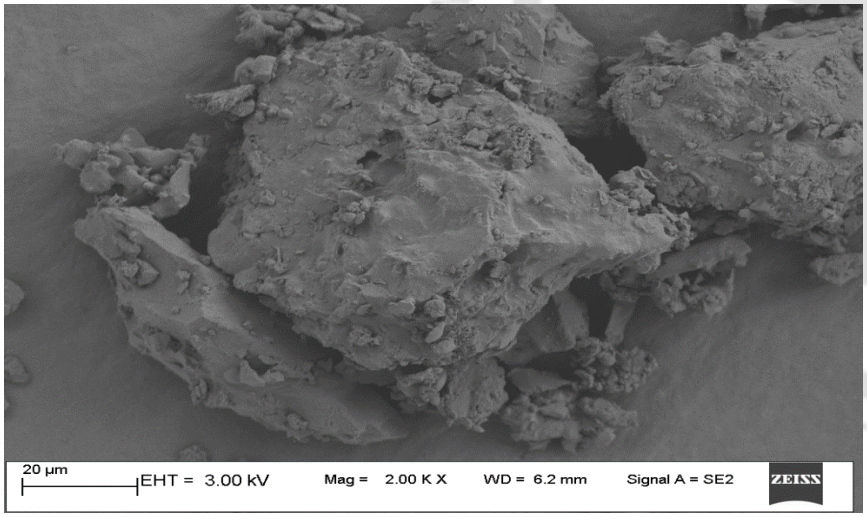

(c) HAC 600ºC

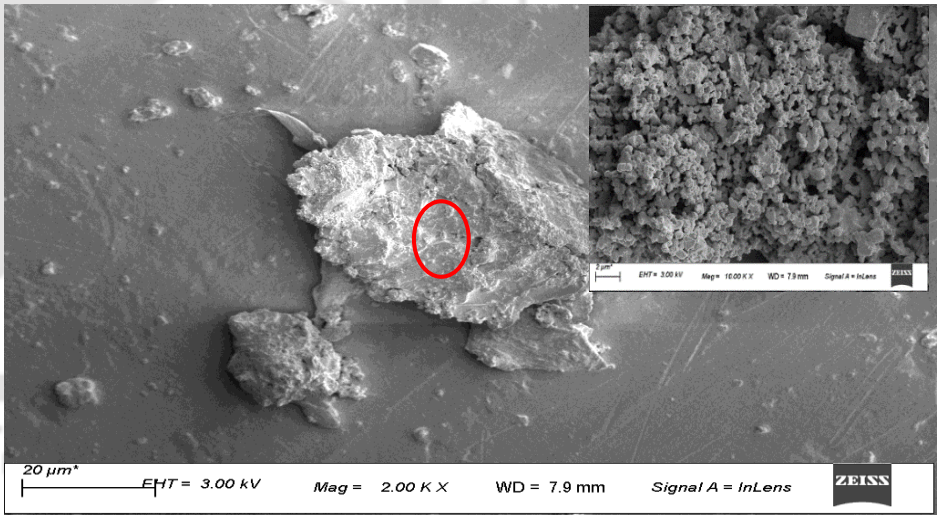

(d) HAC-HDPE 600ºC (2KX and 10KX)

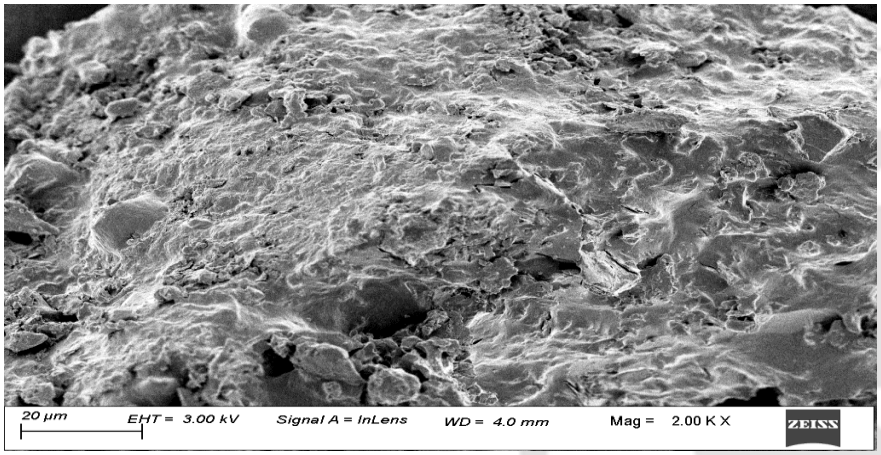

(e) HAC 800ºC

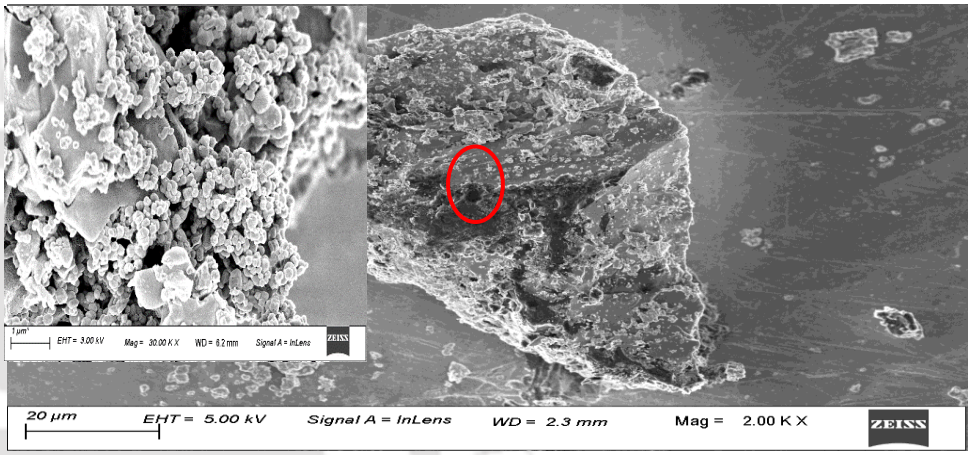

(h) HAC-HDPE 1000ºC

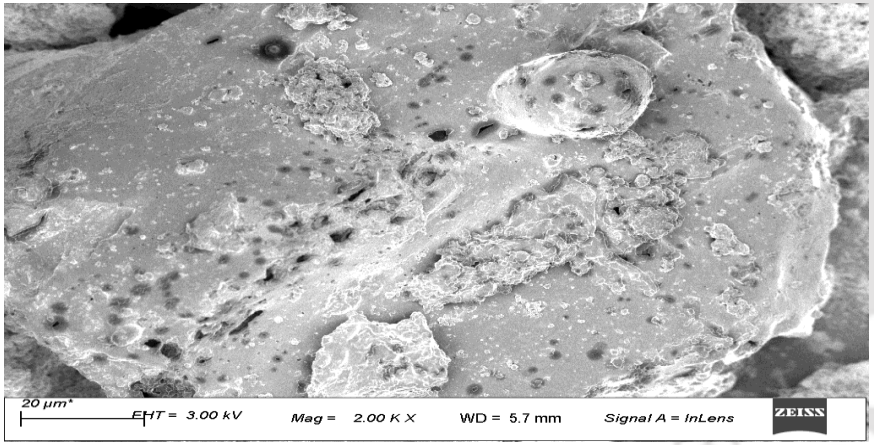

(g) HAC 1000ºC

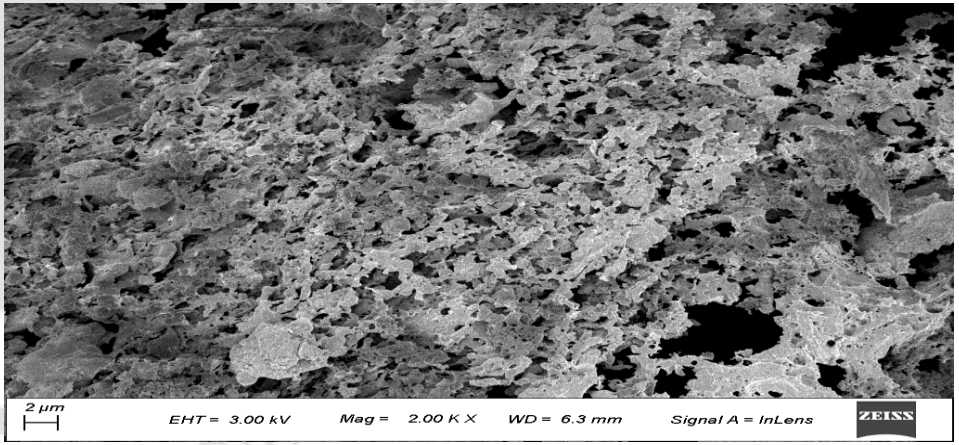

(h) HAC-HDPE 1000ºC

Figure 4.8. SEM images of char formed from HAC and HDPE-HAC blend respectively at different operating temperatures (a)&(b) 400ºC, (c)&(d) 600ºC, (e)&(f) 800°C and (g)&(h) 1000°C

4.3. Summary of the chapter

The present study shows the novel results for the effective utilization of non-reactive Indian coals with waste plastics such as HDPE.

- CO_2 pyrolysis of HDPE and HAC by thermogravimetric analysis and fixed bed experimentation at 400, 600, 800, and 1000˚C have been performed. The formation of acid and ester groups during the co-pyrolysis of HAC and HDPE at 400°C reveals the chemical interaction between coal volatiles, CO_2, and ethylene molecules. The plugging and dispersion of ethylene species at 400°C into the pores of coal having a higher content of inorganics may enlarge the pore diameter at 1000°C.
- There is an enhancement of surface area in the char, which favours the progress of the Boudouard reaction with CO_2 gas. Hence, the addition of HDPE created appropriate morphological and structural changes in the non-reactive high ash Indian coal, thereby increasing syngas calorific value.
- The co-gasification of HAC with HDPE enhanced the content of CO in the syngas at above 800°C. The estimated percentage of CO during the gasification of pure HAC is found as high as 14.2%, whereas, under blending, the CO gas had increased to 24.4%. The highest calorific value of syngas obtained using HAC was in the range of 2.5 - 2.7 MJ/Nm^3. Under co-gasification conditions, the addition of HDPE significantly raised the calorific value of syngas to 20 MJ/Nm^3.
- The kinetic analysis of fuel blends revealed that the CO_2 pyrolysis and gasification had followed two different kinetic models. At the volatile matter stage (400-600°C), the first-order kinetics is observed and at the gasification stage (800-1000°C), the 3-D diffusion model is found as the most accurate.
- The calorific value of syngas for whole experiment increases by 1 to 7 MJ/Nm^3 when HDPE is mixed with HAC. Irrespective of operating temperature calorific value of syngas by mixing HDPE increases as compared to HAC alone. Concentration of CO in syngas increases by 7 and 15% when final temperature of HAC and HAC-HDPE mixture increases from 800 to 1000°C.

References

Basu, T.K., Mitra, P.K., Chowdhury, S.G., Roy, S.G., Chowdhury, A. (1996). *Coal*

carbonization. CFRI (Central Fuel Research Institute).

Fernandez, A., Soria, J., Rodriguez, R., Baeyens, J., & Mazza, G. (2019). Macro-TGA steam-assisted gasification of lignocellulosic wastes. *Journal of Environmental Management*, *233*(December 2018), 626–635. https://doi.org/10.1016/j.jenvman.2018.12.087

Gulmine, J. V., Janissek, P. R., Heise, H. M., & Akcelrud, L. (2002). Polyethylene characterization by FTIR. *Polymer Testing*, *21*(5), 557–563. https://doi.org/10.1016/S0142-9418(01)00124-6

Guo, Y., & Bustin, R. M. (1998). Micro-FTIR spectroscopy of liptinite macerals in coal. *International Journal of Coal Geology*, *36*(3–4), 259–275. https://doi.org/10.1016/S0166-5162(97)00044-X

Janajreh, I., Adeyemi, I., & Elagroudy, S. (2020). Gasification feasibility of polyethylene, polypropylene, polystyrene waste and their mixture: Experimental studies and modeling. *Sustainable Energy Technologies and Assessments*, *39*(December 2019), 100684. https://doi.org/10.1016/j.seta.2020.100684

Melendi-espina, S., Alvarez, R., Diez, M. A., & Casal, M. D. (2015). Coal and plastic waste co-pyrolysis by thermal analysis – mass spectrometry. *Fuel Processing Technology*, *137*, 351–358. https://doi.org/10.1016/j.fuproc.2015.03.024

Meng, A., Chen, S., Long, Y., Zhou, H., Zhang, Y., & Li, Q. (2015). Pyrolysis and gasification of typical components in wastes with macro-TGA. *Waste Management*, *46*, 247–256. https://doi.org/10.1016/j.wasman.2015.08.025

Nomura, S., Kato, K., Nakagawa, T., & Komaki, I. (2003). *The effect of plastic addition on coal caking properties during carbonization q*. *82*, 1775–1782. https://doi.org/10.1016/S0016-2361(03)00120-0

O'Reilly, J. M., & Mosher, R. A. (1983). Functional groups in carbon black by FTIR spectroscopy. *Carbon*, *21*(1), 47–51. https://doi.org/10.1016/0008-6223(83)90155-0

Singh, R. K., Ruj, B., Sadhukhan, A. K., & Gupta, P. (2020). A TG-FTIR investigation on the co-pyrolysis of the waste HDPE, PP, PS and PET under high heating conditions. *Journal of the Energy Institute*, *93*(3), 1020–1035.

https://doi.org/10.1016/j.joei.2019.09.003

Tommasi, I. (2017). Direct carboxylation of C(Sp3)-H and C(sp2)-H bonds with CO_2 by transition-metal-catalyzed and base-mediated reactions. In *Catalysts* (Vol. 7, Issue 12). https://doi.org/10.3390/catal7120380

Verma, S. K., Masto, R. E., Gautam, S., Choudhury, D. P., Ram, L. C., Maiti, S. K., & Maity, S. (2015). Investigations on PAHs and trace elements in coal and its combustion residues from a power plant. *Fuel*, *162*, 138–147. https://doi.org/10.1016/j.fuel.2015.09.005

This page is left blank intentionally

This page is left blank intentionally

CHAPTER 5

CO-GASIFICATION OF INDIAN HIGH ASH COAL AND COVID-19 PLASTIC WASTES

COVID-19 has severely affected human health and caused lot of fatalities. This has led to a generation of high amount biomedical wastes. In this chapter, COVID-19 plastic wastes are pyrolyzed and gasified at various temperatures. Thermal treatment of overall gowns (OG) used was carried out under inert and reactive conditions with and without HAC at various operating temperatures. The products such as oil, syngas and the solid residue obtained were characterized. The effect of OG on co-gasification with HAC is explored.

5.1. Experimental description

The experimental results of pyrolysis and gasification of COVID-19 based plastic wastes has been discussed in detail in this chapter. Overall gown (OG), which is extensively used during this pandemic period, is used as a feed in this study. A fresh OG is brought from a pharmacy shop in the campus. OG was cut into small pieces for better handling (4mm×4mm). OG consisted of 89% volatile matter, which is around 5 times that of HAC. The photograph of OG is given in Figure 5.1.

Figure 5.1. Overall Gown

Co-gasification of HAC with OG was carried out at different weight ratios to analyse its impact on HAC gasification. In Table 5.1, the list of experiments performed are given. Experiments are performed under isothermal conditions. Maximum weight of OG used

for pyrolysis and gasification is 5 grams as it is a highly volatile feed, which can block inlet and outlet section of the reactor.

Table 5.1. List of experiments performed

Feed	Operating temperature (°C)	Atmosphere	Feed weight (gm)
OG	500	N_2 and CO_2	5
OG	700	N_2 and CO_2	5
OG	900	N_2 and CO_2	5
OG	1000	CO_2	5
HAC	1000	CO_2	15
HAC: OG (19:1)	1000	CO_2	15
HAC: OG (9:1)	1000	CO_2	15
HAC: OG (17:3)	1000	CO_2	15
HAC: OG (4:1)	1000	CO_2	15

5.2. Co-pyrolysis and Co-gasification of HAC with OG

5.2.1. Thermogravimetric analysis

Table 5.2 gives the TGA-based weight loss rate estimated for the overall gown and HAC gasification. Also from Figure 5.2, it can be observed that OG has two stages of weight loss under pyrolysis conditions (N_2 atmosphere). In Table 5.2, Max_r and DTG_{max} represent maximum weight loss rate (%/min.) and the temperature (°C) at which it occurs. Range (°C) represents the temperature range at which weight loss occurs.

Polypropylene is the major component of such type of OG (found by FTIR analysis (Figure 5.7)). The first stage of weight loss of OG occurs between 340 and 515˚C. This represents the release of volatile matter. The second stage of weight loss occurred at 580-750˚C. This second weight loss peak during volatile matter stage is due to the release of volatilization of $CaCO_3$. This weight loss peak was observed at 600-610˚C under CO_2 atmosphere. This delay could be due to the feed CO_2 inhibiting the volatilization of $CaCO_3$. Similar results were also observed by Kwon et al. for chicken manure and Duan et al. for coal (Kwon et al., 2019),(Duan et al., 2009). The presence of $CaCO_3$ was confirmed by XRD peaks of CaO in the OG ash.

Table 5.2. TGA data of Fuels and fuel mixtures

Individual feedstock pyrolysis under N_2 conditions				
	Range	Max_r(%/min.)	DTG_{max} (^{o}C)	Residue %
OG (stage 1)	330-479	20.51	443	12.38
OG (stage 2)	577-700	1.32	682	
HAC	400-592	1.34	515	77.59
Individual feedstock pyrolysis and gasification under CO_2 conditions				
OG (stage 1)	410-497	26.39	466	5.31
OG (stage 2)	915-955	5.07	936	
HAC (Stage 1)	400-572	1.74	508	
HAC (Stage 2)	900-1000	0.7	1000	64.12
Co-pyrolysis under CO_2 environment (Stage 1)				
HAC: OG (Weight %)	Range (^{o}C)	Max_r(%/min.)	DTG_{max} (^{o}C)	Residue %
19:1	368-620	1.94	475.55	73.21
9:1	385-620	2.53	473.67	72.39
17:3	385-585	4.49	472.51	65.24
4:1	388-584	5.54	471.3	62.72
Co-gasification under CO_2 environment (Stage 2)				
HAC: OG (Weight %)	Range (^{o}C)	Max_r(%/min.)	DTG_{max}(^{o}C)	
19:1	850-1000	0.49	1000	
9:1	850-1000	0.54	1000	
17:3	865-1000	0.65	965.51	
4:1	866-1000	0.66	957.3	

A typical result of Table 5.2 showed that the final weight residue for HAC and OG was found 13.5% and 7.1% lower in CO_2 conditions than under N_2 conditions. The temperature range of weight loss under CO_2 conditions is found lower than in N_2 conditions. The decrease in the range was also observed by Gulsac for Tuncbilek lignite(Isik Gulsac, 2021).

Under co-gasification conditions, it was found that the range of volatile matter stage decreases from 252 to 196°C with the increase in the OG from 5 to 20%. In DTG graph, the devolatilization stage between 330 and 620°C consists of a major and a secondary shoulder peak. These two peaks represent the volatile matter loss of OG and HAC, respectively. In the devolatilization stage, the DTG_{max} decreases from 475 °C to 471 °C as quantity of OG in the mixture increases from 5 to 20%. The maximum weight loss rate is increased from 1.94%/min to 5.54%/min when OG in the fuel mixture is enhanced from 5 to 20%. The addition of OG decreased the initial temperature at which the volatile matter loss was initiated.

Positive synergism is observed by adding OG to HAC at the gasification stage. It can be observed that by adding OG, the temperature at which gasification occurs is shifted to a lower temperature. Gasification is initiated at 900°C and 915 °C for HAC and OG, respectively, at this temperature Boudouard reaction between carbon and CO_2 occurs to form CO (Lee et al., 2017). Whereas, under co-feed conditions, the gasification is initiated at low temperatures from 850 and 865 °C. This could be due to the formation of porous structures in the mixed feed by the devolatilization of OG. At a higher concentration of OG in the fuel mixture during the gasification stage, the weight loss peak tends to become flatter. The maximum weight loss rate is improved with the increase in the OG concentration. It increases from 0.49 to 0.66%/min., when OG content in fuel mixture is increased from 5% to 20%.

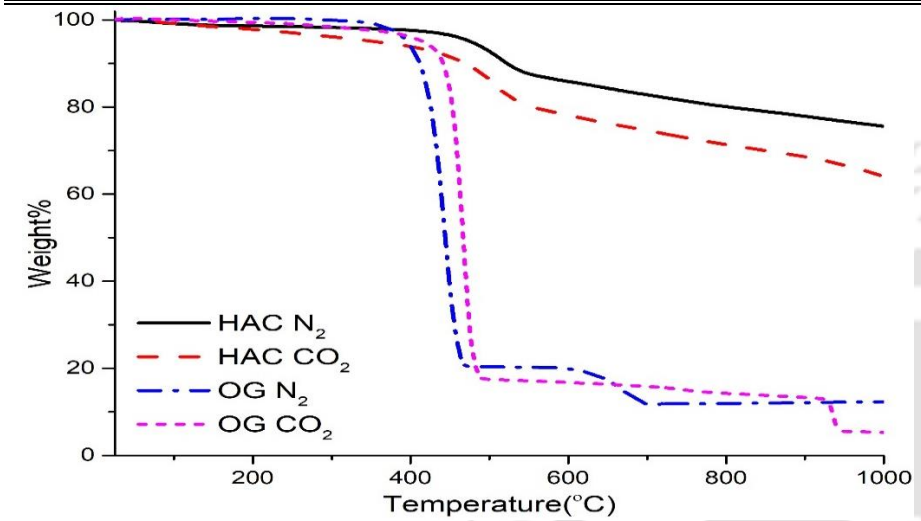

(a) TGA of HAC and OG in N_2 and CO_2

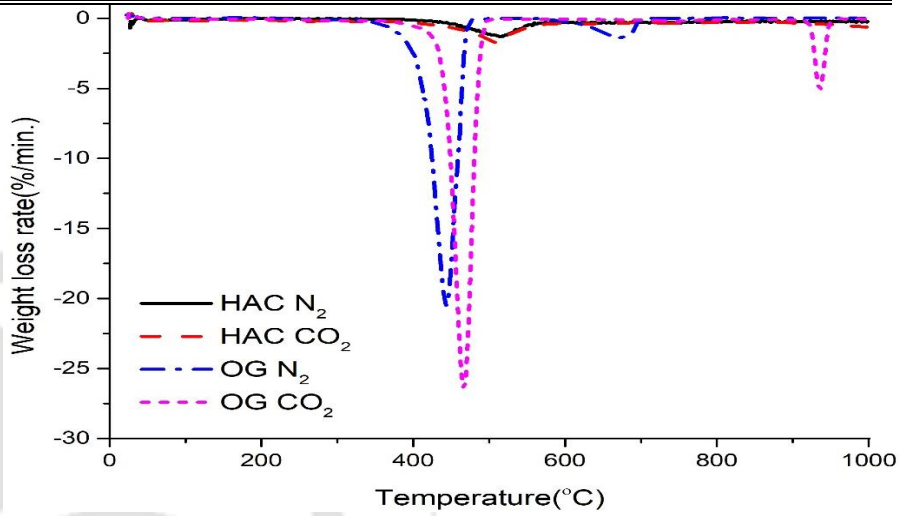

(b) DTG of HAC and OG in N_2 and CO_2

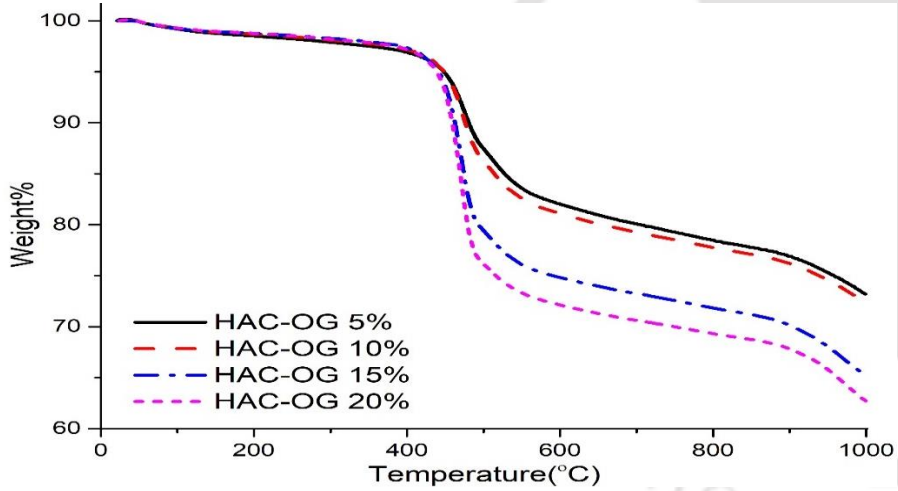

(c) TGA of HAC and OG fuel mixtures

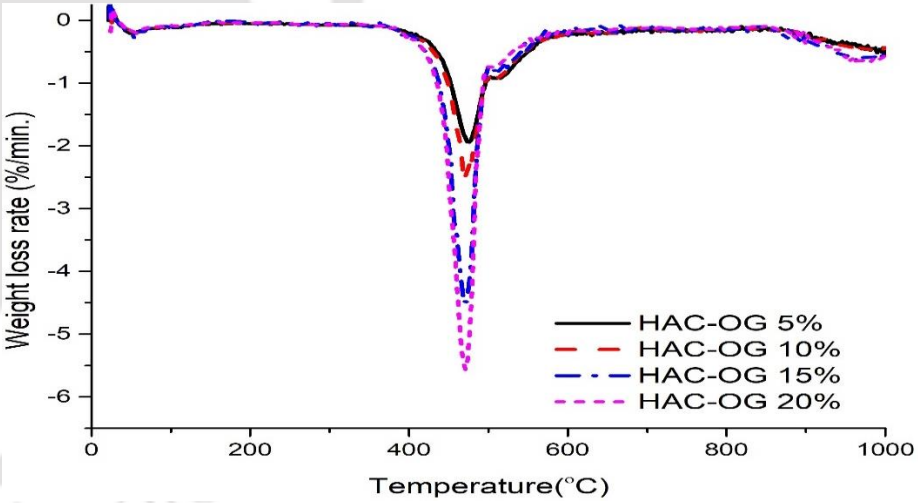

(d) TGA of HAC and OG fuel mixtures

Figure 5.2. TGA and DTG of HAC-OG in N_2 and CO_2

5.2.2. Kinetic analysis

Table 5.3. Activation energy of fuel and fuel mixtures

Volatile matter stage				
Fuel	Model	Activation energy (kJ/mol)	Arrhenius constant (min^{-1})	R^2
HAC N_2	Order 1	62.1	6.8×10^{3}	0.98
HAC CO_2	Order 1	29.1	1.54×10^{6}	0.97
OG N_2 stage 1	Order 1	146.1	6.95×10^{9}	0.99
OG N_2 stage 2	Order 1	9.4	3.4×10^{7}	0.97
OG CO_2	Order 1	221.8	1.4×10^{12}	0.96
HAC-OG 5% CO_2	Order 3	78.9	265.8	0.96
HAC-OG 10% CO_2	Order 3	89.2	208.31	0.96
HAC-OG 15% CO_2	Order 3	134.5	5.93×10^{5}	0.96
HAC-OG 20% CO_2	Order 3	138.5	1.32×10^{6}	0.97
Gasification stage				
HAC CO_2	D3 model	18.1	3.4×10^{8}	0.97
OG CO_2	D4 model	300.3	5.81×10^{8}	0.97
HAC-OG 5% CO_2	D4 model	49.1	2.88×10^{5}	0.96
HAC-OG 10% CO_2	D4 model	36.2	9.21×10^{6}	0.96
HAC-OG 15% CO_2	D2 model	35.2	2.75×10^{6}	0.96
HAC-OG 20% CO_2	D2 model	34.3	2.95×10^{6}	0.96

Activation energy of the reaction of HAC in volatile matter stage has decreased from 62 to 29 kJ/mol during the shift from N_2 to CO_2 conditions. Similar results were also observed for MSW by Lai et al.(Lai et al., 2012). Activation energy of pyrolysis of OG was 221.8 and 146.1 kJ/mol under CO_2 and N_2 conditions (Table 5.3), similar results were observed by Saad et al. (Saad et al., 2021).

In the gasification stage, it was observed that the activation energy of the coal-based reaction is lower than the OG. Gasification peak of OG was comparatively narrower than HAC. Activation energy of fuel mixture in volatile matter stage is dependent on OG in fuel mixture, which could be due to the formation of OG layer over HAC. In the gasification stage, the activation energy is decreased, which could be due to a decrease

in the gasification initiation temperature from 900 to 865ºC as the OG content in the fuel mixture is increased from 0 to 20% (Lee et al., 2017). It also increased the weight loss occurring in gasification stage from 4.4 to 6% and decreased the maximum weight loss rate, which might negatively affect the activation energy

5.2.3. HAC and OG co-gasification

In Figure 5.3, the gas composition profiles of H_2, CO, CH_4, and C2 and C3 hydrocarbons are shown. The maximum concentration of H_2 in the syngas is directly dependent on the OG concentration in the fuel mixture. The maximum concentration of H_2 has obtained from 29.4 to 37.6% with an increase in the OG concentration from 0% to 20% in the fuel mixture. Similar to H_2 profile, the maximum concentration of CO increases with PPE in the fuel mixture. The CO gas is obtained as high as 68.9%, which increases from 49.9% when OG content in the fuel mixture is increased from 0 to 20%. This could be due to the progress of dry reforming reactions where polypropylene is converted into H_2 and CO.

Two stages of gas evolution can be observed from the composition profile of CO throughout the experiment. The volatile matter stage lasts for the first 40 to 60 minutes, whereas the gasification stage lasts for the rest of the experiment. When the OG content in the fuel mixture is 5 and 10%, the CO gas obtained during the devolatilization stage is about 35.6%, which remains the same as that of HAC. From Figure 5.3(c), it can be noticed that the maximum concentration of CH_4 increased from 20.1 to 39.1% with the increase in the OG content up to 15%. However, with a further increase in the OG content to 20%, the percentage of CH_4 decreases to 33.8%, which could be due to the formation of OG layer over the coal. This results in the slow release of CH_4 throughout the experiment extended by around 7 to 8 minutes. From Figure 5.3(d), one can see that the addition of OG in fuel mixture increases the maximum concentration of C2 and C3 compounds in the syngas increases from 2.9% to 6.8%. In HAC, C2 and C3 compounds are released only in the first 5 minutes of the experiment. With the increase in the OG, C2 and C3 contents are increased to 20% and released up to 23 min. Hence, the addition of OG improves the yield of C2+C3 compounds in the syngas.

The calorific value of syngas is shown in Figure 5.3(e). In volatile matter stage, the maximum calorific value of syngas obtained has increased from 13.9 to 24.96 MJ/Nm^3 with an increase in the OG content from 0 to 15%. However, with a further increase in

the OG content, the maximum calorific value of syngas decreased to 23.5 MJ/Nm^3. This was due to the reduction in the CH_4 concentration in the syngas, which could be due to the formation of OG layer over coal preventing reactions between CO_2 and OG. After devolatilization, the concentration of CO becomes stable at around 30% when 5% OG is maintained and the CO is found 10% higher under co-gasification conditions, compared to HAC alone. This could be due to the fixed carbon in OG, which might form a porous structure, compared to HAC alone. However, with the increase in the OG content in the fuel mixture from 15 to 20%, the CO content in the syngas becomes lower than the HAC alone, which might be due to the formation of ash from OG. It was observed from Figure 5.3(f) that the syngas flow rate during initial decomposition and stable gasification conditions increases with the addition of OG due to the presence of a high amount of volatile matter. Stable gasification conditions can be defined as the reaction between fixed carbon and CO_2 after the maximum release of volatile matter. Maximum syngas flow rate was observed in the range of 0.95 lpm to 1.5 lpm during devolatilization stage. Under stable gasification conditions, the syngas flow rate was found in the range of 0.32 lpm to 0.44 lpm. The residue formed from gasification is found greyish when the OG content in the mixture is increased from 5 to 20%, contrary to HAC residue, which is blackish (Figure 5.4). From Figure 5.4, it was observed that the greyish particles are ash obtained from OG particles. The calorific value of the syngas is shown in Table 5.4. It can be observed that the addition of OG improves the calorific value of the syngas produced due to the generation of CH_4 and C2 and C3 hydrocarbons. In HAC-OG 20% experiment, the concentration of H_2 and CO improves because of dry reforming reactions occurring between OG and CO_2 in initial stages of gasification (0-60 minutes) or devolatilization of high volume of OG. The calorific value of syngas increases by 51.77% as the OG content in fuel mixture increases from 0 to 20%.

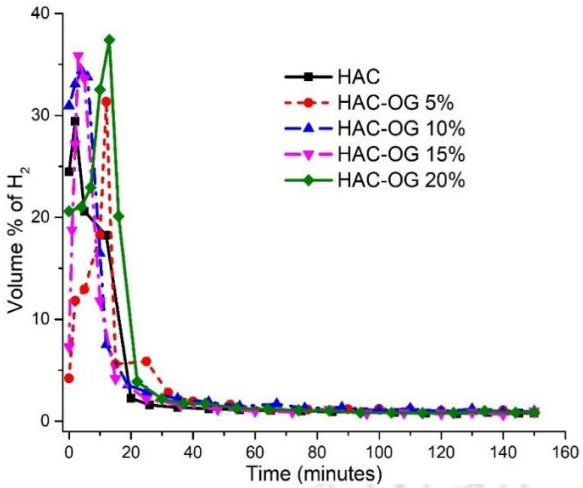

Figure 5.3(a). Volume% of H_2

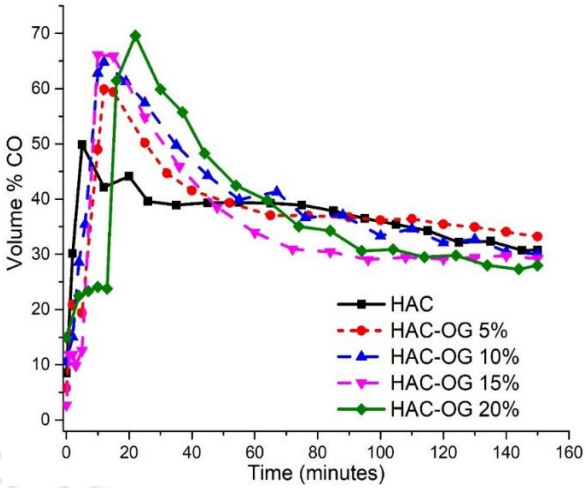

Figure 5.3(b). CO concentration

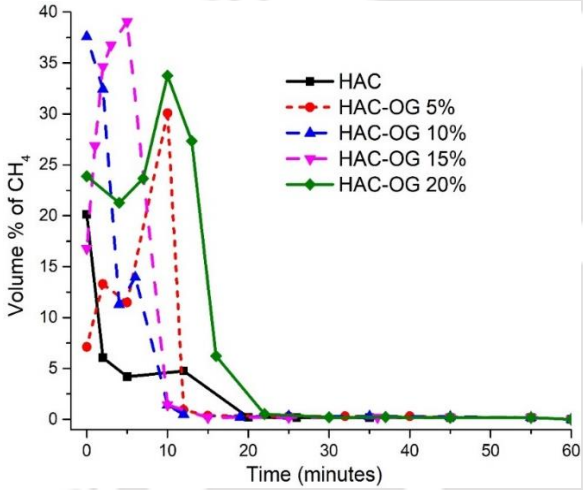

Figure 5.3(c). CH_4 concentration

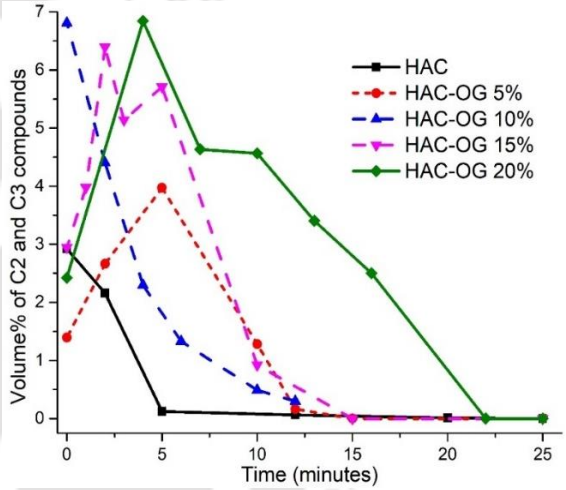

Figure 5.3(d). C2 and C3 gas concentration

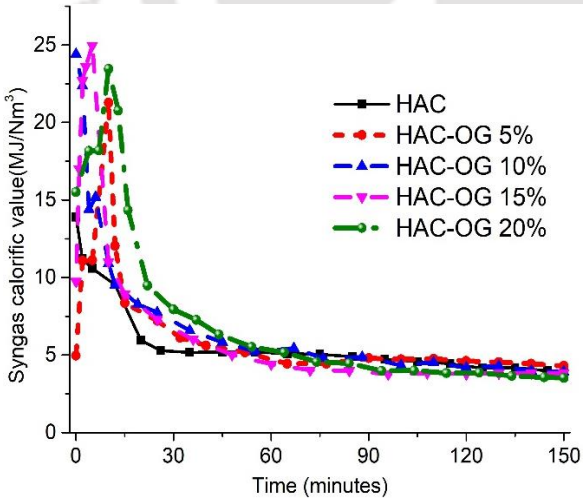

Figure 5.3(e). Syngas calorific value

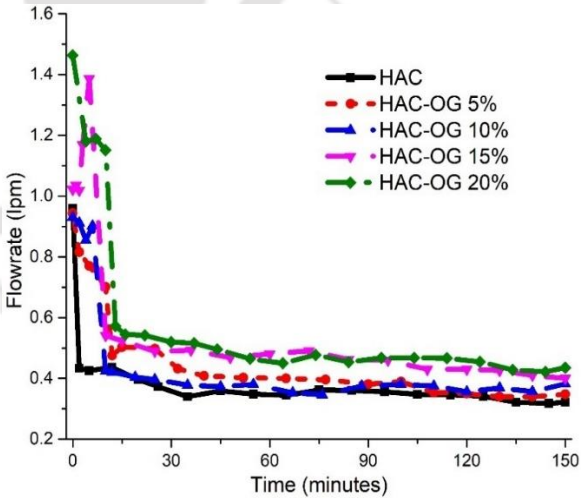

Figure 5.3(f). Syngas flowrate

Figure 5.3. Syngas properties by co-gasification of HAC with OG

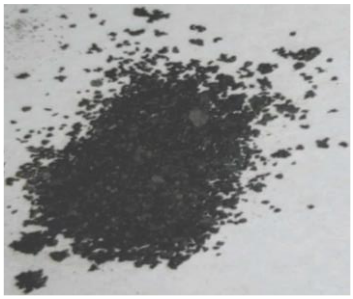

5.4(a) HAC residue

5.4(b) HAC-OG residue 5%

5.4(c) HAC-OG residue 10 %

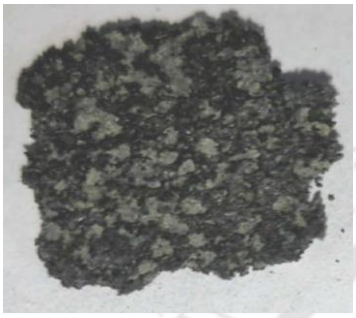

5.4(d) HAC-OG residue 15%

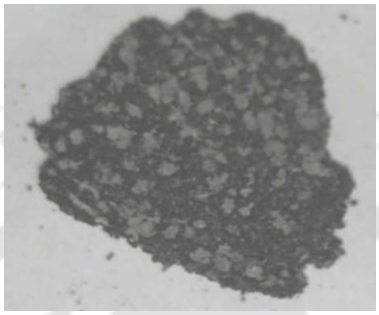

5.4(e) HAC-OG 20% residue

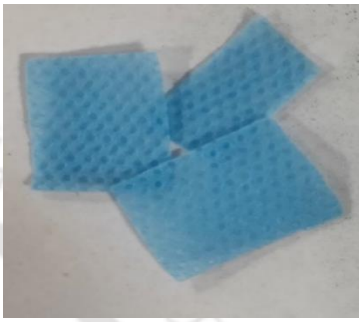

5.4(f) OG raw

Figure 5.4. Photographs of residues and OG raw obtained

Table 5.4. Syngas composition and calorific value

Case	H_2	CO	CH_4	C_2H_2	C_2H_4	C_2H_6	C_3H_6	Calorific value (MJ/Nm^3)
HAC 1000ºC	3.83±0.03	37.03±0.6	0.96±0.03	0.07±0.01	0.08±0.01	-	-	5.64
HAC-OG (19:1)	4.58±0.06	38.02±0.8	2.95±0.43	-	0.32±0.02	0.05	0.0031	6.79
HAC-OG (9:1)	7.4±0.04	39±0.9	3.23±0.19	-	0.42±0.03	0.06	0.0049	7.59
HAC-OG (17:3)	6.86±0.11	32.84±0.7	5.22±0.23	-	0.67±0.02	0.12	0.011	8.20
HAC-OG (4:1)	7.29±0.12	35.32±0.5	5.93±0.9	-	1.16±0.01	0.13	0.02	8.56
OG 700°C N_2	1.5±0.1	0.25±0.03	2.2±0.08	-	0.99±0.03	0.35	-	1.95
OG 700°C CO_2	1.5±0.09	1.12±0.04	2.2±0.55	-	1.6±0.02	0.4	-	2.46
OG 900°C N_2	6.7±0.06	3.71±0.11	5.97±0.73	-	2.26±0.06	0.12	-	5.16
OG 900°C CO_2	7.23±0.09	8.43±0.13	7.7±0.9	-	1.5±0.03	0.21	0.21	6.33
OG 1000°C CO_2	10.99±0.1	15.33±0.6	4.9±0.61	-	1.4±0.04	0.13	0.14	6.37

5.2.4. Pyrolysis and gasification of Overall Gown (OG)

Pyrolysis and gasification of OG were carried out at different operating temperatures. The pyrolysis of OG carried out under N_2 and CO_2 conditions showed that the melting of OG only took place and no conversion of feed to gas and liquid products was observed. The photographs of the residue taken are given in Figure 5.5. At 700ºC, the residue retained under CO_2 and N_2 conditions is 16% and 20.67%, respectively. In N_2 conditions, the color of the residue is black, which changes to greyish in CO_2 conditions and this denotes the utilization of fixed carbon even at low temperatures where Boudouard reaction would not occur. At 900 ºC, a significant quantity of oil was released. Under N_2 conditions, the quantity of oil obtained was higher than in CO_2 conditions owing to the reactions between CO_2 and heavy volatiles to form gaseous products. With a further increase in the operating temperature, the yield of tar component decreases from 16% to 9.4% under CO_2 conditions. Almost 95.8% of OG is utilized at 1000ºC under CO_2 conditions.

Figure 5.6 shows the gas composition, syngas calorific value, and outlet flow rate of syngas at various operating temperatures. It can be noticed that with an increase in the temperatures, the gas yield is high. At 900ºC, the CO was obtained as high as 20% due to the cracking of OG at higher temperatures. The concentration of CH_4 and C2-C3 compounds are comparatively higher at 900ºC as compared to 1000ºC. This may be due to dry reforming reactions taking place between CO_2 and hydrocarbons, which would result in the increased production of H_2, and CO with a higher outlet flow rate of syngas high as 3.7 lpm at 1000ºC. The calorific value of the obtained syngas in the first 30 minutes ranges from 5 to 27 MJ/Nm^3. The maximum calorific value of syngas obtained at 700ºC under N_2 and CO_2 conditions is 13.5 MJ/Nm^3 and 14.6 MJ/Nm^3, respectively and at 900ºC, 18.43 MJ/Nm^3 and 26.73 MJ/Nm^3 of calorific value of syngas are obtained. As the operating temperature is increased further to 1000ºC, the calorific value of syngas obtained in CO_2 conditions decreases whereas the quantity of syngas generated is higher than 900ºC. The quantity of syngas generated at 900ºC under N_2 and CO_2 conditions is 59.51 and 60.22 liters, respectively. Whereas at 1000ºC under CO_2 conditions, a higher quantity of syngas of 68.54 liters was generated due to the progress of dry reforming and Boudouard reactions.

(a) OG CO_2 500 ºC

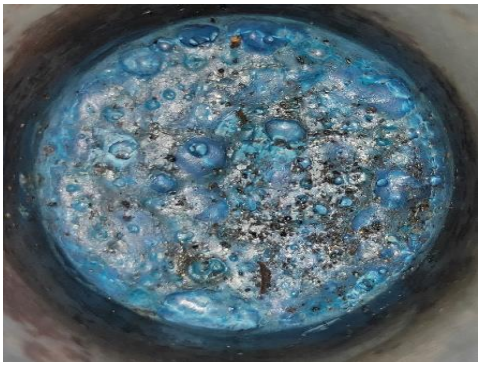

(b) OG N_2 500ºC

(c) OG N_2 500ºC

(d) OG CO_2 700ºC

(e) OG N_2 900 ºC

(f) OG CO_2 900ºC

OG CO_2 1000 ºC

Figure 5.5. Residue from OG pyrolysis and gasification

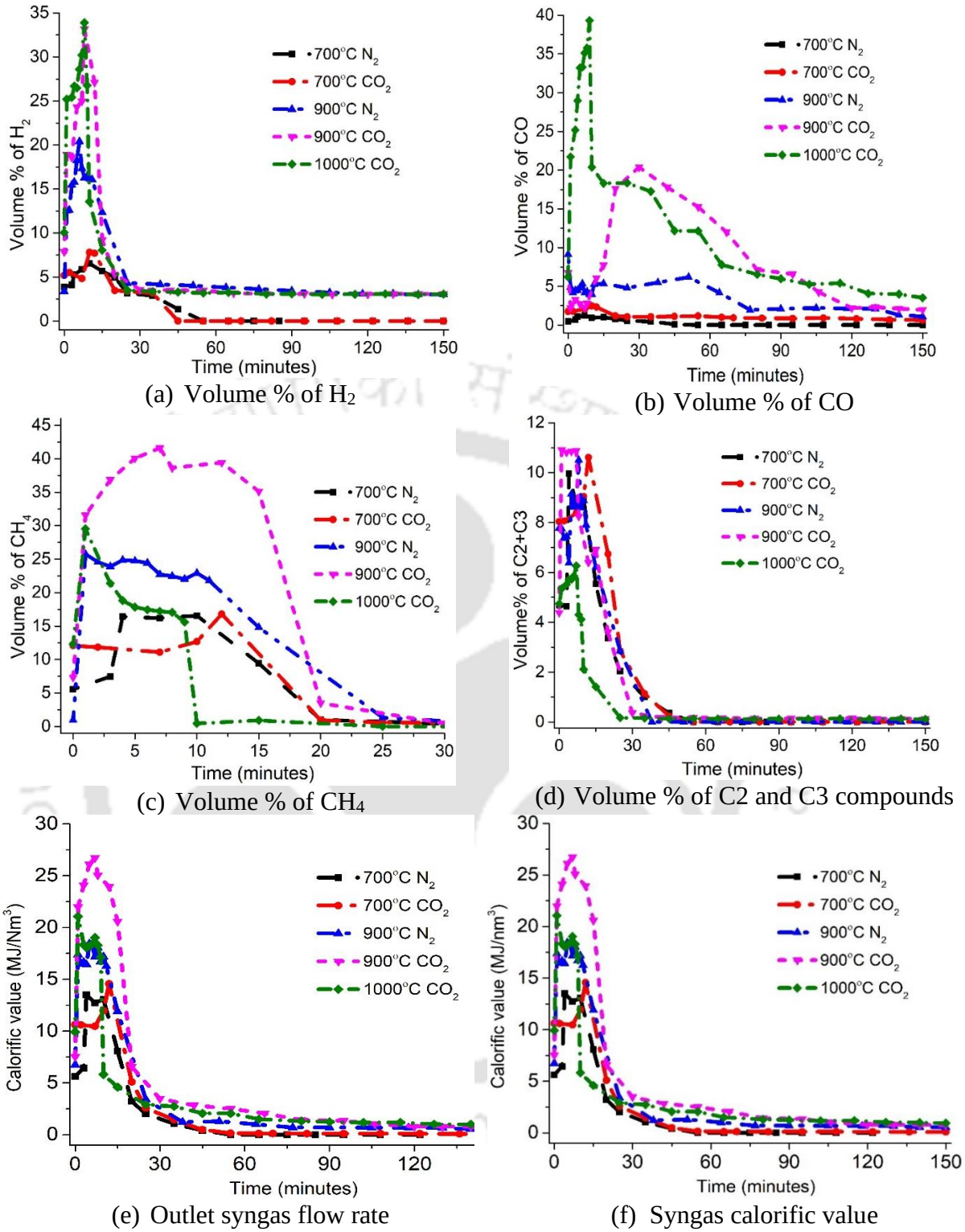

(a) Volume % of H_2 (b) Volume % of CO

(c) Volume % of CH_4 (d) Volume % of C2 and C3 compounds

(e) Outlet syngas flow rate (f) Syngas calorific value

Figure 5.6. Syngas composition and flow rate by OG pyrolysis and gasification

From Table 5.4 it can be observed that as the operating temperature is increased the thermal cracking of OG increases. This leads to increase in calorific value and H_2, CO concentration. Under CO_2 conditions mole % of CO is higher than N_2 conditions owing to gasification reactions between OG and CO_2. Concentration of CO in CO_2 atmosphere

increases from 1.12% to 15.33% as operating temperature increased from 700°C to 1000°C. This denotes the increase in reforming and Boudouard reactions with temperature. This is also reflected in calorific value of syngas; calorific value of syngas increases from 2.46 MJ/Nm^3 to 6.37 MJ/Nm^3 in CO_2 conditions.

5.2.5. FTIR analysis of feed and products

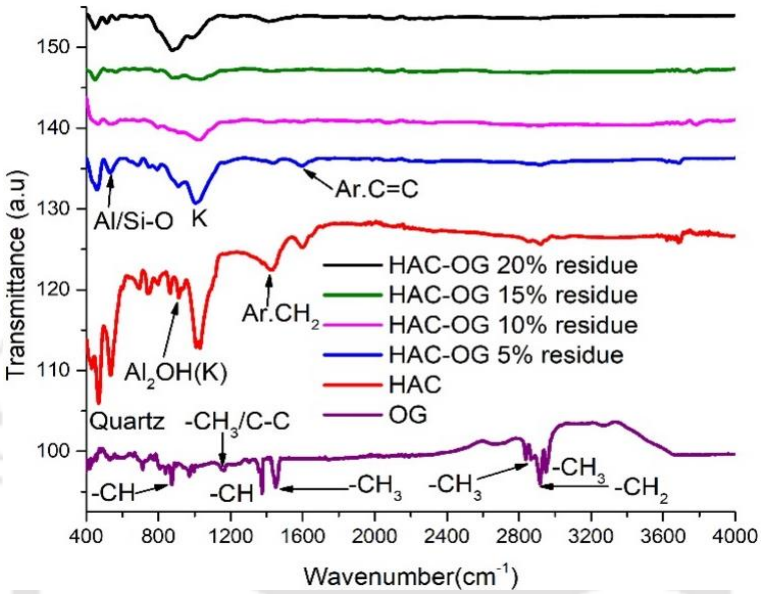

(a) FTIR of residue and Feed

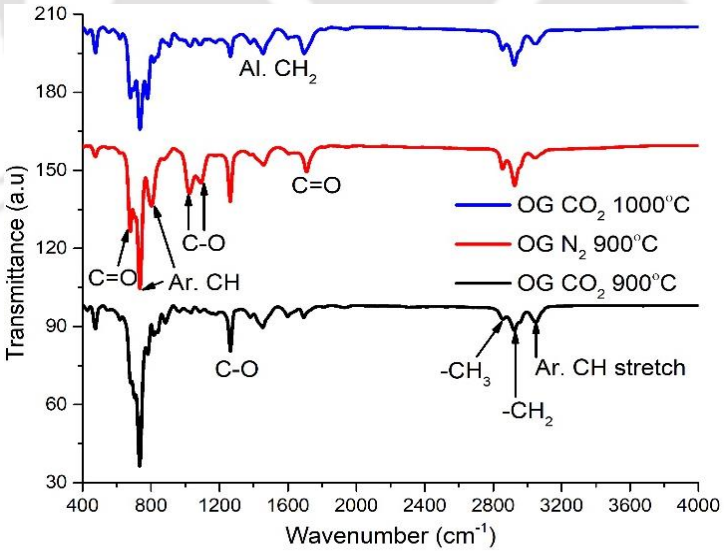

(b) FTIR of tar from OG pyrolysis and gasification

Figure 5.7. FTIR of the residue obtained after the gasification of HAC and OG

FTIR peaks and their assignments are given in Table 5.5. According to the studies conducted by Yousef et al., polypropylene is the major component of such PPE kits. FTIR peaks appeared between 500 and 1000 cm^{-1} representing aromatic C-H out of plane

bending in coal(Yousef et al., 2021). The residues obtained by the co-gasification of HAC and OG contain a major peak at 1000 cm^{-1} and 915 cm^{-1}. The intensity of these peaks varies according to the percentage of OG in the feed mixture. It can be noticed from Figure 5.7(a) that with the increase in the OG content in the fuel mixture, the peak intensity at 1000 cm^{-1} keeps decreasing whereas, at 915cm^{-1}, the peak intensity increases. This denotes that the volume of ethers/alcohols in the residue decreases as the OG content decreases, whereas ash content in the residue increases.

Table 5.5. FTIR peak and assignment (Eterigho-Ikelegbe et al., 2021), (Fang et al., 2012), (Franco et al., 2019), (Rodríguez-Luna et al., 2021), (Zhang et al., 2021)

OG	
Wavenumber (cm^{-1})	Assignment
841	C-H Rocking vibration
972	Rocking CH_3/Stretching C-C
1165	C-H Wagging
1375	Symmetrical bending CH_3
1450	Symmetrical bending CH_3
2897	CH_3 stretching
2917	Asymmetrical CH_2 stretching
2950	Asymmetrical CH_3 stretching
HAC	
1600	Aromatic C=C
1437	CH_2 aromatic
1035	Kaolinite
1000	C-O-C aliphatic ethers/alcohols
915	Al_2OH from kaolinite
536	Al/Si-O
468	Quartz

FTIR of tar from OG gasification and pyrolysis at obtained at 900 and 1000ºC is shown in Figure 5.7(b). Mostly aliphatic and aromatic structures are found. Aliphatic peaks of alkanes are observed at 2859 cm^{-1} and 2929 cm^{-1} (Fang et al., 2012), which are the characteristic peaks of polypropylene. Flatter peaks at 3058 cm^{-1} observed denote the formation of aromatic compounds (Taherian et al., 2021). The formation of oxygen-based compounds is observed in both N_2 and CO_2 conditions at 1265 and 1712 cm^{-1} (Shi et al.,

2012), (Yang et al., 2001). In N_2 conditions, C-O peaks are observed at 1027 and 1096 cm^{-1}(Patel et al., 2020), (Amit et al., 2020). This could be due to the consumption of such groups in CO_2 conditions.

5.2.6. SEM images

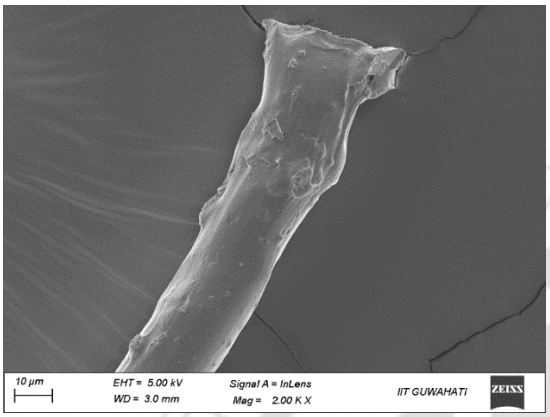

(a) OG Raw

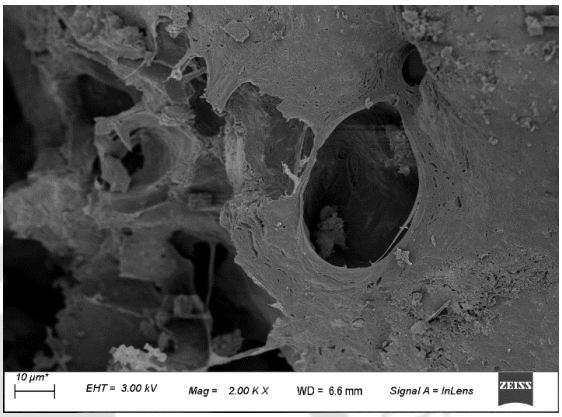

(b) HAC residue

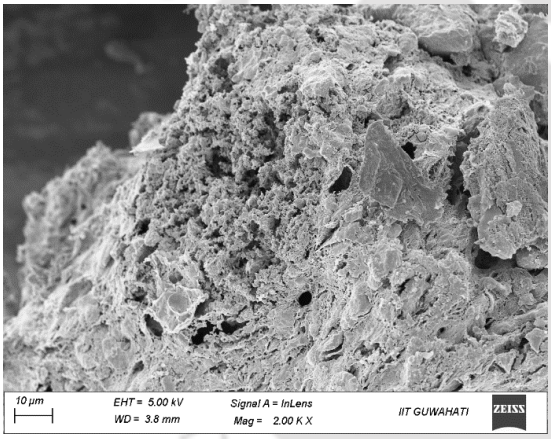

(c) HAC-OG 5% residue

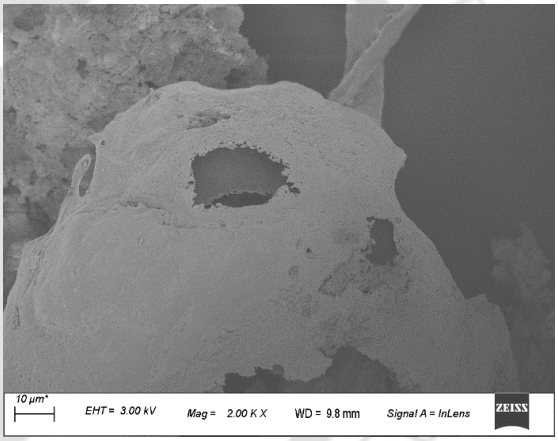

(d) HAC-OG 10% residue

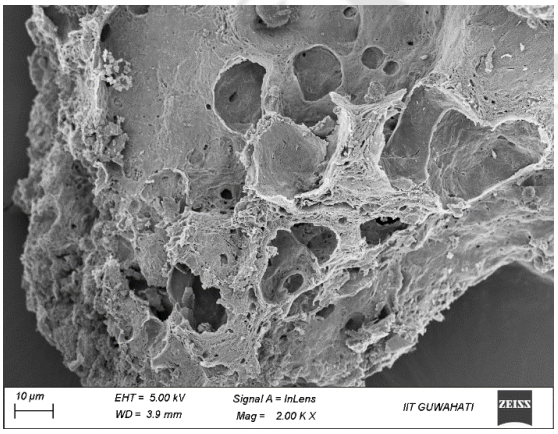

(e) HAC-OG 15% residue

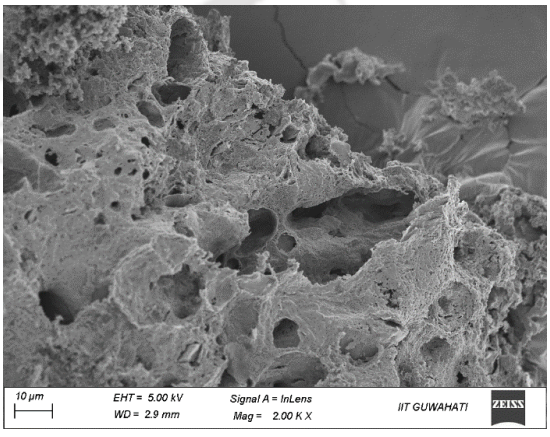

(f) HAC-OG 20% residue

Figure 5.8. SEM images of the residues obtained after the gasification of HAC and OG

To analyse the morphology of residue SEM analysis was carried out. SEM images of the residue obtained from various experiments are given in Figure 5.8. OG was found to be made of fibers (Figure 5.8(a)). These fibers are made up of plastic and at higher temperatures, OG fiber structures were rarely observed due to the devolatilization of polypropylene. It is observed only at a 10% OG mixture. In Figure 5.8(b), HAC residue pores are observed with large pore diameters. These pores are formed due to the sustained gasification of the coal with the diffusion of CO_2 along the pores. Further, the addition of OG to HAC results in the formation of highly porous structures. As soon as the volatile matter from OG is released, voids are created. From Figures 5.8(e) and 5.8(f), it can be noted that with the increase in the percentage of OG in the fuel mixture, the porosity of the solid mixture increases, which results in the formation of channels inside the residue.

5.2.7. Mass balance and residue analysis

Table 5.6 shows the mass and energy of the products obtained during gasification. Tar content is found high with an increase in the OG content. The surface area of the solid residue produced decreases with an increase in the OG. This could be due to partial coverage of pores by OG. Carbon yield of the experiment follows the same trend, it increases from 22.83 % to 37.83% when OG fraction in fuel is 20%. This reflects unconverted OG particles on coal. Adding OG to coal had a positive effect on the volume of syngas generated per mass of fuel. Volume of syngas generated increased from 39.72 liters (2.65 m^3/kg) to 50.15 liters (3.96m^3/kg). This was due to high amount of volatile matter present in OG. Ultimate analysis of the residue experiments is given in Table 5.7. When pyrolysis and gasification of OG were carried out under N_2 and CO_2 conditions, the volume of gas produced under CO_2 conditions was higher than N_2 conditions. It could be due to higher thermal cracking and gasification reactions.

Table 5.6. Mass analysis and surface area

Case	Residue weight %	Tar weight %	Gas weight %	BET surface area (m^2/gm)	Pore diameter (nm)	Carbon yield (%)	Syngas volume (m^3/kg)
HAC	51.07±1.09	1.53±0.4	47.4±2.83	147.61	2.88	22.83	2.65
HAC-OG (19:1)	50.8±2.05	1.7±0.56	47.5±2.02	116.23	2.22	28.98	3.14
HAC-OG (9:1)	50.31±0.83	1.84±0.41	47.85±1.88	118.76	2.49	35.23	3.2
HAC-OG (17:3)	49.86±1.1	2.06±0.33	48.08±1.54	84.38	2.22	35.77	3.78
HAC-OG (4:1)	49.7±2	2.18±0.41	48.12±2.03	77.87	2.26	37.83	3.96
OG 700ºC N_2	20.67±1.36	0	79.33±3	-	-	-	6.8
OG 700ºC CO_2	16±1.55	0	84±2.66	-	-	-	7.1
OG 900ºC N_2	10.2±1	17±0.96	72.8±2.56	-	-	-	7.68
OG 900ºC CO_2	7.2±0.5	16±1	76.8±3.6	-	-	-	8.41
OG 1000ºC CO_2	4.2±0.9	9.4±0.74	86.4±2.5	-	-	-	9.69

The higher volume of syngas (9.69 m^3/kg) is observed in CO_2 conditions at 1000ºC. Syngas volume produced for OG increased from 6.8 m^3/kg to 8.41 m^3/kg under N_2 conditions when temperature is increased from 700ºC to 900ºC. Similarly, under CO_2 conditions, it increases from 7.1 to 9.69 m^3/kg when operating temperature is increased from 700ºC to 1000ºC.

Table 5.7. Ultimate analysis of the residue obtained

Experiment	C	H	N	S	O	Ash%
HAC	25.66	0.495	0.28	0	13.78	59.78
HAC-OG (19:1)	33.2	1.01	0.35	0	7.95	57.48
HAC-OG (9:1)	41.32	0.5	0.54	0	2.23	55.41
HAC-OG (17:3)	42.9	0.6	0.42	0	2.83	53.24
HAC-OG (4:1)	46.12	0.6	0.61	0	1.92	50.74

5.2.8. XRD analysis

XRD of the obtained ash and char particles was carried out to analyse the presence of minerals. XRD of the residue obtained from the gasification and OG ash is shown in Figure 5.9. It can be observed that the OG ash contains a high amount of CaO and $CaCO_3$(Kumar & Ali, 2013),(Sánchez-Cantú et al., 2011). The residue contains clay (montmorillonite, illite, kaolinite), quartz and hematite particles, which was also reported by Barma et al. (Deb Barma et al., 2018). The presence of $CaCO_3$ and CaO can be observed from XRD peaks of the co-gasified residue at 32º, 37.4º, and 40.34º. It can be seen from the XRD peaks that the intensity of CaO is significantly lesser than quartz/clay particles. OG ash can act as a source of CaO and $CaCO_3$, which have been widely used as catalysts for the gasification of fuels (Murakami et al., 2015). This denotes the utility of char obtained from co-gasification of HAC and OG.

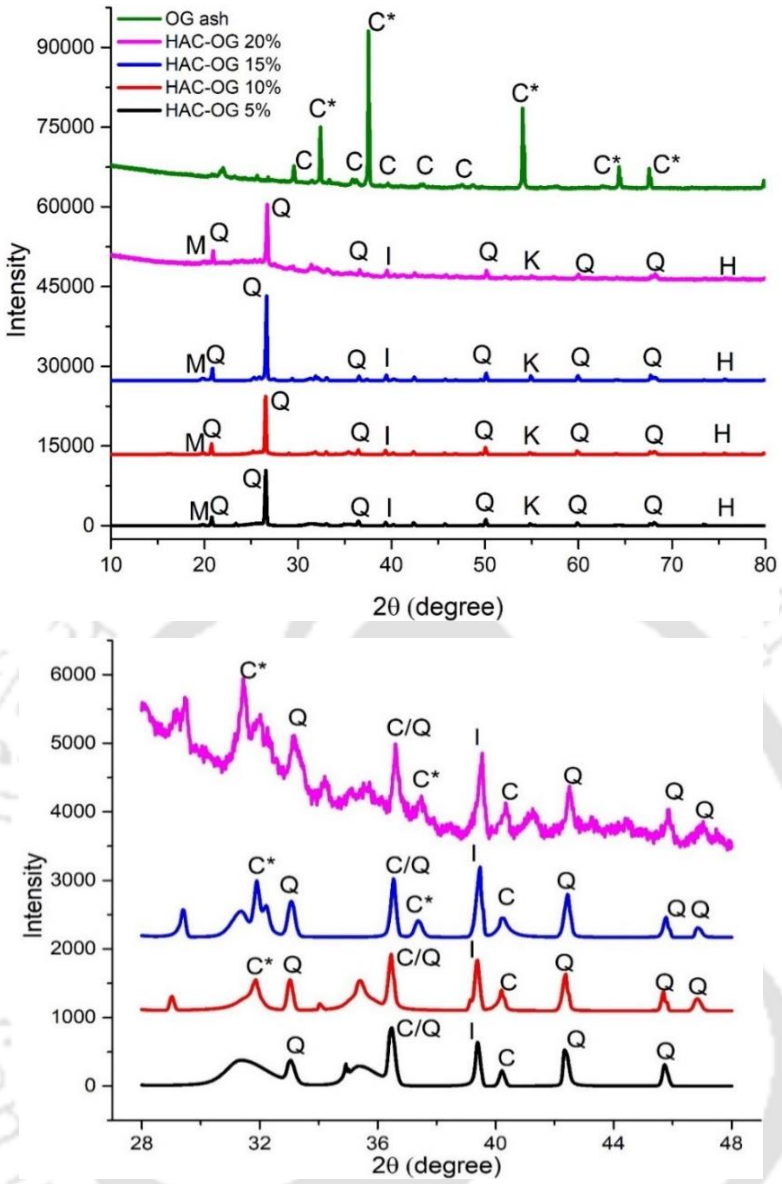

Figure 5.9. XRD peaks of residue and OG ash (C: $CaCO_3$, C*: CaO, K: Kaolinite, I: Illite, H: Hematite, Q: Quartz, M: Montmorillonite)

5.2.9. Reaction mechanism between coal and OG

Figure 5.10 summarises the physical activities between coal and OG. When coal and OG are fed into the reactor at 1000°C, rapid devolatilization of coal and OG takes place. Devolatilization of coal releases volatile matter resulting in the formation of pores (Figure 5.8(b)). OG is mostly devolatilized at the start of the reaction. The leftover OG deposits over the coal char. As the OG is mostly made up of polypropylene, due to steric hindrance, the molten propylene slowly flow into the coal pores (Ishaq et al., 2006). With progress in time, the OG volatile matter is almost released completely, however, the fixed

carbon in OG reacts with CO_2 and this reaction is comparatively faster than the CO_2-coal based char (Table 5.2, 5.07%/min v/s 0.7%/min.). This results in the deposition of the OG ash over the coal surface/pores and further this prevents the reaction between CO_2 and coal char as the CO_2 path is blocked by the OG ash in the pores. The minor of amounts of the leftover OG based volatile matter or fixed carbon react with CO_2 and form CO or other gases.

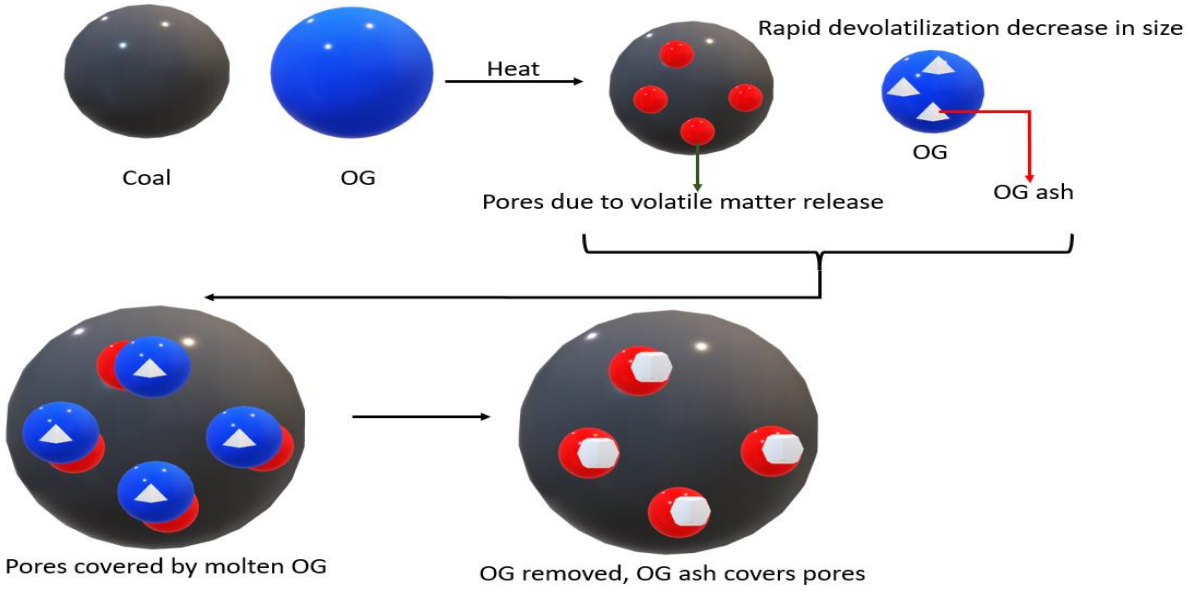

Figure 5.10. Physical activities between coal and OG

5.3. Summary of the chapter

Pyrolysis and gasification of PPE gown were carried out at 500ºC, 700ºC, and 900ºC. Tar was obtained at the operating temperatures of 900ºC and 1000ºC with low oxygen content under CO_2 conditions. Co-gasification of HAC and OG (overall gown) was carried out by varying the percentage of the gown from 0 to 20%. The addition of OG to HAC significantly increased the calorific value of syngas by 45.4% and 51.8% with the increase in the OG content in the fuel mixture by 15 and 20%. Hydrogen, methane, and C2-C3 hydrocarbons in the syngas increased by 3.46, 6.2, and 8.73 times, respectively, during the 20% addition of OG content in the fuel mixture. Gown ash is rich in CaO (~32%) and $CaCO_3$ (~67%) (EDX analysis), which can act as a catalyst during gasification for the generation of syngas.

References

Amit, Jamwal, R., Kumari, S., Dhaulaniya, A. S., Balan, B., Kelly, S., Cannavan, A., &

Singh, D. K. (2020). Utilizing ATR-FTIR spectroscopy combined with multivariate chemometric modelling for the swift detection of mustard oil adulteration in virgin coconut oil. *Vibrational Spectroscopy*, *109*(February), 103066. https://doi.org/10.1016/j.vibspec.2020.103066

Deb Barma, S., Sathish, R., Baskey, P. K., & Biswal, S. K. (2018). Chemical Beneficiation of High-Ash Indian Noncoking Coal by Alkali Leaching under Low-Frequency Ultrasonication. *Energy and Fuels*, *32*(2), 1309–1319. https://doi.org/10.1021/acs.energyfuels.7b03291

Duan, L., Zhao, C., Zhou, W., Qu, C., & Chen, X. (2009). Investigation on coal pyrolysis in CO2 atmosphere. *Energy and Fuels*, *23*(7), 3826–3830. https://doi.org/10.1021/ef9002473

Eterigho-Ikelegbe, O., Trammell, R., & Bada, S. (2021). Preparation and characterization of ceramic composites from South Africa coal discard. *Construction and Building Materials*, *302*(June), 124164. https://doi.org/10.1016/j.conbuildmat.2021.124164

Fang, J., Zhang, L., Sutton, D., Wang, X., & Lin, T. (2012). Needleless melt-electrospinning of polypropylene nanofibres. *Journal of Nanomaterials*, *2012*. https://doi.org/10.1155/2012/382639

Franco, P., Incarnato, L., & De Marco, I. (2019). Supercritical CO_2 impregnation of α-tocopherol into PET/PP films for active packaging applications. *Journal of CO_2 Utilization*, *34*(February), 266–273. https://doi.org/10.1016/j.jcou.2019.06.012

Ishaq, M., Ahmad, I., Shakirullah, M., Khan, M. A., Habib ur Rehman, & Bahader, A. (2006). Pyrolysis of some whole plastics and plastics-coal mixtures. *Energy Conversion and Management*, *47*(18–19), 3216–3223. https://doi.org/10.1016/j.enconman.2006.02.019

Isik Gulsac, I. (2021). Thermochemical conversion behavior of turkish lignite/poppy capsule pulp blends in N_2 and CO_2 atmospheres. *Gazi University Journal of Science*, *34*(2), 355–368. https://doi.org/10.35378/gujs.737055

Kumar, D., & Ali, A. (2013). Transesterification of low-quality triglycerides over a Zn/CaO heterogeneous catalyst: Kinetics and reusability studies. *Energy and Fuels*, *27*(7), 3758–3768. https://doi.org/10.1021/ef400594t

Kwon, G., Cho, D. W., Hyun Moon, D., Kwon, E. E., & Song, H. (2019). Beneficial use of CO_2 in pyrolysis of chicken manure to fabricate a sorptive material for CO_2. *Applied Thermal Engineering*, *154*(February), 469–475. https://doi.org/10.1016/j.applthermaleng.2019.03.110

Lai, Z., Ma, X., Tang, Y., & Lin, H. (2012). Thermogravimetric analysis of the thermal decomposition of MSW in N_2, CO_2 and CO_2/N_2 atmospheres. *Fuel Processing Technology*, *102*, 18–23. https://doi.org/10.1016/j.fuproc.2012.04.019

Lee, J., Lee, T., Ok, Y. S., Oh, J. I., & Kwon, E. E. (2017). Using CO_2 to mitigate evolution of harmful chemical compounds during thermal degradation of printed circuit boards. *Journal of CO_2 Utilization*, *20*(May), 66–72. https://doi.org/10.1016/j.jcou.2017.05.009

Murakami, K., Sato, M., Tsubouchi, N., Ohtsuka, Y., & Sugawara, K. (2015). Steam gasification of Indonesian subbituminous coal with calcium carbonate as a catalyst raw material. *Fuel Processing Technology*, *129*, 91–97. https://doi.org/10.1016/j.fuproc.2014.08.023

Patel, N., Shadangi, K. P., & Kar, P. K. (2020). Characterization of waste engine oil derived pyrolytic char (WEOPC): SEM, EDX and FTIR analysis. *Materials Today: Proceedings*, *38*, 2866–2870. https://doi.org/10.1016/j.matpr.2020.09.138

Rodríguez-Luna, L., Bustos-Martínez, D., & Valenzuela, E. (2021). Two-step pyrolysis for waste HDPE valorization. *Process Safety and Environmental Protection*, *149*, 526–536. https://doi.org/10.1016/j.psep.2020.11.038

Saad, J. M., Williams, P. T., Zhang, Y. S., Yao, D., Yang, H., & Zhou, H. (2021). Comparison of waste plastics pyrolysis under nitrogen and carbon dioxide atmospheres: A thermogravimetric and kinetic study. *Journal of Analytical and Applied Pyrolysis*, *156*(April), 105135. https://doi.org/10.1016/j.jaap.2021.105135

Sánchez-Cantú, M., Pérez-Díaz, L. M., Rosales, R., Ramírez, E., Apreza-Sies, A., Pala-Rosas, I., Rubio-Rosas, E., Aguilar-Franco, M., & Valente, J. S. (2011). Commercial hydrated lime as a cost-effective solid base for the transesterification of wasted soybean oil with methanol for biodiesel production. *Energy and Fuels*, *25*(7), 3275–3282. https://doi.org/10.1021/ef200555r

Shi, J., Xing, D., & Li, J. (2012). FTIR studies of the changes in wood chemistry from wood forming tissue under inclined treatment. *Energy Procedia*, *16*(PART B), 758–762. https://doi.org/10.1016/j.egypro.2012.01.122

Taherian, Z., Dehaghani, A. H. S., Ayatollahi, S., & Kharrat, R. (2021). A new insight to the assessment of asphaltene characterization by using fortier transformed infrared spectroscopy. *Journal of Petroleum Science and Engineering*, *205*(March), 108824. https://doi.org/10.1016/j.petrol.2021.108824

Yang, X. F., Vang, C., Tallman, D. E., Bierwagen, G. P., Croll, S. G., & Rohlik, S. (2001). Weathering degradation of a polyurethane coating. *Polymer Degradation and Stability*, *74*(2), 341–351. https://doi.org/10.1016/S0141-3910(01)00166-5

Yousef, S., Eimontas, J., Striūgas, N., & Abdelnaby, M. A. (2021). Pyrolysis kinetic behaviour and TG-FTIR-GC–MS analysis of Coronavirus Face Masks. *Journal of Analytical and Applied Pyrolysis*, *156*(April). https://doi.org/10.1016/j.jaap.2021.105118

Zhang, G., Ranjith, P. G., Li, Z., Vongsvivut, J., & Gao, M. (2021). Application of synchrotron ATR-FTIR microspectroscopy for chemical characterization of bituminous coals treated with supercritical CO_2. *Fuel*, *296*(February), 120639. https://doi.org/10.1016/j.fuel.2021.120639

This page is left blank intentionally

This page is left blank intentionally

CHAPTER 6

CO-GASIFICATION OF HIGH ASH COAL WITH PRINTED CIRCUIT BOARD

In this section, pyrolysis and gasification of printed circuit board (PCB) obtained is performed under N_2 and CO_2 conditions to evaluate the products obtained (gas, residue and tar). In this study, the PCB of computers are separated into three components such as plastics, resins and metals. Thermal treatment is carried out using the individual components as well as under mixed condition at various temperatures of 500, 700 and 900°C. Further, co-gasification of PCB with HAC is performed under CO_2 conditions and the synergism among the feedstock is explored.

6.1. Experimental description

In the present study, printed circuit boards (PCB) are obtained from a computer waste based shop in Guwahati City. PCB's are disassembled and their components are separated. The components derived from PCB are resin, plastics and metals. These segregated components are thermally treated individually with HAC. Further, these individual PCB components are mixed as per the composition given in Table 6.1. These mixed components are termed as "PCB mixture". The mixed components are used as one of the feedstocks for thermal treatment. Three types of metals are obtained copper, aluminium and tin/aluminium alloy. The presence of these metals are confirmed by XRD analysis. In Table 6.1, the weight percentage of individual components of PCB mixture is given.

The resin and plastics in PCB possess a high amount of ash and oxygen severely affecting the calorific value. The calorific value of the mixed components of PCB is estimated as 6.04 MJ/kg whereas the plastic component of PCB mixture has 9.4 MJ/kg. The maximum combustible mass in the PCB mixture is found to be 34.78 wt.%. Figure 6.1 shows the photographs of components recovered from PCB mixture.

Table 6.1. Composition of PCB mixture

Component	Weight, %
Copper	2.25
Aluminum	12.68
Tin aluminum alloy	5.49
PCB resin	60.95
PCB plastic	18.63

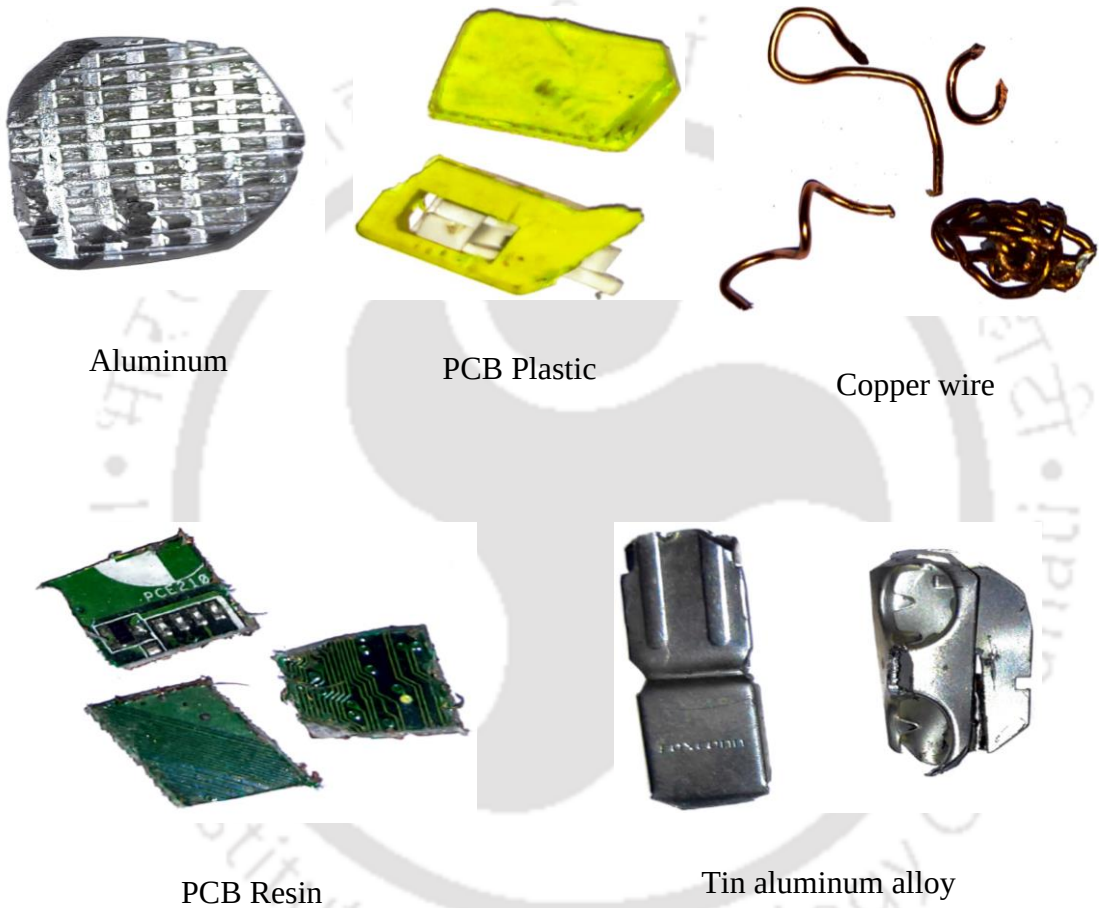

Figure 6.1. Components of printed circuit board mixture

Pyrolysis and gasification experiments are performed in isothermal conditions. The list of experiments performed in this section are given in Table 6.2.

Table 6.2. List of experiments carried out using PCB and HAC

PCB pyrolysis and gasification						
S. No.	Fuel (weight ratio)	Fuel weight (gm)	Temperature (ºC)	Atmosphere	Flow rate (lpm)	Experiment type
1	PCB mixture	50	500	N_2	0.3	Pyrolysis
2			700			Pyrolysis
3			900			Pyrolysis
4			500	CO_2		Pyrolysis
5			700			Pyrolysis
6			900			Gasification
7	PCB mixture	15	1000			Gasification
HAC and PCB based co-gasification						
8	HAC:PCB mixture (4:1)	15		CO_2	0.3	Gasification
9	HAC:PCB resin (4:1)					Gasification
10	HAC:PCB plastic (4:1)					Gasification
11	HAC		1000			Gasification
12	HAC		900			Gasification

6.2. Co-pyrolysis and co-gasification of PCB with HAC

6.2.1. XRD of Metals

XRD analysis of the obtained metals is reported in Figure 6.2. Peaks at 43.6, 50.8, and 74.4˚ confirm the presence of copper metal (Yu et al., 2019). Aluminium peaks are observed at 38.42, 44.7, 65.02, and 78.26˚(Ji et al., 2022). Third metal contains major peaks at 30.8˚, 32.16˚, and 44.82˚, corresponding to tin (Hu et al., 2014). The peak at 38.62˚ may correspond to the alloy of tin and aluminium. It can be noticed from Figure 6.2 that pure metals like copper and aluminium can be reasonably recovered without complicated metallurgical processes.

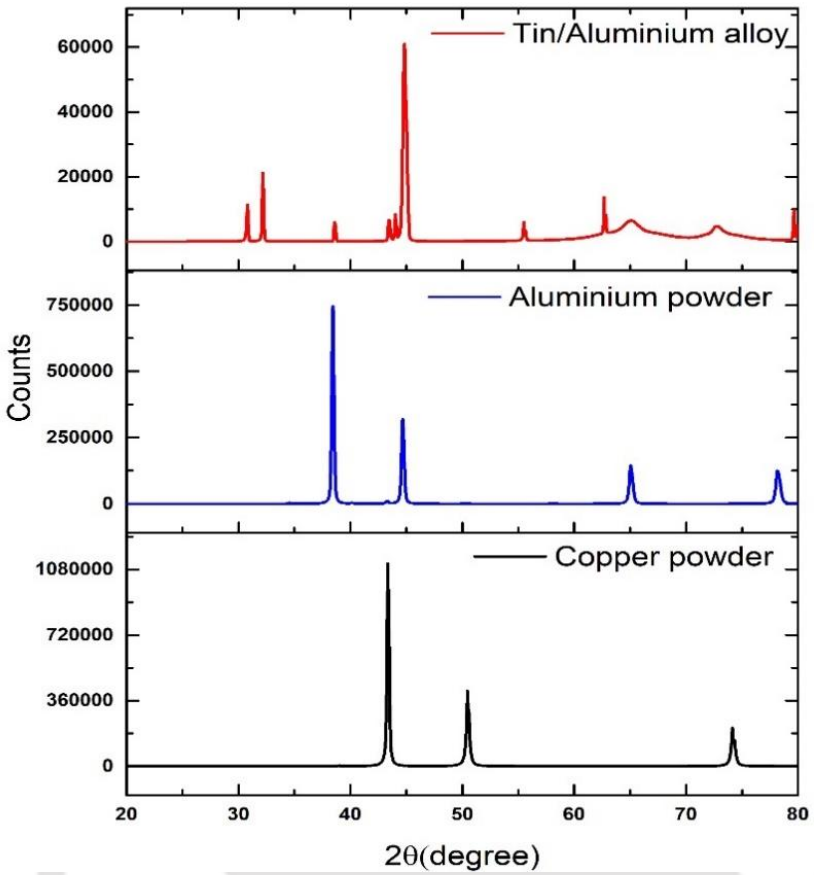

Figure 6.2. XRD of metals found in PCB

6.2.2. TGA analysis

Table 6.3. TGA analysis of fuels under N_2 and CO_2 conditions at low-temperature

	CO_2 conditions			
	Residue %	Weight loss range (˚C)	DTG_{max}(˚C)	Maximum weight loss rate (%/min.)
HAC	64.12	400-572	508.66	1.74
PCB resin	68.87	270-379	335.73	5.34
PCB plastic	28.62	330-417	391.72	33.88
	N_2 Conditions			
	Residue %	Weight loss range (˚C)	DTG_{max}(˚C)	Maximum weight loss rate (%/min.)
HAC	77.59	400-592	515	1.34
PCB resin	69.31	250-424	344.04	3.91
PCB plastic	41.1	300-410	386.84	20.02

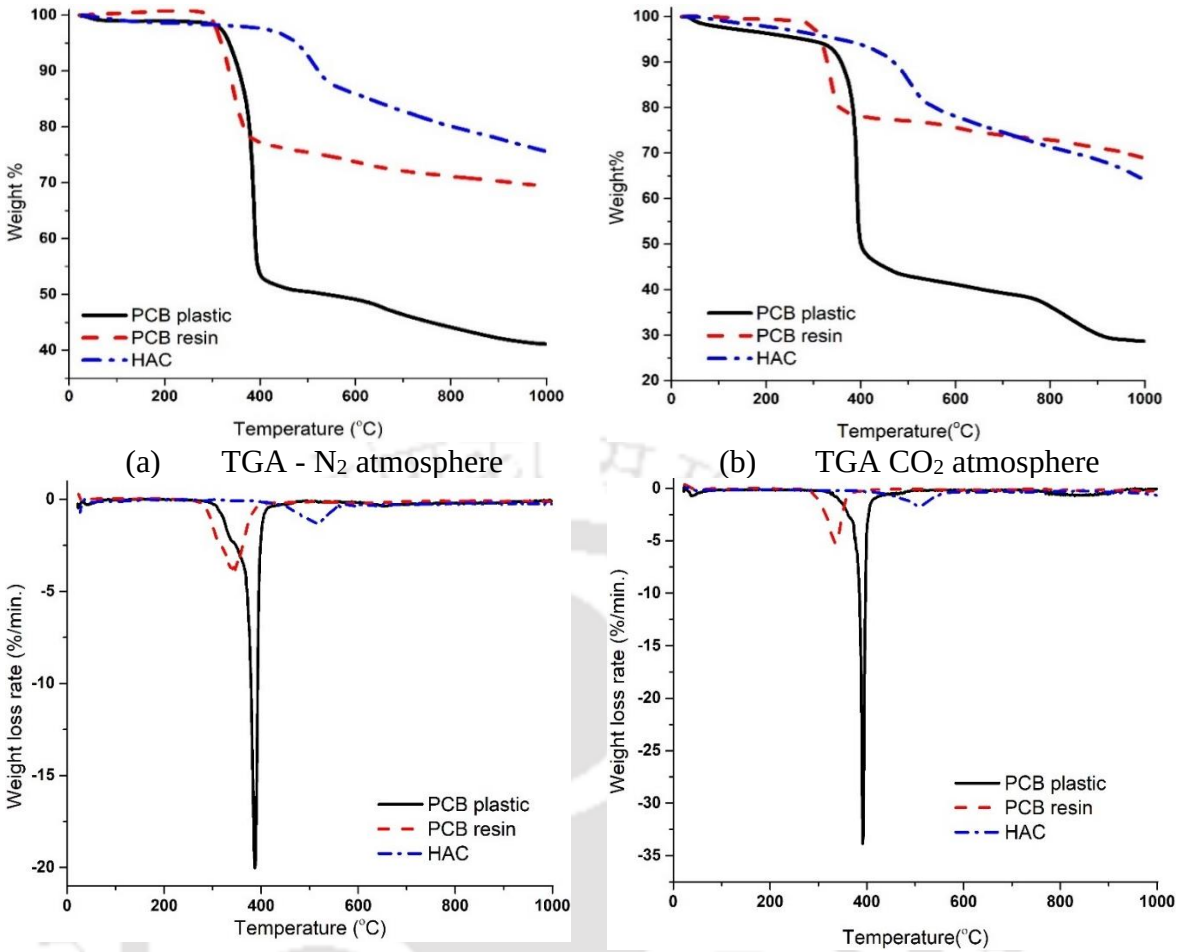

Figure 6.3. TGA curves of fuels under (a) N_2, (b) CO_2 conditions, and DTG curves of fuels under (c) N_2, (d) CO_2 conditions

TGA analysis of the fuels is given in Table 6.3. The maximum weight loss rate of PCB plastics with CO_2 is 13.8%/min higher than the N_2 conditions, which ensures CO_2 reactivity with PCB plastics at 392°C. Figure 6.3 shows the weight loss and derivative thermogravimetric (DTG) curves of PCB and HAC under N_2 and CO_2 conditions. During CO_2 conditions, Boudouard reaction occurs between 950˚C and 1000˚C. The gasification of PCB plastic reactions happened between 774˚C and 923˚C. PCB resin has low fixed carbon content, resulting in little progress in gasification reactions between 800-880 ˚C. As a typical result, the weight loss rate under CO_2 conditions is higher than N_2 conditions, and the range of weight loss decreases under CO_2 gasification conditions. This could be due to higher thermal conductivity of CO_2 (Guo-dong et al., 2016). The additional weight loss due to the gasification in HAC, PCB resin, and PCB plastic was 13.47%, 12.48%, and 0.33%, respectively. Boudouard reaction begins at different temperatures for different fuels. This could be due to the variations in char structures, which are formed

after the release of volatile matter. Due to the high ash content in HAC and PCB resin, the Boudouard reactions occur at a higher temperature (950°C and 800°C) than PCB plastic (774ºC). The ash content in fuels also has a significant amount of silicon and aluminium, negatively affecting gasification.

Kinetic studies are carried out using reaction order and diffusion models. First, second, and third order reactions are considered for reaction order models. The 2D and 3D reaction models are used in the diffusion models. Activation energy is calculated in two separate stages by Coats-Redfern method. The activation energy of HAC-based pyrolysis reactions under N_2 and CO_2 conditions is 62.07 kJ/mol and 29.1 kJ/mol, respectively. In Table 6.4 Kinetic analysis of HAC, PCB resin and PCB plastics are given.

Table 6.4. Kinetic parameters under N_2 and CO_2 conditions

	Volatile matter pyrolysis (400-600˚C)							
	N_2 pyrolysis				CO_2 pyrolysis			
Sample	E(kJ/mol)	A (min^{-1})	R^2	Model	E(kJ/mol)	A (min^{-1})	R^2	Model
HAC	62.07	6.8×10^3	0.98	Order 1	29.1	1.54×10^6	0.97	Order 1
PCB resin	171.29	1.1×10^7	0.99	Order 3	153.39	6.9×10^9	0.97	Order 3
PCB plastic	123.2	1.4×10^6	0.98	Order 1	59.57	2125.7	0.97	Order 1
	CO_2 gasification conditions (800-1000˚C)							
	E		A		R^2		Model	
HAC	18.09		3.4×10^8		0.973		D3-model	
PCB resin	16.38		2.6×10^5		0.96		D3-model	
PCB plastic	14.11		4.23×10^5		0.994		D2- model	

The activation energy under CO_2 conditions for PCB resin and PCB plastics is found lower by 17.9 kJ/mol and 63.6 kJ/mol than N_2 conditions, respectively. Plastic and resin reactions with CO_2 in the temperature range of 400 to 600°C have the best fit for first order and second order reaction models, respectively. The activation energy for the pyrolysis reactions with PCB resin and plastic is found two to three times higher than the HAC. This may be due to the higher energy required for thermal cracking of polymers in the PCB. At temperatures above 900˚C, the activation energy of HAC and PCB resin based reactions is found similar due to uniform char gasification. Activation energy

obtained in the current study for pyrolysis conditions is compared with literature and is found to be reasonably accurate. The activation energy of PCB resin and PCB plastic based reactions under N_2 conditions was found to be 171.29 kJ/mol and 123.2 kJ/mol, respectively.

6.2.3. FTIR of feed and tar samples

$$R - NH_2 + CO_2 \rightarrow COOCNR \quad (6.1)$$

FTIR analysis of the feed (HAC, PCB plastic, PCB resin) and tar residues is shown in Figure 6.4. It can be observed that the functional groups containing oxygen are highly prevalent, which is already confirmed by ultimate analysis. Oxygen-containing functional groups in plastics are observed at 1031 cm^{-1}, 1637 $cm^{-1,}$ and 1738 cm^{-1}. These are due to the presence of ether functional groups, epoxy resins, and carbonyl groups, respectively (Reena et al., 2011), (Wang & Zhang, 2004), (Jain et al., 2002). The presence of C-Br bond is identified in PCB plastic and resins, possibly due to brominated epoxide resin (Shen et al., 2018). The presence of amine groups is observed in PCB plastic at 3296 cm^{-1} and 939 cm^{-1}, which is found in phenolic resin curing agent and –NH- bending vibrations (Jain et al., 2002), (Sahoo et al., 2012). FTIR peaks at 688 and 731 cm^{-1} represent C-H bending vibrations in benzene rings (Lakshminarayana et al., 2020). FTIR analysis of PCB resin, PCB plastic, and HAC based on the literature ((Bodzay et al., 2009; Gokulakumar & Narayanaswamy, 2008; Guo & Wu, 2018; Lakshminarayana et al., 2020; Luda et al., 2007; Nie et al., 2020; Reena et al., 2011; Sahu & Vairakannu, 2021; Sanapala, 2008; Shen et al., 2018; Tahir et al., 2021; Wu & Qiu, 2014; Yanti et al., 2016),(Singh et al., 2020) is given Table 6.5. High ash coal contains kaolinite clay, aluminium, and silicon oxides. Further, aromatic structures are observed at 1437 cm^{-1} and 1600 cm^{-1} (Bhui & Prabu, 2021).

FTIR of tar products formed by pyrolysis and gasification of PCB mixture at 500, 700, and 900ºC is shown in Figure 6.4(b). The tar obtained by CO_2-pyrolysis contains -CN group (2233cm^{-1}), which was due to the reaction between -NH_2 groups in PCB plastic and CO_2 gas (Sajjan et al., 2020)(Huang et al., 2021). Equation 6.1 gives the reaction between CO_2 and amines in the plastic, which does not occur under N_2 conditions. Irrespective of operating temperatures, the major functional groups obtained in the tar are C-H, C-Br, C=C, OH, and CH_2. The peaks of tar at 754 cm^{-1} and 1232 cm^{-1} represent benzene structures. The peaks at 1232 cm^{-1} and 754 cm^{-1} represent the bending vibration

of C-H bond in benzene ring and plane bending of benzene ring vibration (Nie et al., 2020). The peak at 500 cm^{-1} represents C-Br bond revealing the presence of bromine in tar, which is highly corrosive, and its presence is detrimental to its applicability (Evangelopoulos et al., 2020). The peaks at 889 cm^{-1} represent C-H deformation of alkene groups, which would improve knocking resistance of oil (Bodzay et al., 2009), (C. W. Zhou et al., 2022).

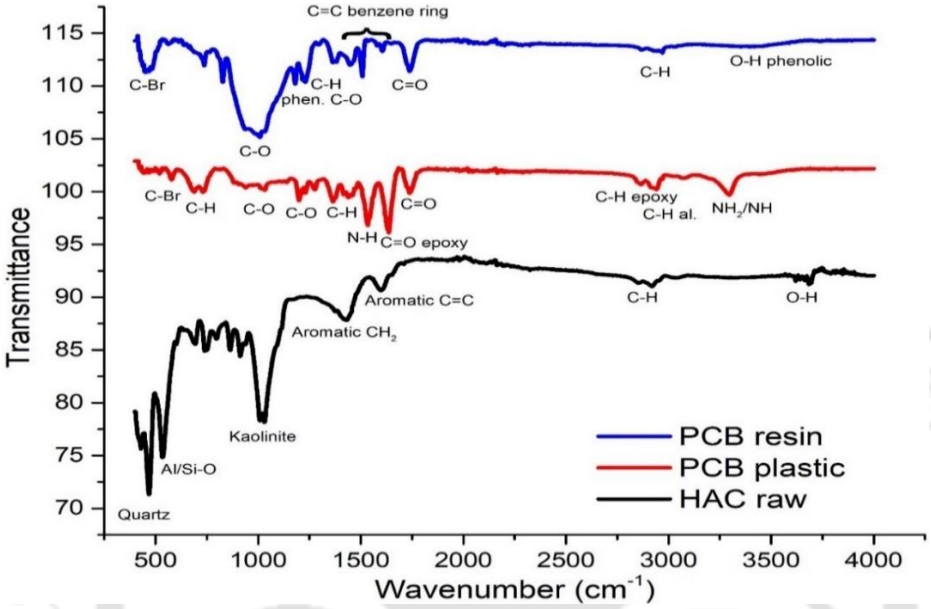

(a) FTIR spectra of PCB and HAC fuels

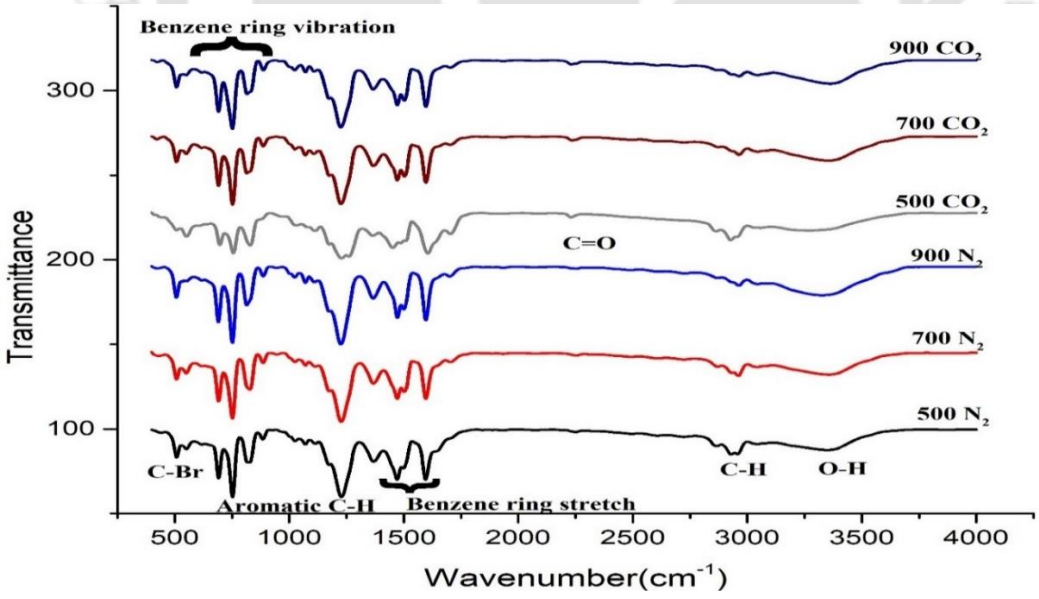

(b) FTIR spectra of PCB tar

Figure 6.4. FTIR spectra of (a) PCB and HAC fuels and (b) PCB tars

Peaks at 693 cm^{-1}, 829 cm^{-1}, 1473 cm^{-1}, and 1502 cm^{-1} represent bending of benzene rings. Like feed, OH phenolic groups are also observed at 3387 cm^{-1} and the presence of

aldehyde is detected at 2859 cm^{-1}. Oil's phenolic and aldehydic functional groups are known to affect flow properties and increase its corrosiveness (Lohitharn & Shanks, 2009). Bending vibrations of CH_2 groups are obtained at 2935 cm^{-1} due to the presence of alkane groups, which decreases the oil's boiling and freezing point, improving the jet-fuel properties (Jiménez-Díaz et al., 2017).

Figure 6.4 shows that the intensity of FTIR peak at 2935 cm^{-1} (CH_2 alkanes) decreases with temperature. This could be due to thermal cracking of such functional groups at high temperatures to a gaseous state. Aromatic structures are highly prevalent in tar. As the operating temperature increases, the aromatic peaks start becoming sharper. This could be due to the removal of other functional groups at higher temperatures. Blunt aromatic peaks are observed at 500˚C during CO_2 pyrolysis at 1234 cm^{-1}. Aromatic CH groups and saturated hydrocarbons decrease with an increase in the operating temperature due to thermal cracking reactions. These aromatic groups are observed in the tar because of the thermal cracking of PCB resin and PCB plastics. The high amount of aromatics in bio-oil improves the oil's octane number (Beims et al., 2018). The representation of peaks in Figure 6.4 are also given in Table 6.5.

Table 6.5. FTIR data of fuels and tar

Wavenumber (cm^{-1})	Functional group	Reference
	PCB Resin	
452	C-Br	Shen et al., 2018
871 and 1000	C-O epoxy resin	
1181 and 1231	C-O stretching phenolic compounds	Yanti et al., 2016
1365	C-H deformation methyl groups	
1450, 1508 and 1606	C=C benzene ring stretching	Shen et al., 2018
1740	C=O	
2970	Methyl and methylene groups	Yanti et al., 2016
3402	O-H	Nie et al., 2020
	PCB Plastic	
578	Aromatic ring from DGEBA-DGETBBA	Sanapala, 2008
688-731	C-H out of plane vibrations	Lakshminarayana et al., 2020
1031	C-O primary alcohols/ester	Bodzay et al., 2009
1076	CO-H Secondary alcohols	Alenezi & Al-Fadhli, 2018
1199	P=O from flame retardant	Bodzay et al., 2009
1277	Phenyl-O brominated epoxy	
1439	Aromatic C-C	Luda et al., 2007
1535	Aromatic C-C	
1637	-C=O cured epoxy systems	Bodzay et al., 2009
1738	-C=O carbonyl bond	
2907	-CH epoxy resin	
2940	C-H aliphatic stretch	Reena et al., 2011
3296	NH_2/NH bond	Bodzay et al., 2009

PCB Oil		
Wavenumber (cm^{-1})	Functional group	Reference
500	C-Br	Nie et al., 2020
558	Aromatic ring from DGEBA-DGETBBA	Evangelopoulos et al., 2020
693,754 and 829	bending vibration of C-H bond in benzene ring	Nie et al., 2020
889	C-H deformation peak from alkenes	Evangelopoulos et al., 2020
1232	C-H bond in benzene ring	Nie et al., 2020
1371	CH_2 bending vibrations in benzene ring	Wu & Qiu, 2014
1473,1502 and 1598	Aromatic benzene ring C=C	Nie et al., 2020
2962	C-H saturated hydrocarbon	
2935	OH stretching	Gokulakumar & Narayanaswamy, 2008
2859	CH stretching vibrations aldehyde groups	
3387	O-H phenolic resin	Nie et al., 2020

6.2.4. SEM analysis

Figure 6.5 shows the SEM images of PCB resin and residue at different operating temperatures and atmospheric conditions. Raw PCB resin showed rod-shaped particles (Fig. 6.5(a)). These are glass fibers generally used in PCB (Shen et al., 2018). When thermal treatment of PCB is performed at 500°C, the glass fibers thermally join with plastics and other particles irrespective of atmospheric conditions (Fig. 6.5(b) and 6.5(f)). At 700°C, volatile matters get released resulting in pore formation, and hence the glass fiber structures remain intact in the pores. The pores are large enough to accommodate glass fibers in CO_2 conditions, compared to N_2 conditions (Fig. 6.5(c), 6.5(d), and 6.5(g)). At 900°C, it can be observed that a network of pores is formed due to Boudouard reaction between CO_2 and fixed carbon in feed. CO_2 easily diffuses inside the pores in the char matrix resulting in the formation of channels. Under N_2 conditions at 900°C, due to the excessive and rapid release of volatile matter, porous channels with larger diameters are formed (Fig. 6.5(e), 6.5(h)), as compared to 700°C.

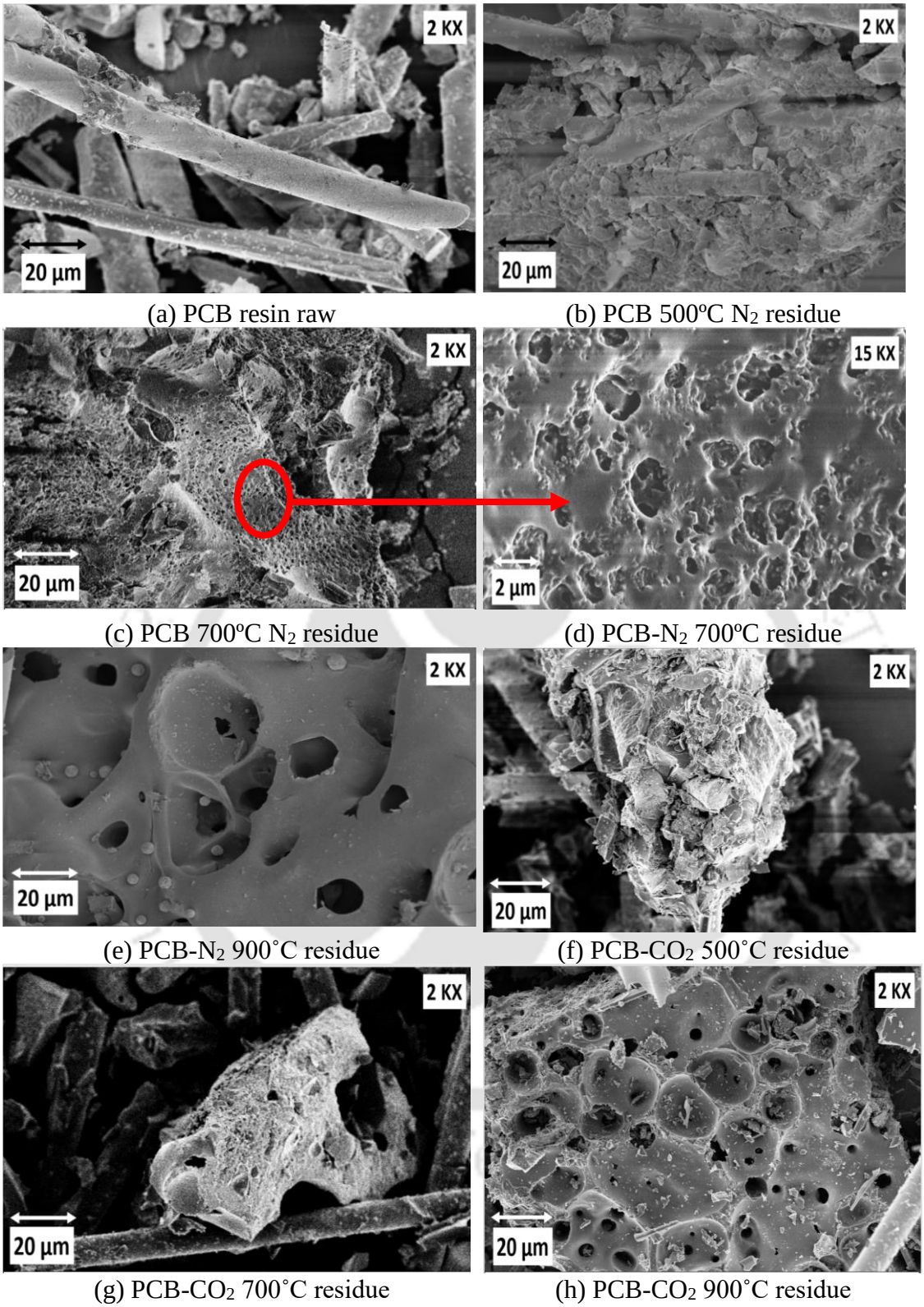

(a) PCB resin raw (b) PCB 500ºC N_2 residue

(c) PCB 700ºC N_2 residue (d) PCB-N_2 700ºC residue

(e) PCB-N_2 900˚C residue (f) PCB-CO_2 500˚C residue

(g) PCB-CO_2 700˚C residue (h) PCB-CO_2 900˚C residue

Figure 6.5. SEM analysis of the PCB residue by pyrolysis and gasification

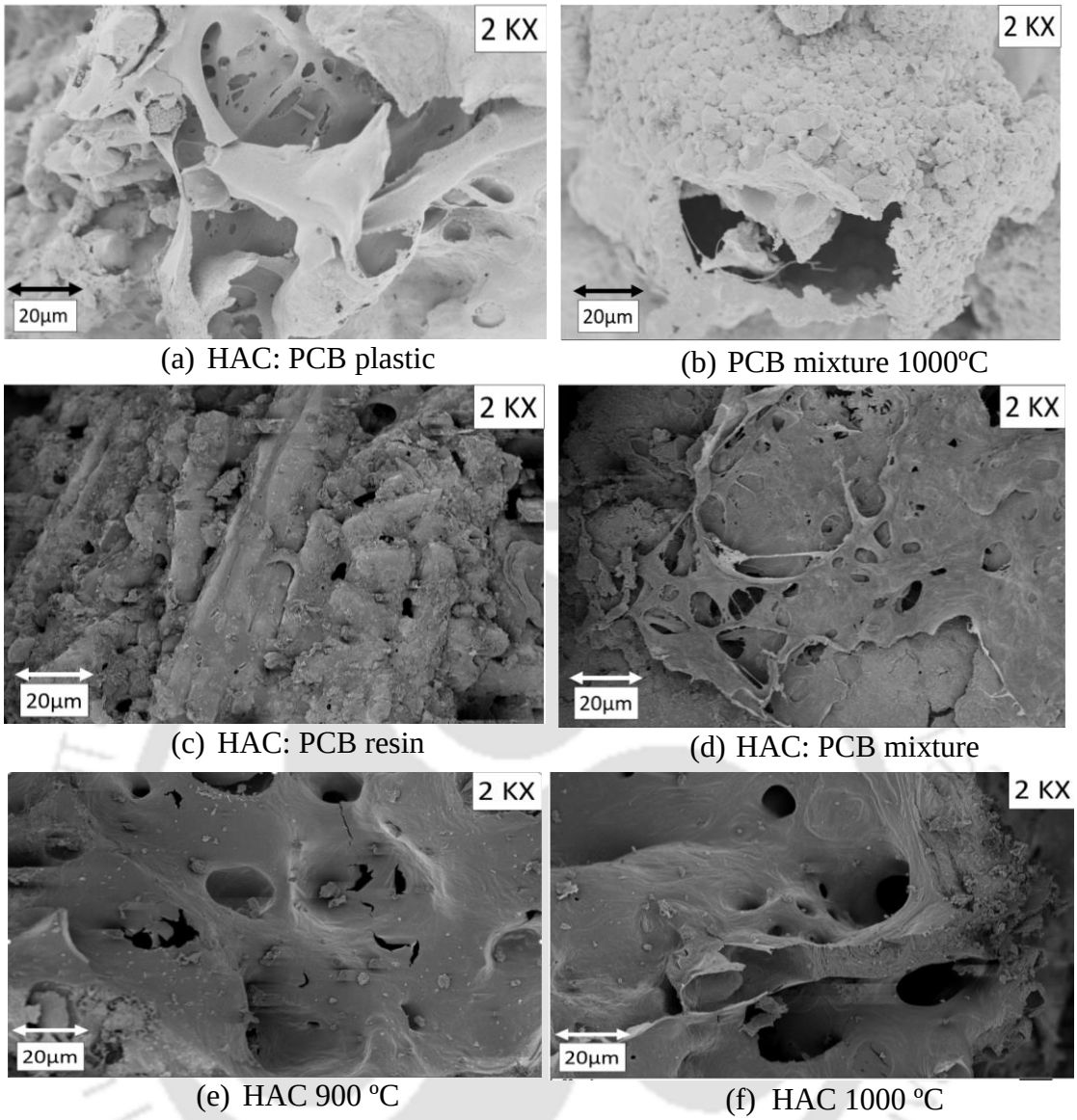

(a) HAC: PCB plastic (b) PCB mixture 1000ºC

(c) HAC: PCB resin (d) HAC: PCB mixture

(e) HAC 900 ºC (f) HAC 1000 ºC

Figure 6.6. SEM images of residue from co-gasification of HAC and PCB components

Figure 6.6 shows the SEM images of the gasification residue obtained. Pure HAC residue obtained at 900ºC and 1000ºC (Fig. 6.6(e) & 6.6(f)) showed the presence of larger pores, compared to co-gasification residue. The addition of PCB-based fuels changes the morphology of the char obtained (Fig. 6.6(a), 6.6(c), and 6.6(d)). During co-gasification of plastics and coal, the volatile matter in coal is released from the char matrix leaving porous structure bonded with higher molecular weight polymers. These co-residue porous structures are different, compared to the char of HAC alone. Plastic based co-gasification residue is highly porous and the pores formed are deep penetrated inside the residue, whereas the HAC pores are formed on the surface. However, the mixing HAC with PCB resin showed distinct rod shape structures in the residue. These structures covered the pores formed by HAC; thus, the pore development is hindered in the PCB

resin. This effect is found to be low in the co-gasification of PCB mixture with HAC. It can be observed in Figure 6.6(d) that the addition of PCB mixture with HAC decreases the surface area of the residue. As discussed earlier, the plastics tend to form a layer over HAC and hence two layers are observed. The top layer is plastic and the coal char layer is formed below it.

6.2.5. Pyrolysis and gasification of PCB mixture

Figure 6.7 shows the gas composition and the calorific value of syngas released at various operating temperatures. Under CO_2 conditions, PCB cracking is more severe than in N_2 conditions, which was confirmed by the mass balance. At 500°C and 700°C, only the volatile matter is released during the initial phase (0-30 min). With increase in the temperature to 900°C under CO_2 conditions, the gasification of char occurs due to the formation of channels (Figure 6.5(e)). This results in the consistent release of CO after the initial phase of devolatilization around 9% (Figure 6.7(d)). After the initial pyrolysis phase, almost 8-9% of H_2 is continuously liberated in both atmospheres. Under the CO_2 pyrolysis conditions, the liquid/tar product weight is at least 0.24 to 0.64% less than N_2 pyrolysis conditions. A 2.5-2.7% methane gas is observed under N_2 and CO_2 pyrolysis conditions. Methane is not released at 500ºC, which affects syngas' calorific value.

The maximum concentration of methane is found similar irrespective of the reactive conditions (Figure 6.7(g) and 6.7(h)). The maximum calorific value of the syngas produced under N_2 and CO_2 conditions is 1.83 MJ/Nm^3 and 2.24 MJ/Nm^3 at 500ºC, respectively. At 700°C, the maximum calorific value of pyrolysis gas under N_2 and CO_2 increases to 2.51 and 4.17 MJ/Nm^3. This could be due to the improved thermal cracking of volatile matter. At 900°C, the calorific value of the syngas obtained under initial pyrolysis conditions is estimated as 5.87 MJ/Nm^3 under CO_2 conditions. The syngas calorific value after devolatilization is found higher than any other conditions due to the production of CO after 20 minutes. The calorific value of the syngas is observed to be twice that of N_2 conditions.

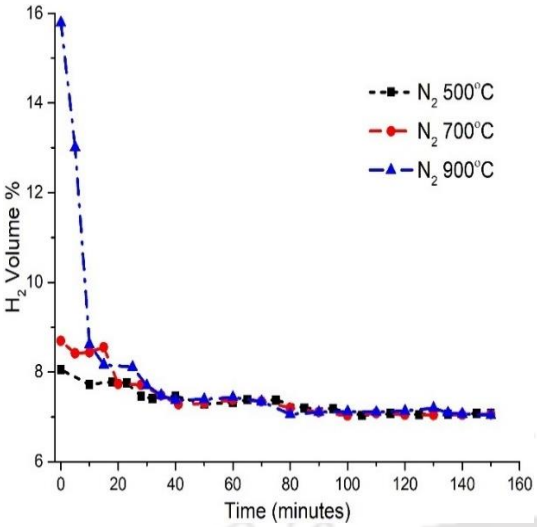

(a) H_2 concentration in N_2

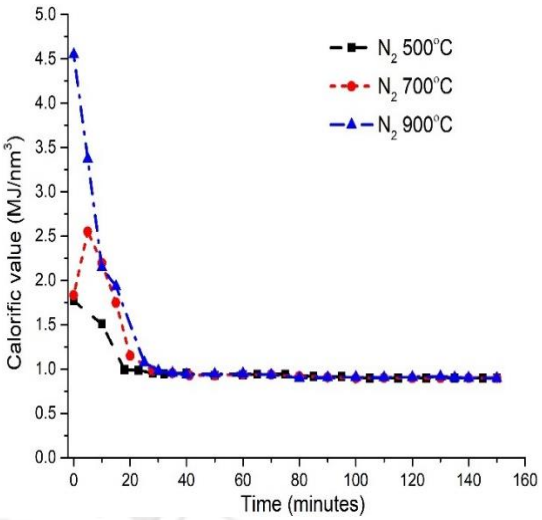

(b) H_2 concentration CO_2

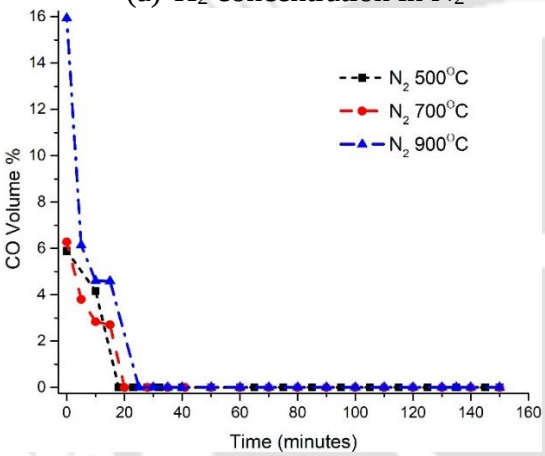

(c) CO concentration in N_2

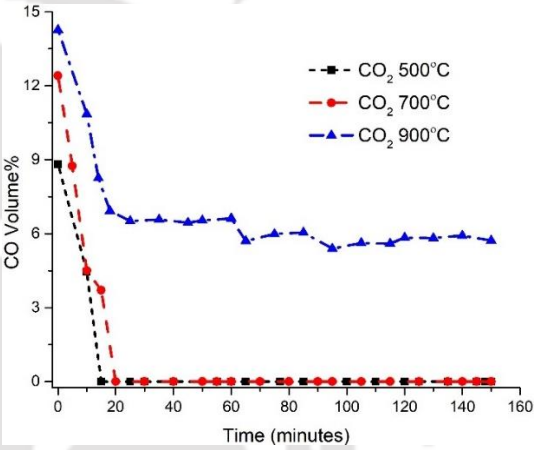

(d) CO concentration in CO_2

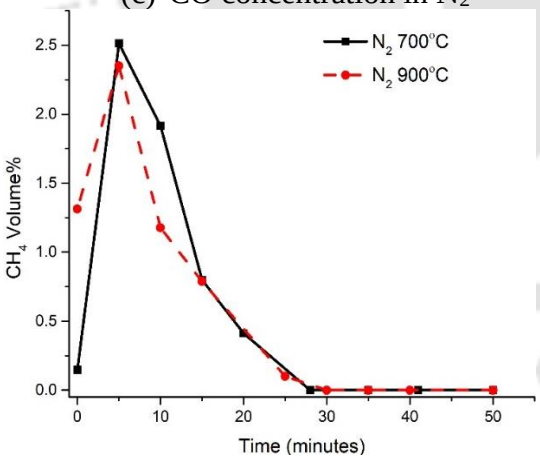

(e) CH_4 concentration in N_2

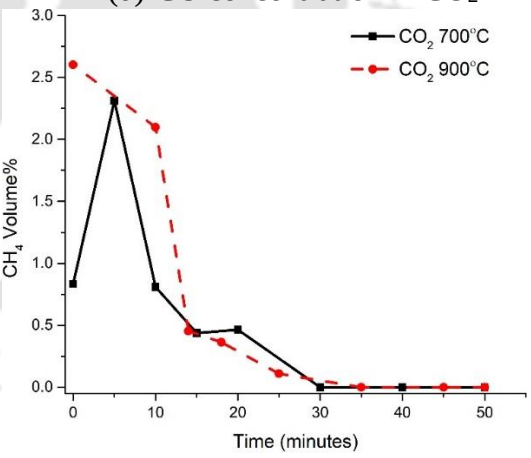

(f) CH_4 concentration in CO_2

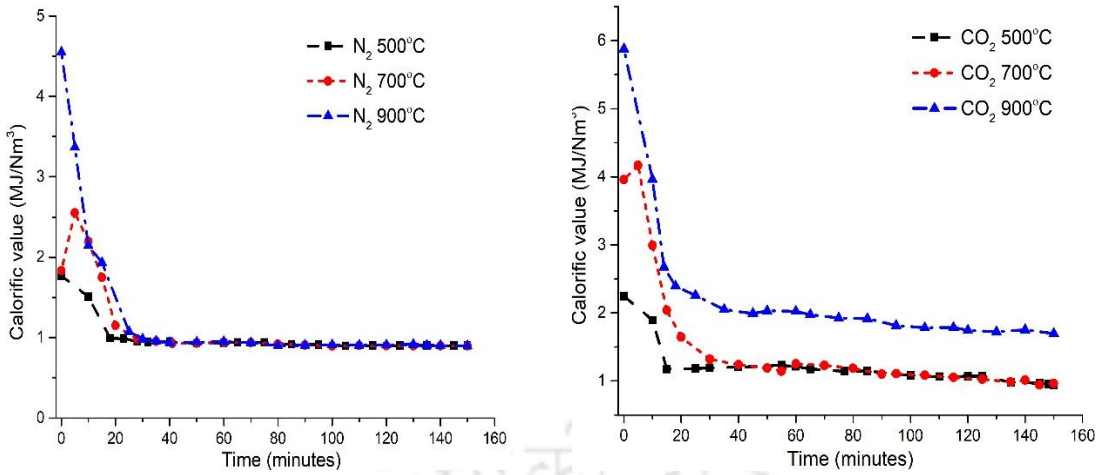

(g) Syngas calorific value in N_2 (h) Syngas calorific value in CO_2

Figure 6.7. Gas composition and calorific value of PCB at various temperatures under N_2 and CO_2 conditions (a) & (b) H_2, (c) & (d) CO, (e) & (f) CH_4, (g) & (h) syngas calorific value, respectively

6.2.6. Co-gasification of HAC and PCB-based fuels

Figure 6.8 gives the syngas composition and calorific value under co-gasification conditions of HAC and PCB fuels. To evaluate the impact of operating temperature on gasification, HAC is gasified at 900˚C and 1000˚C. A higher syngas yield is obtained at 1000°C with an improved quantity of CO by nearly 2 to 3 times compared to the gasification at 900°C. This effective gasification of HAC with PCB is due to the channel formation. Similarly, the volume percentage of H_2 also increased from 14.1% to 29.4%. The initial CH_4 volume percentage is high at 22.13% and gradually decreased to 1% within 20 minutes of operation. Syngas obtained at 1000°C using HAC has a maximum heating value of 14.7 MJ/Nm^3 which then stabilizes at around 5-6 MJ/Nm^3 (Figure 6.8(g)). This reflects the occurrence of volatile matter release stage and Boudouard reaction stage. Table 6.6 shows the average calorific value of the syngas. The standard deviation for the composition of various syngas components is estimated based on the repeatability tests. It varies from 0.002 to 0.79. HAC syngas calorific value increases from 1.91 to 5.64 MJ/Nm^3 as the temperature increases from 900 to 1000ºC. It was mainly due to H_2 and CO concentration improvement by 1.92 and 25%. Under stable gasification conditions, syngas calorific values vary from 1.43-2.34 MJ/Nm^3 at 900ºC, which increases to 3.98-5.31 MJ/Nm^3 at 1000 ºC.

Co-gasification experiments of HAC with PCB and its components are performed at 1000°C as the syngas calorific value of HAC is better at 1000ºC. HAC is co-gasified with

PCB fuels in a 4:1 ratio. Due to the higher release rate of volatile matter in the case of PCB resin and PCB plastic, the H_2 percentage in the syngas is increased to the maximum percentage of 39% (Fig. 6.8(b)) and the CO of 54% (Fig. 6.8(d)) at the initial gasification conditions. The maximum CO content increased by 3.48%, 7.42%, and 7.9% when HAC was co-gasified with resin, plastic, and PCB mixture during the initial stages (Fig. 6.8(c)). Co-gasification conditions produce slightly lower CO than the case of HAC alone during experiment. PCB resin contains only 2.3 wt.% fixed carbon, which may not be sufficient to produce a higher quantity of syngas. The ash-content PCB resin also contains aluminum and silicon, which are unsuitable for gasification reactions. PCB plastic has high amount of oxygen (25.53%), which may be converted into CO_2 instead of CO formation. Similar results were also reported for PET gasification in the air atmosphere, where the CO_2 content in syngas was increased (Choi et al., 2021).

The maximum volume concentration of H_2 produced is in the order HAC:PCB resin (38.91%)> HAC:PCB mixture (29.97%)> HAC (29.41%) > HAC:PCB plastic (22.61%). This could be due to the higher amount of hydrogen in PCB resin, which improved the production of H_2 by 1.1%, compared to HAC. Due to the presence of aluminium and copper, the release of H_2 in the PCB resin is restricted.

Adding PCB plastic and PCB mixture with HAC decreased the calorific value of syngas by 9.4% and 9.22%, respectively. Although the PCB resin increases the H_2 content, the calorific value of syngas is still reduced by 8.16% because the percentage of CO content is decreased by 4.01%. As explained earlier, glass fibers in the resin covered the pores and thereby restricted the progress of gasification reactions.

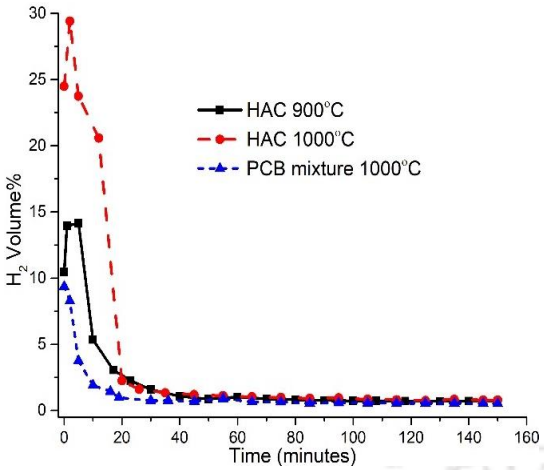

(a) H_2 - Pure fuels

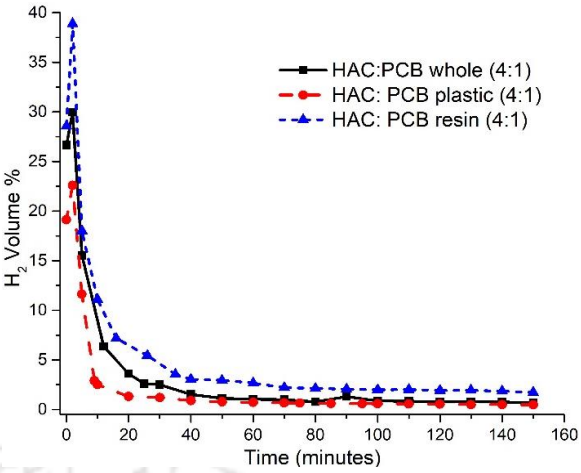

(b) H_2 - HAC and PCB fuel mixture

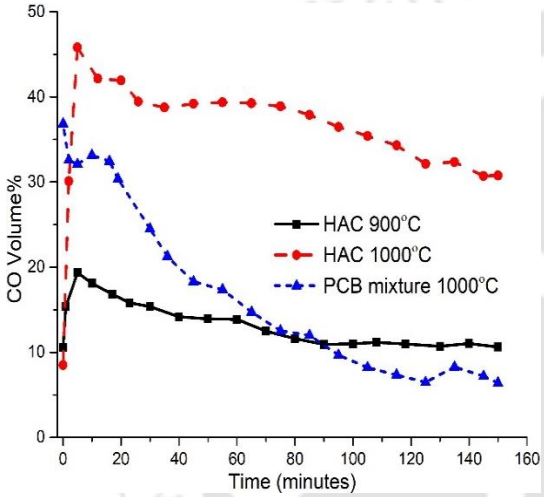

(c) CO - Pure fuels

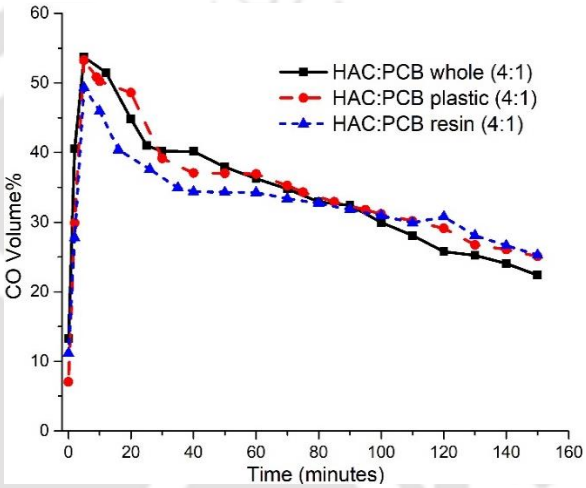

(d) CO - HAC and PCB fuel mixture

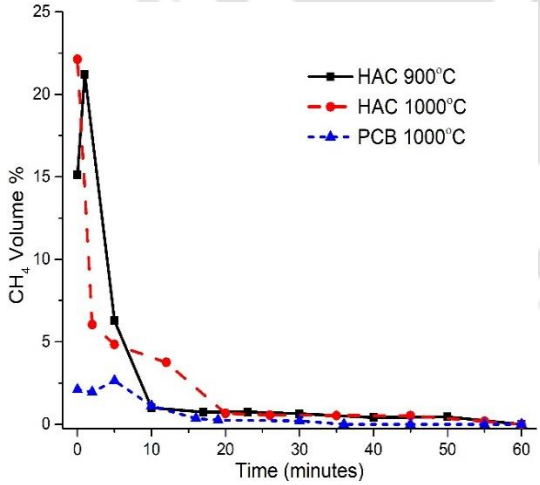

(e) CH_4 - Pure fuels

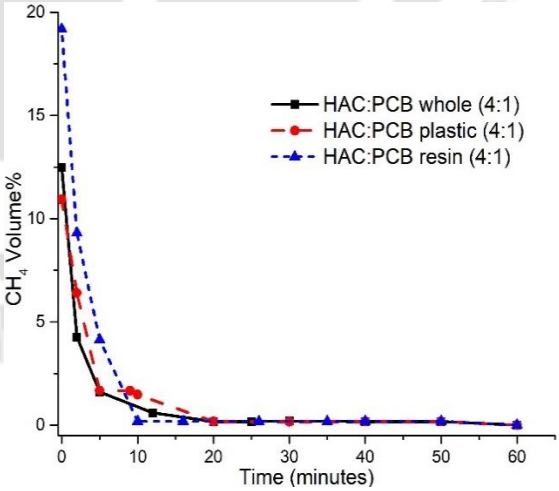

(f) CH_4 - HAC and PCB fuel mixture

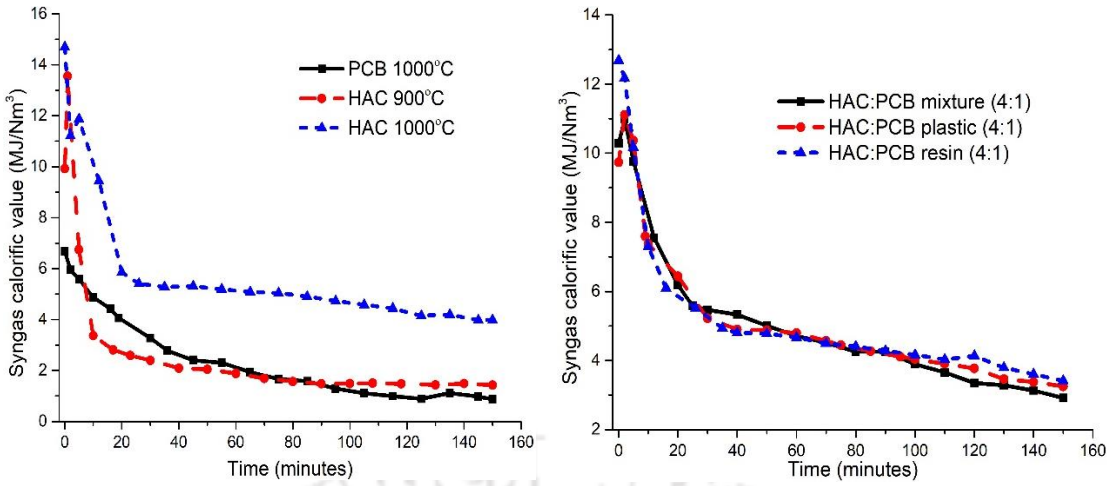

(g) Syngas heating value - Pure Fuels

(h) Syngas heating value - HAC and PCB fuel mixture

Figure 6.8. Gas composition and the calorific value of syngas released

Surface area and average pore diameter of the residue obtained are given in Table 6.6. The surface area of HAC increased significantly with an increase in the operating temperature from 900ºC to 1000ºC. Due to the restructuring of surface at higher temperatures, the gasification reaction is progressed through the pores generated. The PCB mixture is estimated with a low surface area of 1.6 m^2/gm due to the high amount of non-combustibles. Adding PCB mixture and PCB resin to HAC decreased the surface area of the residue by 15-40 m^2/gm compared to HAC. The inorganics (glass fibers and metallic elements) in these PCB components blocked the pores. However, the co-gasification of the PCB plastics with HAC increased 40 m^2/gm of the surface area of the residue. This may be due to the accumulation of plastics in the pores of the HAC at low temperatures and get released at gasification temperature (1000ºC). This led to an increase in the porosity of the obtained residue.

6.2.7. Mass and Residue analysis

Table 6.6 shows the mass and residue analysis of HAC and PCB fuels gasification/pyrolysis. A maximum tar yield of 7.46% is obtained from PCB mixture at 500°C under N_2 conditions. The tar yield reduces under CO_2 conditions, which confirms the tar reactivity with CO_2 by dry reforming reactions. Tar yield is inversely related to the operating temperature, which was due to thermal cracking of higher hydrocarbons to form syngas. The highest calorific value of the tar is found to be 31.28 MJ/kg at 500˚C under N_2 conditions.

Solid yield is also inversely proportional to operating temperature. HAC gasification reactions begin at above 950°C (TGA analysis). This can result in a significant decrease in the solid yield of HAC at 900°C and 1000°C (72.2% and 51.07%). Thermal treatment of PCB mixture at 1000°C and under CO_2 conditions produces a maximum syngas yield of 31.9% due to improved thermal cracking and gasification of PCB. However, a low yield is noticed compared to HAC (47.4%) due to the lower amount of combustibles in PCB mixture.

The volume of syngas generated for HAC increases from 2.38 to 2.65 m^3/kg as the operating temperature is increased from 900°C to 1000°C. Adding PCB plastic increases the volume of syngas generated by 0.04 m^3/kg, which could be due to higher amount of volatiles in PCB plastic as compared to PCB resin. PCB mixture addition decreases the amount of syngas generated as compared to HAC due to ash and metals in PCB mixture (2.62 m^3/kg).

Table 6.6. Average syngas composition with standard deviation, average calorific value during HAC-PCB gasification

Experiment	H_2 vol.%	CO vol.%	CH_4 vol.%	C_2H_2 vol.%	C_2H_4 vol.%	Calorific value (MJ/Nm^3)	BET surface area (m^2/gm)	Average pore diameter (nm)	Volume of syngas produced (m^3/kg)
HAC 900ºC	1.91±0.04	12.79±0.07	0.11±0.03	0.006±0.003	0.008±0.002	1.91	1.58	21.06	2.38
HAC 1000ºC	3.83±0.11	37.03±0.13	0.96±0.12	0.07	0.08	5.64	147.61	2.88	2.65
PCB mixture 1000ºC	0.76±0.16	11.97±0.79	0.06±0.019	0	0	1.63	1.6	7.55	2.35
HAC:PCB mixture (4:1)	3.14±0.21	34.55±0.37	0.45±0.07	0.3±0.007	0.01±0.007	5.12	108.67	2.58	2.62
HAC:PCB plastic (4:1)	3.04±0.24	35.1±0.44	0.57±0.17	0.08±0.007	0.03±0.006	5.11	186	2.65	2.69
HAC:PCB resin (4:1)	4.93±0.17	33.02±0.63	0.76±0.15	0.08±0.008	0.06±0.014	5.18	132.66	2.57	2.65

Table 6.7. Product yields under various conditions

Sample	Atmosphere	Temperature (ºC)	Solid Yield,%	Tar yield,%	Tar calorific value (MJ/kg)	Gas yield,%
PCB mixture	N_2	500	81.1±1.38	7.46±0.37	31.28	11.44±0.53
	N_2	700	77.2±0.87	6±0.79	30.97	16.8±0.89
	N_2	900	73.02±1.49	2.66±0.36	30.61	24.32±1.84
	CO_2	500	79.4±1.26	6.82±0.19	28.73	13.78±1.46
	CO_2	700	76.02±0.81	5.76±0.27	28.12	18.22±0.55
	CO_2	900	69.8±0.95	2.4±0.31	27.81	27.8±0.64
HAC	CO_2	900	72.2±1.41	5±0.2	3.83	22.8±1.21
HAC	CO_2	1000	51.07±0.77	1.53±0.14	14.96	47.4±0.91
PCB mixture	CO_2	1000	66.07±1.38	1.99±0.19	0.24	31.94±1.18
HAC:PCB mixture (4:1)	CO_2	1000	51.07±0.73	1.44±0.19	1.05	47.49±0.92
HAC:PCB resin (4:1)	CO_2	1000	53.4±1.15	1.51±0.23	4.97	45.09±1.38
HAC:PCB plastic (4:1)	CO_2	1000	41.53±1	1.86±0.17	8.86	56.61±0.95

6.2.8. Residue calorific value from PCB pyrolysis and gasification

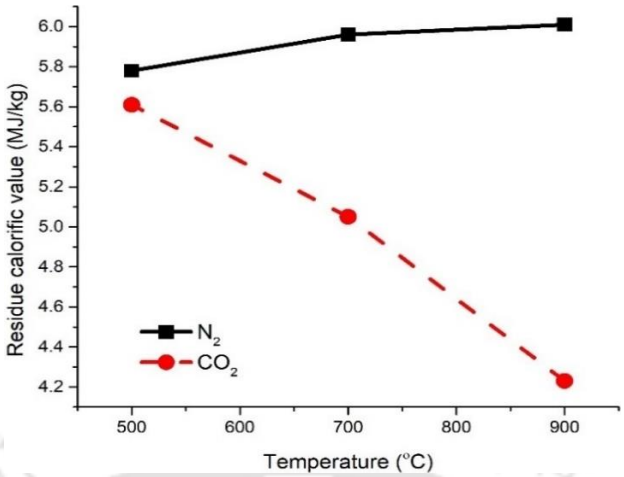

Figure 6.9. Effect of operating temperature on calorific value PCB mixture residue

Figure 6.9 shows the heating value of the PCB mixture residues obtained after pyrolysis and gasification conditions. The calorific value of residues obtained under CO_2 conditions is 0.2-1 MJ/kg lower than N_2 conditions. It was due to the conversion of combustibles to syngas. The CO_2 based residues have found with low calorific values reducing from 5.6 MJ/kg to 4.2 MJ/kg with the increase in the operating temperatures. Under N_2 conditions, the calorific value of residue increases with the operating temperatures. This could be due to the increase in the energy density of residues by releasing the gaseous matter in the PCB under N_2 conditions.

6.2.9. XRD of ash and char obtained

XRD analyzes the ash content of the fuels under blended and unblended conditions; their peaks are shown in Figure 6.10. PCB resin ash contains SnO_2, SiO_2, Al_2O_3, and CuO, similar to Batnasan et al. (Batnasan et al., 2019). Calcium, tin and titanium containing compounds are found PCB plastic ash (Mihai et al., 2012), (J. Zhou & Kong, 2019), (El-Mekkawi et al., 2017), (Loan et al., 2021). Indian high ash coal contains a significant amount of silica and clay particles and a small amount of iron oxides. By co-gasifying PCB resin and HAC ash, the residue obtained contains the mixture of these particles. Ash can be mixed with concrete, which can improve the matrix's strength and decrease the matrix's permeability.

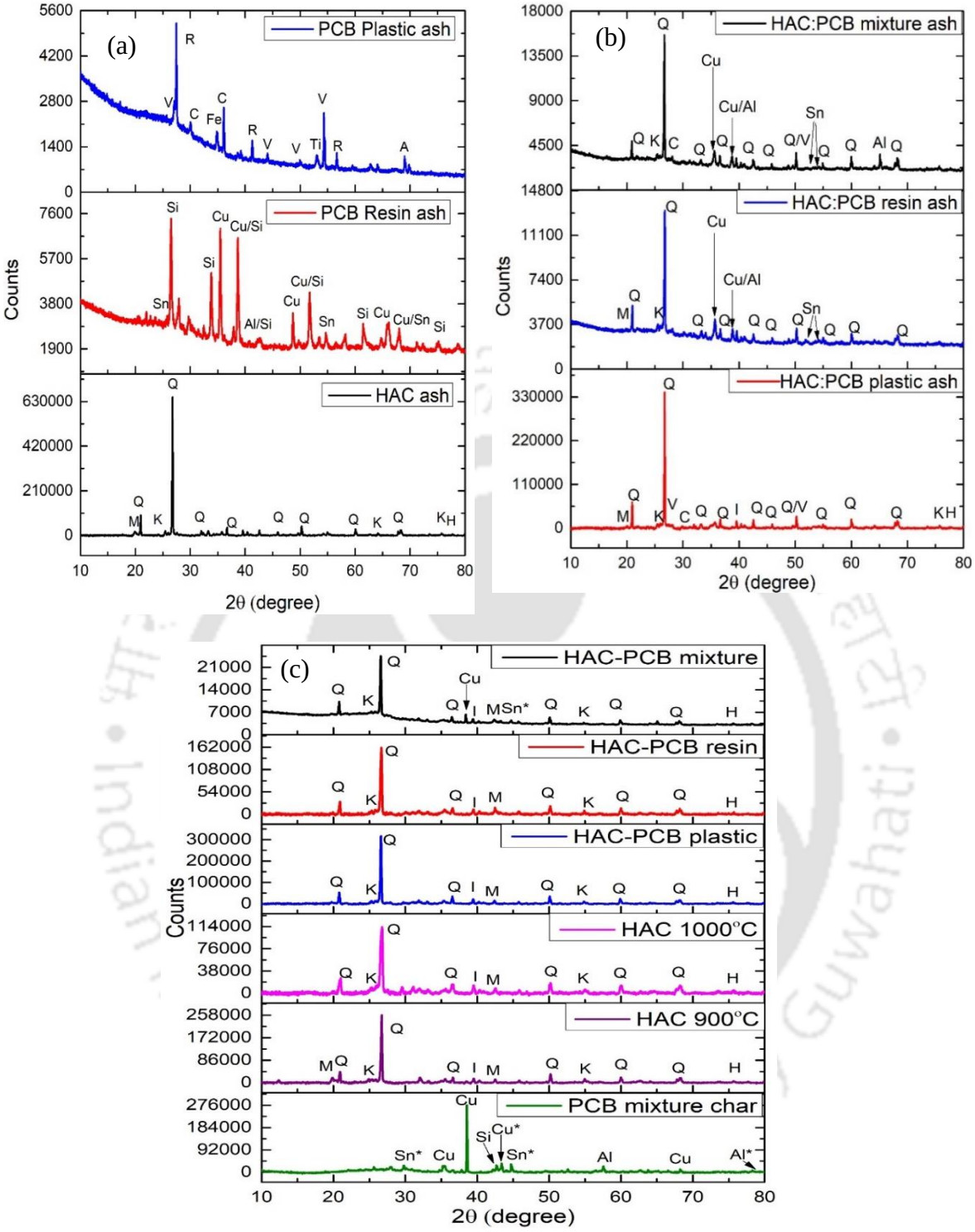

Figure 6.10. XRD of (a) feed ash, (b) HAC:PCB ash and (c) char (Q: Quartz, K: Kaolinite, H: Hematite, M: Montmorillonite, Sn: SnO_2, Si: SiO_2, Cu: CuO, Al: Al_2O_3, V: Vaterite, R: Rutile, A: Anatase, C: Calcite, Fe: Iron, Cu*: copper metal, Sn*: Tin metal, Al*: Aluminium metal)

The residue, such as bottom ash can be used in concrete material for construction purposes. TiO_2 nanoparticles in the bottom ash used in concrete mixture are known to

improve the durability and compressive strength of the concrete. The presence of calcium carbonate up to 1% can decrease porosity and voids in the concrete. $CaCO_3$ nanoparticles can improve the water absorption property of cement (Nejad et al., 2018). Hence, the PCB plastic containing both TiO_2 and $CaCO_3$ under co-gasification conditions with high ash coal can produce the bottom ash suitable as an additive for concrete production. According to the studies conducted by Mojdeh et al. (Khotbehsara et al., 2018), adding SnO_2 nanoparticles can improve the density of concrete microstructure, thus increasing its compressive strength. Hence, the addition of HAC-PCB resin/PCB mixture ash can improve the compressive strength of the concrete produced.

Residue contains metal oxides such as SnO_2, Fe_2O_3, and CuO (Figure 6.10(c)). Residues having Fe_2O_3 particles can be used as a catalyst for cracking coal or biomass tar (Jiang et al., 2022), (Du et al., 2021). Further, the SnO_2 and CuO nanoparticles can be involved in char cracking reactions of cellulose (Donar & Sinağ, 2016). Hence, HAC char and mixed char can be suitable for catalyst use.

6.2.10. Reaction mechanism

The proposed reaction mechanism between PCB mixture and CO_2 is given in Figure 6.11. Initially, at low temperatures, the adhesive force between the layers of PCB resin loosens and it breaks into its components. The PCB plastics are cracked, melted, and deposited over the different layers of PCB. The bond between PCB plastic and other layers hardens over time. CO_2 reacts with amines in the PCB plastic and forms cyanide groups in PCB tar (from FTIR analysis) whereas, in N_2 conditions, the cyanide groups are not formed. The metals in the PCB mixture generally remain unreacted and do not change structure except tin-aluminium alloy, which melts and forms spheres, even at low temperatures (500°C). As PCB plastic contains a higher amount of fixed carbon than PCB resin, at 900°C, Boudouard reaction occurs between PCB plastic and CO_2 and forms CO. Al metal can react with CO_2 to form Al_2O_3 and CO/C, and C can be deposited on PCB (Equations 6.2 and 6.3). Reactions 6.2 and 6.3 are confirmed by XPS analysis (given in appendix).

Reaction mechanism proposed between coal particles and PCB fuel is given in Figure 6.11(b). The coal particles release volatile matter at 1000°C, forming pores. In initial conditions, due to thermal shock experienced by coal, small hydrocarbons are formed. Polymerization reactions between these hydrocarbons can form polyaromatic hydrocarbons (PAH). These PAH can react with CO_2 or O_2 and depolymerizes the

hydrocarbons forming smaller hydrocarbons (Wijayanta et al., 2012). Aromatic hydrocarbons can also be found in the syngas due to their presence in the feed samples. The reactions occurring due to PAH are given in Equation 6.4.

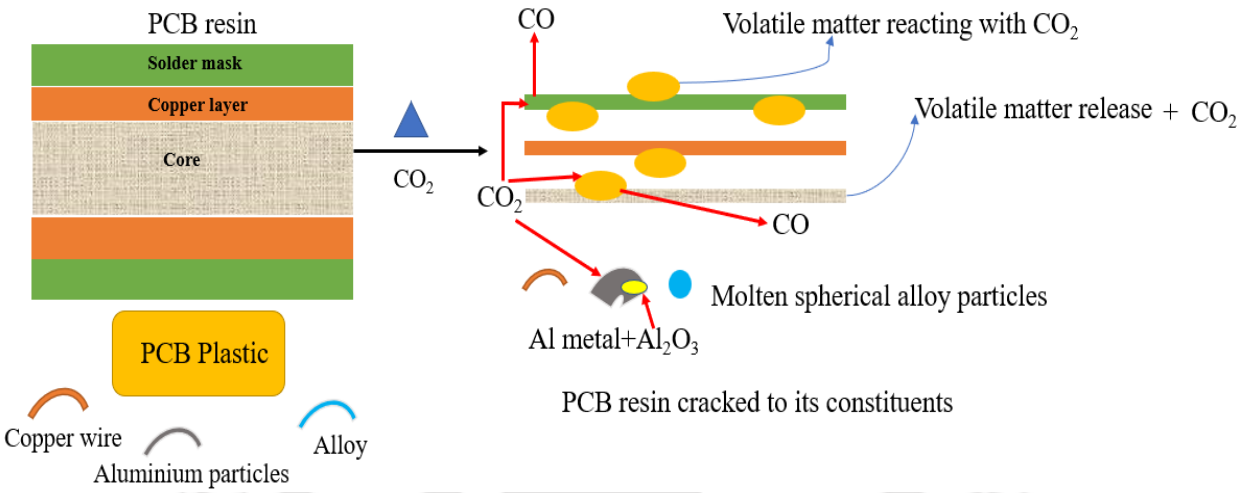

Figure 6.11(a). Reaction between PCB mixture and CO_2

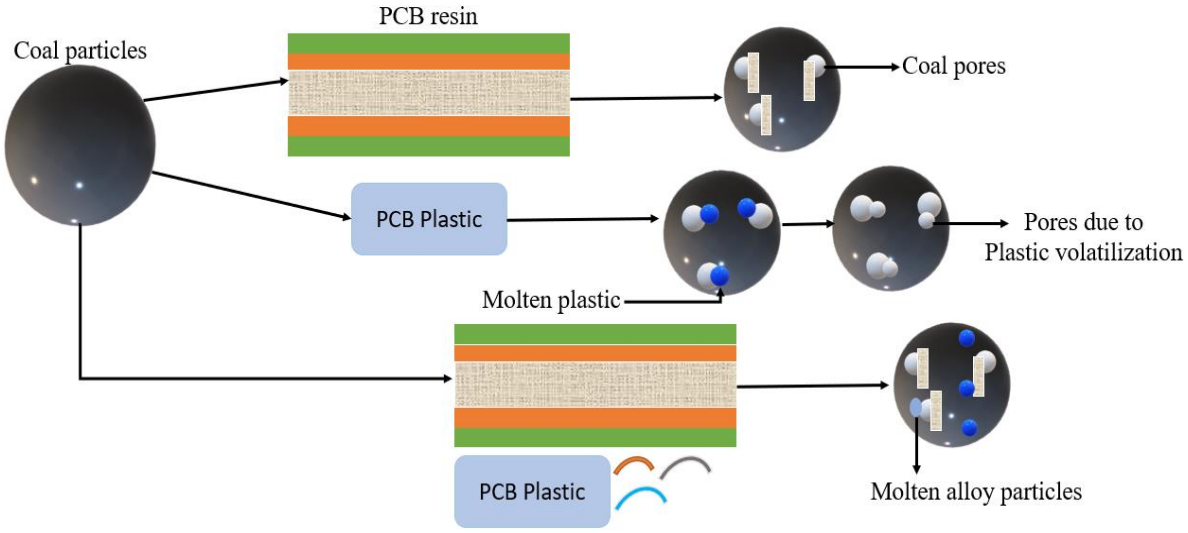

Figure 6.11(b). Reaction between PCB fuels and coal

Figure 6.11. Reaction mechanism of PCB

$$2Al + 3CO_2 \rightarrow Al_2O_3 + 3CO \quad (6.2)$$

$$4Al + 3CO_2 \rightarrow 2Al_2O_3 + 3C \quad (6.3)$$

The core of PCB resin made up of glass fibers tends to cover coal pores, decreasing the surface area of particles. When coal is mixed with PCB plastic, plastics melt over coal pores, covering the pores initially. However, as time progresses, the plastics are devolatilized and removed from the residue. This increases the surface area and pore

diameter. Similarly, when PCB mixture is added to coal, alloy and resin deposit over coal pores thus decreasing the surface area and pore diameter.

$$PAH/PAH^{*} + O/OH \rightarrow PAH^{*} + CO + H \quad (6.4)$$

6.3. Summary of the chapter

PCB mixture-based pyrolysis and gasification processes are performed under N_2 and CO_2 conditions at 500ºC, 700ºC, and 900ºC. A maximum tar yield of 7.46% with a calorific value of 31.28 MJ/kg is obtained at 500ºC under N_2 conditions. CGE and exergy efficiency of the process at 1000ºC under CO_2 conditions are estimated as 91.88% and 82.85%. The activation energy of PCB resin and plastic based CO_2 gasification reaction is estimated as 17.9 and 63.63 kJ/mol, respectively, which are 10.45% and 51.65% lower than N_2 conditions. The co-gasification of HAC with PCB (PCB resin, PCB plastic, and PCB mixture) under a 4:1 ratio generated the syngas with as high as 33-35% CO and 3.0-4.9% H_2 under CO_2 conditions with a net calorific value of 5.1-5.2 MJ/Nm^3. The solid residue of the gasification process is suitable for commercial applications as catalysts. The co-gasification residue has a BET surface area of 108.67-186 m^2/gm. Further, the presence of $CaCO_3$, TiO_2, and SnO_2 in PCB plastic and PCB resin ash, is confirmed by XRD. These ash particles can be mixed with concrete materials for the construction purpose to improve compressive strength and water absorption capacity.

References

Alenezi, R. A., & Al-Fadhli, F. M. (2018). Thermal degradation kinetics of waste printed circuit boards. *Chemical Engineering Research and Design*, *130*(December 2017), 87–94. https://doi.org/10.1016/j.cherd.2017.12.005

Batnasan, A., Haga, K., & Huang, H. H. (2019). High-pressure oxidative leaching and iodide leaching followed by selective precipitation for recovery of base and precious metals from waste printed circuit boards ash. *Metals*, *9*(3). https://doi.org/10.3390/met9030363

Beims, R. F., Botton, V., Ender, L., Scharf, D. R., Simionatto, E. L., Meier, H. F., & Wiggers, V. R. (2018). Effect of degree of triglyceride unsaturation on aromatics content in bio-oil. *Fuel*, *217*(October 2017), 175–184. https://doi.org/10.1016/j.fuel.2017.12.109

Bhui, B., & Prabu, V. (2021). Chemical looping based co-combustion of high ash Indian coal and rice straw operating under CO_2 in-situ gasification mode. *Journal of the Energy Institute*, *94*, 176–190. https://doi.org/10.1016/j.joei.2020.07.004

Bodzay, B., Marosfoi, B. B., Igricz, T., Bocz, K., & Marosi, G. (2009). Polymer degradation studies using laser pyrolysis-FTIR microanalysis. *Journal of Analytical and Applied Pyrolysis*, *85*(1–2), 313–320. https://doi.org/10.1016/j.jaap.2008.11.016

Choi, M. J., Jeong, Y. S., & Kim, J. S. (2021). Air gasification of polyethylene terephthalate using a two-stage gasifier with active carbon for the production of H_2 and CO. *Energy*, *223*. https://doi.org/10.1016/j.energy.2021.120122

Donar, Y. O., & Sinağ, A. (2016). Catalytic effect of tin oxide nanoparticles on cellulose pyrolysis. *Journal of Analytical and Applied Pyrolysis*, *119*, 69–74. https://doi.org/10.1016/j.jaap.2016.03.016

Du, S., Dong, Y., Guo, F., Tian, B., Mao, S., Qian, L., & Xin, C. (2021). Preparation of high-activity coal char-based catalysts from high metals containing coal gangue and lignite for catalytic decomposition of biomass tar. *International Journal of Hydrogen Energy*, *46*(27), 14138–14147. https://doi.org/10.1016/j.ijhydene.2021.01.179

El-Mekkawi, D. M., Labib, A. A., Mousa, H. A., Galal, H. R., & Mohamed, W. A. A. (2017). Preparation and characterization of nano titanium dioxide photocatalysts via sol gel method over narrow ranges of varying parameters. *Oriental Journal of Chemistry*, *33*(1), 41–51. https://doi.org/10.13005/ojc/330105

Evangelopoulos, P., Persson, H., Kantarelis, E., & Yang, W. (2020). Performance analysis and fate of bromine in a single screw reactor for pyrolysis of waste electrical and electronic equipment (WEEE). *Process Safety and Environmental Protection*, *143*, 313–321. https://doi.org/10.1016/j.psep.2020.07.006

Gokulakumar, B., & Narayanaswamy, R. (2008). Fourier Transform – Infrared Spectra (FT-IR) Analysis of Root Rot Disease in Sesame (Sesamum Indicum). *Romanian Journal of Biophysics*, *18*(3), 217–223.

Guo-dong, S., Zhi-qi, W., Jing-li, W. U., Tao, H. E., Jian-qing, L. I., Jing, Y., & Jin-hu,

W. U. (2016). Combustion characteristics of low-rank coal chars in O_2/CO_2 , O_2/ N_2 and O_2/Ar by TGA. *Journal of Fuel Chemistry and Technology*, *44*(9), 1066–1073. https://doi.org/10.1016/S1872-5813(16)30048-2

Guo, X., & Wu, Y. (2018). IN SITU visualization of water adsorption in cellulose nanofiber film with micrometer spatial resolution using micro-FTIR imaging. *Journal of Wood Chemistry and Technology*, *38*(5), 361–370. https://doi.org/10.1080/02773813.2018.1488869

Hu, R., Sun, W., Zeng, M., & Zhu, M. (2014). Dispersing SnO_2 nanocrystals in amorphous carbon as a cyclic durable anode material for lithium ion batteries. *Journal of Energy Chemistry*, *23*(3), 338–345. https://doi.org/10.1016/S2095-4956(14)60156-X

Huang, K., Wei, Z., & Cooks, R. G. (2021). Chemical Science Accelerated reactions of amines with carbon dioxide driven by superacid at the microdroplet. *Chemical Science*, 2242–2250. https://doi.org/10.1039/d0sc05625a

Jain, P., Choudhary, V., & Varma, I. K. (2002). FLAME RETARDING EPOXIES WITH PHOSPHORUS. *Journal of Macromolecular Science, Part C: Polymer Reviews*, *1797*, 139–183. https://doi.org/10.1081/MC-120004762

Ji, Y., Sun, Y., Zhu, B., Liu, J., & Wu, Y. (2022). Calcium fluoride promoting the combustion of aluminum powder. *Energy*, *250*, 123772. https://doi.org/10.1016/j.energy.2022.123772

Jiang, Y., Zong, P., Bao, Y., Zhang, X., Wei, H., Tian, B., Tian, Y., Qiao, Y., & Zhang, J. (2022). Catalytic conversion of gaseous tar using coal char catalyst in the two-stage downer reactor. *Energy*, *242*, 123013. https://doi.org/10.1016/j.energy.2021.123013

Jiménez-Díaz, L., Caballero, A., Pérez-Hernández, N., & Segura, A. (2017). Microbial alkane production for jet fuel industry: motivation, state of the art and perspectives. *Microbial Biotechnology*, *10*(1), 103–124. https://doi.org/10.1111/1751-7915.12423

Khotbehsara, M. M., Miyandehi, B. M., Naseri, F., Ozbakkaloglu, T., Jafari, F., & Mohseni, E. (2018). Effect of SnO_2, ZrO_2, and $CaCO_3$ nanoparticles on water

transport and durability properties of self-compacting mortar containing fly ash: Experimental observations and ANFIS predictions. *Construction and Building Materials*, *158*, 823–834. https://doi.org/10.1016/j.conbuildmat.2017.10.067

Lakshminarayana, B., Kumar, K. V. A., Selvaraj, M., Satyanarayana, G., & Subrahmanyam, C. (2020). Journal of Environmental Chemical Engineering PVP-PS supported ultra-small Pd nanoparticles for the room temperature reduction of 4-nitrophenol. *Journal of Environmental Chemical Engineering*, *8*(4), 103899. https://doi.org/10.1016/j.jece.2020.103899

Loan, T. T., Huong, V. H., Huyen, N. T., Van Quyet, L., Bang, N. A., & Long, N. N. (2021). Anatase to rutile phase transformation of iron-doped titanium dioxide nanoparticles: The role of iron content. *Optical Materials*, *111*(September 2020), 110651. https://doi.org/10.1016/j.optmat.2020.110651

Lohitharn, N., & Shanks, B. H. (2009). Upgrading of bio-oil: Effect of light aldehydes on acetic acid removal via esterification. *Catalysis Communications*, *11*(2), 96–99. https://doi.org/10.1016/j.catcom.2009.09.002

Luda, M. P., Balabanovich, A. I., Zanetti, M., & Guaratto, D. (2007). Thermal decomposition of fire retardant brominated epoxy resins cured with different nitrogen containing hardeners. *Polymer Degradation and Stability*, *92*(6), 1088–1100. https://doi.org/10.1016/j.polymdegradstab.2007.02.004

Mihai, M., Bucătariu, F., Aflori, M., & Schwarz, S. (2012). Synthesis and characterization of new $CaCO_3$/poly(2-acrylamido-2- methylpropanesulfonic acid-co-acrylic acid) polymorphs, as templates for core/shell particles. *Journal of Crystal Growth*, *351*(1), 23–31. https://doi.org/10.1016/j.jcrysgro.2012.04.010

Nejad, F. M., Tolouei, M., Nazari, H., & Naderan, A. (2018). Effects of calcium carbonate nanoparticles and fly ash on mechanical and permeability properties of concrete. *Advances in Civil Engineering Materials*, *7*(1), 651–668. https://doi.org/10.1520/ACEM20180066

Nie, C., Wang, Y., Zhang, H., Zhang, Y., Zhang, Y., Yan, Z., Li, B., Lyu, X., Tao, Y., Qiu, J., Li, L., Zhang, G., & Zhu, X. (2020). Cleaner utilization of non-metallic components in separation tailings of waste printed circuit board : Pyrolysis oil , calori fi c value and building aggregate. *Journal of Cleaner Production*, *258*,

120976. https://doi.org/10.1016/j.jclepro.2020.120976

Reena, G., Sangita, & Verinder, K. (2011). Ft-ir studies of e-plastic obtained from obsolete computers. *Journal of Chemical and Pharmaceutical Research*, *3*(5), 660–667.

Sahoo, S., CK, C., PK, B., & SC, M. (2012). FTIR and Raman Spectroscopic Investigations of a Norfloxacin / Carbopol934 Polymeric Suspension. *Journal of Young Pharmacists*, *4*(3), 138–145. https://doi.org/10.4103/0975-1483.100017

Sahu, P., & Vairakannu, P. (2021). CO_2 based synergistic reaction effects with energy and exergy (2E) analysis of high density polyethylene with high ash bituminous coal for syngas production. *Fuel*, *June*, 122500. https://doi.org/10.1016/j.fuel.2021.122500

Sajjan, V. A., Aralekallu, S., Nemakal, M., Palanna, M., Prabhu, C. P. K., & Sannegowda, L. K. (2020). Nanomolar detection of lead using electrochemical methods based on a novel phthalocyanine. *Inorganica Chimica Acta*, *506*(March), 119564. https://doi.org/10.1016/j.ica.2020.119564

Sanapala, R. (2008). CHARACTERIZATION OF FR-4 PRINTED CIRCUIT BOARD LAMINATES BEFORE AND AFTER EXPOSURE TO LEAD-FREE SOLDERING CONDITIONS. In *University of Maryland*. University of Maryland.

Shen, Y., Chen, X., Ge, X., & Chen, M. (2018). Thermochemical treatment of non-metallic residues from waste printed circuit board : Pyrolysis vs . combustion. *Journal of Cleaner Production*, *176*, 1045–1053. https://doi.org/10.1016/j.jclepro.2017.11.232

Singh, R. K., Ruj, B., Sadhukhan, A. K., & Gupta, P. (2020). A TG-FTIR investigation on the co-pyrolysis of the waste HDPE, PP, PS and PET under high heating conditions. *Journal of the Energy Institute*, *93*(3), 1020–1035. https://doi.org/10.1016/j.joei.2019.09.003

Tahir, M. H., Mubashir, T., Hussain, M. B., Cheng, X., Karim, A., Ali, N., Jamil, M., Khan, A. M., & Irfan, R. M. (2021). Selective catalytic conversion of tea waste biomass into phenolic-rich bio-oil and subsequent extraction. *Journal of Analytical and Applied Pyrolysis*, *159*(August), 105315.

https://doi.org/10.1016/j.jaap.2021.105315

Wang, X., & Zhang, Q. (2004). Synthesis , characterization , and cure properties of phosphorus-containing epoxy resins for flame retardance. *European Polymer Journal*, *40*, 385–395. https://doi.org/10.1016/j.eurpolymj.2003.09.023

Wijayanta, A. T., Saiful Alam, M., Nakaso, K., & Fukai, J. (2012). Numerical investigation on combustion of coal volatiles under various O_2/CO_2 mixtures using a detailed mechanism with soot formation. *Fuel*, *93*, 670–676. https://doi.org/10.1016/j.fuel.2011.10.003

Wu, W., & Qiu, K. (2014). Vacuum co-pyrolysis of Chinese fir sawdust and waste printed circuit boards. Part I: Influence of mass ratio of reactants. *Journal of Analytical and Applied Pyrolysis*, *105*, 252–261. https://doi.org/10.1016/j.jaap.2013.11.011

Yanti, Nurhayati, T., Royani, I., Widayani, & Khairurrijal. (2016). Synthesis and characterization of MAA-based molecularly-imprinted polymer (MIP) with D-glucose template. *Journal of Physics: Conference Series*, *739*(1). https://doi.org/10.1088/1742-6596/739/1/012143

Yu, J., Liu, S., Cardoso, A., Han, Y., Bikane, K., & Sun, L. (2019). Catalytic pyrolysis of rubbers and vulcanized rubbers using modified zeolites and mesoporous catalysts with Zn and Cu. *Energy*, *188*, 116117. https://doi.org/10.1016/j.energy.2019.116117

Zhou, C. W., Farooq, A., Yang, L., & Mebel, A. M. (2022). Combustion chemistry of alkenes and alkadienes. *Progress in Energy and Combustion Science*, *90*(December 2021), 100983. https://doi.org/10.1016/j.pecs.2021.100983

Zhou, J., & Kong, D. (2019). Effects of Ni addition on corrosion behaviors of laser cladded FeSiBNi coating in 3.5% NaCl solution. *Journal of Alloys and Compounds*, *795*, 416–425. https://doi.org/10.1016/j.jallcom.2019.05.012

This page is left blank intentionally

This page is left blank intentionally

CHAPTER 7

MSW-COAL BASED POWER GENERATING SYSTEMS

Incineration of municipal solid waste (MSW) can generate thermal energy for electricity generation and reduces its accumulation in the environment. MSW has low calorific value and its utilization would lead to low thermal efficiency in power plants due to higher auxiliary power consumption. Alternatively, this problem can be overcome by co-utilizing MSW with coal in thermal power plants. The capture of the generated CO_2 from MSW can lead to carbon-negative energy production. Hence to evaluate its feasibility, energy and techno-economic analysis of subcritical and supercritical based steam turbines using MSW and its co-utilization with Indian high ash and low ash coals are performed using Aspen plus software (v 8.8). The effect of integrating post combustion and oxy-combustion based carbon capture on the net thermal efficiency of power plants and its subsequent impact on levelized cost of electricity (LCOE) are analysed.

In this chapter, the feasibility of co-utilization of high and low ash coal with MSW for power generation is studied. A very few literature reported the economic analysis of MSW with coal for electricity generation. MSW is a low calorific fuel and the gasification of these waste along with coal produces a low quality syngas. Direct burning of MSW after prior treatment is a better option than co-gasification with coal inorder to recover its heating value. Hence, the impact of MSW blending with high and low coal on the net power generation capacity of steam turbine based power plants is evaluated with and without carbon capture. Post combustion and oxy-fuel combustion mode of CCS is assessesd with the co-utilization of MSW with coal.

MSW has comparatively lower calorific value than conventional fuels such as coal and natural gas. The net efficiency of coal based power plants is around 32-35% without CO_2 capture under subcritical conditions (U. Singh et al., 2017), (Surywanshi et al., 2019). When MSW is combusted under subcritical conditions, the net efficiency of waste to energy plants is estimated around 18-22% (Ding et al., 2018), (Yassin et al., 2009), (Sadi & Arabkoohsar, 2019). It was recommended that the co-combustion of coal with MSW

could increase the efficiency of power plants (Sebastian & Alappat, 2016). Economic analysis of waste to energy plants was carried out by Zhao et al. (2016) (Xin-gang et al., 2016). They found that the net profit margin grew from 14.7% in first year to 26.7% in 18 years. They concluded that the use of locally made equipment would be able to decrease investment costs by 30-35%. By improving the efficiency of fuel utilization with simultaneous production of power and heat, the pollutant gas emissions can be reduced (Goh & Ang, 2021).

In Changchun, China, the co-combustion of MSW was carried out with lignite coal using a circulating fluidized bed (Cheng et al., 2007). They utilized 78% of MSW in their fuel blend having a moisture content of 50% and estimated NO_x emission in the range of 130-170 mg/m^3. Natural gas and MSW are used as fuels in Zabalgarbi power plant Bilbao, Spain, in a combined cycle operation. The waste heat in the flue gas was used to heat the feed gas of the combustor. As a consequence, the overall efficiency of the power plant was increased from 31.6% to 34.5% (Kimberlin & Ribeiro, 2010). Cormos (2013) conducted a simulation study based on gasification integrated combined cycle power plants (C. C. Cormos, 2013). The net electrical efficiency of the coal-based power plant and coal-MSW (mixed in the ratio of 4:1 (by weight)) based power plant was estimated as 36% and 35.7%, respectively . Their results had shown the flexibility of using MSW with coal, which impacts only a minimal reduction in the net thermal efficiency of power plants. Pour et al. (2018) carried out a techno-economic analysis on MSW combustion with and without a carbon capture unit (CCU) (Pour et al., 2018). They estimated that the levelized cost of electricity (LCOE) with CCU and without CCU was 225 $/MWh and 140 $/MWh, respectively. Further, they reported that using coal as the fuel, the LCOE values were estimated as 100 $/MWh and 55 $/MWh with and without CCU, respectively. Hence, a higher value of LCOE makes MSW utilization for power generation uneconomical, compared to coals. Further, it was reported in the literature that the LCOE of supercritical power plants is found to be lower than subcritical power plants. This is due to the improved net efficiency of the power plants at higher operating temperature and pressure under supercritical conditions (Surywanshi et al., 2019). This could lead to lower greenhouse gas emissions per MW of electricity generated. Further, the supercritical power plants have comparatively a low start-up start time and are more flexible to handle different coal grades (Rai, 2017). Auxiliary power consumption,

materials requirement for infrastructure development, water requirement, blow down loss, etc. in supercritical power plants are lower than the subcritical power plants.

NO_x emissions are directly related to the level of oxygen in the feed oxidant mixture(Ma et al., 2019). The co-combustion of coal and MSW can reduce the peak flame temperature, compared to coal alone as the fuel, and as a consequence, the formation of thermal NO_x is reduced (Vekemans & Chaouki, 2016). The experimental and simulation studies on the co-combustion of coal and hydrothermally treated MSW (HT-MSW) proved that the 30% addition of HT-MSW decreased NO_x emissions in a bubbling fluidized bed reactor (Lu et al., 2016). The NH radicals from the HT-MSW convert the NO generated from coal into N_2 gas in the reducing atmosphere. Hence, MSW can be utilized under co-combustion conditions with coal for NO_x reduction. Further, NO_x can be removed by post-combustion treatment method using a selective catalytic reduction unit. Although the above mechanism may result in decreased NO_X emissions as compared to pure coals, but the amount of N in MSW would play an important role in net NO_X emissions. Hence, proper capital investment and further improvement in the separation processes of MSW are essential for efficient and clean energy production (Xu et al., 2020).

Fouling, slagging, agglomeration, and corrosion are several problems associated with the coal and MSW's co-combustion. MSW ash consists of minerals with lower melting temperatures than coal ash. As a consequence, a viscous layer of ash is formed during the combustion of MSW in the boiler of the power plant. Further, alkali chlorides in the ash content of MSW get evaporated and deposited on the cold surfaces of the convective sections (superheater, reheater, economizer) of the boiler. They form adhesive layer over the cold heat exchanger surfaces and this adhesive layer traps ash particles, which act as resistance for heat transfer during steam production(Moradian et al., 2015). These ash deposits can be removed by blowing dry saturated steam or slightly superheated steam on heat exchanger surfaces (Vekemans & Chaouki, 2016). Agglomeration issue can be avoided by co-firing of MSW with coal. In fluidized bed conditions, the addition of kaolin clay along with the feed mixture prevents biomass ash agglomeration (Miller & Francisco, n.d.). Further studies on kaolin-sand mixture under fluidized bed condition showed that the agglomeration temperature of wheat straw ash had increased by 100°C (Ohman & Nordin, 2000). The ash content of Indian high ash coal (HAC) contains kaolinite, which would help to reduce agglomeration of ash particles during co-

combustion conditions (Bhui & Prabu, 2021). MSW and coal ash mineralogy was studied by Cormos. CaO and Na_2O are low melting point minerals present in higher amount in MSW ash (Cormos 2013). Ash fusion temperature of Indian coals was calculated by Sharma et al., which was around 1500°C (Sharma et al. 2014). Melting point of MSW ash was around 1200°C as reported by Gao et al., (Gao et al. 2021).

Table 7.1. Minerals present in coal and MSW ash (Cormos 2013)

Mineral (wt.%)	Coal ash	MSW ash
SiO_2	52.2	52.45
Al_2O_3	27.3	16.21
Fe_2O_3	5.1	7.17
CaO	6.4	16.92
MgO	2.1	0
TiO_2	1.5	0
K_2O	1	0
Na_2O	0.3	7.25
SO_3	2.4	0
P_2O_5	1.3	0
SrO	0	0

Techno-economic analysis of the co-combustion of coal with MSW under subcritical and supercritical conditions of steam turbines has not yet been reported in the literature. Further, no studies are available yet for the incorporation of CCU (carbon capture unit) with MSW based subcritical and supercritical based power plants. Hence the novelty of the present study is to assess the process feasibility of co-utilization of of coal and MSW by economic analysis using Aspen plus software. To utilize Indian coals suitably with MSW of Indian origin for power production, energy, and economic analysis are performed. High sulfur coal with low ash content is found in the north-eastern region of India, whereas the rest of India contains high ash bituminous coals. Sustaining the stability of a combustion flame during the incineration of high ash coal is a critical issue due to low volatile matter and high fixed carbon of the coal. This issue can be minimized by the co-utilization of coal with MSW, which contains high quantity of volatile matter (Zhang, 2013). Further, high sulfur coals from the northeastern region of India can generate SO_x based pollutants in the flue gas during the combustion process. Hence, the

mixing of MSW with high sulfur coals can reduce the level of SO_x in the flue gas. In this context, the synergistic effects during the co-utilization of Indian coals with MSW in steam turbine based power plants are evaluated. Further, the pollutants generated such as CO_2, SO_x, and NO_x are captured, and the impact of their capture cost on the net thermal efficiency is assessed. SO_x gases are captured in the form of gypsum, and NO_x gases are converted into nitrogen gas using a catalytic deNO_x reactor. Further, the viability of increasing the process efficiency by using supercritical power plant is investigated. In the process simulation, co-combustion is performed using various blend ratios of MSW and Indian coals and their blending effect on the net thermal efficiency of the power plants is estimated. Further, the economic impact of MSW drying on the net thermal efficiency of the power plants is evaluated. The impact of post-combustion and oxy-combustion based carbon capture methods on net thermal efficiency of power generating systems is assessed.

7.1. Feedstocks of power plants

Table 7.2 (a). Proximate and ultimate analysis of the fuels considered

Proximate analysis	MSW (wt. %) (Mboowa et al., 2017)	High ash coal (HAC) (wt. %)	Low ash coal (LAC) (wt. %)
Moisture content	25.49	2	3.35
Volatile matter (dry basis)	60.77	19.38	38.53
Fixed carbon (dry basis)	6.08	50	59.46
Ash (dry basis)	33.15	30.53	2.01
Ultimate analysis (dry basis)			
Carbon	36.38	57.41	76.64
Hydrogen	4.56	5.02	4.41
Oxygen	23.62	6.06	11.22
Nitrogen	1.88	0.98	1.33
Sulfur	0.41	0	4.39
Gross calorific value (MJ/kg)	14.85	22.3	26.13

The impact of low and high ash Indian coals are evaluted in the present study. The inherent properties of Jharia mine based high ash coal and Assam based low ash coal

(high sulfur) are considered in the power plant studies. The ultimate and proximate analyses of HAC, LAC, and MSW are listed in Table 7.2(a). HAC and MSW fuels contain high ash content in the range of 30-33%. Table 7.2(b) shows the composition of MSW, which contains 92% biomass and 6% plastics. The higher amount of biomass result in a high moisture content in MSW.

Table 7.2 (b). The composition of MSW (Mboowa et al., 2017)

Component	Weight %
Organic component	92
Hard plastic	0.9
Soft plastic	5.1
Papers	0.3
Glass	0.4
Textiles	0.9
Metals	0.1
Others	0.3

The detailed analysis of the power plant simulation studies based on post combustion and oxy-combustion CCS methods are presented in the sub-chapters.

7.2. Power plant efficiency calculation

The power produced by the steam turbines such as high pressure steam turbine (HPST), medium pressure steam turbine (MPST) and low pressure steam turbine (LPST) is denoted as P_{HPST6}, P_{MPST} and P_{LPST}, respectively. The gross efficiency of the power plants is calculated as per the Equation No. (7.1). The net efficiency is calculated based on the power consumption in the CCU (P_{CCU}) units as per Equation No. (7.2).

$$Gross\ efficiency = \frac{P_{HPST} + P_{MPST} + P_{LPST}}{Total\ energy\ input\ from\ feedstock} \quad (7.1)$$

$$Net\ efficiency = \frac{P_{HPST} + P_{MPST} + P_{LPST} - P_{CCU} - P_{PUMP}}{Total\ energy\ input\ from\ feedstock} \quad (7.2)$$

P_{PUMP} is the power consumed by the pump to pressurize the water from ambient conditions to the required pressure. P_{CCU} is the power consumption in the CCU unit, including reboiler and compressor duty for stage wise compression of CO_2 to 110 bar.

7.3. Economic analysis

The economic analysis is performed to estimate the LCOE of the proposed power plants. Table 7.3 shows the cost of feedstock, chemicals and capital investments considered in the economic analysis. The cost of fuels according to their calorific value provided by the coal producing company, Coal India Limited is considered(Coal India Ltd., 2011). The cost of MSW in India is considered as per the recommendations of the National Capital Territory for solid waste management in Delhi (India) (Grover, 2017). The cost of turbines, combustor and other auxiliary equipment is calculated using Equation 7.3 (Mishra et al., 2019).

$$C_E = (Q_E/Q_B)^n \times C_B \quad (7.3)$$

C_E is the cost of the equipment to be estimated with a capacity Q_E and, C_B is the known cost of an equipment with a capacity Q_B and, n is scaling factor ranging from 0.6 to 0.7. In the present study, the scaling factor is assumed to be 0.7. The cost of the steam turbines with known capacity is taken from the report of the central electricity commission, India (*Thermal_Model_Consolidated_v*, n.d.). The costs of the carbon capture units (CCU) such as CO_2 compression system, transport and injection system are found from the studies of Pettinau et al. 2017 (Pettinau et al., 2017). The cost of MSW pre-treatment equipment with known capacity was found in the literature(*Detailed Project Report Integrated MSW Management for GMADA Cluster*, 2017). In the economic analysis, the parameters such as capital recovery factor (CRF), power capital cost index (PCCI) and purchasing power parity index (PPPI) are calculated. These parameters are defined as follows

Capital recovery factor (CRF): The total cost of the capital investment of the power plant would be paid in equal installments throughout the lifetime of the power plant (~25 years). In the present study, the CRF was found to be 0.086, which signifies 8.6% of the entire loan taken would be paid each year over 25 years (Harvey, 2020).

Power capital cost index (PCCI): It is the ratio of equipment cost (upstream/downstream) or labour cost in the current year to that of the base year. It signifies the increase in machinery cost price over the years compared to base year (Pauschert, 2009).

Purchasing power parity index (PPPI): It compares the purchasing power of two different currencies. It is a measure of relative consumer prices of goods and services across the countries (Callen, 2012).

Table 7.3. Cost of feedstocks considered in the economic analysis of power plants

Feed	Cost
Low ash coal (LAC)	0.043 $/kg (Coal India Ltd., 2011)
High ash coal (HAC)	0.033 $/kg (Coal India Ltd., 2011)
Municipal solid waste (MSW)	0.021 $/kg (Grover, 2017)
Mono-ethanolamine (MEA)	2200 $/t (A. Cormos & Cormos, 2017)
Limestone	22.4 $/t (Pettinau et al., 2017)
Hydrogen Peroxide	0.23 $/gallon (Chen et al., 2013)
Assumptions for economic analysis (Mishra et al., 2019),(Pettinau et al., 2017)	
Owner's Cost	15% of total installed cost
Land purchase, surveying cost	5% of total installed cost
Annual discount rate	7%
Plant life	25 years

LCOE is estimated using the following Equations (7.4), (7.5), and (7.6). The annual capital cost (ACC) and capital recovery factor (CRF) are calculated as,

$$ACC = Total\ capital\ cost\ (TC)\ \times\ Capital\ recovery\ factor\ (CRF) \tag{7.4}$$

$$CRF = \frac{r(1+r)^t}{(1+r)^t - 1} \tag{7.5}$$

'r' is the rate of capital discharge (7%) and the CRF is estimated as 0.086 (A. Cormos & Cormos, 2017).

$$LCOE = \frac{Annual\ capital\ cost\ (ACC) \times\ Total\ operating\ and\ maintenance\ cost}{Net\ electricity\ produced} \tag{7.6}$$

The cost of machines such as heat exchangers and compressors is calculated by Aspen plus as per the cost based on the USA. These values are converted to Indian basis by the following equation (Surywanshi et al., 2019).

$$C_{India} = C_{USA} \times \left(\frac{PCCI\ for\ current\ year}{PCCI\ for\ original\ year}\right) \times PPPI_{India} \tag{7.7}$$

C_{India} is the cost of the equipment in India, C_{USA} is the cost of equipment in the USA. PCCI and PPPI are the power capital costs index and purchasing power parity index, respectively. The values of PCCI and PPPI are taken from the report of organisation for economic co-operation and development (OECD) (*Purchasing Power Parities*, n.d.). The maintenance costs associated with the power plants including fixed cost and variable cost are considered as 1% and 2% of total capital costs, respectively. The land surveyor and owner's costs are taken as 5% and 15% of the total installed cost, respectively(Mishra et al., 2019). In the present study, MEA is used as a solvent for CO_2 capture in post-combustion method and its cost considered in the economic analysis is 2200 $/t (A. Cormos & Cormos, 2017).

7.4. Aspen plus process simulation

The main objective of the present study is to simulate the co-combustion of the Indian coals with MSW. The power plants are modelled according to the operating conditions mentioned by National Thermal Power Corporation Limited (NTPC), India (Suresh et al., 2010). The co-combustion of coals and MSW is carried out at different mass ratios to predict the optimized conditions leading to the least negative effect on the cost of electricity. Figure 7.1 describes the process followed for energy and economic analysis of sub-critical and supercritical power plants with and without incorporation of CCU. The utilization of MSW requires pre-treatment operation, and it is described in section 7.5. For the economic analysis of the power plants operating under various conditions, the details of equipment cost, labour cost, utilities etc. are necessary. The cost of the equipment related to the power plants is found and scaled up according to the required capacity (*Thermal_Model_Consolidated_v*, n.d.),(*Detailed Project Report Integrated MSW Management for GMADA Cluster*, 2017). In the present study, a pulverised coal burner is considered for the incineration of the fuels. The power plant simulations are performed using Aspen Plus v8.8 software. The combustion of MSW, HAC, and LAC with and without blending has been performed under subcritical and supercritical conditions. The net thermal efficiency of power plants with CCU units is estimated. Economic analysis is performed for the following cases (Table 7.4) of feed composition (by weight) with and without CCU under subcritical and supercritical conditions:

Table 7.4. List of fuel blends used in the power plant simulation

HAC (without blending)	HAC: MSW (3:1)	LAC: MSW (3:1)
LAC (without blending)	HAC: MSW (1:1)	LAC: MSW (1:1)
MSW (without blending)	HAC: MSW (1:3)	LAC: MSW (1:3)

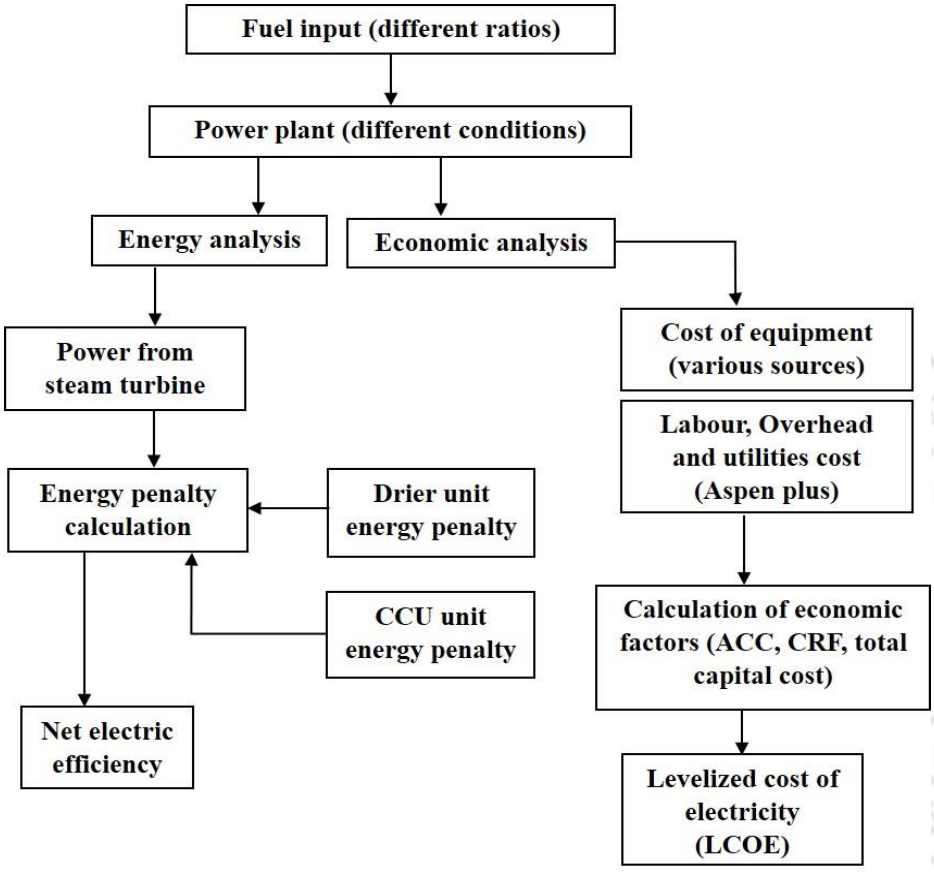

Figure 7.1. Block diagram of the procedure followed for energy and economic analysis

7.5. MSW treatment unit

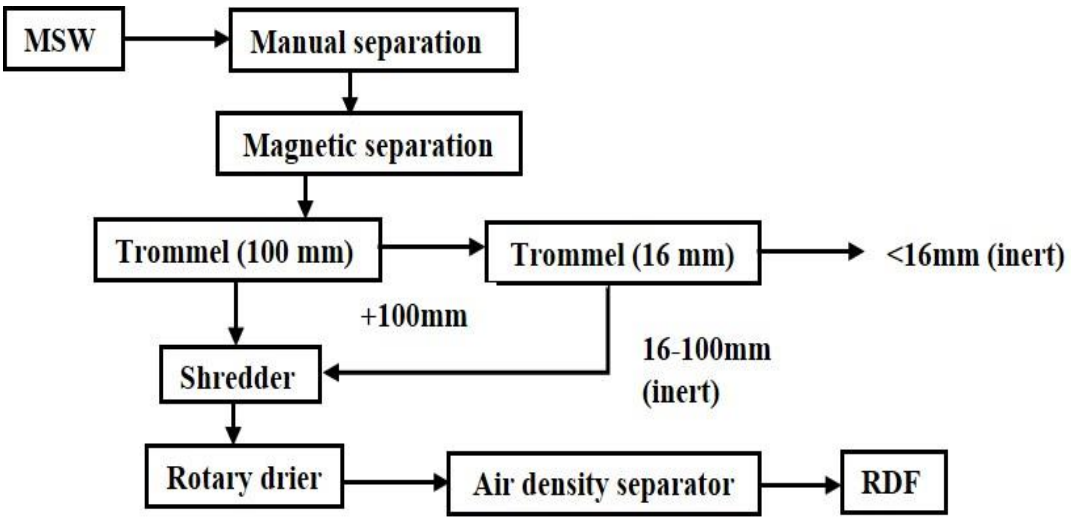

Figure 7.2. Block diagram for treatment of MSW

The issues related to MSW blending with coal are (i) high sulfur, chlorine content in MSW, (ii) high moisture in MSW, (iii) chipping and milling of MSW, (iv) low calorific value of MSW. Further, the feeding techniques of MSW and coal into the boiler are different. Coal and MSW are fed into a circulating fluidized bed by a screw feeder and a rotary feeder, respectively(Dong et al., 2002). The costs of the pre-processing equipment of coal and MSW feeders are considered in the economic analysis. Due to the high moisture content of MSW, the flame sustainability of combustion is one of the main concerns for blending of MSW with coal. Hence, MSW is completely dried in the preprocessing unit and further 60% of volatile matter in the MSW supports the sustainability of the combustion flame. In the present study, the MSW treatment is carried out based on the process treatment of waste to energy plant at Ghazipur, Delhi, India ("12 MW Waste to Energy Project (Ghazipur , Delhi)," n.d.). The block diagram of the MSW treatment plant is shown in Figure 7.2. The cost of MSW pretreatment equipment is considered from the report of Municipal corporation of Mohali and Medak, India (*Detailed Project Report Integrated MSW Management for GMADA Cluster*, 2017),(*Detailed Project Report on Municipal Solid Waste Management*, 2017). The quantity of inert materials in MSW is insignificant (<1%), and these are removed as inert and magnetic materials. Most of the inert materials in the MSW are manually removed using a slow-moving belt. A belt magnetic separator removes magnetic impurities of MSW. Further, an air density separator removes the inert materials found in the MSW.

With the help of trommels, the inert particles below 16 mm size are almost removed. To get the dried MSW with a size in the range of 16-25 mm, a shredder is used to produce fine particles. A rotary drier is used to reduce the moisture content of MSW to 10%.

CHAPTER 7A

CO-COMBUSTION OF MSW AND COAL IN POST COMBUSTION CCS BASED POWER PLANTS

The effect of integrating post combustion carbon capture on the net thermal efficiency of power plants and its subsequent impact on levelized cost of electricity (LCOE) are analysed. The feedstock with an equal proportion of coal and MSW had shown a reasonable LCOE in the range of 60 to 67 $/MWh without carbon capture. The results had shown that the addition of 25% MSW to low ash coal could give a similar plant thermal efficiency and LCOE to that of high ash coal under subcritical conditions without carbon capture.

7.6. Post combustion CCS based power plants

7.6.1. Subcritical and supercritical steam power plants

Power plant simulations are carried out as per the studies of Suresh et al. (2010)(Suresh et al., 2010). Figure 7.3 shows the schematic diagram of power generation unit. Water is pumped to a pressure of 242.2 bar and 190.8 bar to produce high-pressure steam for operating steam turbines under supercritical and subcritical conditions, respectively. The power plant cycle uses three turbines based on the operating pressure, namely, high-pressure steam turbine (HPST), medium-pressure steam turbine (MPST), and low-pressure steam turbine (LPST). Initially, MSW is processed using a drier, and its moisture content is reduced from 25% to 10% at 120°C (Ragazzi et al., 2007). An optimal quantity of air is supplied for drying as per the heat balance. A rotary dryer, operating under continuous mode, is used to dry MSW and coal(Perazzini et al., 2016). A flue gas desulfurizing unit (FGD) is used to capture sulfur from the flue gas. Further, a post-combustion CO_2 capture unit separates CO_2 from N_2, and the captured CO_2 gas is compressed for geological storage.

Table 7.5. Operating conditions of the subcritical and supercritical power plants

Units	Temperature (°C)	Pressure (bar)
Subcritical condition (Suresh et al., 2010), (Kuo & Wu, 2016)		
Combustor	1200	1.01
Air inlet to combustor	25	1.01
High pressure steam turbine (HPST)	501	190.8
Medium Pressure steam turbine (MPST)	542	31.8
Low pressure steam turbine (LPST)	306	5.18
Water pump	25	190.8
MSW drier	105	1.01
Supercritical condition (Suresh et al., 2010)		
Combustor	1773	1.01
HPST	537	242.2
MPST	565	42
LPST	215	2.9
Water pump	25	242.2
CCUand FGD unit (Carpenter, 2012), (Stec et al., 2016)		
Absorber	40	1.05
Stripper	100	1.9
Compressor pressure conditions [46]	--	3, 13.6, 33.5, 70, 110
MEA solution concentration (weight, %)	30%	
Ratio of MEA to flue gas	3.9-4.5	
CO_2 recovery	90%	
FGD unit inlet	125	
SO_2 removal efficiency	98%	
Lime solution solids inlet%	25%	
Gypsum solids %	45%	

The operating parameters of subcritical and supercritical power plants are given in Table 7.5. The reactor models used in the present study are given in Table 7.6. Figure 7.4 shows the flow sheeting of the air combustion-based steam turbine power plant. Under the subcritical conditions, the pumped feed water is heated by using four preheater units

(FW1, FW2, FW3, and FW4). The preheaters can raise the temperature of water to 277°C. The first preheater (FW1) heated the raw water to 70°C using the residual heat of the flue gas at 166°C. The warm water from the first preheater (FW1) goes into the other preheaters (FW2 and FW3) where the water is heated by the outlet steam from the HPST and the MPST units, respectively. The outlet hot water from the FW3 preheater goes to the subsequent preheater, FW4, where the flue gas preheats it. The preheated water from FW4 at 277°C enters into the boiler, which converts the hot water into steam at 446°C. The saturated steam from the boiler is superheated by using two superheater units (SH1 and SH2). The SH1 superheats the saturated steam to 500°C and this steam drives the HPST to produce electricity. A significant proportion of the outlet steam (89%) from the HPST goes to the SH2 superheater for reheating. After reheating, the resultant steam at 542°C is sent to the MPST for power generation. Further, the outlet steam from the MPST (~83%) is sent to the LPST. The residual steam from the HPST (~11%) and the MPST is sent to the FW2 and FW3 for preheating the feed water. The split ratio of steam in HPST and MPST is maintained as per the data provided by Suresh et al. (2010) (Suresh et al., 2010).

Table 7.6. Models and properties used in Aspen simulation

Equipment	Model	Explanation
Combustor	RGibbs	In RGibbs reactor model, stoichiometry of the reaction is not required. It solves the model by minimizing Gibbs free energy of the products and estimates the composition of products.
Decomp	RYield	This component is used for the decomposition of solid fuel into its constituents for known product composition. Stoichiometry and kinetics of the reactor model can be unknown.
FGD and SCR (Flue gas desulfurization and selective catalytic reduction)	RStoic	Stoichiometry and conversion of the reaction are essential and kinetics may not be known. In the FGD unit, the stoichiometry and conversion are found from the literature.
Air and steam properties	Peng-Rob	Peng-Robinson model is used to accurately calculate the thermodynamic properties of air and steam at high temperature and pressure conditions.

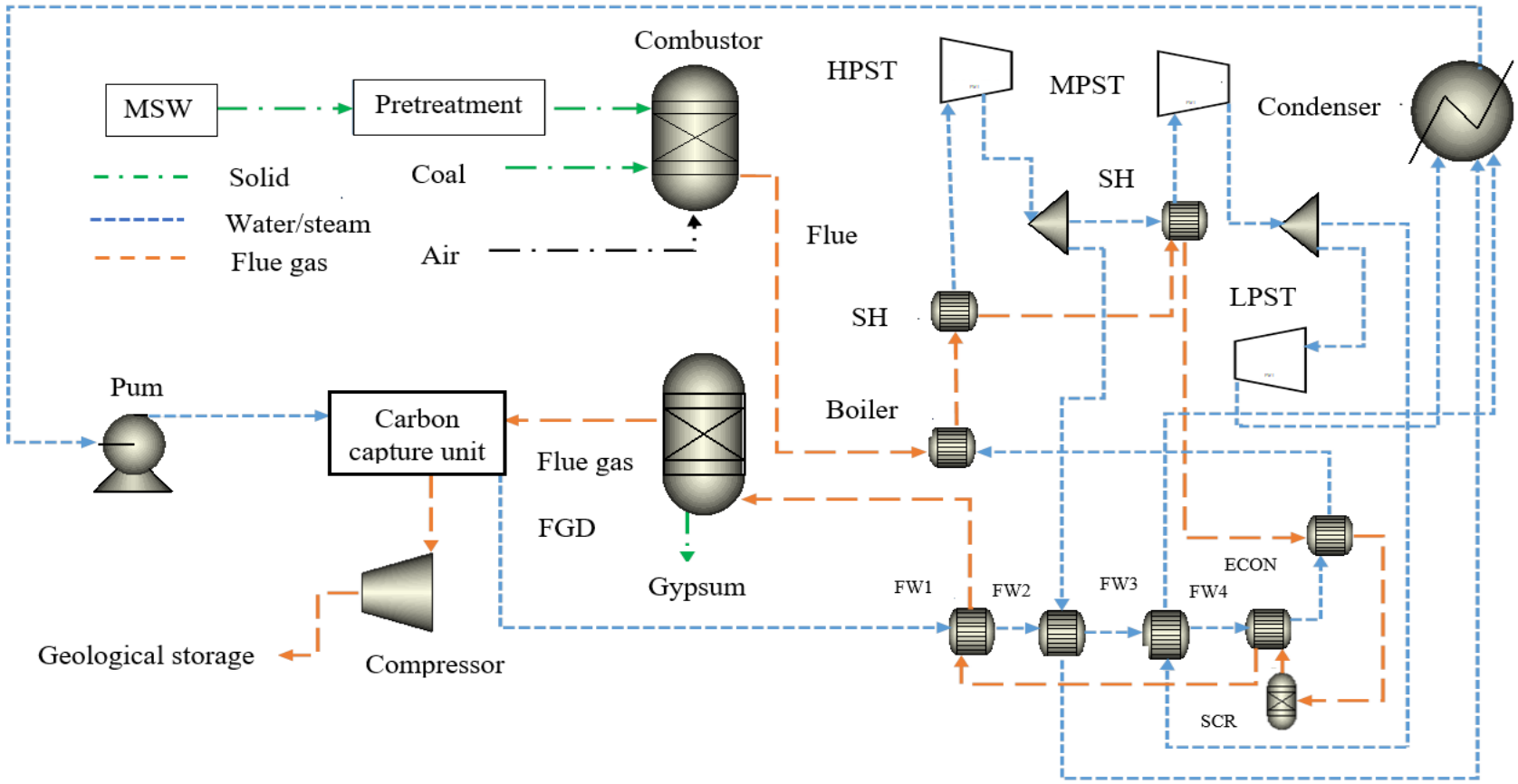

SH: Superheater, FW: Feedwater preheaters, HPST, MPST, LPST: High pressure steam turbine, Medium pressure steam turbine, Low pressure steam turbine, blue line: water, steam stream, Orange dash: Gas stream, SCR: Selective catalyst reduction unit

Figure 7.3. The schematic diagram of the CCU incorporated steam turbine power plant

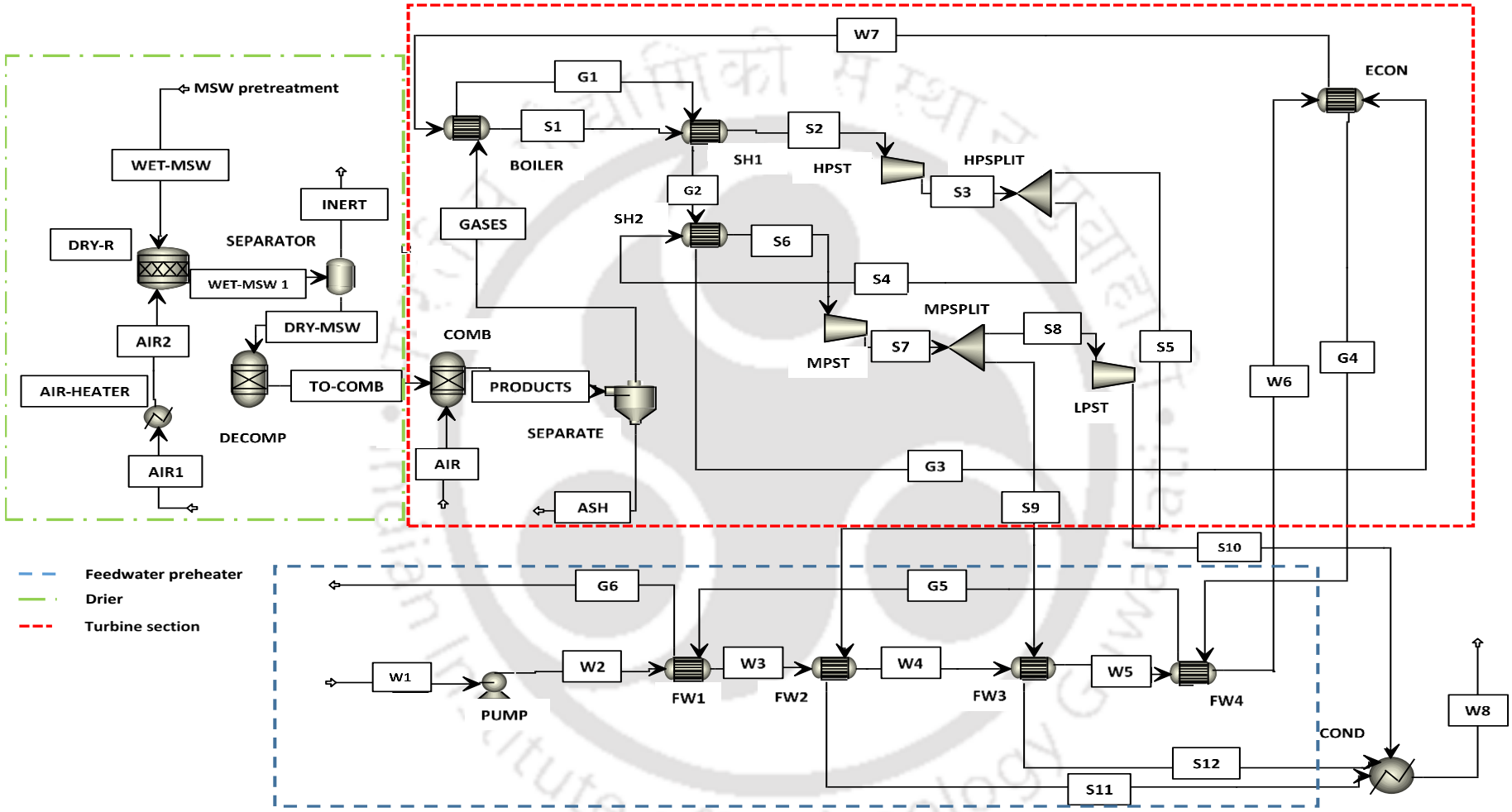

S: steam, W: water, G: gas, FW: feed water heater, HPST: High pressure steam turbine, MPST: Medium pressure steam turbine, LPST: Low pressure steam turbine, Comb: Combustor, SH: superheater, COND: Condenser, B: Boiler, DECOMP: Decomposer, ECON: Economiser, Separator:Air density separator

Figure 7.4. Flowsheeting of the MSW based air combustion operated steam turbine power plan

In the supercritical condition-based power plant operation, the pumped water at 242.2 bar is heated at 277°C using a series of preheaters units. Further, the hot water from the preheating units is converted into steam at 341°C using an economizer. By using a superheater (SH1) and a boiler unit, the steam is superheated to 537°C and sent to the HPST unit. Almost 85% of the outlet steam from the HPST is sent to the SH2 for reheating. The reheated steam from SH2 at 838 K is sent to the MPST, which operates at 42 bar. The outlet steam (68% of steam) from the MPST is sent to the LPST for electrical power generation. The rest of the steam from the HPST and MPST is used for preheating the feed water.

7.6.2. Flue gas DeNO$_x$ and DeSO$_x$ unit

Gas cleaning section has a flue gas desulfurization unit (deSO$_x$) followed by a selective catalytic NO$_x$ reduction unit. In the present study, the flue gas desulfurization process is performed using a wet scrubbing system. Limestone is used for the removal of sulfur by 99% by the formation of gypsum (Eq. (1), (2) and (3)). In the deSO$_x$ unit, the flue gas at 393 K is cooled to 353 K and scrubbed by contacting a mixture of limestone and oxygen to form calcium sulphate (gypsum) and calcium sulphite product. The limestone slurry is passed into the deSO$_x$ unit through spray nozzles under counter-current mode of operation for efficient contact between the flue gas and limestone. The gypsum formed can be used for commercial purposes.

$$SO_2 + H_2O \rightarrow H_2SO_3 \tag{7.8}$$

$$CaCO_3 + H_2SO_3 \rightarrow CaSO_3 + H_2O + CO_2 \tag{7.9}$$

$$CaSO_3 + 1/2O_2 + 2H_2O \rightarrow CaSO_4.2H_2O \tag{7.10}$$

After the removal of SO$_x$ pollutants, the flue gas is sent to a selective catalytic reduction (SCR) unit for the removal of NO$_x$. In this unit, a stream of NH$_3$ is mixed with the flue gas to decompose NO$_x$ into N$_2$ and H$_2$O as per the chemical reaction (7.11) and (7.12) with the support of V_2O_5-TiO_2 catalysts. The SCR unit is operated at around 673 K with a pressure drop of 0.015 to 0.02 bar, which increases the energy penalty associated with the flue gas cleaning unit (Srivastava et al., 2005). The feed NH$_3$ also can react with SO$_2$ and SO$_3$ in the flue gas and may form $(NH_4)_2SO_4$ and $(NH_4)HSO_4$ as side products. These undesired products can block the gas flow path in the solid mixture system. The side

reactions are suppressed in the SCR unit by employing suitable catalysts, compared to the selective non-catalytic reduction unit (SNCR) (Srivastava et al., 2005).

$$2NH_3 + 2NO + 0.5O_2 \rightarrow 2N_2 + 3H_2O \quad (7.11)$$

$$4NH_3 + 2NO_2 + O_2 \rightarrow 3N_2 + 6H_2O \quad (7.12)$$

7.6.3. Post combustion based CO_2 absorption unit

Mono-ethanolamine (MEA) solution absorbs CO_2 from the flue gas in an absorber unit. The CO_2 rich MEA solution from the absorber unit is regenerated using a stripper column. The MEA solution is heated in the reboiler section of the stripper unit for desorbing the CO_2. The regenerated MEA solution at 100°C is used to preheat the CO_2 enriched MEA in a heat exchanger. The desorbed CO_2 from the stripper unit is sent to a compression unit. This unit consists of five compressors with interstage coolers. The heat produced during the compression is used to preheat the water for steam generation. The operating pressure of each compressor unit is given in Table 7.5. A 30% (by weight) MEA solution is used for the absorption operation. A ratio of MEA solution to the flue gas is maintained in the range of 3.9 to 4.7. CO_2 loading (mol CO_2/mol MEA) in the lean solvent is maintained as 0.29 (Stec et al., 2016).

The operating parameters of the post CO_2 capture unit are taken from the literature Stec et al. (2016) (Stec et al., 2016). They conducted pilot scale studies based on post-combustion CCU by amine absorption method and showed 90% CO_2 removal efficiency. In the present study, the amine absorption and stripper units are modelled as separators. Temperature, liquid/gas ratio, MEA concentration etc. are taken from their studies (Stec et al., 2016). The post-combustion CO_2 capture unit is integrated with a compression unit to obtain a high pressure CO_2 stream for storage. Figure 7.5 shows the schematic representation of the CCU system. The cold flue gas from the preheater, FW4, goes into the FGD unit for the removal of sulfur. The desulfurized flue gas is sent to the absorber for CO_2 separation. In the present study, the CCU unit is modelled based on the pilot plant studies conducted by. The MEA to flue gas ratio is maintained in the range of 3.9-4.5 (Stec et al., 2016). The operating parameters such as temperature and pressure of the CCU unit are taken from the studies of Santos et al. (2016) (Santos et al., 2016). The flue gas (G9) from the FGD unit enters into the CCU section, where it is heated to 40°C using a heater (HEX7). After heating, the flue gas (G12) is sent to the absorber section where

90 to 92.5% of CO_2 in the flue gas is absorbed using the 30% (weight %) MEA solution. The rest of the flue gas enriched with nitrogen (G14) is released into the atmosphere. The absorber unit is operated at 60°C and 1.05 bar. The CO_2 rich MEA solution (G13) from the absorber is heated to 100°C using a heat exchanger (HEX1) with the help of the MEA solution from the reboiler outlet (LM1). Further, the heated CO_2 rich MEA solution (G15) is pressurized to 1.9 bar (G16) and sent to the stripper section. In this section, the CO_2 gas is desorbed from the MEA solution, and the CO_2 lean flue gas (G17) is sent to a heat exchanger (HEX6) for cooling.

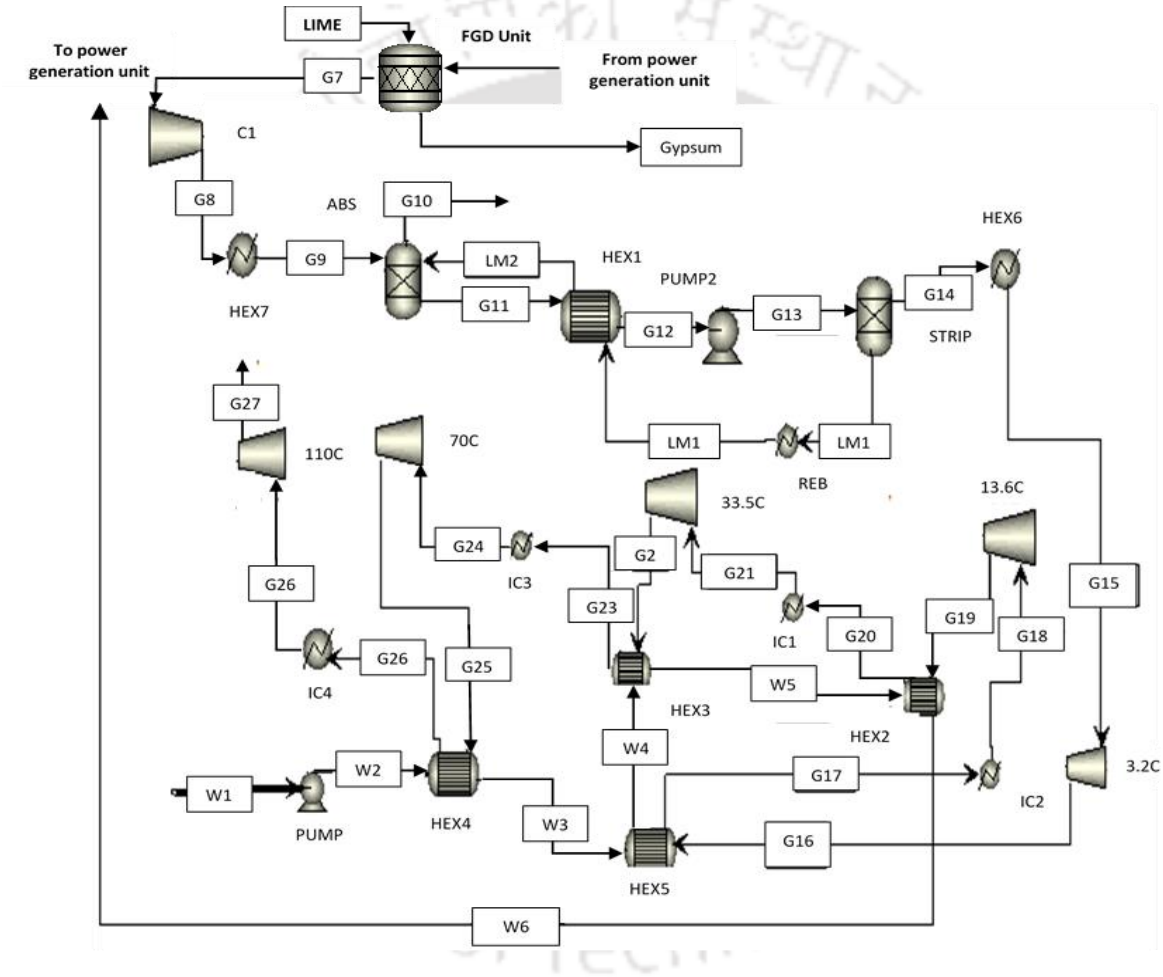

W: water, G: gases, 3bar,13.5 bar, 34 bar, 70 bar, 110 bar: stage compressors, FGD: Flue gas desulfurization unit; ABS: absorber; STRIP: Stripper, IC: interstage coolers, HEX: heat exchanger, C: compressors

Figure 7.5. Flow sheeting of the post-combustion CCU unit for flue gas treatment

In the CO_2 compression unit, the captured CO_2 gas (G18) is pressurised to 3 bar (G19), 13.6 bar, and finally to 110 bar using several compressor units. The heat generated during compression is utilized to preheat the raw water (W3 (33°C), W4 (37), W5 (40°C), W6 (46°C)) for steam generation using the heat exchangers (HEX2, HEX4, and HEX5). The

residual heat energy in the flue gas is removed using several inter-stage coolers (IC1, IC2 and IC3).

7.6.4. Assumptions in the aspen plus study

In the present study, the following technical specifications are considered.

a. The isentropic efficiency of the steam turbines is considered as 0.89, 0.903, 0.851 for HPST, MPST and LPST, respectively, under subcritical conditions. Under the supercritical conditions, the isentropic efficiency of the steam turbines is 0.896, 0.917 and 0.857 for HPST, MPST and LPST, respectively (Suresh et al., 2010).
b. The mass flow rate of the solid fuels is estimated for 100 MW based on the heating value of the fuels. During the co-combustion conditions, the weight % of MSW in the blend is varied from 0 to 100% with the increment of 25%.
c. The combustor operating temperature is considered as 1200°C under subcritical conditions. At this operating temperature, the complete combustion of the organic and toxic materials such as polychlorinated dibenzofurans, polychlorinated dibenzodioxins and polychlorinated biphenyls can be achieved to reduce the pollutant emissions (Kokalj & Samec, 2013). Under supercritical conditions, the operating temperature is fixed as 2045 K (Suresh et al., 2010).
d. HAC, LAC, and MSW fuels are assumed as non-conventional components, and their properties are defined by HCOALGEN and DCOALIGT options of Aspen Plus software (Dattatray & Shilapuram, 2019).
e. Peng Robinson's model is used to estimate the physical properties of steam and gas. This model accurately predicts the properties of gases in hydrocarbon processing applications and polar non-ideal chemical systems (Dattatray & Shilapuram, 2019).
f. RGibbs reactor model is used to simulate the combustor unit to predict the chemical and phase equilibrium using Gibbs energy minimization method (Dattatray & Shilapuram, 2019).
g. RYield reactor is used to decompose the feedstock into its elements (Dattatray & Shilapuram, 2019)
h. Ambient conditions are assumed to be one atmospheric pressure and 25°C.
i. CO_2 removal is assumed to be 90% in the absorber section of the CCU unit (Stec et al., 2016)

j. The cost of the required equipment with known capacity is taken from central electricity commission report of India. The techno economic parameters based on the operating conditions of the power plants found in Talcher, Odisha (India) and Jhajjar, Haryana (India) are considered for the simulation of subcritical and supercritical power plants, respectively (*Thermal_Model_Consolidated_v*, n.d.).

7.6.5. Model Validation

The model developed in the present study is validated with the results of the subcritical based power plants without CCU from the studies of Singh et al. (2017) (U. Singh et al., 2017). Their study is based on the subcritical power plant with a net capacity of 500 MW using high ash Indian coal with a flow rate of 89 kg/s. The developed model in the present study is used to perform economic and energy analysis of the Talcher based thermal power plant with a capacity of 500 MW. The operating parameters of the steam turbines and other process equipment and the properties of the coal used in their studies are considered for validation. Table 7.7 shows the comparison of energy and economic analysis of the developed model with the results reported in the literature(U. Singh et al., 2017). A relative error of 1% is obtained for the estimated net efficiency and LCOE values. This shows that the model in the present study has good agreement with the studies reported in the literature.

Table 7.7. Aspen model validation with literature

	Model validation in the present study	(U. Singh et al., 2017)	Error %
Net power produced (MW)	494.81	500.00	1.04
Net efficiency (%)	33.98	34.34	1.04
LCOE ($/MWh)	37.59	37.96	0.96

7.7. Detailed energy analysis of post combustion based power plants

The energy and economic analysis of the power plants are performed for various proportions of the chosen feedstocks and are discussed in the following section. The effect of CCU on the net thermal efficiency of the power plants is evaluated. A complete combustion of the fuels and their blends in the combustor is achieved with excess air.

7.7.1. Subcritical and supercritical power plants without carbon capture

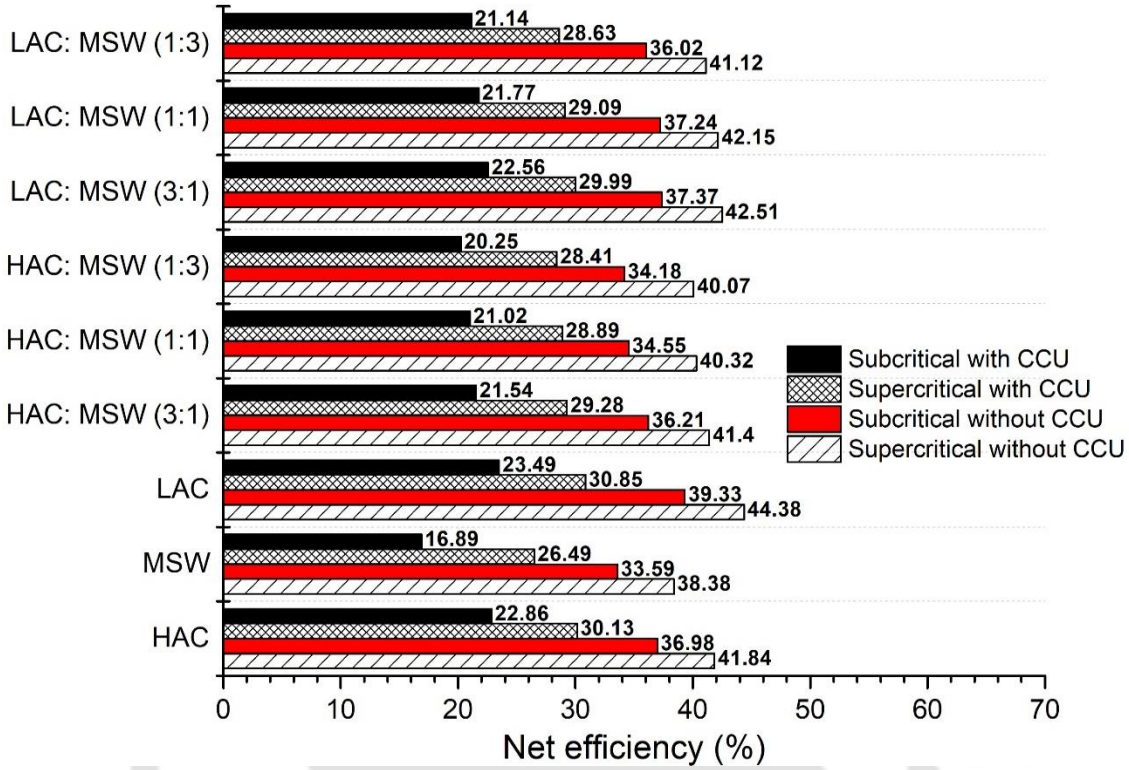

Figure 7.6. Net thermal efficiency of power plants at various operating conditions

In the subcritical power plants, the complete combustion is achieved with excess air ranging from 78-86%. The excess flow of air maintains the boiler temperature at 1200°C under subcritical condition, and at 1772°C under supercritical conditions. The air flow rate in the range of 67-79 kg/s is maintained in the combustor depending on the percentage of combustible matter in the fuels. Figure 7.6 show the comparison of the net efficiency of the power plants for various fuels and their blend. The LAC feedstock with 2% ash content achieved higher net efficiency of 39.3%, which is 2.3% higher than the HAC feedstock. Whereas the MSW fuel has shown a reasonable net efficiency of 33.6%, which is 3.4% lower than the HAC. The efficiency of the MSW based power plants reported in various literature is found in the range of 18-22%. This may be due to the low calorific value of MSW, and further the high power requirement in the auxiliary units for MSW based power plants. Further, the steam temperature and pressure were also comparatively lower (400°C and 40 bar) (Yassin et al., 2009) Further, a typical result can be seen that the addition of MSW had dropped the efficiency of the power plants due to the energy penalty associated with drying of MSW (~0.46 MW for MSW alone). The estimated net thermal efficiency of the power plants without the CCU unit is shown in

Table 7.8. The net efficiency of HAC-MSW based power plants had decreased by 0.77, 2.4, and 2.8%, with the increase in the quantity of MSW in the fuel blend by 25, 50, and 75%, respectively, under the subcritical conditions. In the case of the LAC-MSW based power plants, the MSW fuel blending caused a drop in the net thermal efficiency by 1.96, 2.09 and 3.31% for 25%, 50% and 75% blending conditions, respectively, compared to the LAC alone as the feedstock. Although the overall net thermal efficiency of LAC-MSW based power plants is higher than the HAC-MSW power plants, the drop in the net efficiency is higher in the LAC with the addition of MSW. This is due to the presence of high ash content in MSW leading to heat loss through ash slag. The least quantity of ash slag (~0.07 kg/s) is obtained in the case of LAC alone as the feedstock, whereas MSW has generated ash slag as high as 1.96 kg/s. This leads to a 1.1 MW energy loss in the slag of MSW based power plant whereas the least energy loss of 0.036 MW is estimated in the LAC based power plant. Hence, the addition of 75% MSW with the LAC blend had resulted in the energy loss of 0.63 MW in ash slag in the form of sensible heat. One can note that the 50% addition of MSW with LAC had achieved almost similar net efficiency (~37%) as that of HAC alone as the feedstock. Also, 25% addition of MSW with HAC had shown a marginal drop in the net efficiency by 0.77%.

Under the supercritical-condition, a similar trend is observed. Figure 7.7 shows the increase in the net thermal efficiency of the supercritical power plant, compared to subcritical conditions. Overall, the net thermal efficiency in the range of 4-6% is increased in the power plants from the subcritical condition to the supercritical stage. In the case of 75% addition of MSW with HAC, a maximum increase in the net thermal efficiency by 5.89% is estimated. Further, a higher drop in efficiency by 1.77% and 3.26% is estimated with the addition of 75% MSW with HAC and LAC, respectively. A lesser amount of excess air in the range of 5-13% is needed under the supercritical conditions due to the higher operating temperature of the combustor.

Table 7.8. Net efficiency of the power plants considered without CCU

Subcritical Conditions									
	HAC	LAC	MSW	HAC:MSW (3:1)	HAC:MSW (1:1)	HAC:MSW(1:3)	LAC:MSW(3:1)	LAC:MSW(1:1)	LAC:MSW(1:3)
HPST power (MW)	12.62	13.14	11.62	12.38	12	11.86	12.99	12.76	12.38
MPST power (MW)	11.18	12.48	10.3	10.97	10.5	10.38	11.37	11.31	10.97
LPST power (MW)	13.74	14.3	12.65	13.48	12.76	12.75	13.66	13.89	13.48
Pump power (MW)	0.56	0.59	0.52	0.55	0.54	0.53	0.58	0.57	0.55
Drier power (MW)	0	0	0.46	0.07	0.17	0.28	0.067	0.15	0.26
Steam requirement (kg/s)	26.6	27.7	24.5	26.1	25.4	25	27.5	26.9	26.1
Air requirement (kg/s)	75.5	79.1	67	74.2	72.6	70.3	78.7	75.8	72.6
Gross efficiency %	37.54	39.92	34.57	36.83	35.26	34.99	38.17	37.96	36.83
Net efficiency %	36.98	39.33	33.59	36.21	34.55	34.18	37.37	37.24	36.02
Supercritical Conditions									
	HAC	LAC	MSW	HAC:MSW (3:1)	HAC:MSW (1:1)	HAC:MSW(1:3)	LAC:MSW(3:1)	LAC:MSW(1:1)	LAC:MSW(1:3)
HPST power (MW)	13.69	14.52	12.62	13.69	13.25	13.06	13.94	13.84	13.54
MPST power (MW)	16.71	17.72	15.48	16.41	16.17	16.12	17	16.89	16.53
LPST power (MW)	12.19	12.94	11.43	12.12	11.8	11.89	12.41	12.33	12.06
Pump power (MW)	0.75	0.8	0.69	0.75	0.73	0.72	0.77	0.76	0.75
Drier power (MW)	0	0	0.46	0.07	0.17	0.28	0.067	0.15	0.26
Steam requirement (kg/s)	28.2	29.2	25.8	28	27.1	26.7	28	28.3	27.6
Air requirement (kg/s)	45.8	48.5	39.5	44.8	43.4	41.75	47.8	45.9	43.6
Gross efficiency %	42.59	45.18	39.53	42.22	41.22	41.07	43.35	43.06	42.13
Net efficiency %	41.84	44.38	38.38	41.4	40.32	40.07	42.51	42.15	41.12

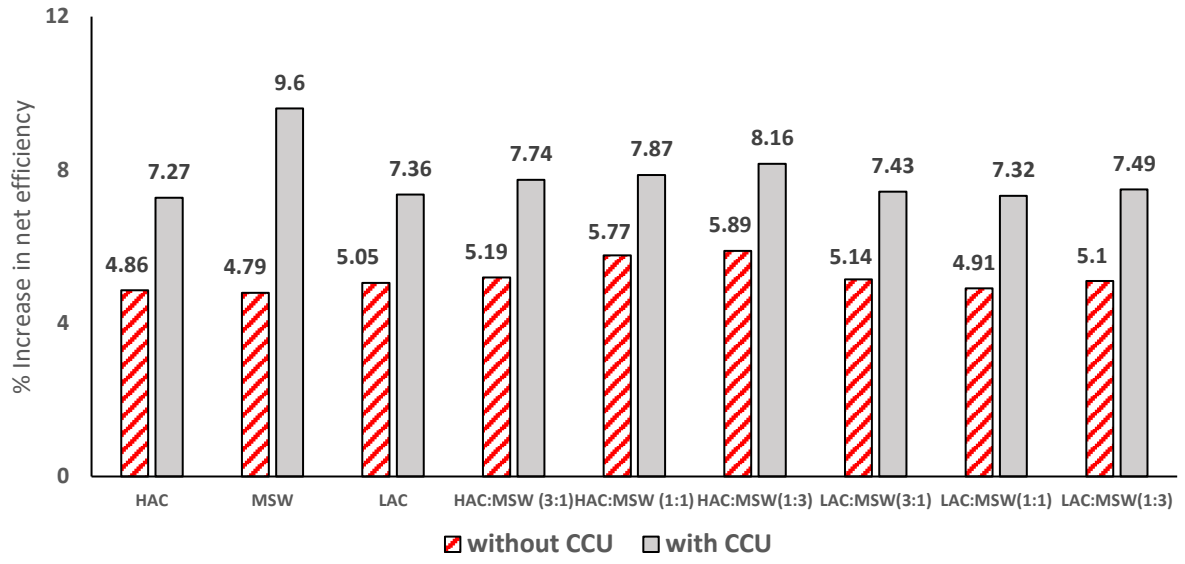

Figure 7.7. Increase in the net efficiency of power plants in supercritical conditions compared to subcritical condition.

7.7.2. Effect of carbon capture unit on net thermal efficiency

The details of the net efficiency of the power plants with the incorporation of CCU units are given in Table 7.9. Figure 7.8 shows the decrease in the net thermal efficiency of LAC and HAC by the incorporation of CCU.

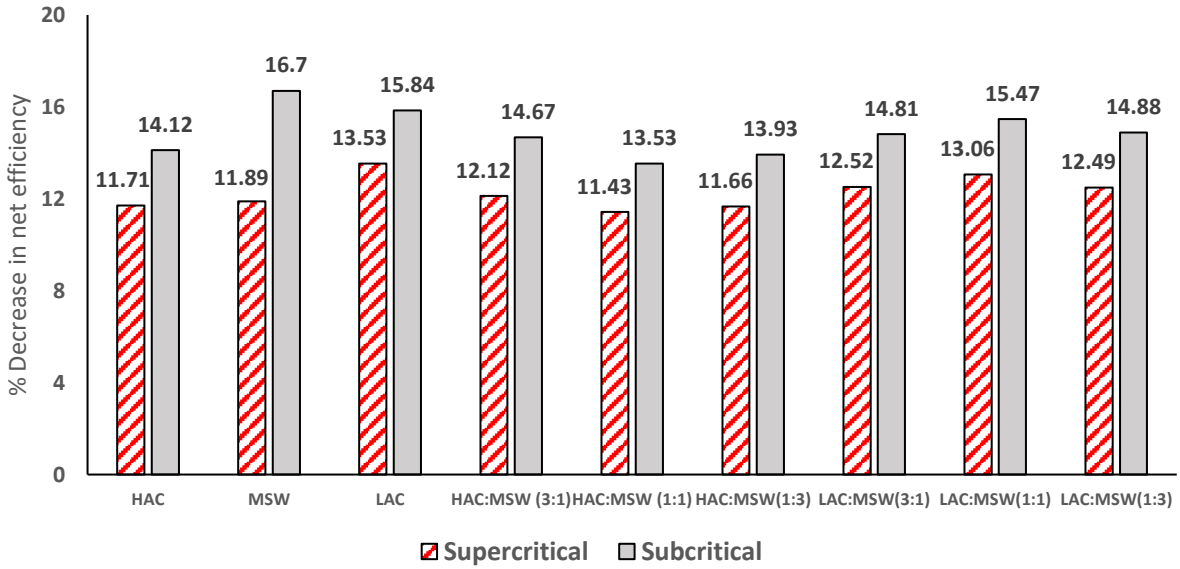

Figure 7.8. Net efficiency decrease of power plants due to the incorporation of CCU

The integration of CCU unit in the power plants decreased the net efficiency by 14-16% under subcritical conditions; whereas the efficiency drop in the range of 10-13% is estimated under supercritical conditions. This is due to the low percentage of excess air

required for combustion leading to the production of smaller quantity of flue gas. As a consequence, a low energy penalty in the reboiler duty is estimated for heating the MEA solution in the supercritical power plants. The quantity of MEA required is high for subcritical power plants and estimated in the range of 115 to 120 kg/s. It can be noted that the energy penalty due to the CCU is lower in the supercritical power plants than the subcritical conditions. Further, it is estimated that the energy penalty of the CCU is higher for the MSW feedstock due to the higher energy loss in the ash slag, although a low quantity of air is required for combustion. Hence, the variation in the net efficiency loss due to the CCU depends on the quantity of the ash slag formed and the air supplied. Further, it can be noted that the addition of the CCU unit leads to a higher loss in the net thermal efficiency of the LAC based power plants, compared to the HAC based power plants, in both subcritical and supercritical conditions.

Table 7.9. Net efficiency of the power plants considered with CCU

Subcritical Conditions									
	HAC	LAC	MSW	HAC:MSW (3:1)	HAC:MSW (1:1)	HAC:MSW(1:3)	LAC:MSW(3:1)	LAC:MSW(1:1)	LAC:MSW(1:3)
HPST power (MW)	13.19	13.71	11.86	12.9	12.52	12.14	13.47	13.04	12.62
MPST power (MW)	11.68	12.15	10.51	11.43	11.1	10.76	11.94	11.56	11.18
LPST power (MW)	14.36	14.92	12.91	14.04	13.63	13.22	14.67	14.2	13.73
Pump power (MW)	0.6	0.61	0.53	0.58	0.56	0.54	0.6	0.58	0.56
Drier power (MW)	0	0	0.46	0.07	0.17	0.28	0.067	0.15	0.26
Energy penalty (MW)	15.76	16.68	14.49	16.18	15.5	15.05	16.85	16.3	15.56
Steam requirement (kg/s)	27.8	28.4	24.7	27.2	26.4	25.6	28	27.5	26.1
Air requirement (kg/s)	75.5	79	67	75.6	72.6	70.4	78	75.7	72.6
Gross efficiency	39.23	40.78	32.37	38.37	37.25	36.12	39.51	38.8	37.53
Net efficiency	**22.86**	**23.49**	**16.89**	**21.54**	**21.02**	**20.25**	**22.56**	**21.77**	**21.14**
Supercritical Conditions									
	HAC	LAC	MSW	HAC:MSW (3:1)	HAC:MSW (1:1)	HAC:MSW(1:3)	LAC:MSW(3:1)	LAC:MSW(1:1)	LAC:MSW(1:3)
HPST power (MW)	13.54	14.18	12.13	13.59	13.4	13.15	13.89	13.45	13.15
MPST power (MW)	16.53	17.31	14.8	16.1	15.88	15.59	16.95	16.45	16.05
LPST power (MW)	12.06	12.63	10.8	11.9	11.73	11.51	12.37	11.98	11.71
Pump power (MW)	0.76	0.79	0.68	0.75	0.75	0.73	0.77	0.75	0.74
Drier power (MW)	0	0	0.46	0.07	0.17	0.28	0.067	0.15	0.26
Energy penalty (MW)	11.23	12.48	10.09	11.48	11.2	10.83	13.22	12.78	12.28
Steam requirement (kg/s)	27.7	29	24.7	27.8	27.1	26.7	28.3	28.3	27.6
Air requirement (kg/s)	45.8	48.5	39.5	44.8	43.4	41.75	47.8	45.9	43.6
Gross efficiency %	42.13	44.12	37.73	41.59	41.01	40.25	43.21	41.88	40.91
Net efficiency %	**30.13**	**30.85**	**26.49**	**29.28**	**28.89**	**28.41**	**29.99**	**29.09**	**28.63**

7.8. Economic analysis

The detailed economic analyses of the power plants without CCU are given in Tables 7.10 and 7.11 for subcritical and supercritical conditions, respectively. The cost of turbines and boilers is the the major proportion of the capital cost. It can be noted that the addition of MSW increased the capital investment due to the cost associated with MSW pre-treatment unit. The electric power in the range of 0.07 to 0.5 MW is consumed in the MSW pre-treatment process under various operating conditions. Further, the ash handling system of MSW consumed electric power as high as ~1 MW. Under the subcritical conditions without CCU, the LAC based power plants had shown the lowest LCOE of 51.61 $/MWh, whereas, the LCOE of the HAC plant is higher by 5.92 $/MWh. The MSW based power plants had shown the highest LCOE of 81.14 $/MWh; however, MSW blended with coal in the ratio of 1:3 reduces the LCOE to 73.37 and 69.65 $/MWh for the HAC and LAC, respectively. Under the supercritical conditions, the net efficiency of the power plants had increased and subsequently, a decrease in the LCOE can be observed. It can be noted from Table 7.10 and 7.11, the difference in the values of the LCOE under subcritical and supercritical conditions is found in the range of 0.6 - 2.71 $/MWh, which is in line with the reported literature (Surywanshi et al., 2019). MSW based subcritical and supercritical power plant is found with the highest LCOE of 81.14 and 80.44 $/MWh, respectively.

The economic analysis of power plants with CCU is given in Tables 7.12 and 7.13 for subcritical and supercritical conditions, respectively. Under the subcritical condition, the LCOE of the power plants varies from 108.4 to 141.2 $/MWh for the LAC-MSW fuel blend. These values are in line with the literature (Pettinau et al., 2017). The addition of the CCU unit to the subcritical power plants increased the LCOE in the range of 53.4 to 106.7 $/MWh; whereas under supercritical conditions, the LCOE of the power plants is increased in the range from 36.7 $/MWh to 53.2 $/MWh.

Table 7.10. LCOE estimation by economic analysis of the power plants considered under subcritical condition without CCU

Components (million $)	HAC	LAC	MSW	HAC:MSW (3:1)	HAC:MSW (1:1)	HAC:MSW(1:3)	LAC:MSW(3:1)	LAC:MSW(1:1)	LAC:MSW(1:3)
MSW pre-treatment	0	0	0.57	0.17	0.3	0.43	0.16	0.28	0.41
Water system	2.29	2.05	3.05	2.44	2.6	2.81	2.22	2.43	2.7
Heat exchangers	0.066	0.072	0.054	0.045	0.065	0.065	0.064	0.063	0.063
Turbine	38.23	34.25	50.83	40.68	43.48	46.81	37.09	40.58	45.03
Boiler	57.68	51.69	76.7	61.38	65.6	70.64	55.96	61.24	67.94
Coal handling cost	1.02	0.92	-	0.89	0.71	0.47	0.81	0.67	0.46
Total installed cost	99.29	88.99	131.19	105.61	110.36	121.23	96.3	104.99	116.6
Land surveyor cost	4.96	4.45	6.56	5.28	5.51	6.06	4.81	5.25	5.83
Owner's cost	14.89	13.35	19.67	15.84	16.55	18.18	14.44	15.75	17.49
utilities	0.40	0.42	0.39	0.402	0.404	0.405	0.42	0.416	0.414
Total capital cost	119.56	107.2	157.83	127.14	132.83	145.88	115.99	126.41	140.33
Operating and maintenance cost (per year)	3.69	3.31	4.86	3.95	4.12	4.51	3.62	3.93	4.35
Plant overhead (per year)	0.053	0.053	0.072	0.072	0.072	0.072	0.072	0.072	0.072
Fuel cost (per year)	3.94	5.21	4.45	4	4.11	4.23	5.08	4.91	4.7
Ash Handling System (per year)	0.69	0.026	0.92	0.52	0.57	0.63	0.67	0.73	0.82
Total operating and maintenance cost (per year)	8.38	8.58	10.32	8.55	8.87	9.45	9.44	9.65	9.93
ACC	10.26	9.2	13.55	10.91	11.4	12.52	9.95	10.84	12.04
LCOE ($/MWh)	57.53	51.61	81.14	61.35	66.98	73.37	59.26	62.84	69.65

Table 7.11. LCOE estimation by economic analysis of the power plants considered under supercritical condition without CCU

Components (million $)	HAC	LAC	MSW	HAC:MSW (3:1)	HAC:MSW (1:1)	HAC:MSW(1:3)	LAC:MSW(3:1)	LAC:MSW(1:1)	LAC:MSW(1:3)
MSW pre-treatment	0	0	0.57	0.17	0.3	0.43	0.16	0.28	0.41
Water system	2.67	2.39	3.54	2.89	3.03	3.26	2.59	2.83	3.14
Heat exchangers	0.077	0.124	0.136	0.063	0.076	0.078	0.087	0.089	0.09
Turbine	35.82	33.3	54.33	43.49	46.48	50.05	39.67	43.39	48.14
Boiler	71.78	64.32	95.44	76.38	81.63	87.9	69.66	76.21	84.54
Coal handling cost	1.15	1.03	-	1	0.8	0.53	0.91	0.75	0.51
Total installed cost	111.5	101.17	154.03	123.95	132.33	142.26	113.08	123.55	136.84
Land surveyor cost	5.57	5.05	7.7	6.19	6.61	7.11	5.65	6.17	6.84
Owner's cost	16.72	15.17	23.1	18.59	19.85	21.34	16.96	18.53	20.53
utilities	0.43	0.45	0.43	0.432	0.431	0.429	0.43	0.433	0.435
Total capital cost	134.22	121.85	185.26	149.17	159.23	171.14	136.13	148.7	164.64
Operating and maintenance cost (per year)	4.12	3.75	5.7	4.61	4.91	5.27	4.22	4.6	5.08
Plant overhead (per year)	0.055	0.055	0.074	0.074	0.074	0.074	0.074	0.073	0.073
Fuel cost (per year)	3.94	5.21	4.45	4	4.11	4.23	5.08	4.91	4.7
Ash Handling System (per year)	0.69	0.026	0.92	0.52	0.57	0.63	0.67	0.73	0.82
Total operating and maintenance cost (per year)	9.34	9.02	11.14	9.21	9.66	10.21	9.38	9.66	10.66
ACC	11.52	10.46	15.89	12.8	13.66	14.68	11.68	12.76	14.12
LCOE ($/MWh)	56.92	50.11	80.44	60.7	66.05	70.93	56.55	60.72	68.83

Under supercritical conditions, the obtained LCOE values are lower than the power plants at subcritical conditions even though the total installed cost is higher in the supercritical power plants. The LCOE values are higher for the subcritical based power plants in the range of 17 – 54 $/MWh with the incorporation of CCU. The MSW based power plants are the least economical with the highest LCOE values of all the cases considered with CCU. The estimated LCOE values for the MSW-based power plants are 187.87 $/MWh and 133.95 $/MWh under subcritical and supercritical conditions, respectively. The LCOE based on LAC, HAC, MSW and their blends with CCU under supercritical conditions is almost twice as the LCOE of those fuels and blends without CCU. However, the CCU energy penalty is reduced under supercritical conditions by a factor of 0.3 to 0.5, compared to the subcritical conditions of the power plant.

The effect of the incorporation of CCU on the LCOE for LAC and HAC fuels is shown in Figure 7.9. With CCU, the LCOE of HAC based feedstock is higher than the LAC by 0.83 $/MWh and 3.29 $/MWh for the subcritical and supercritical conditions, respectively. However, without CCU, the difference is higher by 5.92 $/MWh and 6.81 $/MWh for the subcritical and supercritical conditions, respectively. One can observe from Table 7.7 and Table 7.10, the fuel blend of LAC-MSW at 3:1 ratio under supercritical conditions without CCU had a similar performance, compared to the power plant with HAC alone. The LCOE of LAC-MSW with 3:1 ratio is 56.55 $/MWh, which is equivalent to the LCOE, 56.9 $/MWh, of the HAC based feedstock. The net electrical efficiency of the HAC based power plant is 41.8%, which is comparable to the efficiency, 42.51%, achieved in the power plant with 3:1 ratio of LAC-MSW feedstock.

Table 7.12. LCOE estimation by economic analysis of the power plants considered under subcritical condition with CCU

Components (million $)	HAC	LAC	MSW	HAC:MSW (3:1)	HAC:MSW (1:1)	HAC:MSW(1:3)	LAC:MSW(3:1)	LAC:MSW(1:1)	LAC:MSW(1:3)
MSW pre-treatment	0	0	0.57	0.17	0.3	0.43	0.16	0.28	0.41
Water system	2.29	2.05	3.05	2.44	2.61	2.81	2.22	2.43	2.7
Heat exchangers	0.66	0.7	0.75	0.68	0.7	0.73	0.72	0.73	0.74
Turbine	38.23	34.25	50.83	40.68	43.48	46.82	37.09	40.59	45.02
Boiler	57.68	51.69	76.7	61.38	65.6	70.64	55.95	61.24	67.94
Coal handling cost	1.02	0.92	-	0.89	0.71	0.47	0.81	0.67	0.46
CO_2 compressors	1.43	1.48	1.41	1.43	1.42	1.41	1.44	1.44	1.43
CO_2 removal infrastructure	11.58	12.02	10.39	11.51	11.11	10.8	12.04	11.67	11.17
Gas cleaning	1.8	7.3	5.89	7.07	6.89	6.79	7.25	7.12	6.23
Total installed cost	115	110.43	150	126	133	141	117.7	126	136.11
Land surveyor cost	5.73	5.52	7.48	6.31	6.64	7.05	5.89	6.3	6.81
Owner's cost	17.2	16.6	22.44	18.94	19.92	21.13	17.7	18.92	20.4
utilities	6.23	6.51	5.63	6.24	6.01	5.84	6.48	6.29	6.03
Total capital cost	144	139	185.13	157.76	165.41	174.92	148	157.69	169
Operating and maintenance cost (per year)	4.53	4.42	5.55	5.02	5.25	5.53	4.72	5.01	4.83
Plant overhead (per year)	0.16	0.18	0.2	0.2	0.2	0.2	0.2	0.2	0.2
Fuel cost (per year)	3.94	5.21	4.45	4	4.11	4.23	5.08	4.91	4.7
Ash Handling System (per year)	0.69	0.026	0.92	0.52	0.57	0.63	0.67	0.73	0.82
CO_2 transport and limestone cost	0.55	0.91	0.54	0.56	0.55	0.54	0.86	0.79	0.69
Total operating and maintenance cost (per year)	9.88	10.7	11.9	10.29	10.5	11.1	11.5	11.7	11.8
ACC	12.35	11.9	15.88	13.54	14.19	15.01	12.7	13.53	14.5
LCOE ($/MWh)	110.93	110.1	187.87	126.27	135.05	147.42	122.54	132.08	142.04

Table 7.13. LCOE estimation by economic analysis of the power plants considered under supercritical condition with CCU

Components (million $)	HAC	LAC	MSW	HAC:MSW (3:1)	HAC:MSW (1:1)	HAC:MSW(1:3)	LAC:MSW(3:1)	LAC:MSW(1:1)	LAC:MSW(1:3)
MSW pre-treatment	0	0	0.57	0.17	0.3	0.43	0.16	0.28	0.41
Water system	2.67	2.39	3.54	2.84	3.03	3.27	2.58	2.83	3.14
Heat exchangers	1.11	1.48	0.96	1.38	1.53	1.4	1.36	1.31	1.28
Turbine	40.87	36.62	54.33	43.5	46.48	50.04	39.64	43.39	48.14
Boiler	71.78	64.32	95.43	76.38	81.64	87.9	69.63	76.21	84.54
Coal handling cost	1.15	1.03	-	1	0.8	0.53	0.91	0.75	0.51
CO_2 compressors	1.45	1.48	1.37	1.48	1.47	1.47	1.48	1.46	1.45
CO_2 removal infrastructure	11.58	12.02	10.39	9.09	11.15	10.88	12.07	11.67	11.2
Gas cleaning	3.81	5.29	4.5	5	4.93	4.83	5.25	5.13	4.98
Total installed cost	134	124.64	171	141	151	161	133.11	143	155.7
Land surveyor cost	6.72	6.23	8.56	7.04	7.57	8.04	6.66	7.15	7.78
Owner's cost	20.16	18.7	25.7	21.1	22.7	24.1	20	21.5	23.3
utilities	4.41	4.65	3.84	4.37	4.27	4.13	4.68	4.49	4.26
Total capital cost	166	154	209.19	173	185.89	197	164	176.16	191
Operating and maintenance cost (per year)	5.18	4.87	6.56	5.49	5.86	7.27	5.22	5.57	6.02
Plant overhead (per year)	0.15	0.17	0.18	0.18	0.18	0.18	0.18	0.18	0.18
Fuel cost (per year)	3.94	5.21	4.45	4	4.11	4.23	5.08	4.91	4.7
Ash Handling System (per year)	0.69	0.026	0.92	0.52	0.57	0.63	0.67	0.73	0.82
CO_2 transport and FGD operation	0.55	0.91	0.54	0.55	0.55	0.55	0.87	0.79	0.69
Total operating and maintenance cost (per year)	10.5	11.2	12.7	10.7	11.3	12.9	12	12.2	12.4
ACC	14.22	13.2	17.95	14.88	15.95	16.91	14.1	15.11	16.4
LCOE ($/MWh)	93.59	90.3	133.95	99.9	107.57	119.65	99.46	107.16	114.84

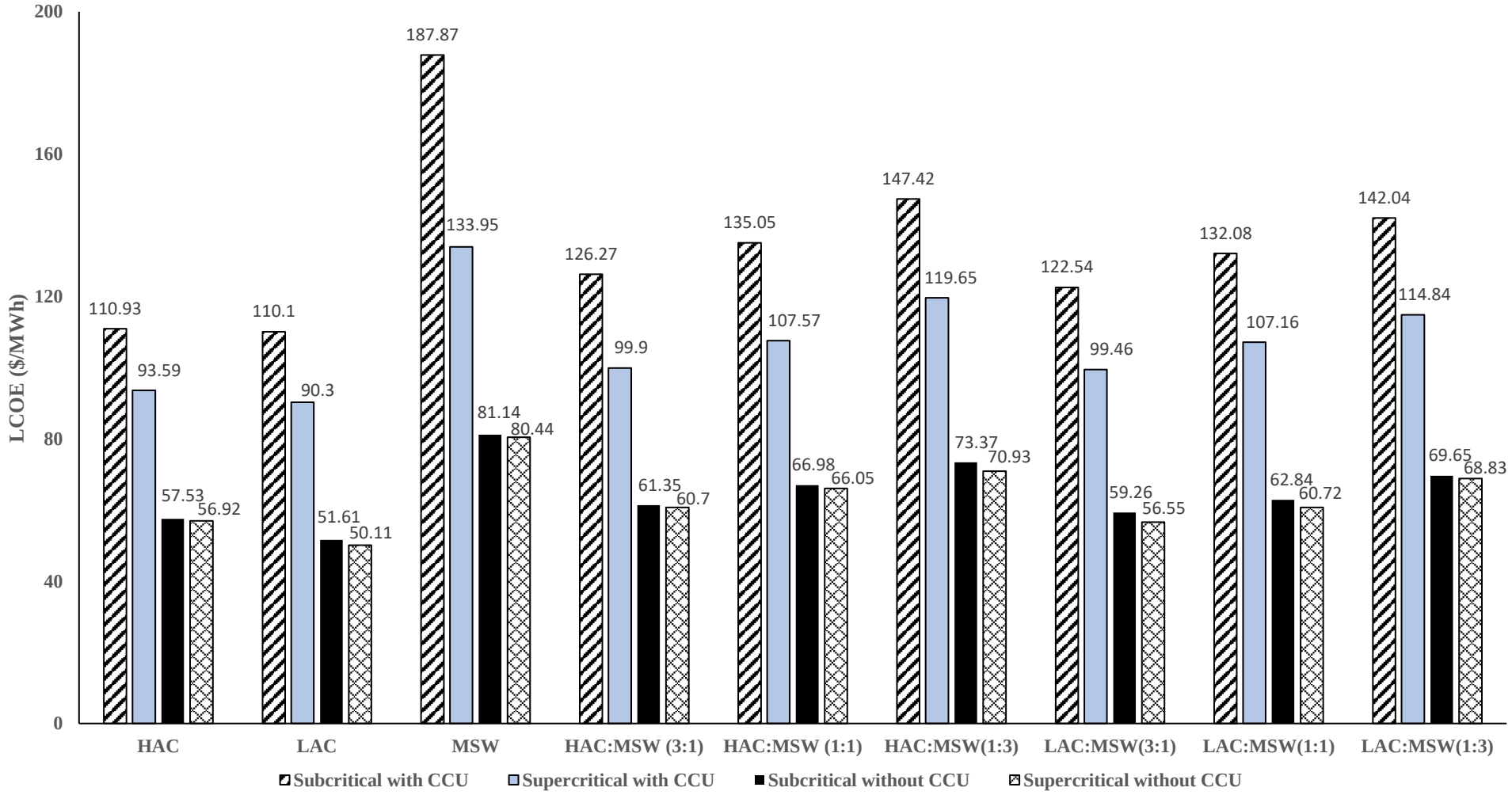

Figure 7.9. LCOE values of different blends with and without CCU

7.9. CO_2, SO_x and NO_x emissions

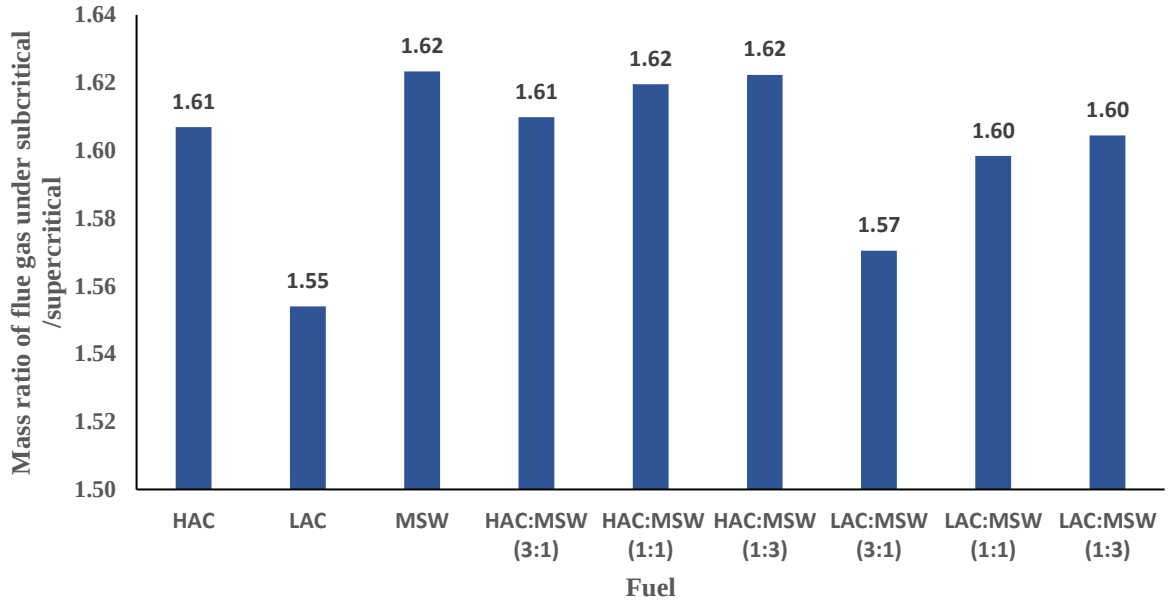

Figure 7.10. Mass ratio of the flue gas generated under subcritical to supercritical stage without CCU

The incorporation of gas cleaning units such as deNO_x and deSO_x units had decreased the net electrical efficiency of the power plants by 1 to 1.5%. These units increased the LCOE of the power plants by 10 to 20 $/MWh. The outlet gas composition of the power plants is given in Table 7.14(a) and 7.14(b) for subcritical and supercritical conditions, respectively. One can see that a larger quantity of flue gas is generated for LAC feedstock, compared to HAC (difference ~ 4 kg/s) and MSW (difference ~11 kg/s), owing to its higher amount of air requirement. The quantity of the flue gas and CO_2 generated is reduced with the addition of MSW. Figure 7.10 shows the mass ratio of the flue gas generated in the subcritical stage to the supercritical condition of the power plants. It can be seen that the flue gas generated in the subcritical conditions is almost 1.56 to 1.62 times higher than the supercritical conditions leading to the high energy penalty for the incorporation of CCU. The percentage of CO_2 in the flue gas varies from 11 to 12% under the subcritical condition; whereas it is increased to 17 to 18% under supercritical condition. Figure 7.11 shows the emission level of the pollutants such as SO_2, NO_x and CO_2 from the power plants with and without treatment unit. According to the Indian standards, the allowable limit of SO_2 and NO_x in the flue gas from thermal power plants is 100 mg/m^3 (Wiatros-Motyka, 2019). It can be seen from Figures 7.11(a) and 7.11(b) that the NO_x and SO_x emissions are found higher under the supercritical conditions. It could be due to the higher thermal NO_x formation at higher operating temperatures. Further, this is due to the

reduction in the quantity of the generated flue gas at higher operating temperature of the combustor (Bienstock et al., 1966). With the incorporation of the treatment units such as SCR and FGD, the allowable limit of NO_x and SO_x in the flue gas is achieved. It can be seen from Figure 7.11(a) that the MSW combustion produces higher NO_x emissions under the subcritical and supercritical conditions with a level of 520 mg/m^3 and 120 mg/m^3, respectively. After the treatment in the SCR unit, the NO_x emissions are limited to 98.5 and 18 mg/m^3 under the supercritical and subcritical conditions, respectively. The increase in the MSW quantity in the blend mixture along with HAC from 0 to 75%, the NO_x emission is increased from 490 to 506 mg/m^3 under the supercritical conditions without CCU. It is estimated that the ratio of NO_x emissions in the supercritical condition to the subcritical condition is 5.5 and 4.5 for the power plant with CCU and without CCU, respectively. This ratio remains same for the both the coals, HAC and LAC. The blending of HAC with MSW at equal proportion decreased the SO_2 emissions from 10953 mg/m^3 to 3960 mg/m^3 under the supercritical conditions without CCU. In the case of LAC, MSW blending decreased the SO_2 emissions from 57340 mg/m^3 to 29314 mg/m^3 at 1:3 ratio of LAC-MSW blending under the supercritical conditions without CCU. The highest SO_2 emission of 57340 mg/m^3 is estimated for LAC alone as the feedstock. After the treatment of flue gas in the FGD unit, the SO_2 emission is reduced to 1.31 and 0.9 mg/m^3 for the HAC-MSW mixture at 3:1 ratio under subcritical and supercritical conditions with CCU, respectively. The ratio of SO_2 emission in the power plants for subcritical condition to the supercritical condition with CCU is found between 1.45 - 1.5 and 2 - 3.2 for HAC-MSW and LAC-MSW blends, respectively.

Table 7.14 (a). Flue gas composition obtained under subcritical conditions with and without CCU unit (weight% basis)

Without CCU	HAC	LAC	MSW	HAC:MSW (3:1)	HAC:MSW (1:1)	HAC:MSW (1:3)	LAC:MSW (3:1)	LAC:MSW (1:1)	LAC:MSW (1:3)
H_2O	2.62	2.40	4.29	2.89	3.23	3.68	2.70	3.04	3.52
N_2	73.70	73.32	71.91	73.40	73.04	72.57	73.19	72.91	72.54
O_2	11.94	12.09	12.69	12.08	12.28	12.47	12.17	12.27	12.50
NO	0.01	0.01	0.01	0.01	0.01	0.01	0.01	0.01	0.01
SO_2	0.00	0.22	0.04	0.01	0.01	0.03	0.01	0.01	0.02
SO_3	0.00	0.19	0.03	0.01	0.01	0.02	0.00	0.01	0.02
CO_2	11.73	11.75	11.02	11.60	11.41	11.23	11.91	11.73	11.39
Total emissions (kg/s)	78.64	82.86	71.62	77.61	76.33	74.43	82.4	79.87	76.9
CO_2 specific emissions (kg/MWh)	898.3	891.3	845.6	895.2	892.2	872.6	928.7	905.5	875.2
With CCU after treatment	HAC	LAC	MSW	HAC:MSW (3:1)	HAC:MSW (1:1)	HAC:MSW (1:3)	LAC:MSW (3:1)	LAC:MSW (1:1)	LAC:MSW (1:3)
N_2	84.87	84.72	83.89	84.68	84.48	84.47	84.55	84.4	84.18
O_2	13.74	13.89	14.8	14.96	14.21	14.97	14.04	14.23	14.48
CO_2	1.35	1.37	1.29	1.34	1.33	1.31	1.38	1.36	1.33
Total emissions (kg/s)	67.94	71.26	61.08	68.2	65.48	63.92	70.51	68.57	65.94
CO_2 specific emissions (kg/MWh)	145.3	149.24	126.13	153.02	149.14	148.56	155.82	154.37	149.36

Table 7.14 (b). Flue gas composition obtained under supercritical conditions with and without CCU (weight% basis)

Without CCU	HAC	LAC	MSW	HAC:MSW (3:1)	HAC:MSW (1:1)	HAC:MSW (1:3)	LAC:MSW (3:1)	LAC:MSW (1:1)	LAC:MSW (1:3)
H_2O	4.18	3.81	6.97	4.66	5.23	5.97	4.22	4.88	5.68
N_2	71.86	71.24	68.89	71.371	70.755	69.97	71.20	70.77	69.97
O_2	5.03	5.56	6.04	5.22	5.44	5.72	5.84	5.68	5.86
NO_2	0.00	0.004	0.005	0.004	0.004	0.004	0.00	0.004	0.004
NO	0.06	0.057	0.059	0.056	0.055	0.057	0.06	0.058	0.056
SO_2	0.00	0.57	0.10	0.017	0.040	0.068	0.01	0.034	0.061
SO_3	0.00	0.034	0.007	0	0.002	0.004	0.00	0.002	0.004
CO_2	18.87	18.73	17.91	18.67	18.47	18.21	18.67	18.579	18.37
Total emissions (kg/s)	48.94	53.32	44.12	48.21	47.13	45.88	52.47	49.97	47.93
CO_2 specific emissions (kg/MWh)	794.4	794.9	741.5	782.8	777.4	750.5	829.5	799.9	773.1
With CCU after treatment	HAC	LAC	MSW	HAC:MSW (3:1)	HAC:MSW (1:1)	HAC:MSW (1:3)	LAC:MSW (3:1)	LAC:MSW (1:1)	LAC:MSW (1:3)
N_2	91.11	90.64	89.81	90.97	90.73	90.43	91.05	90.38	90.1
O_2	6.38	6.89	7.84	6.64	6.84	7.19	7.12	7.23	7.53
CO_2	2.4	2.38	2.35	2.39	2.41	2.38	2.44	2.42	2.38
Total emissions (kg/s)	38.39	40.9	33.68	37.64	36.57	35.32	40.15	38.86	37.04
CO_2 specific emissions (kg/MWh)	110.29	113.61	107.39	110.67	108.99	106.91	117.64	112.59	108.74

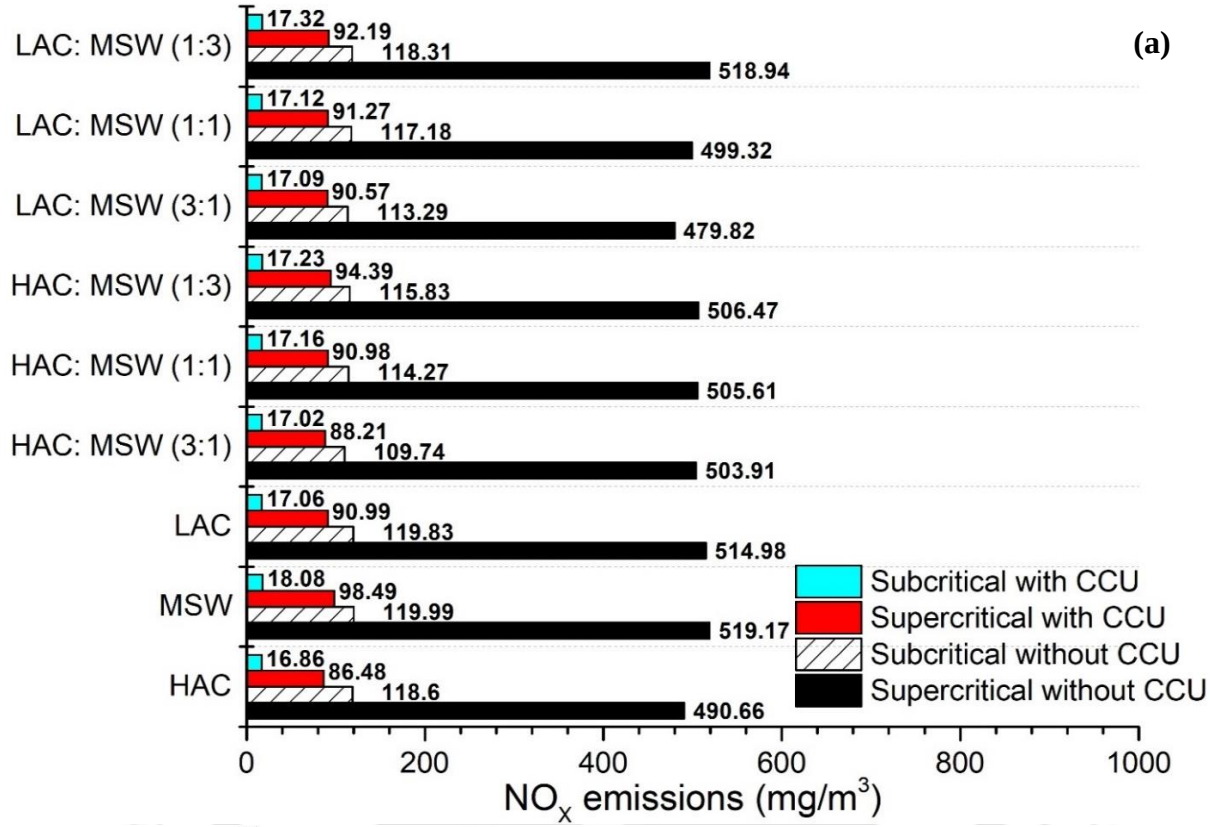

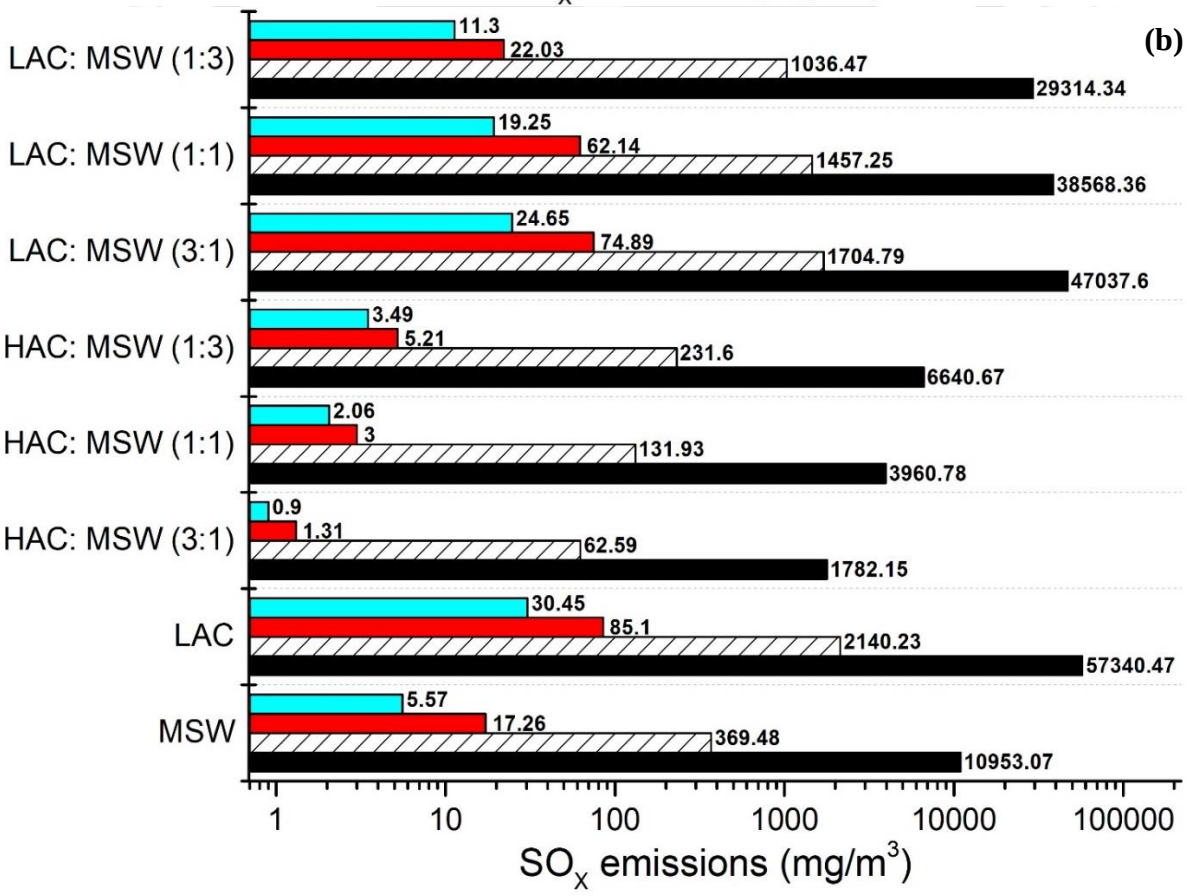

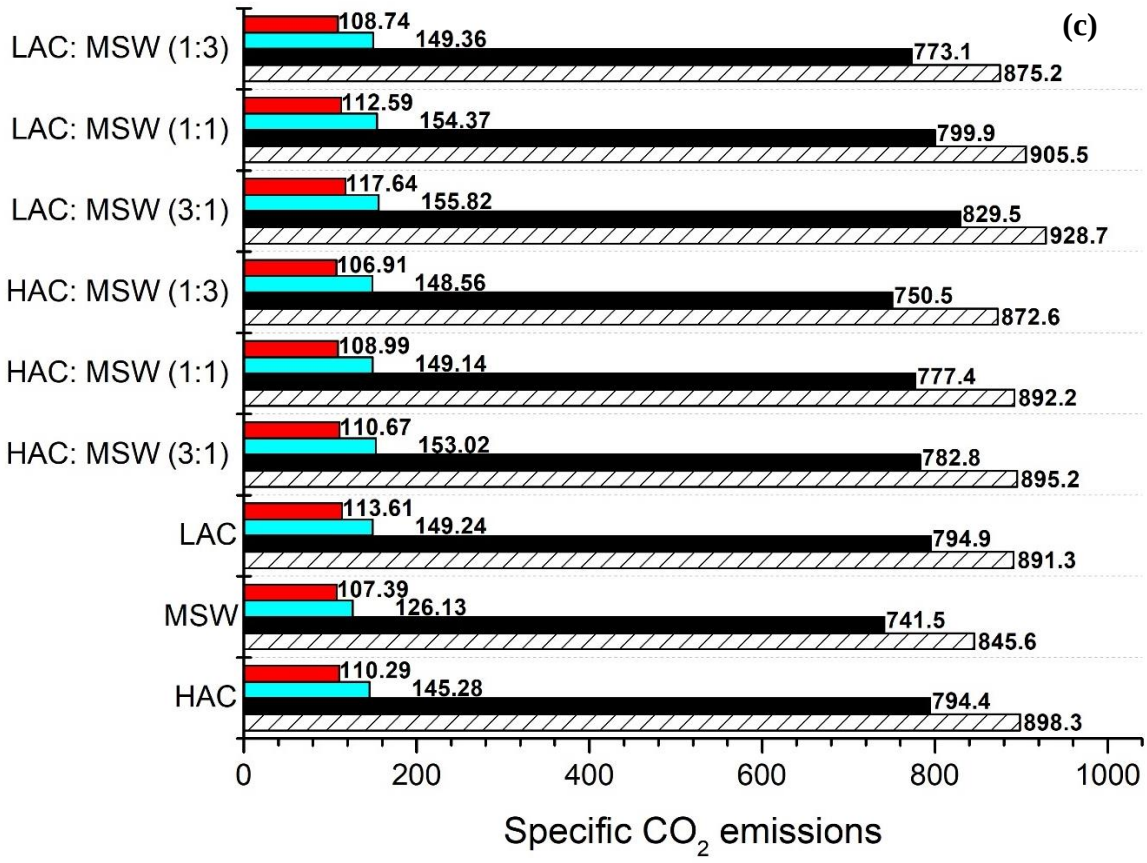

Figure 7.11. (a) SO_X, (b) NO_X emissions, (c) Specific CO_2 emissions

The CO_2 specific emission (kg/MWh) is the least for MSW and its blending with HAC had decreased the CO_2 emission; whereas, MSW blending with LAC had increased the specific CO_2 emission due to the higher drop in the net thermal efficiency of LAC-MSW based power plants. Hence, the blending of LAC and MSW at 3:1 ratio had resulted in the highest specific CO_2 emissions. However, at higher proportion of MSW with LAC (1:3 ratio of LAC and MSW), the specific CO_2 emissions become lower than that of LAC alone. The specific CO_2 emission of LAC are inline with the literature values of 913.2 and 849.12 kg/MWh for subcritical and supercritical conditions without CCU, respectively (Pettinau et al., 2017). The present study estimated the CO_2 specific emissions of 891.3 and 794.9 kg/MWh for LAC under subcritical and supercritical conditions without CCU, respectively. With the incorporation of CCU, the respective CO_2 specific emissions are reduced to 145.3 and 107.3 kg/MWh

7.10. Comparison of LCOE and net efficiency with literature

Table 7.15. Comparison of LCOE and net efficiency with literature

Fuel	References	LCOE ($/MWh)	Net efficiency (%)
	Subcritical		
HAC	Current study	57.53	36.98
LAC	Current study	51.61	39.33
MSW	Current study	81.44	33.59
MSW	(Yassin et al., 2009)	108.64_c*	22.4
Illinois coal (10.91% ash)	(Zhao et al., 2013)	67	38.7
Douglas coal (13.89% ash)	(A. Cormos & Cormos, 2017)	55.03_c	38.51
	Subcritical with CCU		
HAC	Current study	110.93	22.86
LAC	Current study	110.1	23.49
MSW	Current study	187.87	16.89
Illinois coal (10.91% ash)	(Zhao et al., 2013)	117	26.5
Douglas coal (13.89% ash)	(A. Cormos & Cormos, 2017)	100.34_c	29.21
Talcher coal (40 % ash)	(U. Singh et al., 2017)	91.98	23.34
	Super-critical		
HAC	Current study	56.92	41.84
LAC	Current study	50.11	44.38
European bituminous coal	(Zhao et al., 2013)	46	45
Chinese Anthracite coal	(S. Singh et al., 2018)	50.7	40.9
Douglas coal (13.89% ash)	(A. Cormos & Cormos, 2017)	53.3_c	41.42
	Supercritical with CCU		
HAC	Current study	93.59	30.13
LAC	Current study	90.3	30.85
European bituminous coal	(Zhao et al., 2013)	83	31
Chinese Anthracite coal	(S. Singh et al., 2018)	94.3	28.6
Douglas coal (13.89% ash)	(A. Cormos & Cormos, 2017)	94.1_c	32.15

*c = converted from euro, *= operated at comparatively lower temperature*

The estimated LCOE values are compared with the literature results in Table 7.15. The obtained LCOE values are inline with the reported literature. The utilization of Douglas

coal (U.S bituminous coal) (A. Cormos & Cormos, 2017) had shown 55 $/MWh of LCOE, which is almost similar to the results of the present study.

Further, a higher LCOE by 28 $/MWh was reported by Yassin et al. (2019) for MSW fuel, compared to the present study. This could be due to the low operating temperature of the boiler, which generated the steam at low temperature and pressures at 400°C and 40 bar, which affected the net thermal efficiency of the power plant (Yassin et al., 2009).

Table 7.16. Comparison of specific CO_2 emission with literature

Reference	Feed	Subcritical (kg/MWh)	Subcritical with CCU (kg/MWh)
Current study	HAC	898.3	145.3
Current study	LAC	891.3	149.24
(A. Cormos & Cormos, 2017)	Douglas coal (13.89%)	913.2	119.46
(U. Singh et al., 2017)	Talcher coal (40 % ash)	950	140
(Surywanshi et al., 2019)	High ash coal (48.87% ash)	793.6	-
(Zhao et al., 2013)	Illniois coal (10.91% ash)	807	80
Reference	Feed	Supercritical (kg/MWh)	Supercritical with CCU (kg/MWh)
Current study	HAC	794.4	110.29
Current study	LAC	794.9	113.61
(A. Cormos & Cormos, 2017)	Douglas coal (13.89%)	849.12	107.02
(Zhao et al., 2013)	Illniois coal (10.91%)	776	108
(Surywanshi et al., 2019)	High ash coal (48.87%)	759.03	-

In the present study, the incorporation of CCU had increased the LCOE of the power plant by 53-58 $/MWh under the subcritical conditions and 37-40 $/MWh under supercritical conditions for coal fuels. A similar trend is reported in the study based on Douglas coal. The net efficiency of the power plants estimated at various operating conditions is found inline with the literature data at both subcritical and supercritical conditions with and without CCU. In Table 7.16, the specific CO_2 emissions of the power plants proposed in the present study are compared with the literature data. The low carbon

content in high ash coal (48.9% ash) had resulted in lower specific CO_2 emissions, compared to the present study (Surywanshi et al., 2019). Although Talcher coal contains low carbon content (~40%), it shows higher specific CO_2 emissions, which could be due to low net efficiency of the power plant (34.34%) (U. Singh et al., 2017). Similarly, Douglas coal-based power plant had assessed with a similar thermal and economic performance, compared to the LAC-based power plant.

7.11. Summary of the chapter

The impact of the co-combustion of MSW with high and low ash Indian coals in the process efficiency of the conventional steam turbine power plants is studied with carbon capture under post combuation absorption method. The net thermal efficiency of the power plants with and without CCU is estimated using Aspen plus software. Further, the economic analyses of the thermal power plants are carried out. The following conclusions can be drawn from the present study.

- Under subcritical conditions without CCU integration, the addition of 25% MSW with LAC showed the net thermal efficiency of 37%, which is equivalent to that of HAC alone as the feedstock. Further, the 25% addition of MSW with HAC had resulted in only a marginal drop in the net efficiency of 0.77%, compared to the unblended HAC feedstock.
- The LCOE of MSW based power plants under subcritical and supercritical conditions is around 80 $/MWh, which is 40 to 60% higher than that of LAC and HAC based power plants without CCU integration. However, the feedstock with MSW blended coal at 1:3 ratio reduces the LCOE from 80 $/MWh to 73.47 and 69.7 $/MWh for HAC and LAC, respectively.
- The negative impact of ash on the efficiency of thermal power plants can be minimized with the integration of CCU. The LCOE difference between the HAC and LAC is 5.92 $/MWh and 6.81 $/MWh under the subcritical and supercritical conditions without CCU, respectively. This difference can be decreased further by 0.83 $/MWh (subcritical) and 3.29 $/MWh (supercritical) by incorporating the CCU.
- The incorporation of the CCU unit decreases the net efficiency of power plants by 14% to 17% under subcritical conditions and 11% to 13% under supercritical conditions. As a consequence, the LCOE had increased in the range of 53.4 to

106.73 $/MWh and 36.67 to 53.51 $/MWh under subcritical and supercritical conditions, respectively.

- Under supercritical conditions, the quantity of flue gas generated are drastically reduced by ~1.5 times, compared to subcritical conditions. As a result, CO_2 intensity is found higher and increased from 11% to 17% under supercritical conditions. Further, the SO_x emission from the high sulfur coal (LAC) is reduced by 4.76 % while blending with MSW.

Nomenclature

CCU carbon capture unit

PCDD/DF Polychlorinated dibenzo-dioxins/dibenzo difurans

RDF refuse derived fuel

FGD flue gas desulfurization

SCR selective catalytic reduction

SNCR selective non-catalytic reduction

CRF capital recovery factor

PCCI power capital cost index

LCOE levelized cost of electricity

ACC annualized capital cost

MEA monoethanolamine

HPST high pressure steam turbine

MPST medium pressure steam turbine

LPST low pressure steam turbine

TC total capital cost

C_E cost of quimpent to be calculated

Q_E capacity of equipment whose cost is to be calculated

C_B cost of equipment with known capacity

Q_B capacity of equipment with known cost

HAC high ash coal

LAC low ash coal

MSW municipal solid waste

P power consumption or produced (MW)

OECD organisation for economic co-operation and development

References

12 MW Waste to Energy Project (Ghazipur , Delhi). (n.d.). In *IL and FS Environment*.

Bhui, B., & Prabu, V. (2021). Chemical looping based co-combustion of high ash Indian coal and rice straw operating under CO_2 in-situ gasi fi cation mode. *Journal of the Energy Institute*, *94*, 176–190. https://doi.org/10.1016/j.joei.2020.07.004

Bienstock, D., Amsler, R. L., & Bauer, E. R. (1966). Formation of oxides of nitrogen in pulverized coal combustion. *Journal of the Air Pollution Control Association*, *16*(8), 442–445. https://doi.org/10.1080/00022470.1966.10468498

Callen, T. (2012). *Purchasing Power Parity: Weights Matter*. Imf. http://www.imf.org/external/pubs/ft/fandd/basics/ppp.htm#top

Carpenter, A. M. (2012). Low water FGD technologies. In *IEA Clean Coal Center: Vol. December N* (Issue November).

Chen, T., Shen, Y., Lee, W., Lin, C., & Wan, M. (2013). An economic analysis of the continuous ultrasound-assisted oxidative desulfurization process applied to oil recovered from waste tires. *Journal of Cleaner Production*, *39*, 129–136. https://doi.org/10.1016/j.jclepro.2012.09.001

Cheng, H., Zhang, Y., Meng, A., & Li, Q. (2007). Municipal solid waste fueled power generation in China: A case study of waste-to-energy in Changchun City. *Environmental Science and Technology*, *41*(21), 7509–7515. https://doi.org/10.1021/es071416g

Coal India Ltd. (2011). *Coal Price Notification 2018* (pp. 1–30).

Cormos, A., & Cormos, C. (2017). Techno-economic evaluations of post-combustion CO_2 capture from sub- and super-critical circulated fluidised bed combustion (CFBC) power plants. *Applied Thermal Engineering*, *127*, 106–115. https://doi.org/10.1016/j.applthermaleng.2017.08.009

Cormos, C. C. (2013). Assessment of flexible energy vectors poly-generation based on coal and biomass/solid wastes co-gasification with carbon capture. *International Journal of Hydrogen Energy*, *38*(19), 7855–7866. https://doi.org/10.1016/j.ijhydene.2013.04.064

Dattatray, A. D., & Shilapuram, V. (2019). *Detailed parametric investigation of dry gasification oxy-combustion power cycle using ASPEN Plus simulations*. *236*(September 2018), 501–515.

Detailed Project Report Integrated MSW Management for GMADA Cluster. (2017). IL and FS Environment.

Detailed Project Report on Municipal Solid Waste Management. (2017). Medak Municipality.

Dong, C., Jin, B., & Lan, J. (2002). Co-combustion of Municipal Solid Waste and Coal in a Circulating Fluidized Bed. *Developments in Chemical Engineering and Mineral Processing*, *10*(5–6), 639–646. https://doi.org/10.1002/APJ.5500100613

Grover, G. (2017). *Recommendations for Long Term Action Plan for Solid Waste Management in Delhi* (Issue C).

Harvey, L. D. D. (2020). Clarifications of and improvements to the equations used to calculate the levelized cost of electricity (LCOE), and comments on the weighted average cost of capital (WACC). *Energy*, *207*, 118340. https://doi.org/10.1016/j.energy.2020.118340

Kimberlin, T., & Ribeiro, S. G. (2010). High Efficiency Waste to Energy Power Plants Combining Municipal Solid Waste and Natural Gas or Ethanol. *Proceedings of the 18th Annual North American Waste-to-Energy Conference*, 1–7. https://doi.org/10.1115/NAWTEC18-3567

Kokalj, F., & Samec, N. (2013). Combustion of Municipal Solid Waste. *Advances in Internal Combustion Engines and Fuel Technologies*, *1*, 1–16. https://doi.org/10.5772/50231

Kuo, P. C., & Wu, W. (2016). Thermodynamic analysis of a combined heat and power system with CO_2 utilization based on co-gasification of biomass and coal. *Chemical Engineering Science*, *142*, 201–214. https://doi.org/10.1016/j.ces.2015.11.030

Lu, L., Ismail, T. M., Jin, Y., Abd El-Salam, M., & Yoshikawa, K. (2016). Numerical and experimental investigation on co-combustion characteristics of hydrothermally treated municipal solid waste with coal in a fluidized bed. *Fuel Processing Technology*, *154*, 52–65. https://doi.org/10.1016/j.fuproc.2016.08.007

Ma, C., Li, B., Chen, D., Wenga, T., Ma, W., Lin, F., & Chen, G. (2019). An investigation of an oxygen-enriched combustion of municipal solid waste on flue gas emission and combustion performance at a 8 MWth waste-to-energy plant. *Waste Management*, *96*, 47–56. https://doi.org/10.1016/j.wasman.2019.07.017

Mboowa, D., Quereshi, S., Bhattacharjee, C., Tonny, K., & Dutta, S. (2017). Qualitative determination of energy potential and methane generation from municipal solid waste (MSW) in Dhanbad (India). *Energy*, *123*, 386–391. https://doi.org/10.1016/j.energy.2017.02.009

Miller, B. G., & Francisco, S. A. N. (n.d.). *Clean Coal Engineering Technology*. http://www.sciencedirect.com/science/book/9781856177108

Mishra, N., Bhui, B., & Vairakannu, P. (2019). Comparative evaluation of performance of high and low ash coal fuelled chemical looping combustion integrated combined cycle power generating systems. *Energy*, *169*, 305–318. https://doi.org/10.1016/j.energy.2018.12.043

Moradian, F., Pettersson, A., & Richards, T. (2015). Thermodynamic equilibrium model applied to predict the fouling tendency in a commercial fluidized-bed boiler, combusting solid waste. *Energy and Fuels*, *29*(5), 3483–3494. https://doi.org/10.1021/acs.energyfuels.5b00346

Ohman, M., & Nordin, A. (2000). The Role of Kaolin in Prevention of Bed Agglomeration during Fluidized Bed Combustion of Biomass Fuels. *Energy & Fuels*, *14*, 618–624. https://doi.org/https://doi.org/10.1021/ef990198c

Pauschert, D. (2009). Study of Equipment Prices in the Power Sector. *ESMAP Technical Paper*, *122/09*, 121.

Perazzini, H., Freire, F. B., Freire, F. B., & Teixeira, J. (2016). *Thermal Treatment of Solid Wastes Using Drying Technologies : A Review*. *3937*. https://doi.org/10.1080/07373937.2014.995803

Pettinau, A., Ferrara, F., Tola, V., & Cau, G. (2017). Techno-economic comparison between different technologies for CO_2 -free power generation from coal. *Applied Energy*, *193*, 426–439. https://doi.org/10.1016/j.apenergy.2017.02.056

Pour, N., Webley, P. A., & Cook, P. J. (2018). Potential for using municipal solid waste

as a resource for bioenergy with carbon capture and storage (BECCS). *International Journal of Greenhouse Gas Control*, *68*(November 2017), 1–15. https://doi.org/10.1016/j.ijggc.2017.11.007

Purchasing power parities. (n.d.). Organization for Economic Cooperation and Development. https://data.oecd.org/conversion/purchasing-power-parities-ppp.htm

Ragazzi, M., Rada, E. C., Panaitescu, V., & Aposto, T. (2007). Municipal solid waste pre-treatment: A comparison between two dewatering options. *WIT Transactions on Ecology and the Environment*, *102*, 943–949. https://doi.org/10.2495/SDP070902

Rai, A. K. (2017). Super Critical Thermal Power Plant Boiler Efficiency Calculation Using Imported Coal. *International Journal for Research in Applied Science and Engineering Technology*, *V*(IX), 709–717. https://doi.org/10.22214/ijraset.2017.9104

Santos, S., Gomes, J., & Bordado, J. (2016). Scale-Up Effects of CO_2 Capture by Methyldiethanolamine (MDEA) Solutions in Terms of Loading Capacity. *Technologies*, *4*(3), 19. https://doi.org/10.3390/technologies4030019

Singh, S., Lu, H., Cui, Q., Li, C., Zhao, X., Xu, W., & Ku, A. Y. (2018). China baseline coal-fired power plant with post-combustion CO_2 capture: 2. Techno-economics. *International Journal of Greenhouse Gas Control*, *78*(April), 429–436. https://doi.org/10.1016/j.ijggc.2018.09.012

Singh, U., Rao, A. B., & Chandel, M. K. (2017). Economic Implications of CO_2 Capture from the Existing as Well as Proposed Coal-fired Power Plants in India under Various Policy Scenarios. *Energy Procedia*, *114*(November 2016), 7638–7650. https://doi.org/10.1016/j.egypro.2017.03.1896

Srivastava, R. K., Hall, R. E., Khan, S., Culligan, K., & Lani, B. W. (2005). Nitrogen oxides emission control options for coal-fired electric utility boilers. *Journal of the Air and Waste Management Association*, *55*(9), 1367–1388. https://doi.org/10.1080/10473289.2005.10464736

Stec, M., Tatarczuk, A., Więcław-Solny, L., Krótki, A., Spietz, T., Wilk, A., & ̄piewak, D. (2016). Demonstration of a post-combustion carbon capture pilot plant using

amine-based solvents at the Łaziska Power Plant in Poland. *Clean Technologies and Environmental Policy*, *18*(1), 151–160. https://doi.org/10.1007/s10098-015-1001-2

Suresh, M. V. J. J., Reddy, K. S. Ã., & Kolar, A. K. (2010). 3-E analysis of advanced power plants based on high ash coal. *International Journal of Energy Research*, *March 2009*, 716–735. https://doi.org/10.1002/er

Surywanshi, G. D., Pillai, B. B. K., Patnaikuni, V. S., Vooradi, R., & Anne, S. B. (2019). 4-E analyses of chemical looping combustion based subcritical , supercritical and ultra-supercritical coal-fired power plants Unites States of America. *Energy Conversion and Management*, *200*(August), 112050. https://doi.org/10.1016/j.enconman.2019.112050

Thermal_Model_Consolidated_v. (n.d.). Central Electricity Regulatory Commission.

Vekemans, O., & Chaouki, J. (2016). Municipal Solid Waste Cofiring in Coal Power Plants: Combustion Performance. *Intech*, 225–240. https://www.intechopen.com/books/advanced-biometric-technologies/liveness-detection-in-biometrics

Wiatros-Motyka, M. (2019). NOx control for high-ash coal-fired power plants in India. *Clean Energy*, *3*(1), 24–33. https://doi.org/10.1093/ce/zky018

Xu, J., Huang, Q., & Wang, F. (2020). Co-combustion of municipal solid waste and coal for carbon emission reduction: A bi-level multi-objective programming approach. *Journal of Cleaner Production*, *272*, 121923. https://doi.org/10.1016/j.jclepro.2020.121923

Yassin, L., Lettieri, P., Simons, S. J. R., & Germanà, A. (2009). Techno-economic performance of energy-from-waste fluidized bed combustion and gasification processes in the UK context. *Chemical Engineering Journal*, *146*, 315–327. https://doi.org/10.1016/j.cej.2008.06.014

Zhang, D. (2013). *Ultra-Supercritical Coal Power Plants Materials, Technologies and Optimisation* (First). Woodhead Publishing.

Zhao, M., Minett, A. I., & Harris, A. T. (2013). A review of techno-economic models for the retrofitting of conventional pulverised-coal power plants for post-combustion capture (PCC) of CO_2. *Energy and Environmental Science*, *6*(1), 25–40.

https://doi.org/10.1039/c2ee22890d

CHAPTER 7-B

CO-COMBUSTION OF MSW AND COAL IN OXY-COMBUSTION CCS BASED POWER PLANTS

A techno economic analysis is performed for electricity generation using supercritical and subcritical based steam turbines operating in the oxy-fuel co-combustion mode of municipal solid waste with Indian coals. The impact of capture of direct and indirect greenhouse gases such as CO_2, NO_X and SO_X on the net thermal efficiency of the power plants is assessed. The supercritical based steam turbine achieved a higher net thermal efficiency by 8.8% using municipal solid waste based feedstock, compared to sub-critical conditions. The co-combustion mode reduced the levelized cost of electricity (LCOE) by 48-73 $/MWh. Techno-economic analysis for sulfur removal in coal using ultrasonification technology is not yet reported in the literature. The incorporation of an ultrasonicator (a pre-combustion sulfur remover) and a duct sorbent injector (a post-combustion SOx absorber) increased the LCOE by 1.39-2.75 $/MWh. In high sulphur coals, the SO_X emissions has decreased from 224.79 mg/m^3 to 9.2 mg/m^3.

7.12. Oxy-fuel combustion based power plants

MSW can be effectively utilized along with coal in thermal power industries for electricity generation. Oxy-fuel combustion technology ensures the sustainability of combustion flame in boilers especially for high ash coals and MSW. In this technology, the obtained flue gas is free of nitrogen and can be stored without any further treatment. As Indian coals possess high ash content, oxy-fuel combustion technology is beneficial for effective utilization. However, this technology produces fuel and thermal NO_X at higher operating temperatures. Further, the Northeast Indian coals possess high sulfur about 4% and on combustion, they produce SO_X pollutants. NO_X and SO_X in the flue gas need to be captured before CO_2 storage. SO_X produced during coal combustion corrodes heat exchangers and boiler tubes and the sulfur in the coal need to be removed under pre-combustion stage. Although several literature are available on the utilization of MSW with coal for power generation, oxy-fuel combustion with carbon capture and storage (CCU) is not employed with NO_X and SO_X removal. Yassin et al., (2009) had performed

economic and energy analysis considering the wastes to energy under non-oxy combustion mode in the UK (Yassin et al., 2009). Incorporation of the oxy-fuel technology with CO_2 compression and storage and NOx and SOx treatment of flue gas in the co-combustion mode of MSW with Indian coals is not yet studied. Hence, the techno-economic feasibility study of these operations for electricity generation using the conventional steam turbine power plant under subcritical and supercritical conditions is essential for commercialization. The effect of the use of high ash coal (HAC) and low ash coal (LAC) in waste to energy plants incorporating CO_2, NO_X and SO_X capture has not yet been performed. Hence, in the present study, the energy and economic analysis of the co-combustion of MSW with Indian coals were performed using Aspen Plus software for waste to energy plant in context to Indian scenario. In the present study, pre-combustion removal of sulfur by ultrasonification (UC) method and post-combustion capture by flue gas desulfurization unit (FGD) using duct sorbent injection (DSI) are employed to use the high sulfur coals from North eastern India. Ultrasonification of high sulfur coals using solvents like H_2O_2, HCl and HNO_3 could aid in the removal of organic and inorganic sulfur of coals (Ambedkar et al., 2011). To enhance the removal of sulfur compounds in LAC and LAC blended feed, the additional sulfur removal units DSI and UC are added. Energy economic efficiency takes into account the operational parameters with cost of the implementation of the technology to achieve the optimal solution (Du et al., 2020). The impact of the treatment units on the cost of electricity has not yet been reported in the literature whereas it is estimated in the present study.

7.12.1. Power plant configurations

The power plants consist of three major units such as air separation unit (ASU), power generation unit (PGU) and carbon capture unit (CCU). The schematic diagram of the proposed power plant is shown in Figure 7.12. In the proposed system, MSW is pre-treated to remove the moisture content. Under the co-combustion conditions, the net thermal efficiency of steam turbine based power plants is estimated for the various ratios of MSW and coal in the feedstock. MSW is mixed with coal varying from 0 to 100% by weight with 25% increment in each case. In this chapter, the feasibility of co-utilization of high and low ash coal with MSW for power generation is studied. A very few literature reported the economic analysis of MSW with coal for electricity generation. MSW is a

low calorific fuel and the gasification of these waste along with coal produces a low quality syngas.

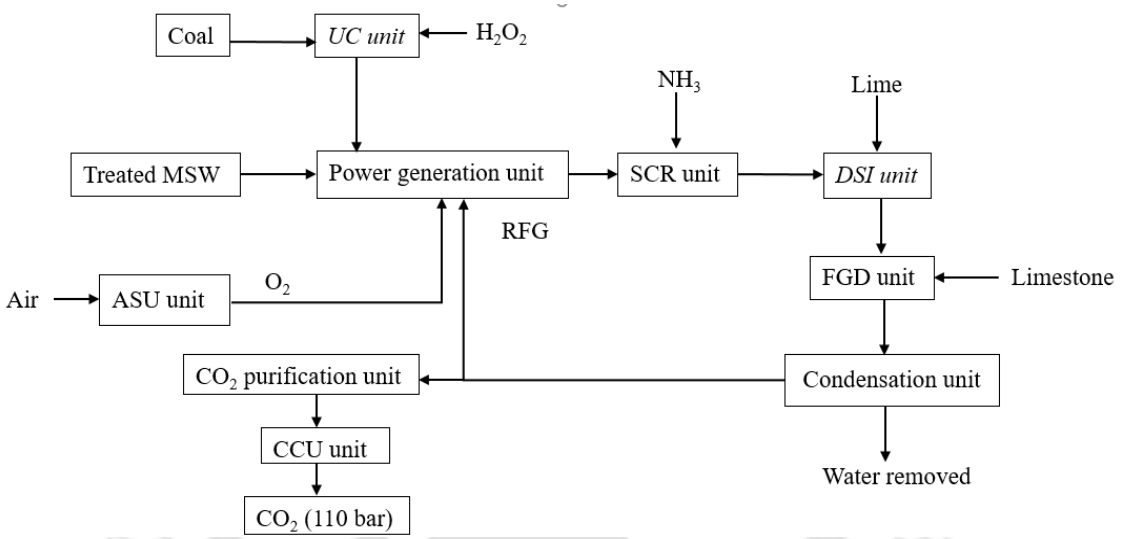

Figure 7.12. Block diagram of oxy-fuel power plant (UC and DSI units are optional)

Direct burning of MSW after prior treatment is a better option than co-gasification with coal inorder to recover its heating value. Hence, the impact of MSW blending with high and low coal on the net power generation capacity of steam turbine based power plants is evaluated with and without carbon capture. Post combustion and oxy-fuel combustion mode of CCS is assessesd with the co-utilization of MSW with coal.The various operating conditions of the power plants of the present study are listed in Table 7.17. MSW after treatment and coal is fed to power generation unit. Flue gas generated is sent to flue gas cleaning in FGD (flue gas desulfurization) and SCR (selective catalyst reduction) unit to remove SO_X and NO_X. UC (ultrasonication) and DSI (duct sorbent injection) units are optional for decreasing sulphur emissions. After SO_X and NO_X are removed, flue gas is sent to condensation unit to remove water from flue gas. After water removal part of flue gas is recycled to combustor and part is sent to CO_2 purification unit. In Table 7.18 models used for additional SO_X removal units are given.

Table 7.17. Operating parameters of power plants used in Aspen Plus simulation

Efficiency of Turbine	Subcritical	Supercritical	Reference
High pressure steam turbine (HPST)	0.89	0.896	(Suresh et al., 2010)
Medium pressure steam turbine (MPST)	0.903	0.917	
Low pressure steam turbine (LPST)	0.851	0.857	
ASU assumptions			
Efficiency of compressors in ASU	0.8		(Aneke & Wang, 2015), (Lockwood, 2014)
Output pressure of compressors	1.98 ,3.46,6.35 bar		
Specific power consumption	164 kWh/t		
CCU Unit			
Compressors	5		(Prabu & Geeta, 2015)
Operating Pressure of Compressors (bar)	3.2,13.6,33.5,70,110		
FGD Unit			
FGD unit inlet temperature (°C)	110		(Carpenter, 2012)
SO_2 removal efficiency	98%		
Lime solution solids inlet%	25%		
Gypsum solids %	45%		
DSI Unit			
Inlet temperature (°C)	150		(Carpenter, 2012)
SO_2 removal efficiency	50%		
SO_3 removal efficiency	80%		
Ultrasonication unit			
Solvent used	H_2O_2		(Ambedkar et al., 2011)
Reagent concentration	0.5mole/l		
Sulfur removal efficiency	80%		

Table 7.18. Reactor types used in Aspen plus simulations

Unit	Reactor type
Flue gas desulfurisation (FGD)	Rstoic
Selective catalytic reduction (SCR)	Rstoic
Duct sorbent injection	Rstoic
Decomposer	Ryield

7.12.2 Additional Flue Gas Desulfurization unit

7.12.2.1. Duct sorbent injection unit

Duct sorbent injection is a post combustion SO_x removal technique. This process is capable of removing SO_2 and SO_3. The operating temperature of the DSI unit is found in the range of 120°C to 180°C. The low operating temperature of the DSI is favourable for the SO_2 removal. The various sorbents such as lime, trona (a compound of Na_2CO_3) and ammonia are used in this method. In the present study, lime is used as a sorbent for SO_x removal. Lime is capable of removing 50-60% of SO_2 and >80% of SO_3. DSI unit consumes 0.2% of net power generated. Lime slurry is sprayed over the flue gas in the form of fine droplets, which makes it more reactive under dry conditions (Carpenter, 2012). The chemical reactions occurring in this unit are given below (Basu & Debnath, 2019).

$$Ca(OH)_2 + SO_2 \rightarrow CaSO_3 + H_2O \quad (7.13)$$

7.12.2.2. Desulfurization by ultrasonification unit

It is one of pre-combustion sulfur removal techniques. Recent studies showed that ultrasonification technology was able to remove organic and inorganic sulfur from coals(Ambedkar et al., 2011),(Saikia et al., 2014). In the present study, H_2O_2 solvent is used for the dissolution of sulfur from coal(Ambedkar et al., 2011),(Baruah & Khare, 2007). During the ultrasonification process, the cavitation effect produces bubbles, which collapse producing high local temperature and high pressure on coal particle surfaces. These shockwaves produce shear forces, which break coal surfaces exposing sulfur sites in coal to the solvent. Ultrasonification technology eliminates the mass transfer resistance and allows the solvent to diffuse easily into the sulfur site for dissolution. By employing low cost solvent, this technology can be easily implemented for commercialization.

7.12.3. Power generation unit (PGU)

The pure oxygen obtained from the ASU unit and the recycled flue gas, which is almost a pure CO_2 stream, are sent to the boiler operating at 1200°C under subcritical conditions and 1772°C under supercritical conditions. In the boiler, the oxygen levels were maintained in the range of 24-26% as similar to the percentage of O_2 in the air(Saikia et al., 2014). Ryield reactor in the Aspen model is used to dissociate the solid feedstock

component into individual species. The pumped water is preheated from 70°C to 80°C using the heat generated during compression of air and flue gas in the ASU and CCU unit, respectively. The warm water from the ASU and the CCU unit is sent to the feed water preheater section (FW). The power plant consists of three steam turbines operating under high pressure (HPST), medium pressure (MPST) and low pressure (LPST) (Figure 7.13).

A fraction of the outlet steam from SH1 is sent to the feed water preheater (FW2) and the rest of steam is reheated using a superheater (SH2). The steam form SH2 is used to drive the MPST. Further, a fraction of outlet steam outlet from the MPST is sent to the feed water preheater (FW3) and the rest is sent to the LPST for electricity generation. The flue gas from the superheater SH2 is sent to an economizer to heat the preheated water at 341°C, which is further sent to the boiler. The flue gas from the economizer is sent the gas cleaning units (DSI and SCR unit) to capture the SOx and NOx gases. The DSI is an optional process depending on the level of SO_x in the flue gas. After the gas cleaning process, a portion of flue gas is recycled to the boiler for temperature moderation. The rest of the flue gas is sent to the water condensation unit. After the removal of water, the obtained dry flue gas is sent to CO_2 purification unit (CPU) to further remove SO_X and NO_X and obtain high purity CO_2(Cau et al., 2018). The cleaned CO_2 is pressurised to 110 bar using a series of compressors in the CO_2 compression unit (CCU) (Figure 7.14)(Prabu & Geeta, 2015).

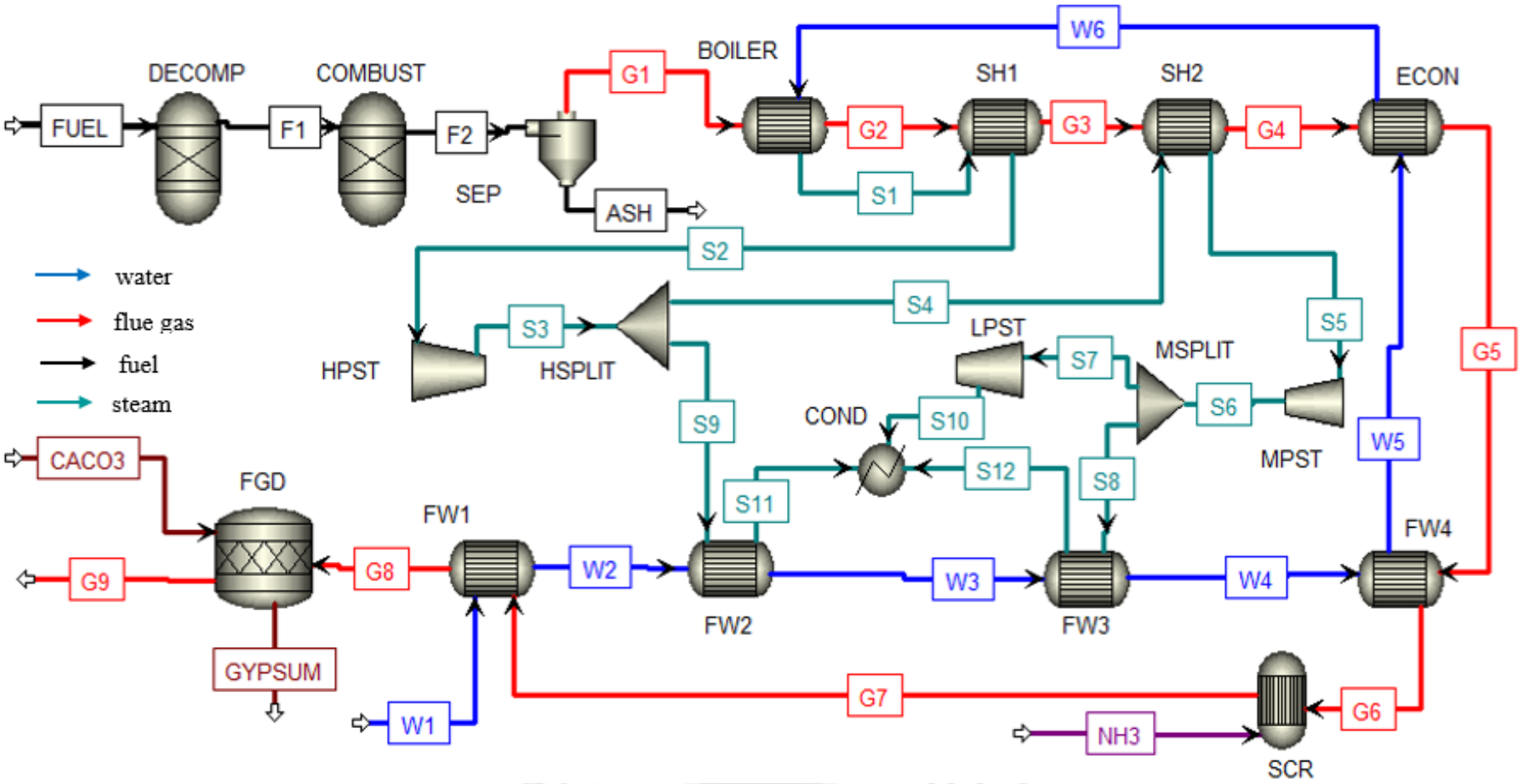

Figure 7.13. Power generation unit (PGU): FW: Feed water preheater, S: steam, W: water, G: gases, COMBUST: combustor, COND: condenser HSPLIT, MPSPLIT: Splitter after HPST and MPST, ECON: economizer SH: superheater, FW: feedwater preheater

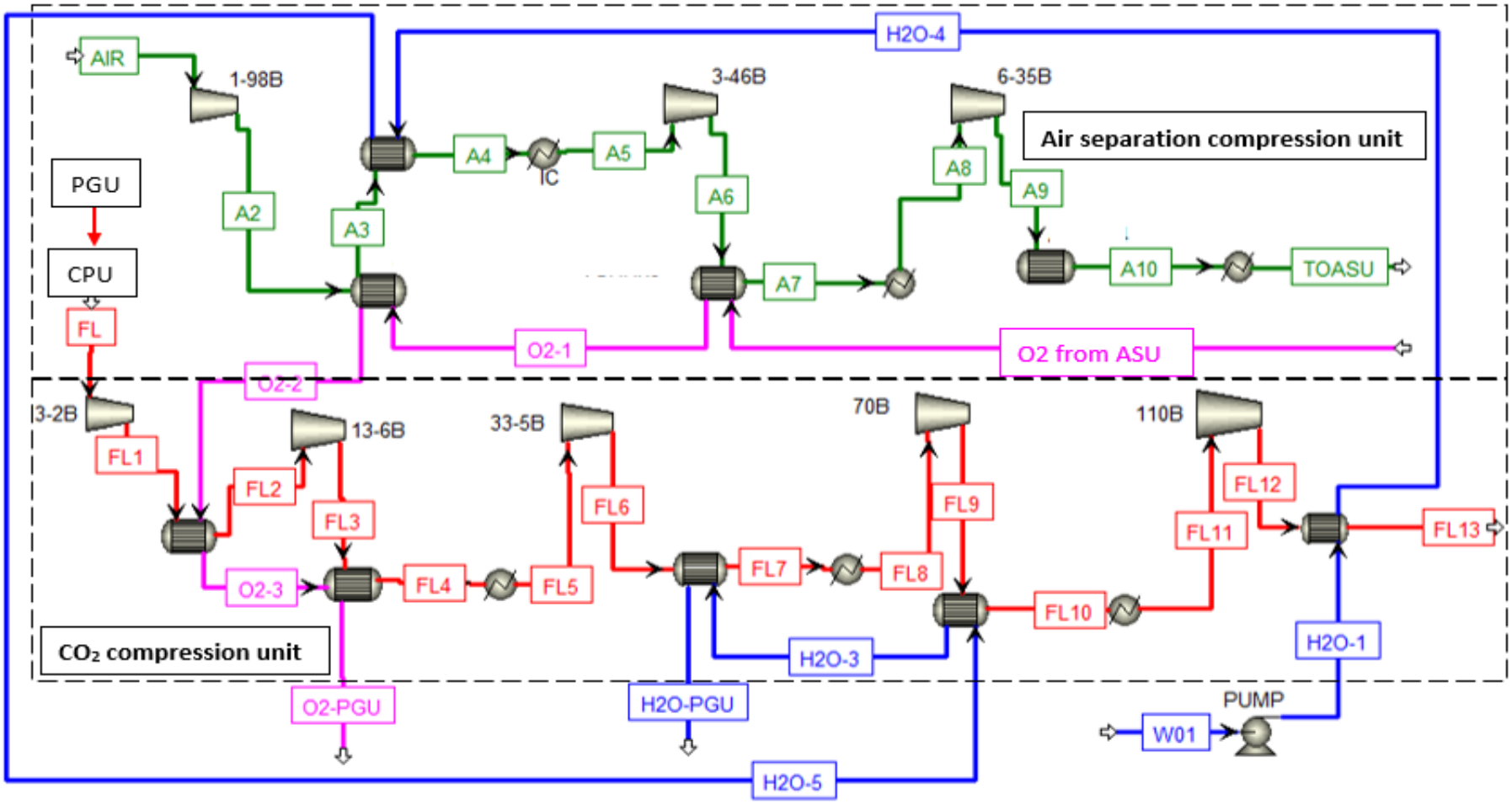

Figure 7.14. Auxiliary unit CCU and ASU with PGU; FL: flue gas, O_2: oxygen; H_2O: water; A: Air; PGU: power generation unit, B: compressor, CPU: CO_2 purification unit, B: compressors, PR: Preheater

7.13. Detailed energy analysis of oxy-fuel combustion based power plants

The energy analysis of the power plants is performed in terms of their gross and net efficiency. Tables 7.19(a) and 7.19(b) show the estimation of the net thermal efficiency of the proposed steam turbine power plants under subcritical and supercritical conditions, respectively. The electric power produced by the steam turbines and the energy penalty associated in the auxiliary units such as ASU, CCU, FGD and SCR are assessed. LAC having the highest calorific value results in the highest net thermal efficiency of the power plants. As LAC contains high quantity of fixed carbon among other fuels, larger quantity of oxygen is required for combustion leading to higher ASU penalty (~7.9 MW). With increase in the MSW content in the feedstock under co-combustion conditions, the oxygen requirement had decreased leading to low energy penalty of the ASU (~5.3 MW). MSW alone as the feedstock produces the least net electric power of 20 MW whereas LAC had achieved 30 MW production of electricity. However, the addition of 25% of LAC with MSW had increased their electric power production (~25 MW) with a net thermal efficiency of 25%. The ash effect in HAC leads to 2% reduction in the net thermal efficiency, compared to LAC feedstock.

Desulfurization of HAC fuel is not required as it contains very negligible amount of sulfur. NOx supercritical reduction unit consumes 0.6 to 1 MW in the subcritical conditions whereas it is 0.3-0.4 MW in the supercritical conditions. The total energy penalty associated with the gas cleaning section is around 0.4 - 0.8 MW in the supercritical conditions and 1 - 1.5 MW in the subcritical conditions. The energy penalty of the NOx and SOx reduction units constitutes 3% to 10% of the overall energy penalty of the power plants.

Table 7.19(a). Energy analysis in subcritical conditions

	HAC	MSW	LAC	HAC:MSW(3:1)	HAC:MSW(1:1)	HAC:MSW(1:3)	LAC:MSW(3:1)	LAC:MSW(1:1)	LAC:MSW(1:3)
HPST (MW)	14.42	10.45	15.35	13.57	12.95	12.33	15.03	13.93	12.81
MPST (MW)	12.78	9.26	13.6	12.17	11.47	10.93	13.16	12.34	11.35
LPST (MW)	15.7	11.34	16.66	15.11	14.09	13.43	15.88	15.18	13.94
Power produced (MW)	42.9	31.05	45.63	40.85	38.51	36.69	44.07	41.45	38.1
Pump penalty (MW)	0.68	0.46	0.7	0.66	0.58	0.54	0.66	0.62	0.57
ASU penalty (MW)	7.58	5.31	7.87	7.44	6.77	6.47	7.84	7.45	6.71
CCU penalty (MW)	4.94	3.66	5.36	4.94	4.63	4.44	5.36	5.10	4.63
SCR penalty (MW)	0.81	0.66	0.94	0.85	0.81	0.75	0.95	0.89	0.8
FGD penalty (MW)	0	0.34	0.55	0.43	0.41	0.41	0.49	0.49	0.41
Total energy penalty (MW)	14.00	10.43	15.43	14.32	13.2	12.61	15.3	14.55	13.12
Net efficiency (%)	**28.89**	**20.62**	**30.18**	**26.53**	**25.31**	**24.08**	**28.77**	**26.90**	**24.99**

Table 7.19(b). Energy analysis in supercritical conditions

	HAC	MSW	LAC	HAC:MSW(3:1)	HAC:MSW(1:1)	HAC:MSW(1:3)	LAC:MSW(3:1)	LAC:MSW(1:1)	LAC:MSW(1:3)
HPST (MW)	14.19	12.15	14.77	13.89	13.69	13.49	14.43	14.13	13.34
MPST (MW)	17.31	14.83	18.02	16.46	16.22	15.99	17.6	17.25	16.29
LPST (MW)	12.58	11.03	13.23	12.16	11.99	11.81	12.85	12.59	11.89
Power produced (MW)	44.08	38.01	46.02	42.51	41.9	41.29	44.88	43.97	41.52
Pump penalty (MW)	0.77	0.7	0.816	0.76	0.75	0.74	0.8	0.78	0.74
ASU penalty (MW)	4.67	4.08	4.96	4.55	4.46	4.35	4.93	4.87	4.52
CCU penalty (MW)	3.29	3.08	3.55	3.29	3	3.19	3.55	3.51	3.13
SCR penalty (MW)	0.38	0.36	0.4	0.38	0.38	0.38	0.45	0.43	0.43
FGD penalty (MW)	0	0.37	0.38	0.36	0.36	0.35	0.37	0.38	0.37
Total energy penalty (MW)	9.1	8.6	10.1	9.34	8.96	9.01	10.1	9.97	9.19
Net efficiency (%)	**34.98**	**29.41**	**35.92**	**33.17**	**32.94**	**32.28**	**34.78**	**34**	**32.33**

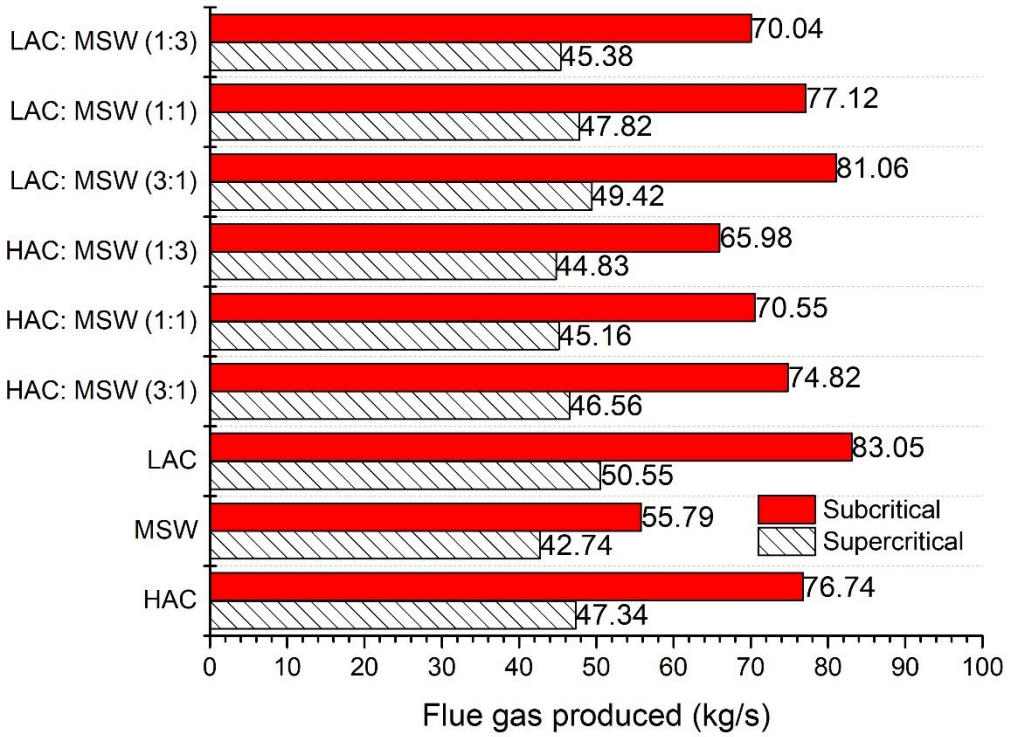

Figure 7.15. Flue gas generated during subcritical and supercritical conditions

The net efficiency of the power plants operating with LAC and MSW at 3:1 mass ratio is found almost similar (~28.8%) to that of HAC based power plants under both subcritical and supercritical conditions. Under supercritical conditions, the net efficiency of the power plants had increased by 5 to 10%. One of the main reasons is the production of higher electrical power under supercritical conditions due to the higher values of the operating temperature and pressure. In MSW based fuel, there is a significant rise in the net thermal efficiency under supercritical conditions by 8.79% due to the low energy penalty associated under these conditions. Energy penalty under subcritical conditions is estimated as 10.43% whereas it is reduced to 8.6% under supercritical conditions. Further, under supercritical conditions, the quantity of temperature moderator used is low by 34-76% and thus the energy penalty for flue gas treatment is reduced by 0.8 to 2.2MW. The amount of flue gas generated under subcritical and supercritical conditions is given in Figure 7.15. The ratio of the flue gas produced in subcritical conditions to supercritical conditions is found in between 1.3 to 1.64 and this ratio is least for MSW and highest for LAC. This could be due to the low oxygen requirement for MSW and higher oxygen requirement for LAC.

7.14. Economic analysis

The economic analysis of the oxy-fuel combustion based power plants under subcritical and supercritical conditions is reported in Tables 7.20(a) and 7.20(b), respectively. The capital recovery factor of the power plants is calculated as 0.086 using Equation 13. The total installed cost under supercritical conditions is found higher (~8-16%) than subcritical conditions, which could be due to the increased costs associated with boiler and turbine. MSW based power plants had shown the highest total installed cost in both subcritical (194 million $) and supercritical (230 million $) power plants. Although the installed costs are higher in the supercritical conditions, the estimated LCOE is found low by 9-11.5 for the coal feedstocks, compared to the subcritical conditions. In the case of MSW, the LCOE is low by 59 million $ in the supercritical conditions. LAC has shown the lowest LCOE among other fuels and their blends.

The operating cost of the power plants depends on the fuel cost and maintenance cost. The fuel cost of LAC is 1.3 to 2 times higher than that of HAC and MSW. With increase in the MSW content in the fuel blend, the operating cost of the power plant increases because higher quantity of MSW would be required to maintain the energy input level to the boiler. MSW has the least amount of carbon and thus requires lower amount of oxygen gas for complete combustion. This directly affects the capital costs associated with the ASU. This is reflected in the installed cost of the ASU unit under the blended feedstock conditions. When MSW proportion in the feedstock increases from 0-75%, the installed cost of the ASU unit decreases by 10.47% and 4.88% for HAC-MSW fuel blends under subcritical and supercritical conditions, respectively. Correspondingly, in the case of LAC-MSW fuel blends, it increases by 10.58% and 6.26% under subcritical and supercritical conditions, respectively.

Overall, the increase in the proportion of MSW in the fuel blend increased the LCOE of the power plants. In HAC-MSW fuel blends, the LCOE increases by 37.7 and 28.15 $/MWh for subcritical and supercritical conditions, respectively, for the increase in the MSW content from 0% to 75% in the fuel blend. Similarly, in LAC-MSW fuel blends, the LCOE increases by 37.21 and 25.38 $/MWh when MSW content increases from 0% to 75%.

Table 7.20(a). Economic analysis of under subcritical conditions

Cost in (million $)	HAC	MSW	LAC	HAC:MSW(3:1)	HAC:MSW(1:1)	HAC:MSW(1:3)	LAC:MSW(3:1)	LAC:MSW(1:1)	LAC:MSW(1:3)
MSW treatment cost	0	0.57	0	0.17	0.3	0.43	0.16	0.28	0.41
Coal handling system	1.02	0	0.92	0.89	0.71	0.47	0.81	0.67	0.46
ASU	20.43	11.5	20.97	19.98	18.86	18.29	20.92	20.17	18.75
Gas cleaning	0.42	8.27	5.79	6.77	7.19	7.7	6.24	6.77	7.43
CO_2 compressor	1.33	1.05	1.38	1.3	1.24	1.21	1.37	1.27	1.19
CO_2 removal and injection infrastructure	11.37	9.05	11.83	11.17	10.67	10.36	11.81	10.91	10.19
Water system	2.29	3.05	2.05	2.44	2.6	2.81	2.22	2.43	2.7
Heat exchangers	0.25	0.18	0.33	0.29	0.48	0.31	0.24	0.26	0.32
Turbine	38.23	50.83	34.25	40.68	43.48	46.82	37.09	40.59	45.02
Boiler	57.68	76.7	51.69	61.38	65.6	70.64	55.96	61.24	67.94
Total installed cost	**133.02**	**161.2**	**129.21**	**145.1**	**151.17**	**159.05**	**136.84**	**144.61**	**154.44**
Land surveyor cost	6.65	8.06	6.46	7.25	7.56	7.95	6.84	7.23	7.72
Owner's cost	19.95	24.2	19.4	21.8	22.7	23.9	20.5	21.7	23.2
Utilities	2.71	1.48	2.19	1.99	1.94	1.69	2.14	2.06	1.85
Total capital cost	**162.35**	**194.93**	**157.25**	**176.1**	**183.3**	**192.25**	**166.36**	**175.59**	**187.15**
Labour and maintenance cost	5.15	9.31	5.03	5.6	5.82	6.1	5.31	5.59	5.93
Plant overhead	0.2	0.23	0.23	0.22	0.22	0.21	0.2	0.22	0.22
Fuel cost	3.94	4.45	5.21	4	4.11	4.24	5.08	4.91	4.7
Slag disposal cost	0.69	0.92	0.026	0.52	0.57	0.63	0.67	0.74	0.82
CO_2 transport	0.57	0.56	0.74	0.7	0.66	0.64	0.74	0.68	0.63
Limestone cost	0	0.045	0.34	0.01	0.02	0.03	0.32	0.25	0.16
Operating and financial cost	10.6	15.5	11.59	11.05	11.4	11.8	12.32	12.4	12.47
ACC	13.93	16.73	13.49	15.1	15.7	16.52	14.28	15.07	16.06
LCOE	**96.77**	**178.62**	**94.85**	**112.59**	**122.35**	**134.47**	**105.53**	**116.53**	**130.33**

Table 7.20(b). Economic analysis under supercritical conditions

Cost in (million $)	HAC	MSW	LAC	HAC:MSW (3:1)	HAC:MSW (1:1)	HAC:MSW (1:3)	LAC:MSW (3:1)	LAC:MSW (1:1)	LAC:MSW (1:3)
MSW treatment cost	0	0.57	0	0.17	0.3	0.43	0.16	0.28	0.41
Coal handling system	1.15	0	1.03	1.02	0.8	0.53	0.91	0.75	0.51
ASU	14.54	13.24	15.17	14.29	14.09	13.83	15.11	14.98	14.22
Gas cleaning	0.69	8.74	6.17	7.06	7.72	8.1	6.69	7.23	8.05
CO_2 compressor	0.97	0.94	1.03	0.98	0.92	0.96	1.03	1.08	0.95
CO_2 removal and injection infrastructure	11.03	10.56	11.63	8.83	10.37	10.82	11.66	12.15	10.67
Water system	2.67	3.55	2.39	2.84	3.03	3.27	2.58	2.83	3.14
Heat exchangers	1.11	0.96	1.48	1.38	1.53	1.4	1.36	1.31	1.28
Turbine	40.87	54.33	36.62	43.49	46.48	50.05	39.64	43.39	48.13
Boiler	71.78	95.44	64.32	76.38	81.64	87.9	69.63	76.2	84.54
Total installed cost	**144.83**	**188.35**	**139.85**	**157.41**	**168.11**	**177.3**	**150.22**	**160.22**	**171.92**
Land surveyor cost	7.24	9.42	6.99	7.87	8.4	8.87	7.51	8.01	8.6
Owner's cost	21.72	28.3	20.98	23.6	25.21	26.6	22.5	24.03	25.8
Utilities	4.41	3.84	4.65	4.37	4.27	4.13	4.68	4.49	4.26
Total capital cost	**178.2**	**229.85**	**172.47**	**193.27**	**206**	**216.89**	**184.94**	**196.76**	**210.57**
Labour and maintenance cost	5.56	7.18	5.42	6.08	6.46	7.87	5.83	6.19	6.6
Plant overhead	0.15	0.18	0.17	0.18	0.18	0.18	0.18	0.18	0.18
Fuel cost	3.92	4.46	5.21	4	4.11	4.24	5.08	4.91	4.7
Slag disposal cost	0.69	0.92	0.026	0.52	0.57	0.63	0.67	0.73	0.82
CO_2 transport	0.52	0.5	0.55	0.52	0.49	0.51	0.55	0.57	0..5
Limestone cost	0	0.053	0.34	0.01	0.02	0.03	0.3	0.24	0.16
Operating and financial cost	10.84	13.29	11.7	11.33	11.84	13.46	12.62	12.83	12.97
ACC	15.29	19.72	14.8	16.58	17.68	18.61	15.87	16.88	18.07
LCOE	**85.27**	**128.15**	**84.2**	**96.05**	**102.27**	**113.42**	**93.5**	**99.37**	**109.58**

7.15. NO_X and SO_X pollutant emissions

Figures 7.16(a) and 7.16(b) show the NO_x and SO_x emission level in the flue gas after treatment in the respective units. The permissible concentration of NO_x and SO_x allowed in the flue gas after flue gas condensation is 640 mg/m^3 and 120 mg/m^3, respectively(Lockwood, 2014). These limits are achieved in the treatment units (Figure 7.16(a)). Under subcritical conditions, the NO_x emissions remain fairly constant about 7 mg/m^3 irrespective of the fuel blend used. Whereas, in the supercritical conditions, NO_x emissions are significantly higher. This could be due to the higher operating temperatures of the boiler and lower flue gas emissions. MSW has the highest NO_x emissions due to the higher nitrogen content in MSW, compared to HAC and LAC. Hence with increase in the MSW content in the fuel blend, the NO_x level in the flue gas also increases. NO_x emissions for HAC-MSW fuel blend increase from 30.65 to 49.67 mg/m^3 and for LAC-MSW fuel blend, the NO_x emissions increase from 35.54 to 55.46 mg/m^3.

One could observe from the Figure 7.16(b) that the SO_x emissions under subcritical conditions are well below the permissible limit in the flue gas (120 mg/m^3). LAC produces the highest SOx level as it contains 4% of sulfur. With the addition of MSW as a fuel blend with LAC (0 to 75%), the SO_x emission has decreased to the permissible level of 119.46 mg/m^3 (1:3 ratio of LAC:MSW). In the HAC-MSW fuel blending conditions, the SOx emission has increased from to the highest level of 12.83 and 27.63 mg/m^3 under subcritical and supercritical conditions, respectively. SO_x emissions can increase by 2-12 times in the supercritical conditions as compared to subcritical conditions. Under the supercritical conditions, it was found that for LAC, LAC: MSW (3:1), LAC: MSW (1:1), the SO_x emissions are higher than the permissible limit of 120 mg/m^3. Hence, the additional SO_x removal techniques such as duct sorbent injection (DSI) and ultrasonication (UC) of coals are employed for the treatment of LAC.

The SO_x emissions after treating the LAC based flue gas in the DSI/UC units is given in Figure 7. The addition of DSI unit and UC effectively decreased the LAC based SO_x emissions by 116.4 and 215.09 mg/m^3, respectively. With LAC-MSW blend at 3:1 mass ratio, the SOx emission has decreased by 106.91 and 159.35 mg/m^3. Ultrasonication method is a pre-combustion sulfur removal technique. The energy penalty for this UC treatment is considered based on the solvent utilization and the electric power

consumption for ultrasound generation per kg of coal treated. A UC reactor consumes 500W of power having working capacity of 8 litres(Chen et al., 2013).

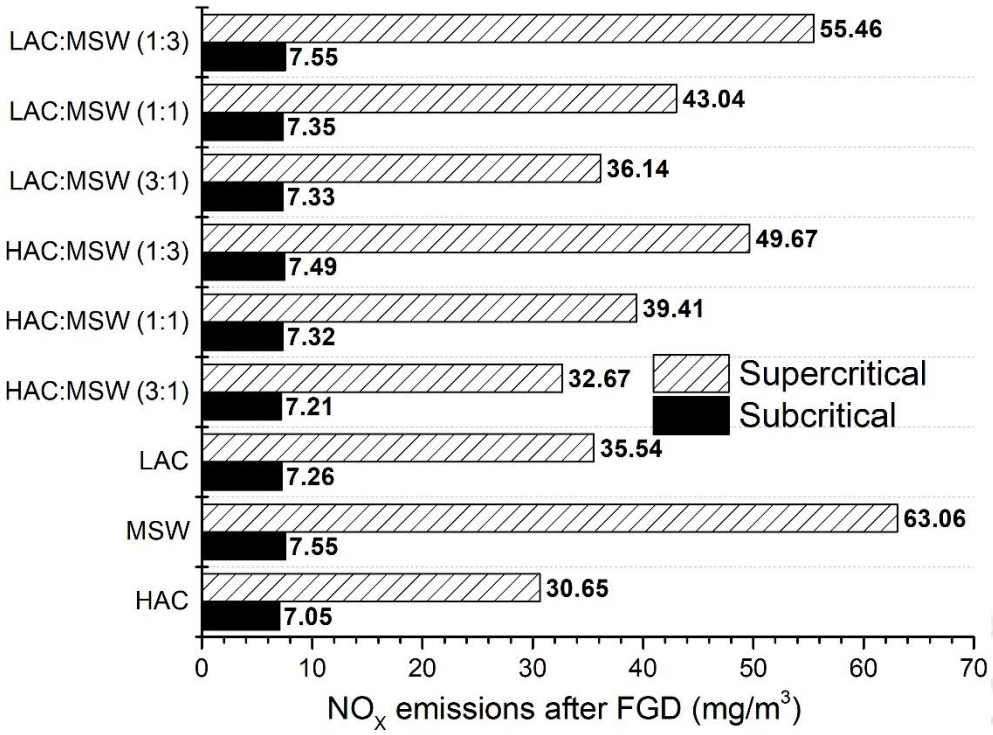

Figure 7.16(a). Estimated NO_x emissions after the treatment of flue gas in the SCR unit

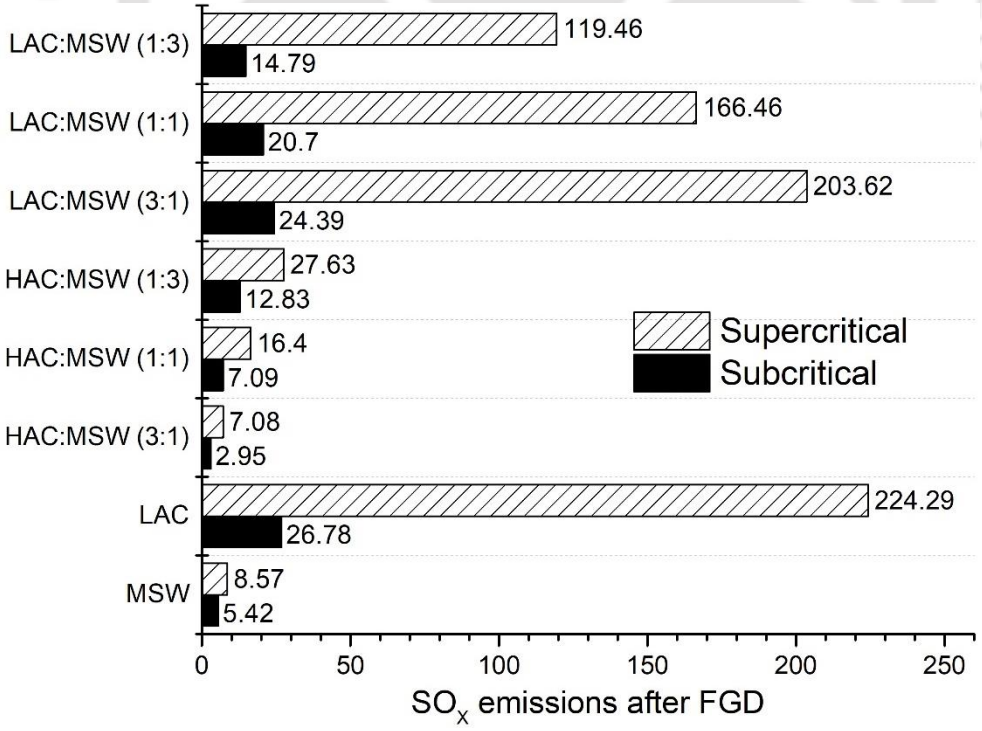

Figure 7.16(b). Estimated SO_x emissions after the treatment of flue gas in the FGD unit

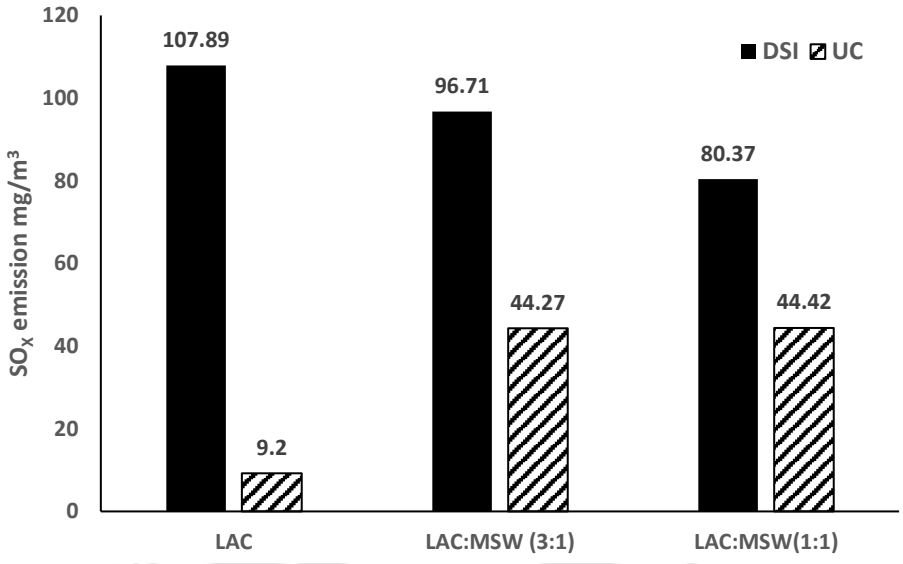

Figure 7.17. SO_x emissions after flue gas desulfurization with DSI/UC

In Figure 7.17, it can be observed that the addition of MSW with LAC decreases the SO_x emissions when FGD and DSI, the post combustion treatment units, are used for SO_x capture. However, in the UC, the pre-combustion deSOx method, the SO_X in the flue gas at LAC-MSW ratio of 1:1 is slightly higher than the flue gas obtained from the feedstock at 3:1 ratio. This is due to the removal of sulfur only from LAC by the UC method at the pre-combustion stage. Hence the SO_x emissions gradually has increased with the addition of MSW content in the LAC-MSW fuel blend.

7.15.1. Energy and economic analysis after addition of UC and DSI unit

Table 7.21 provides the energy analysis of the power plants after the addition of DSI/UC units under supercritical conditions. The LAC based supercritical power plants cause high SOx emissions beyond the permissible level. Hence the techno economic analysis of the power plants incorporating the UC/DSI unit is performed only for the supercritical condition of the turbines. The energy penalty associated with DSI is comparatively lower than the ultrasonication method. The DSI addition decreased the net energy efficiency by 0.09% and by adding the UC, the net efficiency of the power plants decreases even further by 0.34% to 1.06%.

The energy penalty of the UC is directly proportional to the amount of LAC in the LAC-MSW fuel blend. The energy penalty associated with UC addition decreases from 0.34 to 0.22 MW as the quantity of LAC decreases from 100 to 50%. In the UC method, as sulfur is also a combustible substance, the removal of sulfur before combustion affects

the adiabatic flame temperature of the boiler. On an average, the oxygen content for coal combustion has decreased by 0.5 kg/s, compared to the power plant without the addition of the UC unit.

The ASU energy penalty for UC is lower by 0.06 to 0.12 MW when DSI unit is used for sulfur removal. The amount of flue gas recycled for maintaining combustor temperature declines when UC is used for sulfur removal. This in turn decreases the quantity of flue gas supply to the CCU unit. The CCU energy penalty of the UC based power plants is slightly higher (0.1 to 0.4 MW) than the DSI based energy power plants. The energy penalty for the gas cleaning is highly dependent on the quantity of flue gas generated sent to the SCR and FGD unit. As the volume of the flue gas decreases slightly in the UC based power plants, this in turn decreases the energy penalty by 0.03 to 0.05 MW.

Economic analysis of the supercritical power plants after the addition of DSI/UC unit is given in Table 7.22. The addition of the sulfur removal units such as DSI/UC increases the LCOE by 1-2 $/MWh (compared to the LCOE without DSI/UC unit from Table 7.20(b)). The equipment cost (MSW treatment, coal handling, CO_2 compressor, heat exchanger) and operating cost are common to the power plants with and without DSI/UC units. As discussed earlier, the oxygen required for the UC unit is comparatively low and hence the cost of ASU unit becomes low. However, the cost of UC unit is higher than DSI unit, which affects the capital cost. UC and DSI units employ H_2O_2 and lime for sulfur removal, respectively. As the lime is comparatively costlier than H_2O_2, the operating cost of the DSI unit is higher than the UC unit. Overall, UC based system has shown higher LCOE than DS due to the additional costs incurred for ultrasonication and drying unit. As the MSW quantity in LAC-MSW fuel blend increases from 0 to 50%, the costs of the UC unit declines from 1.22 to 0.89 million $ due to the reduction in amount of LAC treated in UC unit.

Table 7.21. Energy analysis of the power plant after the addition of DSI/UC unit

	LAC (DSI)	LAC:MSW (3:1) (DSI)	LAC:MSW (1:1) (DSI)	LAC (UC)	LAC:MSW (3:1) (UC)	LAC:MSW (1:1) (UC)
HPST (MW)	14.77	14.43	14.13	14.52	14.28	14.08
MPST (MW)	18.02	17.6	17.25	17.72	17.43	17.19
LPST (MW)	13.23	12.85	12.59	12.94	12.72	12.54
Power produced (MW)	**46.02**	**44.88**	**43.97**	**45.18**	**44.43**	**43.81**
Pump power (MW)	0.81	0.8	0.78	0.8	0.79	0.78
ASU penalty (MW)	4.96	4.93	4.87	4.84	4.82	4.81
CCU penalty (MW)	3.55	3.55	3.51	3.58	3.56	3.55
SCR penalty (MW)	0.4	0.45	0.43	0.39	0.43	0.41
FGD penalty (MW)	0.38	0.37	0.38	0.37	0.36	0.37
DSI/UC penalty (MW)	0.092	0.09	0.088	0.43	0.36	0.27
Total energy penalty	**10.18**	**10.19**	**10.06**	**10.4**	**10.33**	**10.2**
Net efficiency (%)	**35.84**	**34.69**	**33.91**	**34.77**	**34.1**	**33.6**
Decrease in net efficiency	0.09	0.09	0.09	1.15	0.68	0.4

Table 7.22. Economic analysis after addition of DSI/UC unit

Costs (million $)	LAC (DSI)	LAC (UC)	LAC: MSW (3:1)(DSI)	LAC: MSW (3:1)(UC)	LAC: MSW (1:1)(DSI)	LAC: MSW (1:1)(UC)
ASU	15.17	14.92	15.11	14.88	14.98	14.86
CO_2 removal and injection infrastructure	11.63	11.71	11.66	11.68	11.56	11.66
DSI/UC capital cost	0.41	1.22	0.37	1.08	0.32	0.89
Dryer cost (with UC unit)	-	0.14	-	0.12	-	0.1
Common installed cost	113.04	113.04	122	122	133.02	133.02
Total installed cost	**140.81**	**141.58**	**150.61**	**151.21**	**159.9**	**160.56**
Land surveyor cost	7.04	7.08	7.53	7.56	7.99	8.03
Owner's cost	21.1	21.2	22.6	22.7	23.98	24.08
Utilities	4.65	4.65	4.68	4.68	4.49	4.49
Total capital cost	**173.62**	**174.55**	**185.41**	**186.13**	**196.37**	**197.15**
Labour and maintenance cost	5.46	5.48	5.85	5.87	6.17	6.2
Common operating cost	5.786	5.786	6.3	6.3	6.19	6.19
Plant overhead	0.17	0.17	0.18	0.18	0.18	0.18
Limestone and lime cost	0.18	0.07	0.16	0.07	0.12	0.063
H_2O_2 cost	-	0.02	-	0.017	-	0.012
DSI operating cost	0.59	-	0.52	-	0.42	-
Total Operating cost	**12.16**	**11.51**	**13.07**	**12.44**	**13.08**	**12.66**
Annual capital cost (ACC)	14.9	14.98	15.91	15.97	16.85	16.92
LCOE	**86.21**	**86.95**	**95.19**	**95.12**	**100.76**	**100.45**

7.16. Comparison with literature

Table 7.23. Comparison of net efficiency and LCOE values with literature for oxy-fuel based coal combustion power plants

References	Net efficiency (%)	LCOE ($/MWh)
(C. C. Cormos, 2020)	34.64	94.56**
(C. C. Cormos, 2016), (Adams II et al., 2017)	34.31	82.3*
(C. C. Cormos, 2016)	32.2	99.16*
(Lockwood, 2014)	33.4	79
(maddahi & Hossainpour, 2019)	26.32	75.07**
(Guandalini et al., 2019)	33.6	106.6
(Xiong et al., 2009)	36.24	55.04
Present values (LAC)	35.92	84.2
Present values (HAC)	34.98	85.27
MSW (compared with post CCU method)		
Present values (MSW)	29.41	128.15
(Yassin et al., 2009)	22.4	108.64**
(Mondal, 2021) (Combined cycle)	44.24	123.5
(Chaiyat, 2021) (Organic Rankine cycle)	37.43	153

**Values calculated from Euro/MWh to Dollar/MWh (1 Euro= 1.12 Dollar),

*converted to 2017-year basis by Adams (2017) (Adams II et al., 2017),

The net efficiency and economic analysis of the power plants are compared with the literature results and are shown in Table 7.23. It can be noted that the LCOE estimated in the present study for LAC and HAC is almost comparable with the literature values for oxy-fuel combustion based technology. Adams et al., (2017) (Adams II et al., 2017) recalculated the net efficiency and LCOE of the power plants reported in the literature on the basis of the year 2017 (Table 7.23). Using MSW as the feedstock, Yassin et al., (2009) (Yassin et al., 2009) reported an LCOE value of 108.64 $/MWh with the integration of post CCU method; whereas the present study under oxy-combustion method had shown a lower LCOE value with a difference of 10.97 $/MWh.

7.17. Summary of the chapter

In the present study, techno-economic analysis of oxy-fuel co-combustion based power plants using high ash and low ash Indian coals with MSW has been performed. It can be concluded that the MSW being a low quality fuel cannot be incinerated alone for the electricity generation as the calculated LCOE values are not economically favourable. The following conclusions can be drawn from the present study.

- The co-combustion of MSW with coals exhibits certain advantages. The addition of 25% of HAC and LAC with MSW raised the net thermal efficiency of steam turbine by 5.91% and 8.15% for HAC and LAC respectively under subcritical conditions. The co-combustion of coal with MSW reduced the LCOE by 48-73, compared to MSW alone as the feedstock for the power plants.
- The net thermal efficiency of the MSW based power plants under supercritical conditions has significantly raised by 8.79%, compared to the subcritical conditions. Further, the LCOE of MSW based power plants is reduced by 50$/MWh under supercritical conditions.
- The addition of MSW from 0-75% in the fuel blend increased the NO_x emissions by 0.44 and 0.29 mg/m^3 for HAC and LAC fuel blends, respectively, under subcritical conditions. Similarly, in supercritical conditions, the emissions increased by ~19 mg/m^3 for HAC and LAC fuel blends. The addition of SCR unit for NO_x reduced the thermal efficiency of the power plant by 0.4-0.45% in supercritical conditions and 0.75-0.95% in subcritical conditions.
- High sulfur coal treatment by duct sorbent injection and ultrasonication method lead to the energy penalty of 0.09 and 0.4 – 1.15 MW in the power plants. These units increased the LCOE by 1.2 – 2.4$/MWh. On an average, DSI operated power plants have 0.25 to 0.98% higher efficiency, compared to UC based power plants.
- With increase in the MSW in the LAC blended feedstock (25% and 50%), the operating cost of UC unit is lower than DSI unit, which decreases LCOE of UC based power plants even though the capital costs associated with UC unit are higher. Power plants based on pure LAC has higher LCOE in UC sulphur treatment method than DSI sulphur treatment method (86.95 versus 86.21$/MWh).

References

Adams II, T. A., Hoseinzade, L., Madabhushi, P. B., & Okeke, I. J. (2017). Comparison of CO_2 Capture Approaches for Fossil-Based Power Generation: Review and Meta-Study. *Processes*. https://doi.org/10.3390/pr5030044

Ambedkar, B., Chintala, T. N., Nagarajan, R., & Jayanti, S. (2011). Chemical Engineering and Processing : Process Intensification Feasibility of using ultrasound-assisted process for sulfur and ash removal from coal. *Chemical Engineering & Processing: Process Intensification*, *50*(3), 236–246. https://doi.org/10.1016/j.cep.2011.02.008

Aneke, M., & Wang, M. (2015). Potential for improving the energy ef fi ciency of cryogenic air separation unit (ASU) using binary heat recovery cycles. *Applied Thermal Engineering*, *81*, 223–231. https://doi.org/10.1016/j.applthermaleng.2015.02.034

Baruah, B. P., & Khare, P. (2007). Desulfurization of Oxidized Indian Coals with Solvent Extraction and Alkali Treatment. *Energy and Fuels*, *25*, 2156–2164.

Basu, S., & Debnath, A. K. (2019). *Power Plant Instrumentation and Control Handbook A Guide to Thermal Power Plants* (G. Nisbet (Ed.); second edi). Candice Janco.

Cau, G., Tola, V., Ferrara, F., Porcu, A., & Pettinau, A. (2018). CO_2-free coal-fired power generation by partial oxy-fuel and post-combustion CO_2 capture: Techno-economic analysis. *Fuel*, *214*(October 2017), 423–435. https://doi.org/10.1016/j.fuel.2017.10.023

Chaiyat, N. (2021). Energy, exergy, economic, and environmental analysis of an organic Rankine cycle integrating with infectious medical waste incinerator. *Thermal Science and Engineering Progress*, *22*(December 2020), 100810. https://doi.org/10.1016/j.tsep.2020.100810

Cormos, C. C. (2016). Oxy-combustion of coal, lignite and biomass: A techno-economic analysis for a large scale Carbon Capture and Storage (CCS) project in Romania. *Fuel*, *169*, 50–57. https://doi.org/10.1016/j.fuel.2015.12.005

Cormos, C. C. (2020). Energy and cost efficient manganese chemical looping air separation cycle for decarbonized power generation based on oxy-fuel combustion

and gasification. *Energy*, *191*, 116579. https://doi.org/10.1016/j.energy.2019.116579

Ding, G., He, B., Cao, Y., Wang, C., Su, L., Duan, Z., Song, J., Tong, W., & Li, X. (2018). Process simulation and optimization of municipal solid waste fired power plant with oxygen/carbon dioxide combustion for near zero carbon dioxide emission. *Energy Conversion and Management*, *157*(May 2017), 157–168. https://doi.org/10.1016/j.enconman.2017.11.087

Dong, C., Jin, B., & Lan, J. (2002). Co-combustion of Municipal Solid Waste and Coal in a Circulating Fluidized Bed. *Developments in Chemical Engineering and Mineral Processing*, *10*(5–6), 639–646. https://doi.org/10.1002/APJ.5500100613

Du, Y. F., Liao, H., & Wei, Y. M. (2020). Integrating cost information in energy efficiency measurement: An empirical study on thermal power companies. *Energy Efficiency*, *13*(4), 697–709. https://doi.org/10.1007/s12053-020-09849-5

Goh, T., & Ang, B. W. (2021). Integrating combined heat and power in index decomposition analysis of the power sector. *Energy Efficiency*, *14*(7), 1–22. https://doi.org/10.1007/s12053-021-09969-6

Guandalini, G., Romano, M. C., Ho, M., Wiley, D., Rubin, E. S., & Abanades, J. C. (2019). A sequential approach for the economic evaluation of new CO2 capture technologies for power plants. *International Journal of Greenhouse Gas Control*, *84*(October 2018), 219–231. https://doi.org/10.1016/j.ijggc.2019.03.006

Lockwood, T. (2014). Developments in oxyfuel combustion of coal Developments in oxyfuel combustion of coal. *IEA Clean Coal Center*, *August*.

Ma, C., Li, B., Chen, D., Wenga, T., Ma, W., Lin, F., & Chen, G. (2019). An investigation of an oxygen-enriched combustion of municipal solid waste on flue gas emission and combustion performance at a 8 MWth waste-to-energy plant. *Waste Management*, *96*, 47–56. https://doi.org/10.1016/j.wasman.2019.07.017

maddahi, L., & Hossainpour, S. (2019). Thermo- economic evaluation of 300 MW coal based oxy-fuel power plant integrated with organic Rankine cycle. *International Journal of Greenhouse Gas Control*, *88*(November 2018), 383–392. https://doi.org/10.1016/j.ijggc.2019.07.004

Mondal, P. (2021). Techno-economic and environmental performance assessment of a MSW to energy plant for Indian urban sectors. *Thermal Science and Engineering Progress*, *21*(April 2020), 100777. https://doi.org/10.1016/j.tsep.2020.100777

Prabu, V., & Geeta, K. (2015). CO_2 enhanced in-situ oxy-coal gasi fi cation based carbon-neutral conventional power generating systems. *Energy*, *84*, 672–683. https://doi.org/10.1016/j.energy.2015.03.029

Purchasing power parities. (n.d.). Organization for Economic Cooperation and Development. https://data.oecd.org/conversion/purchasing-power-parities-ppp.htm

Rai, A. K. (2017). Super Critical Thermal Power Plant Boiler Efficiency Calculation Using Imported Coal. *International Journal for Research in Applied Science and Engineering Technology*, *V*(IX), 709–717. https://doi.org/10.22214/ijraset.2017.9104

Sadi, M., & Arabkoohsar, A. (2019). Exergoeconomic analysis of a combined solar-waste driven power plant. *Renewable Energy*, *141*, 883–893. https://doi.org/10.1016/j.renene.2019.04.070

Saikia, B. K., Dutta, A. M., Saikia, L., Ahmed, S., & Baruah, B. P. (2014). Ultrasonic assisted cleaning of high sulphur Indian coals in water and mixed alkali. *Fuel Processing Technology*, *123*(2013), 107–113. https://doi.org/10.1016/j.fuproc.2014.01.037

Sebastian, R. M., & Alappat, B. (2016). Thermal Properties of Indian Municipal Solid Waste Over the Past, Present and Future Years and Its Effect on Thermal Waste to Energy Facilities. *Civil Engineering and Urban Planning: An International Journal (CiVEJ)*, *3*(2), 97–106. https://doi.org/10.5121/civej.2016.3208

Singh, S., Lu, H., Cui, Q., Li, C., Zhao, X., Xu, W., & Ku, A. Y. (2018). China baseline coal-fired power plant with post-combustion CO_2 capture: 2. Techno-economics. *International Journal of Greenhouse Gas Control*, *78*(April), 429–436. https://doi.org/10.1016/j.ijggc.2018.09.012

Singh, U., Rao, A. B., & Chandel, M. K. (2017). Economic Implications of CO_2 Capture from the Existing as Well as Proposed Coal-fired Power Plants in India under Various Policy Scenarios. *Energy Procedia*, *114*(November 2016), 7638–7650.

https://doi.org/10.1016/j.egypro.2017.03.1896

Thermal_Model_Consolidated_v. (n.d.). Central Electricity Regulatory Commission.

Xin-gang, Z., Gui-wu, J., Ang, L., & Ling, W. (2016). Economic analysis of waste-to-energy industry in China. *Waste Management*. https://doi.org/https:// doi. org/ 10. 1016/j. wasman. 2015. 10. 014

Xiong, J., Zhao, H., Zheng, C., Liu, Z., Zeng, L., Liu, H., & Qiu, J. (2009). An economic feasibility study of O2/CO2 recycle combustion technology based on existing coal-fired power plants in China. *Fuel*, *88*(6), 1135–1142. https://doi.org/10.1016/j.fuel.2008.12.002

Xu, J., Huang, Q., & Wang, F. (2020). Co-combustion of municipal solid waste and coal for carbon emission reduction: A bi-level multi-objective programming approach. *Journal of Cleaner Production*, *272*, 121923. https://doi.org/10.1016/j.jclepro.2020.121923

l Engineering Journal, *146*, 315–327. https://doi.org/10.1016/j.cej.2008.06.014

Zhang, D. (2013). *Ultra-Supercritical Coal Power Plants Materials, Technologies and Optimisation* (First). Woodhead Publishing.

This page is left blank intentionally

This page is left blank intentionally

CHAPTER 8

CONCLUSIONS & FUTURE WORK

In this chapter, conclusions drawn form the present work are listed. Further, future work that can be conducted based on present experiments/simulations are given.

8.1. Major conclusions

From the thesis, the following major conclusions can be drawn.

- During co-gasification of HAC with HDPE, the chemical interaction between coal volatiles, CO_2, and ethylene molecules at 400°C enlarged the pore diameter of HAC at 1000°C. Hence, the structural and morphological changes in the HAC enhanced its reactivity with CO_2 and resulted in high quality syngas.
- The co-gasification of HAC with HDPE enhanced the calorific value of syngas of HAC from 2.6 MJ/Nm^3 to 20 MJ/Nm^3 due to the improvement in the surface area and pore diameter of the char of HAC.
- A 15 to 20% (weight basis) addition of OG plastics to HAC increased the heating value of the syngas as high as 8.56 MJ/nm^3. This is due to the increase in the hydrogen and hydrocarbon gases in the syngas by 8.7 fold. The addition of OG beyond 20% with OG causes adverse effect due to the formation high tarry fluid, which plugs the pores of HAC.
- The co-gasification of HAC with PCB (PCB resin, PCB plastic, and PCB mixture) in a 4:1 ratio (HAC:PCB) generated the syngas with a net calorific value of 5.1-5.2 MJ/nm^3. The addition of excess PCB mixture beyond this ratio retards the progress of gasification due to the hindrance of other non-reactive solid materials.
- The residues of OG after gasification contain CaO (~32%) and $CaCO_3$ (~67%), which can act as catalysts during gasification for the generation of syngas. Further the co-gasification residue of PCB has a significant proportion of $CaCO_3$, TiO_2, and SnO_2 for PCB plastic and PCB resin ash. These ash particles can be used as an additive with concrete materials for the construction purpose to improve compressive strength and water absorption capacity.

- Under post-combustion CCS method, the addition of ¼ proportion of MSW with HAC as a fuel feedstock in thermal power plants operating under subcritical conditions caused only a marginal drop in the net efficiency of 0.77%, compared to the unblended HAC feedstock. Hence, 25% addition of MSW with HAC may be permitted for effective co-utilization.
- The LCOE of MSW based power plants is found higher by 40 to 60% than LAC and HAC based power plants. The blending of HAC with MSW at 1:3 (HAC:MSW) ratio drops the LCOE from 80 to 73.5 $/MWh. Further, the incorporation of post-combustion based CCU unit reduces the impact of ash on the efficiency of thermal power plants.
- Under oxy-fuel combustion conditions, a similar trend is observed with the addition of coal with MSW. The net thermal efficiency of steam turbine based thermal power plants is increased by 5.9% by the addition of 25% of HAC with MSW under sub-critical based power plants.
- Under oxy-fuel combustion conditions, MSW based power plants achieved a net thermal efficiency higher by 8.79% under supercritical conditions compared to subcritical conditions. Further, the LCOE of MSW based power plants is reduced by 50 $/MWh under supercritical conditions.

8.2. Future scope of the study

The present study explored the effective co-utilization of high ash coal with various wastes by thermochemical treatment with municipal solid waste, plastic wastes and electronic wastes. The future work related to thermochemical treatment of wastes is:

- Pilot scale studies must be performed for co-gasification of HAC with these plastic wastes to up-scale the process. The difficulties associated with tar handling along with ash need to be explored.
- Effect of HAC ash on HDPE/OG needs to be evaluated during gasification. Further, the impact of OG ash, which is rich in Ca, on the gasification of HAC, should be explored.
- The co-gasification behaviour of these feedstocks should be explored under fully fluidized and spouted fluidized conditions of the bed.
- In case of PCB processing, post gasification process is required to recover metals from the obtained residue.

- The oil recovered from pyrolysis of PCB contains bromine, which is detrimental for its application. Hence, further purification is necessary without addition of auxiliary units.
- Techno-economic analysis on co-gasification of HAC with these wastes is required to evaluate the feasibility of syngas production. Life cycle analysis can also be executed to compare the process with other thermochemical processes.

This page is left blank intentionally

APPENDIX

(i) XPS survey

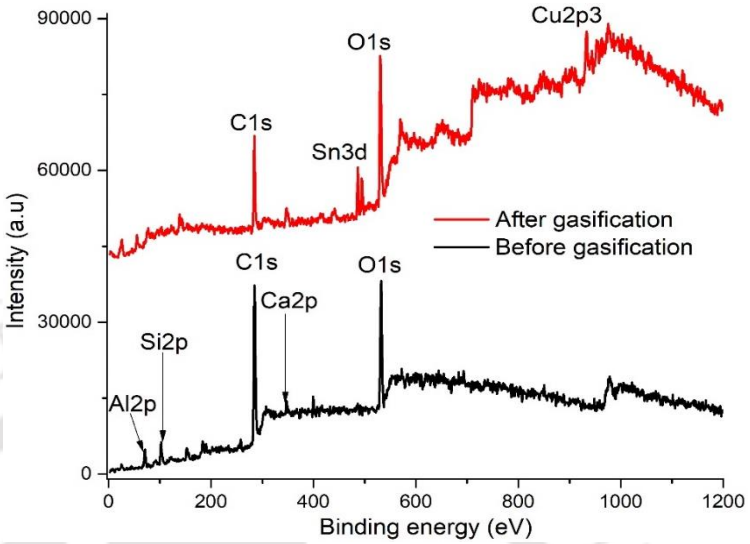

(j) Cu survey

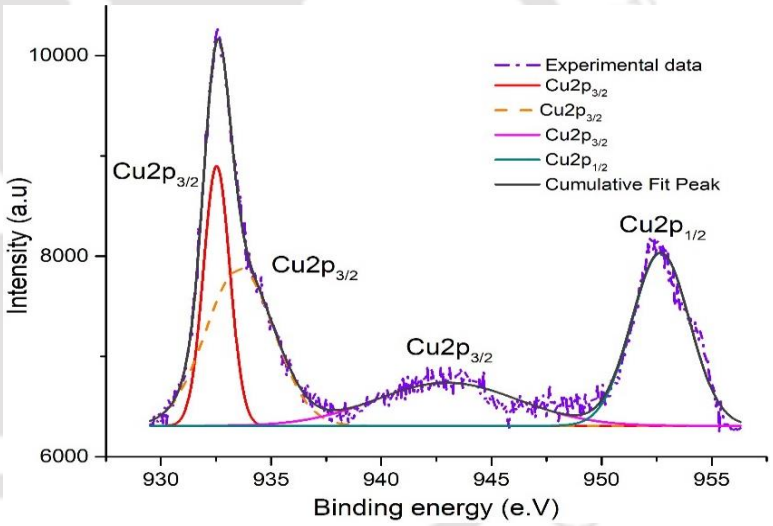

(k) Tin survey

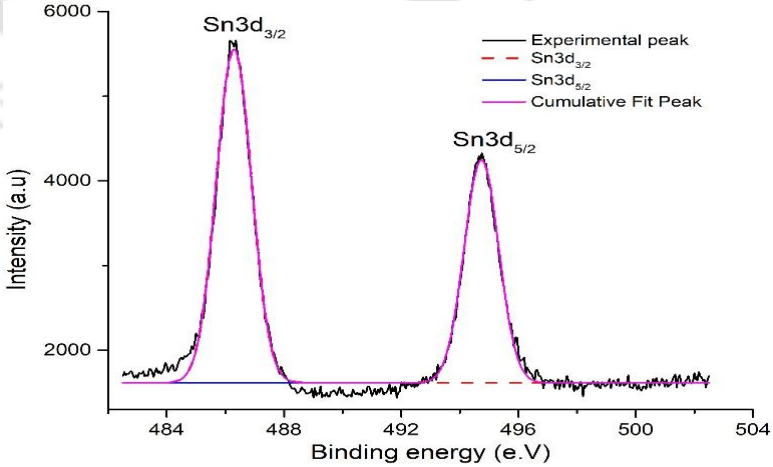

(l) Silicon survey

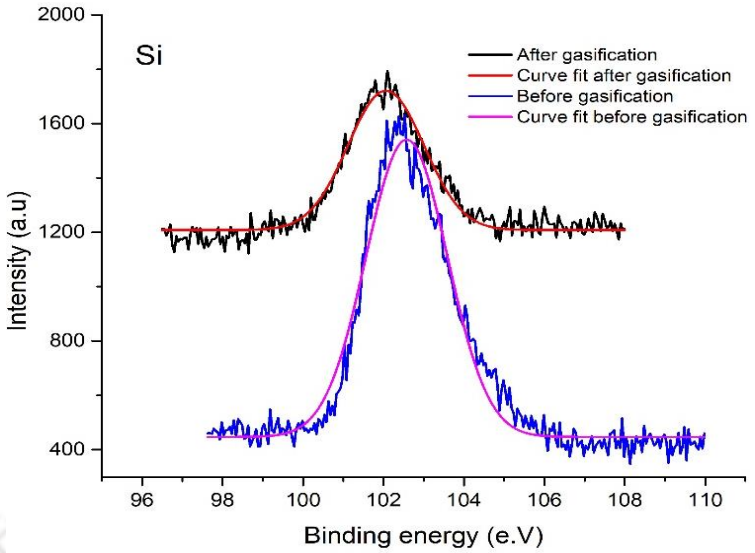

(m) Calcium survey

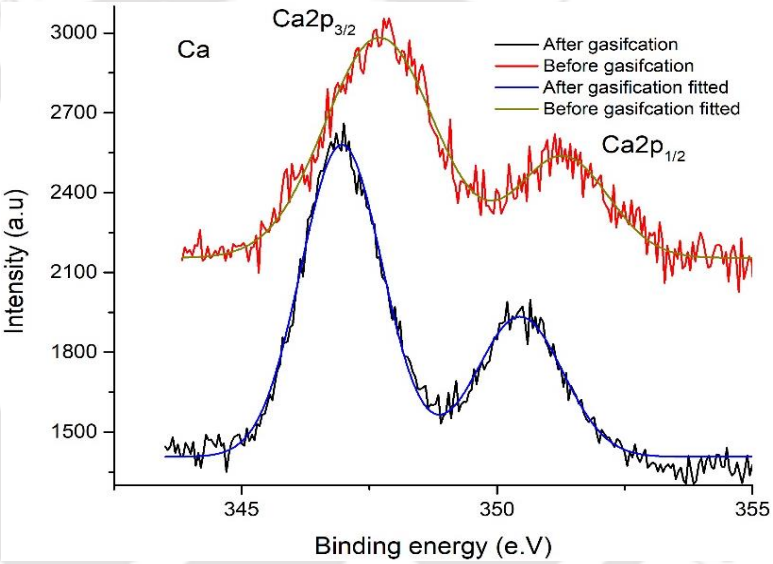

(n) Aluminium survey

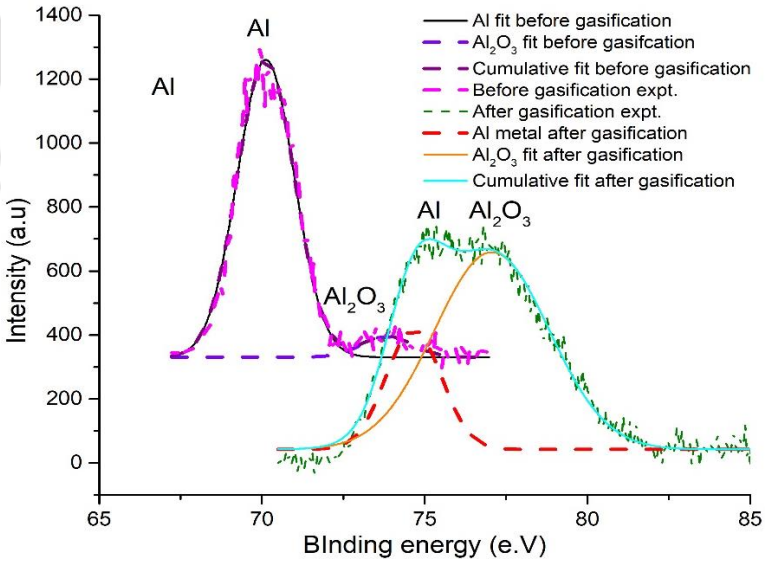

Figure 1. XPS analysis of PCB mixture before and after gasification

XPS analysis of PCB mixture before and after gasification is shown in Figure 1. It shows the presence of aluminium, silica, and calcium before and after gasification. Although tin and copper are present in the PCB feedstock, these are masked by other materials like carbon. Gasification of PCB mixture depletes the amount of carbon in residue, which ultimately unmasks these metals. XPS analysis of aluminium metal before gasification reveals a minor amount of Al_2O_3. However, after gasification, the amount of Al_2O_3 increases as compared to Al. The binding energy of aluminium shifts from 70.24 and 74.18 eV to 75.29 and 77.24 eV. This could be due to the reaction between Al metal and CO_2 at high temperatures to form Al_2O_3, CO, or C, which is deposited on PCB (BREAKSPERE, 1970). Similar observations could be made for Ca and Si and this was due to high temperature CO_2 conditions near these metals. The binding energy of Ca ($2p_{3/2}$ and $2p_{1/2}$) is 347.93 and 351.23 and shifts to 346.99 and 350.65 eV. Further, the binding energy of Si shifts from 102.57 to 102.09 eV. These shifts are caused due to the mobility of oxygen compounds over the surface (Al-Mamoori et al., 2019). Table 1 provides the general binding energy of Ca, Si, and Al.

Table 1. XPS energy of various metals

Metal	Binding energy(eV)	Reference
Ca	347.93 $Ca2p_{3/2}$	Zhai et al., 2022
	350.68 $Ca2p_{1/2}$	
Al	73.1 Al metal	Jilani et al., 2013
	76.2 Al-O	
Si	99.5 Si^0	Radvanyi et al., 2014

$$2Al + 3CO_2 \rightarrow Al_2O_3 + 3CO \quad (1)$$

$$4Al + 3CO_2 \rightarrow 2Al_2O_3 + 3C \quad (2)$$

References

Al-Mamoori, A., Lawson, S., Rownaghi, A. A., & Rezaei, F. (2019). Improving Adsorptive Performance of CaO for High-Temperature CO 2 Capture through Fe and Ga Doping. *Energy and Fuels*, *33*(2), 1404–1413. https://doi.org/10.1021/acs.energyfuels.8b03996

BREAKSPERE, R. J. (1970). High-Temperature Oxidation of Aluminium. *Journal of Applied Chemistry*, *20*, 208–212.

Jilani, S. M., Gamot, T. D., Banerji, P., & Chakraborty, S. (2013). Studies on resistive switching characteristics of aluminum/graphene oxide/semiconductor nonvolatile memory cells. *Carbon*, *64*(August), 187–196. https://doi.org/10.1016/j.carbon.2013.07.051

Radvanyi, E., Vito, E. De, Porchera, W., & Larbi*, S. J. S. (2014). An XPS/AES comparative study of the surface behaviour of nano-silicon anodes for Li-ion batteries. *J. Anal. At. Spectrom.* https://doi.org/https://doi.org/10.1039/C3JA50362C

Zhai, H., Liu, F., Huang, Y., Yang, Q., Tian, C., & Zhou, W. (2022). Preparation of peanut shell-like calcium carbonate from biowaste chicken eggshell and its application for aqueous Victoria Blue B removal. *Microporous and Mesoporous Materials*, *329*(September 2021), 111549. https://doi.org/10.1016/j.micromeso.2021.111549

RESEARCH OUTPUT

PUBLICATIONS BASED ON THE PRESENT WORK

1. **Pradeep Sahu**, Prabu Vairakannu. *Techno-economic analysis of co-combustion of Indian coals with municipal solid waste in subcritical and supercritical based steam turbine power generating carbon-negative systems*. **Energy** DOI https://doi.org/10.1016/j.energy.2021.121053

2. **Pradeep Sahu**, Prabu Vairakannu. *Synergistic reaction effects with energy and exergy (2E) analysis of high-density polyethylene with high ash bituminous coal for syngas production*. **Fuel** DOI https://doi.org/10.1016/j.fuel.2021.122500

3. **Pradeep Sahu**, Prabu Vairakannu. *Techno-economic analysis on oxy-fuel based steam turbine power system using municipal solid waste and coals with ultrasonicator sulfur removal*. **Waste Disposal & Sustainable Energy** DOI https://doi.org/10.1007/s42768-022-00100-8

4. **Pradeep Sahu**, Prabu Vairakannu. *CO_2 based co-gasification of printed circuit board (PCB) with high ash Indian coal*. **Energy** https://doi.org/10.1016/j.energy.2022.125977

5. **Pradeep Sahu**, Prabu Vairakannu. *CO_2 pyrolysis and gasification of COVID-19 based wastes with high ash coal.* (Accepted).

CONFERENCES ATTENDED

1. **Pradeep Sahu**, Prabu Vairakannu. *Pyrolysis and Gasification of Municipal Solid Waste (MSW).* Recycle 2018, 22 February 2018-24 February 2018. Indian Institute of Technology, 2018

2. **Pradeep Sahu**, Prabu Vairakannu. *Thermogravimetric analysis on Co-gasification of Municipal Solid Waste with Indian Coals and Pet coke***.**

Advances in Chemical Engineering (ACES 2019), 7 March 2019-8 March 2019. Indian Institute of Science Education and Research, Bhopal, 2019

3. **Pradeep Sahu**, Prabu Vairakannu. *Co-pyrolysis and co-gasification of kitchen waste with Indian coals.* SEGT 2019, Bangkok, 11-14 December 2019.

4. **Pradeep Sahu** and Prabu Vairakannu, *Thermogravimetric analysis kitchen waste under pyrolysis and gasification conditions.* 3rd Sustainable Waste Management Conference August 4-6, 2021. AICHE Conference.

BOOK CHAPTER PUBLICATION

1. **Pradeep Sahu**, Roni Mallick and Prabu Vairakannu.' Thermochemical treatment of waste for power generation' in *Valorization of Wastes for Sustainable Development*' Elsevier (under review)